論文 / 著書情報
Article / Book Information

題目(和文)	
Title(English)	Infrared Studies of Adsorption and Hydrogenations over ZrO_2_
著者(和文)	野村淳子
Author(English)	JUNKO NOMURA
出典(和文)	学位:理学博士, 学位授与機関:東京工業大学, 報告番号:甲第2324号, 授与年月日:1991年3月26日, 学位の種別:課程博士, 審査員:
Citation(English)	Degree:Doctor of Science, Conferring organization: Tokyo Institute of Technology, Report number:甲第2324号, Conferred date:1991/3/26, Degree Type:Course doctor, Examiner:
学位種別(和文)	博士論文
Type(English)	Doctoral Thesis

Infrared Studies of Adsorption and Hydrogenations over ZrO_2

by Junko Kondo

Thesis submitted to the Tokyo Institute of Technology
for the Degree of Doctor of Science
1991

CONTENTS

Chapter 1

General Introduction

1-1 Vibrational Spectroscopies of Adsorbed Species

Infrared (IR) and Raman spectroscopies have been widely used in investigations of vibrational energy levels of a molecule to analyze the structure of it. Characterization of molecules adsorbed on surfaces are intensively performed by electron energy loss spectroscopy (EELS), which is one of the recently developed electron spectroscopies in addition to IR and Raman spectroscopies. To gain valuable spectra of adsorbed species mainly the following three points are important.

1) High sensitivity: Intermediates during surface reactions are usually unstable and their concentration is less than the other stable species. In dealing with single crystal surfaces the concentration of surface species is very low. Therefore, high sensitivity is required for the analysis of adsorbed species.

2) The existence of the gas phase: Adsorbed species are certainly located only at the gas-solid interface. The presence of a gas phase gives rise to weakly adsorbed species. These weakly adsorbed species are observed under equilibrium condition, in addition to stably adsorbed species. This atmospheric condition is very important for studying catalytic reactions.

3) Range of observable frequency region: The adsorbate-substrate stretching modes are observed at low frequency region (below 500 cm^{-1}). The possibility of observation at low frequency region leads to the study of the direct

interaction of adsorbed moleculs with a surface.

At present EELS is the most widely used technique for studies adsorption on single metal crystal surfaces due to its high sensitivity and the wide spectral region. Another advantage of this technique is its accessibility to the range of electronic transitions (1-50 eV), which provides valuable information on the molecular structure as well as the vibrational data. However, in addition to a low resolution, this technique is restricted to UHV pressures and flat surfaces. This is a serious limitation in the study of catalytic reactions, where it is necessary to carry out over studies at high pressure regime and supported powder catalysts.

This disadvantage can be overcome by IR spectroscopy and Raman spectroscopy. This latter is potentially a powerful technique with high resolution, wide spectral region and virtually no pressure restriction because it is performed in the wavelength region of visible light. The main hindrance for a wide use in adsorption studies, however, is its low sensitivity for nonenhanced Raman scattering.

In contrast, infrared spectroscopy has achieved high sensitivity at high resolution. At present, however, the spectral region is limited to 400-4000 cm^{-1}, a restriction which can be overcome by further technical improvements such as more intensive IR light sources (synchrotron radiation, lasers) or detectors of high sensitivity and wide spectral range (e.g. germanium bolometer). Regardless of further developments, this technique has already at

present state of art proven to be most valuable due to its ability to work at ambient pressure from UHV to high pressure and with a variety of surfaces from single crystal metals to supported catalysts. This enables one to study catalytic adsorption systems on well defined surfaces in UHV. Then these data can be related to those performed on supported catalysts.

1-2 IR Spectroscopy and Catalysis

IR spectroscopy has proven to be an enormously useful technique for obtaining information about the structure of the catalysts and species adsorbed on catalyst surfaces. The widespread application of the method is a consequence of the ease with which samples can be prepared and analyzed, and the absence of a need for complex workup of the spectral data prior to interpretation. A further attraction is that spectra can readily be taken at high temperatures and pressures, and under conditions at which catalysts are used in industrial practice.

The application of IR spectroscopy to the characterization of catalysts and adsorbed species was first carried out by Terenin and other Russian scientists in the late 1940s. These studies focused primarily on silicas and silica-aluminas. In the 1950s Eischens and co-workers pioneered the application of the technique to study supported metal catalysts. Since that time, the range of catalysis examined by IR spectroscopy has widened significantly, and important advances have been made in the techniques for acquiring spectra.

Before the era of Fourier spectrometry, it was difficult to obtain IR spectra of species adsorbed at the monolayer or partial monolayer at high signal-noise (SN) ratio. In the past decade, however, by means of good Fourier-transform infrared spectrometers (FT-IR), spectra of adsorbed species measured using a variety of different sampling techniques have been reported.

The most popular sampling technique is still a conventional absorption measurement in which a powdered adsorbent such as a metal oxide or transition metal supported on alumina or silica is pressed into a very thin wefer.

In spite of the improvement in sensitivity and technique, the effort to make the most of IR spectroscopy to obtain more detailed information about catalytic studies other than studies on single crystal surfaces does not seem to be very much compared with the total amount of catalytic researches. However, there is still a great possibility in catalytic studies by means of FT-IR which is available to give some information about reaction mechanisms with good quality, even without comparison with well defined surfaces. Although the proposed mechanisms by IR studies may not always reflect the practical reaction pathways, acquired information itself is expected to be closer to real catalysis than that obtained with use of spectroscopies which are utilized only under UHV condition.

Catalytical interest for IR studies was initially on supported metals mentioned. In some cases, it becomes difficult to distinguish the observed effect on adsorbed species of the metal itself and the used support. On the other hand, several metal oxides indicate high reactivity for reactions and those catalysts can be used for IR study without any second component. This is a great advantage

for metal oxides to be used as samples for IR studies. IR studies on metal oxide catalysts are much less than those on metal catalysts. A problem of the material is its ability for transmittance as an IR sample, and highly reactive catalysts do not always give good transmittance. Accordingly, it is not necessarily favorable to pursue studies of catalysts with high reactivity but under disadvantageous conditions. It would rather be preferable to accumulate as many information under facile conditions and to extend the acquired knowledge to generalization. In this point of view, IR studies on metal oxide catalysts play an important role to understand catalytic reactions.

1-3 Zirconium Oxide

ZrO_2 which was used in this series of adsorption and kinetics studies has shown its appropriateness for IR studies[1-3] as well as its catalytic property. It has been demonstrated that methanol and iso-butene were produced over ZrO_2 from synthesis gas with high selectivities depending on the reaction temperature. Although CuO-ZnO system is used as a practical catalyst for methanol synthesis[4], this catalyst is easily reduced under reaction condition, and its transmittance falls down. Compared to this, ZrO_2 allows good IR transmittance in a wide range between 4000 and 800 cm^{-1} under reaction condition even after a pretreatment of evacuation above 1000 K. In this point of view, adsorption studies and hydrogenation reactions over ZrO_2 were investigated by means of transmission FT-IR.

1-4 Outline of This Thesis

Chapter 2 gives detailed investigation about activation of hydrogen over ZrO_2. Adsorption studies of ethene and ethane are presented in chapters 3 and 4, respectively. On the basis of these knowledge in chapters 2, 3 and 4, a catalytic reaction of ethene hydrogenation over ZrO_2 is discussed. CO hydrogenation was also considered and described in chapter 6. In addition to those studies on ZrO_2, an adsorption study of methanol on MgO is presented in chapter 7. All the findings are summarizied in chapter 8.

1-5 References

1 H. Abe, K. Maruya, K. Domen and T. Onishi, Chem. Soc. Jpn., Chem. Lett., 1984, 1875.

2 T. Onishi, H. Abe, K. Maruya and K. Domen, J. Chem. Soc., Chem. Commun., 1985, 617.

3 T. Onishi, H. Abe, K. Maruya and K. Domen, J. Chem. Soc., Chem. Commun., 1986, 103.

4 W. Keim, "Catalysis in C1 Chemistry", D. Reidel Publishing Co., 1983.

Chapter 2

Infrared Studies of Hydrogen Adsorbed on ZrO_2

2-1 Summary

The adsorption of H_2 and D_2 at various temperatures and the isotope effect have been studied in detail over a ZrO_2 catalyst by means of FT-IR. Five different types of adsorbed hydrogen were observed as follows: (1) molecularly adsorbed hydrogen, $H_2(a)$, was observed below 173 K and was easily desorbed by evacuation; (2) homolytic dissociative adsorption which produces $Zr<^{H}_{H}$ species was observed below 373 K and was stable below 178 K; (3) heterolytic dissociative adsorption which forms OH and ZrH was observed in the temperature range 223-373 K and the isotope effect of adsorption between H_2 and D_2 was also found; (4) tentatively assigned ZrHZr species was found with a broad band at 1371 cm^{-1}; (5) the adsorption which generates two OH bands at 3778 and 3668 cm^{-1} takes place above room temperature. For the heterolytic dissociative adsorption of H_2 and D_2, both the kinetic and equilibrium isotope effect were observed. The magnitude of these isotope effect is in good agreement with the values calculated via IR data.

2-2 Introduction

Activation of hydrogen over solid surfaces is important not only for basic research but also in the chemical industry for processes such as hydrogenation reaction over catalysts. Associatively adsorbed hydrogen on supported Pt catalysts has been studied by IR spectroscopy[1]. Recently, activated hydrogen adsorption on clean metal surfaces has been reported by means of HREELS[2] and/or IR reflection absorption spectroscopy (IRAS)[3,4].

IR studies of hydrogen adsorbed on oxides such as ZnO[5], MgO[6], ThO_2[7] and ZrO_2[8] have been reported. Among these oxides, ZnO is the only case which has been examined in detail for the adsorption types of hydrogen and their characteristics[9-17]. On ZnO three types of hydrogen adsorption were reported, these are summarized as follows: type 1 adsorption which produces IR active species, ZnH and OH, takes place easily above 78 K and is reversible above 233 K; type 2 adsorption, which causes the change of conductivity of ZnO, proceeds slowly and irreversibly and produces IR inactive H^+ species above room temperature; type 3 adsorption observed below 78 K maintains the molecular form of H_2.

Recently, we have reported that hydrogen is adsorbed on ZrO_2 at room temperature and gives IR active bands at 3668 and 1562 cm^{-1} due to the OH and ZrH stretching modes, respectively[8]. In this chapter, detailed studies are described on relation to adsorption of hydrogen over ZrO_2

from 100 K to above room temperature, isotope effect of H_2 and D_2 adsorption and also values of the heat of adsorption and the activation energy for adsorption calculated via IR data. One of the objectives of the study in this chapter is to give a more generalized idea of hydrogen activation over oxides by comparison of ZrO_2 with ZnO.

2-3 Experimental

The ZrO_2 catalyst was prepared by precipitation from solution of zirconium oxynitrate with NH_4OH and by calcination of the hydroxide at 773 K for 3 h. About 50 mg of the catalyst was pressed into a self-supported IR disc of 20 mm in diameter. The disc was placed in the center of a quartz IR cell which is illustrated in fig. 2-1. The cell was connected to a Pyrex closed gas circulation system connected to a vacuum line which was described in fig. 2-2. The temperature control of the sample in the cell was carried out from 100 to 1073 K with the use of both liquid N_2 and an electronic heater. As shown in fig. 2-3 and 2-4, the apparent temperatures which were measured by a thermocouple outside are very different from those measured by a directly attached thermocouple to a disc inside the cell. The appearance of the difference between these two temperatures were observed differently in warming and cooling procedure when the cell was evacuated (fig. 2-4). For this fact, usually measured temperatures from outside the cell were always corrected to the real ones with use of fig. 2-3 and 2-4 in the presence of gas and in vacuum condition, respectively. Pretreatment of the sample was usually performed first by oxidation with O_2 at 773 K overnight followed by evacuation above 1003 K for 20 min on a closed gas circulation system. The pressure after evacuation was of the order of 10^{-3}-10^{-4} Torr. H_2 gas was refined by passing through Deoxo tube and liquid N_2 trap. IR spectra were recorded on a JEOL JIR-100 FT-IR

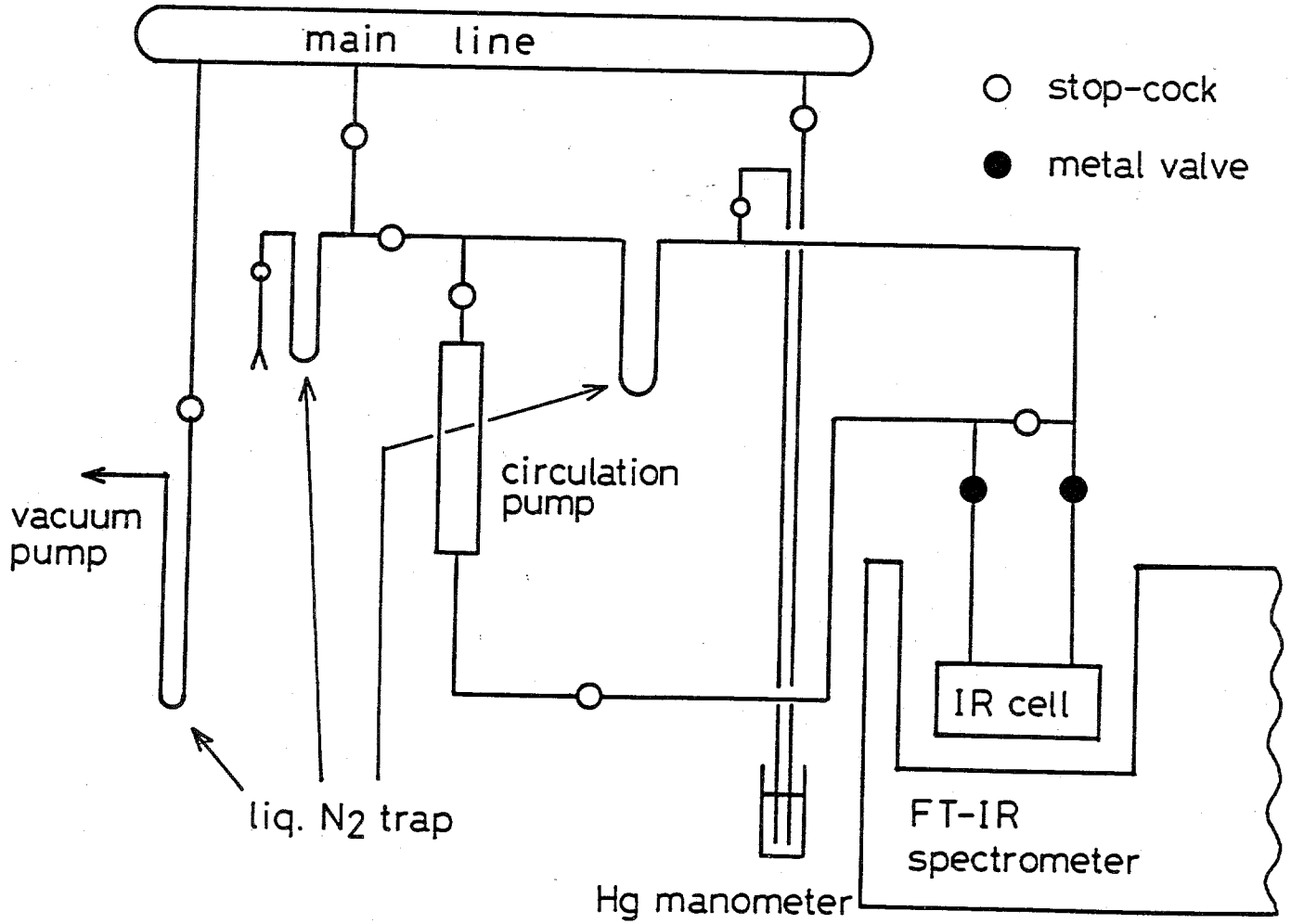

Fig. 2-1 The experimental system used in this study.

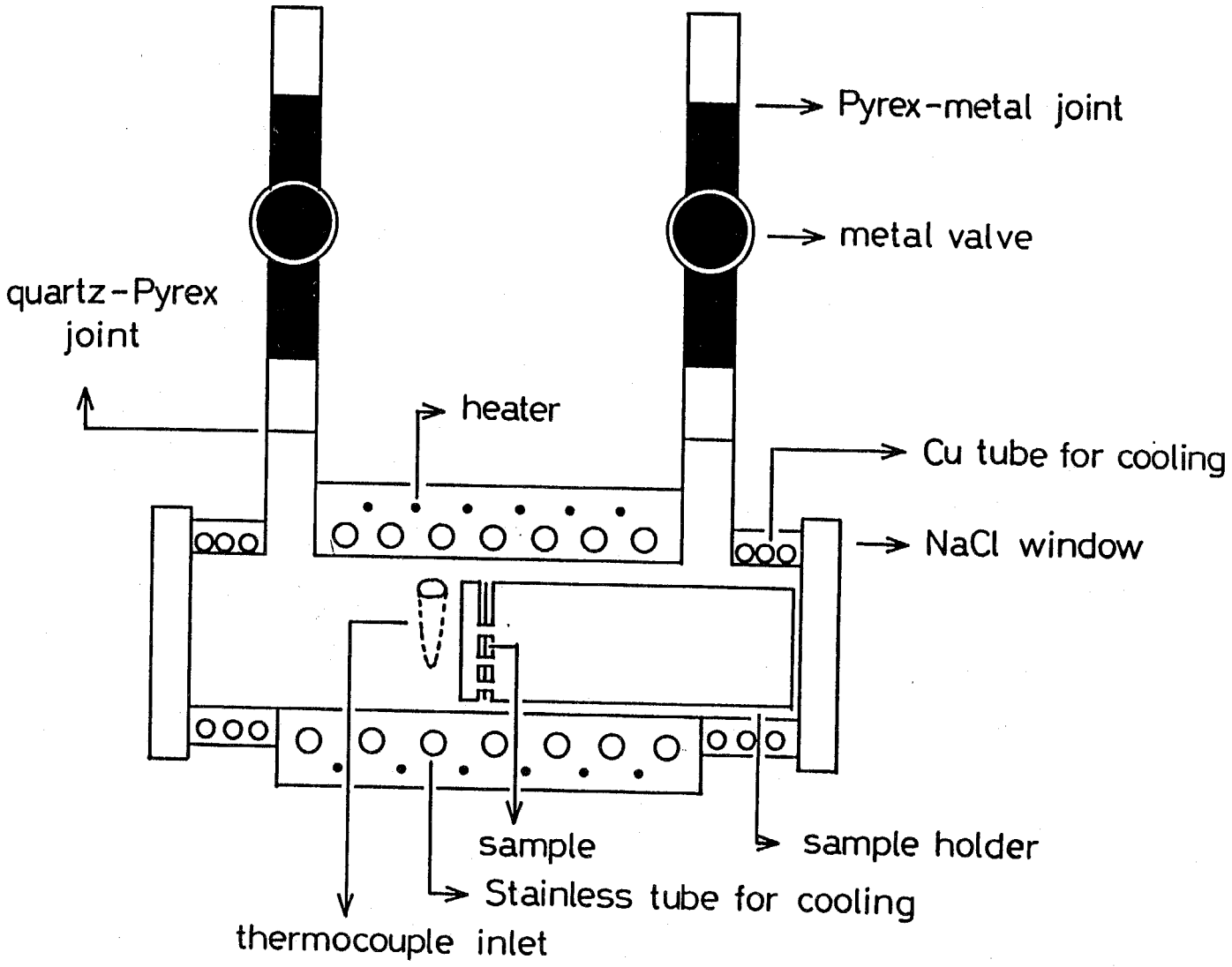

Fig. 2-2 The IR cell used in this study.

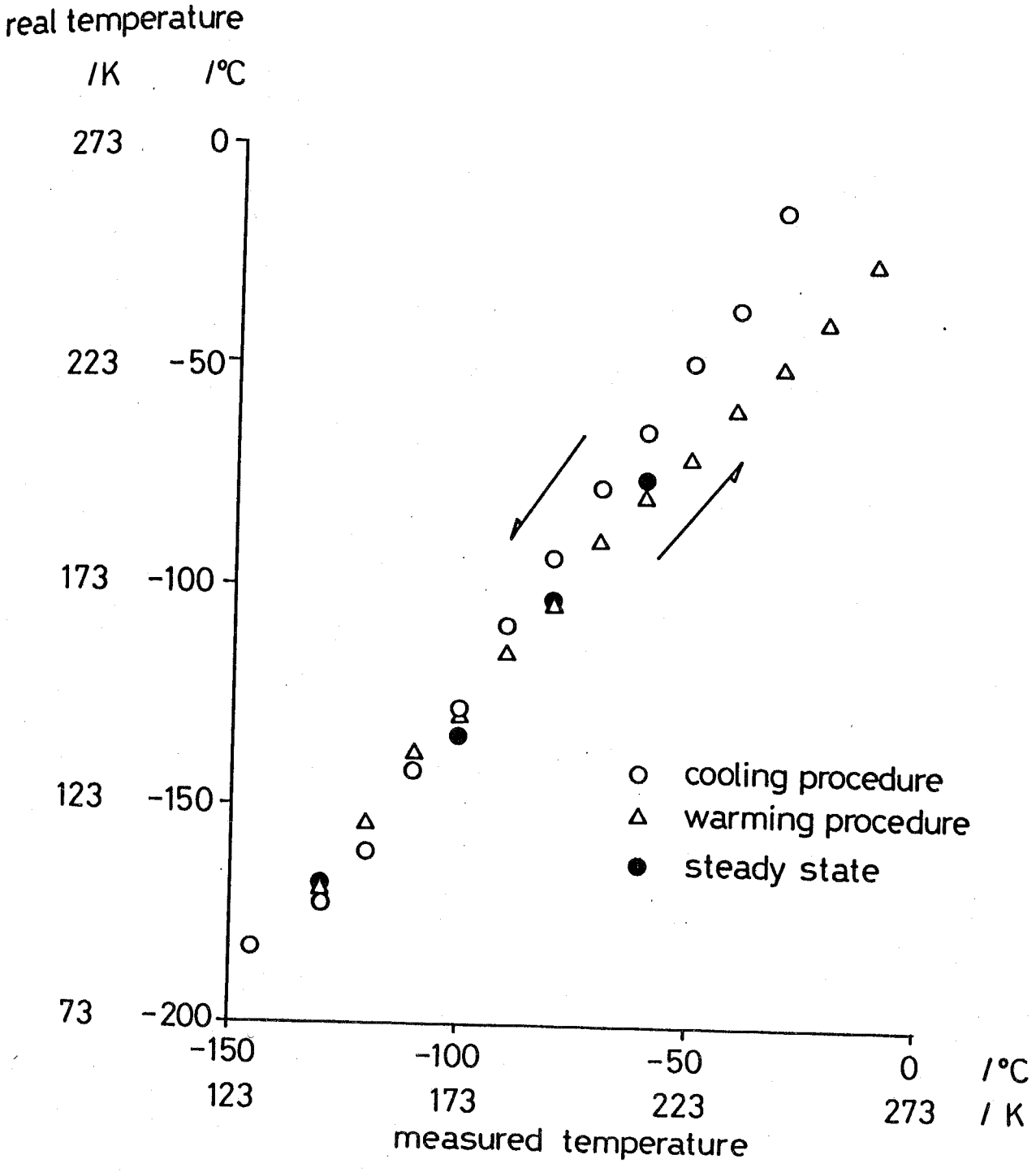

Fig. 2-3 The comparison of the measured and the real temperature when gas exists in a cell.

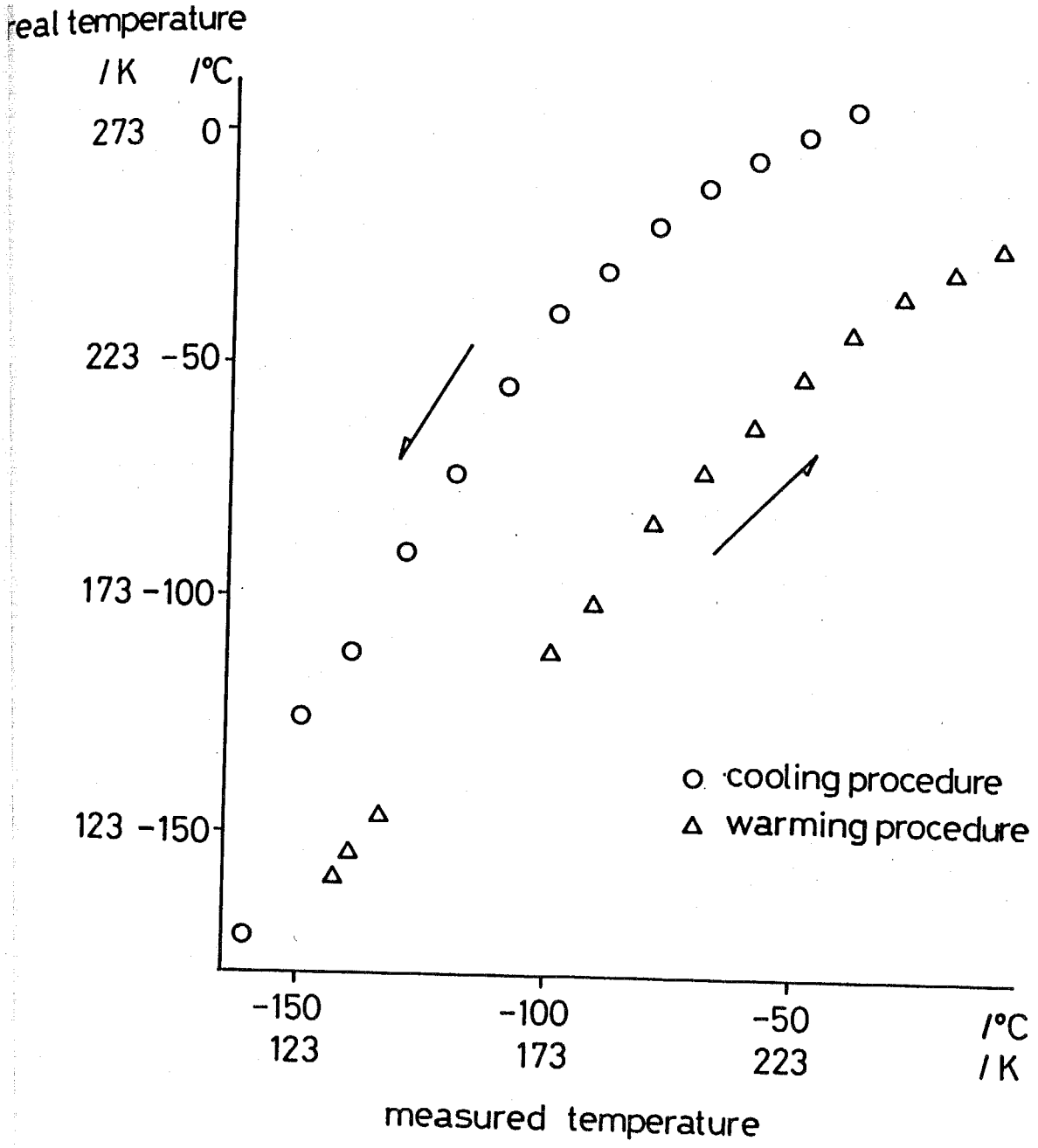

Fig. 2-4 The comparison of the measured and the real temperature under evacuation condition.

spectrometer with a liquid-nitrogen-cooled MCT detector and were taken with 256 scans at 4 cm^{-1} resolution. IR spectra of adsorbed species were obtained by calculating ratio spectra of ZrO_2 and that with surface species. These two spectra, the background (BG) and the sample should be measured at the same temperature in order to avoid the contorted baseline in the resulting ratio spectra. Examples of the distorted baselines are shown in fig. 2-5. The warp in a baseline of a ratio spectrum becomes more intensive especially at ca. 3000 cm^{-1} and below 1200 cm^{-1} when the difference in temperature is large.

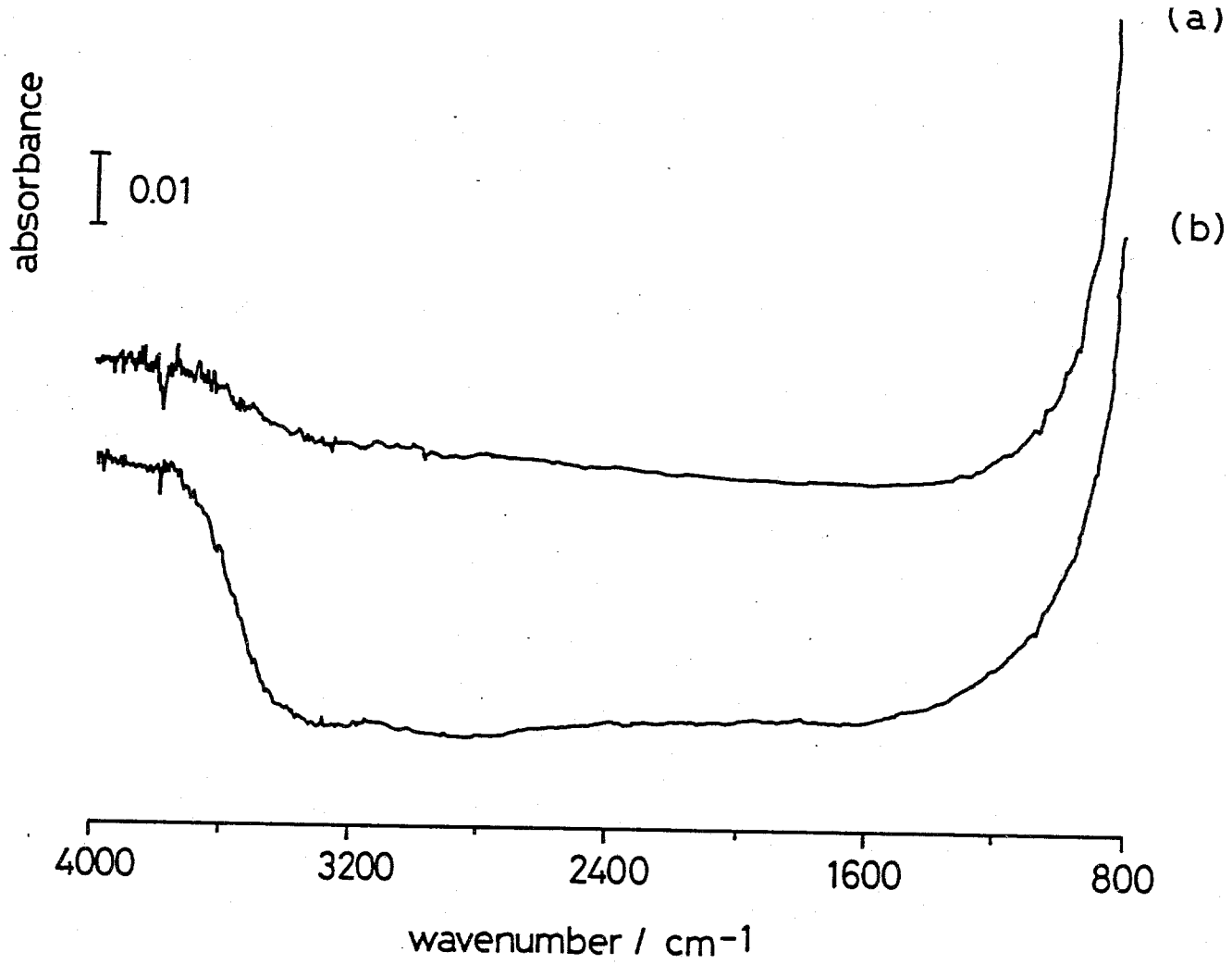

Fig. 2-5 Ratio spectra of ZrO_2 between two different temperatures, (a) 223 K / 203 K and (b) 223 K / 173 K.

2-4 Results and Discussions

2-4-1 The Effect of Pretreatment Temperature

After ZrO_2 was pretreated with O_2 at 773 K overnight the sample was evacuated at various temperatures from 773 to 1003 K (hereafter referred to as the catalyst ZrO_2-773 and ZrO_2-1003). Each of the evacuated ZrO_2 samples was cooled to room temperature under continual evacuation. About 400 Torr of H_2 was introduced to each evacuated sample of ZrO_2 at room temperature. IR spectra of adsorbed hydrogen species are shown in fig. 2-6. Some reverse peaks are due to the shift of bands which exist as background. In fig. 2-6, it is apparent that the spectrum of adsorbed species only appeared over ZrO_2 pretreated at 1003 K and these bands were assigned to adsorbed hydrogen species[8], which will be mentioned in detail below. The ratio spectrum between ZrO_2-1003 and ZrO_2-773 before introduction of H_2 is shown in fig. 2-6(d). Two bands assigned to OH species on the surface indicate that there are larger amounts of OH species on ZrO_2-773 than on ZrO_2-1003. In other words, the surface OH species over ZrO_2-1003 is removed by evacuation at high temperature. It is also found by D_2 treatment that the OH species still remains over ZrO_2-1003 to form OD. Therefore, hydrogen is activated and is adsorbed on the ZrO_2 surface after surface OH is removed to some extent. In this thesis the following studies from chapter 3 to chapter 6 have been carried out over ZrO_2-1003.

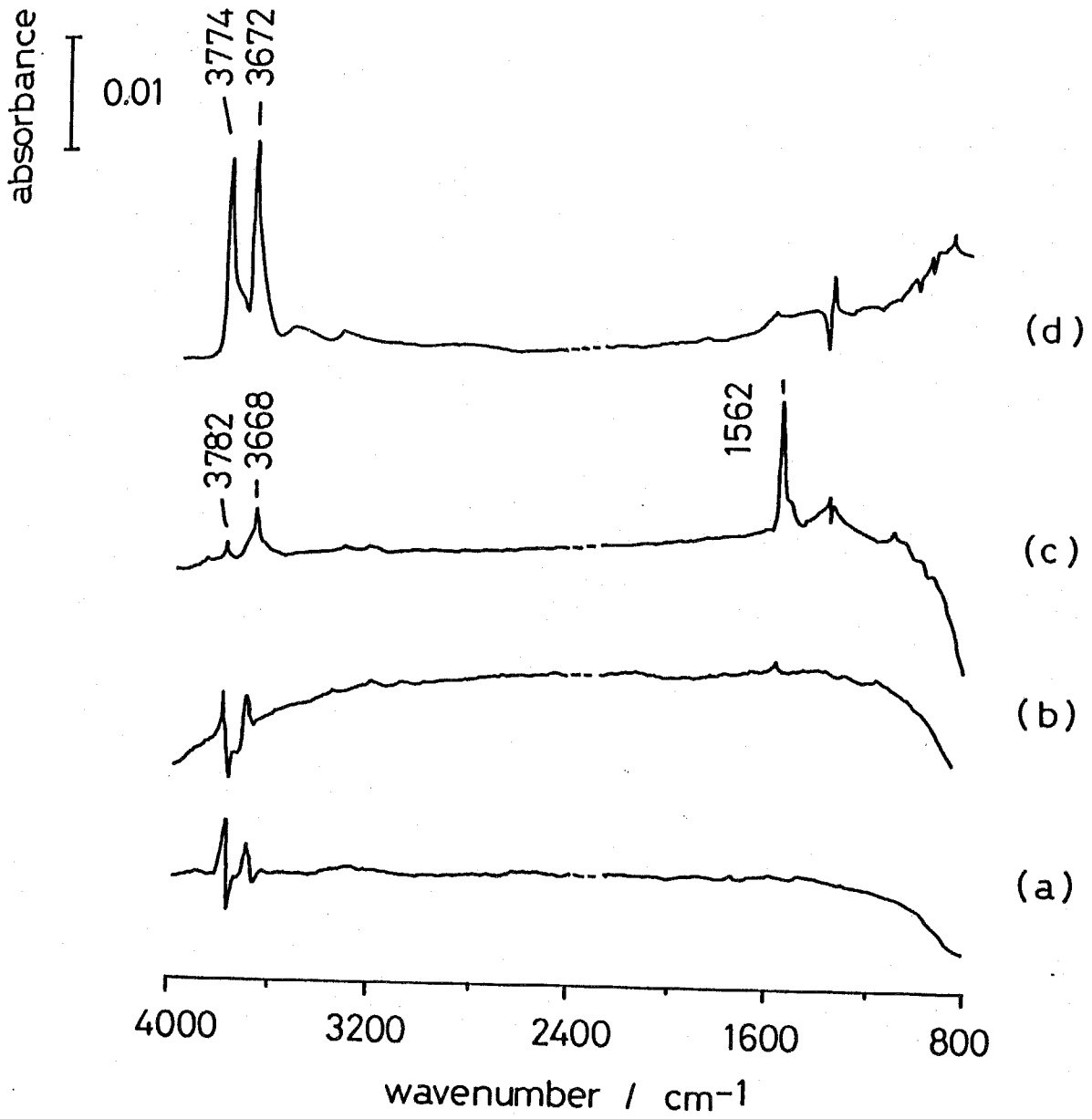

g. 2-6 IR spectra of H_2 adsorption at room temperature after evacuation pretreatment at each of the following temperatures: (a) 773, (b) 923 and (c) 1003 K.
(d) Ratio spectrum (a)/(c) of backgrounds for (a) and (c).

2-4-2 Heterolytic Dissociative Adsorption

When H_2 was exposed to ZrO_2 at room temperature several bands due to the O-H and Zr-H stretching vibrations were observed (fig. 2-6)[8]. When ambient H_2 gas was evacuated at room temperature, the intensities of the band at 3668 (OH) and 1562 cm^{-1} (ZrH) decreased rapidly in the same way. After degassing of H_2 for 1 h at room temperature, H_2 was reintroduced. It was found that the initial amount of the species was completely restored by reintroduction and the intensities of the bands decreased again by re-evacuation. The same results were obtained in case of D_2 adsorption, as shown in fig. 2-7. Fig. 2-7(a) shows the ratio of the spectrum taken after evacuation for 1 h to that before evacuation, where the bands at 2706 (OD) and 1124 cm^{-1} (ZrD) due to decreased species appear below the baseline. Fig. 2-7(b) is also a ratio spectrum which presents the change of the ZrO_2 surface caused by reintroduction of D_2. Restored species appear above the baseline. In fig. 2-8(A) the main bands due to D_2 adsorbed at room temperature are shown and in fig. 2-8(B) the change of the integrated absorbance of the bands at 2760 and 2706 cm^{-1} (OD), and 1124 cm^{-1} (ZrD) against the evacuation times are shown. Two species, which give the bands at 1124 (ZrD) and at 2706 cm^{-1} (OD), were removed rapidly by evacuation of D_2 gas, while the OD band at 2760 cm^{-1} remained unchanged. These results led to the conclusion that the band at 2706 (3668) cm^{-1} due to OD (OH) and at 1224 (1562) cm^{-1}

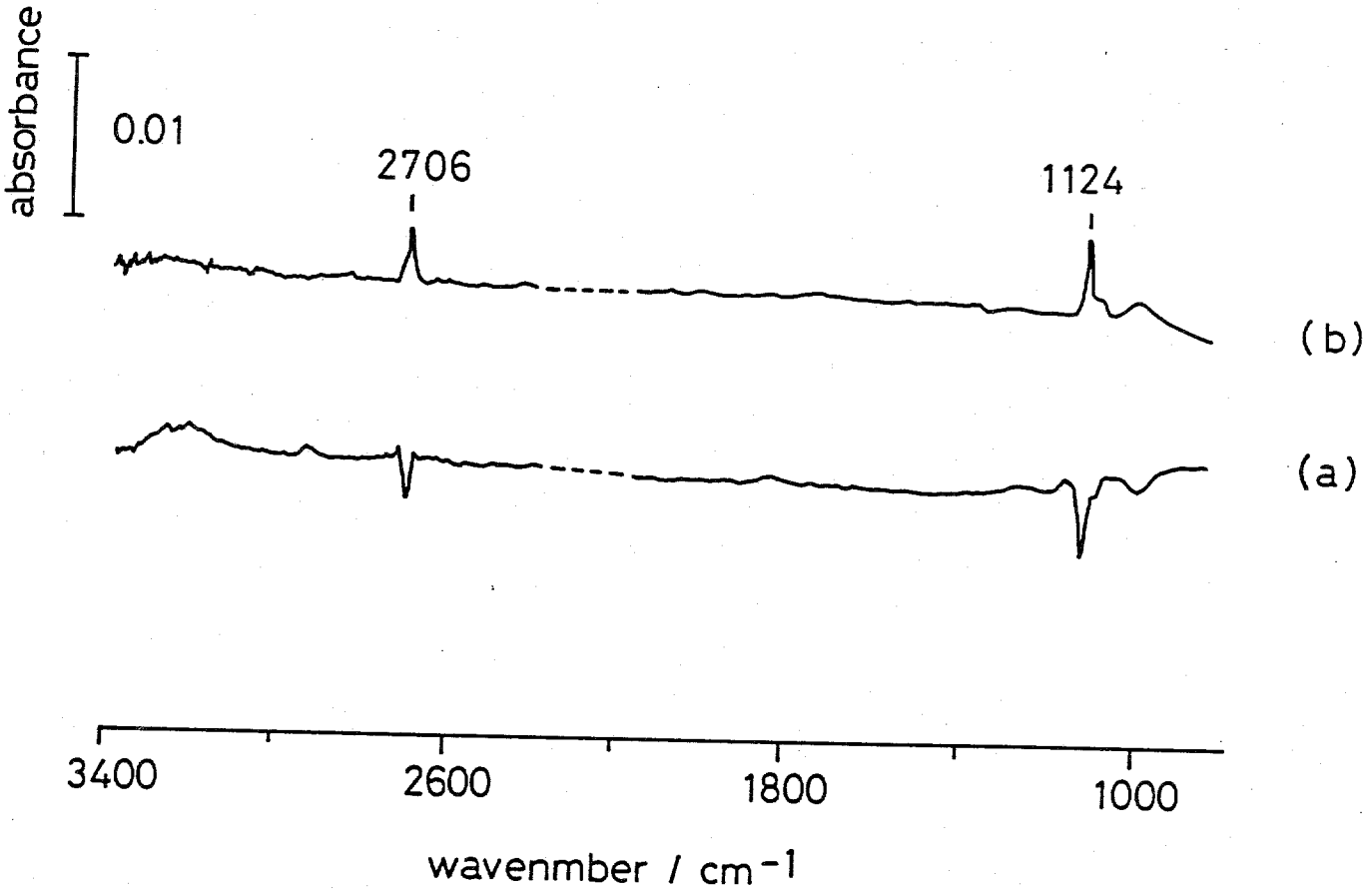

Fig. 2-7 Ratio spectra of D_2 adsorption on ZrO_2 at room temperature and evacuation effect:
(a) after evacuation for 1 h / D_2 adsorption;
(b) reintroduction of D_2 / after evacuation for 1 h.

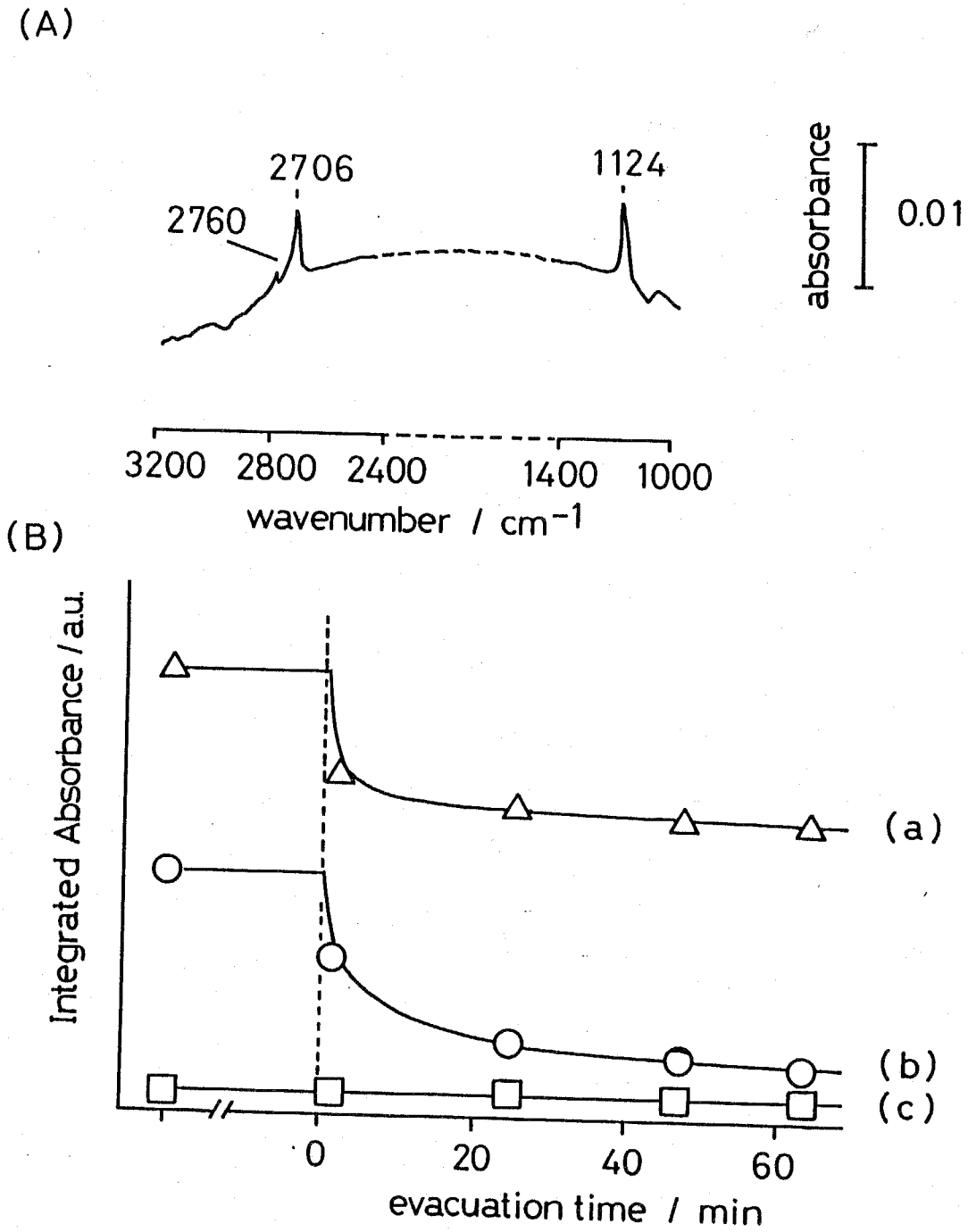

g. 2-8 A; IR spectrum of adsorbed species of D_2 at room temperature. B; Relative amount of each species produced by D_2 adsorption at room temperature, effect of evacuation. (a) OD at 2706 cm^{-1}, (b) ZrD at 1124 cm^{-1} and (c) OD at 2760 cm^{-1}.

due to ZrD (ZrH) are paired. However, some part of the band at 2706 (3668) cm^{-1} due to OD (OH) species still remained at the same position on the surface after complete evacuation of ZrD (ZrH) species. In other words, there exists a different type of OD (OH) species at the same wavenumber. The heterolytic dissociative adsorption of H_2, which produces OH and ZrH species, may occur on the activated Zr-O pair site of ZrO_2, corresponding to type 1 hydrogen adsorption on ZnO.

Gas phase induced ZrH bandshifting

The exchange reaction of H_2 and D_2 over ZnO was examined in early works. It is concluded that the exchange reaction of the species derived from heterolytic dissociative adsorption (type 1) proceed via direct reaction with molecules in gas phase, the so-called Eley-Rideal mechanism. Same type of exchange reaction was studied for heterolytic dissociative adsorption of H_2 on ZrO_2, which gave an unexpected result. ZrH-OH species were produced on the ZrO_2 surface and then, ambient H_2 gas was evacuated below 227 K. Under this condition these species existed stably. No exchange reaction was observed when D_2 was admitted, but an interesting behavior of the ZrH bandshape occurred.

When D_2 was added to ZrH preadsorbed surface at 153 K the peak position and the bandshape immediately changed [fig. 2-9(b)]. This transformation of the peak was kept upto 173 K in warming process under evacuation

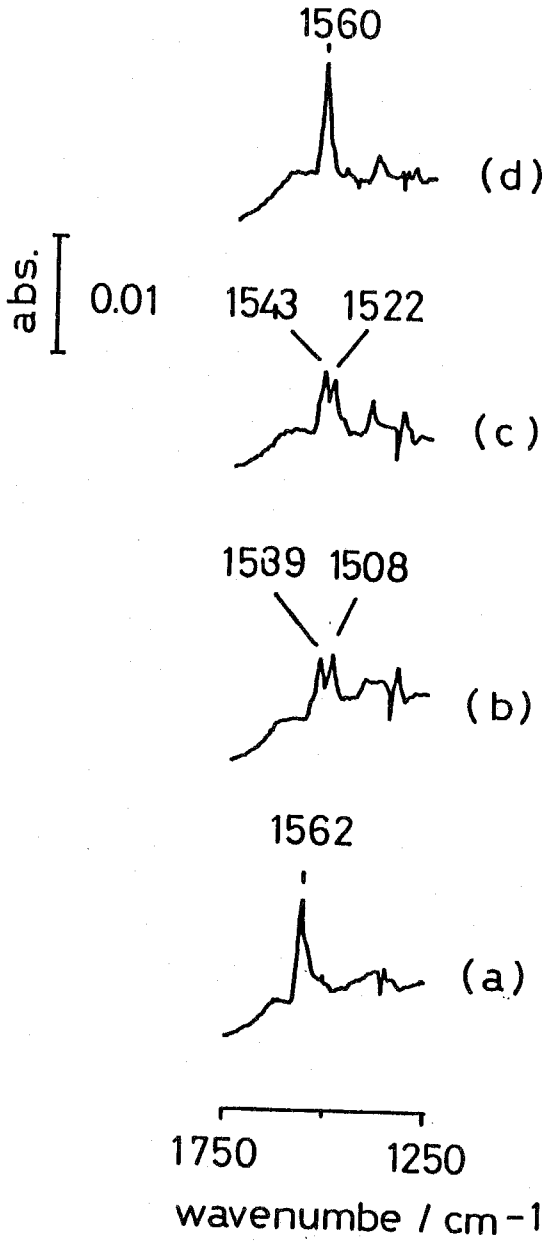

Fig. 2-9 Effect of D_2 in gas phase on ZrH band at low temperature: (a) ZrH band under evacuation at 153 K; (b) after addition of D_2 at 153 K; (c) at 173 K and (d) at 193 K. (b), (c) and (d) were taken in warming procedure at the same experiment.

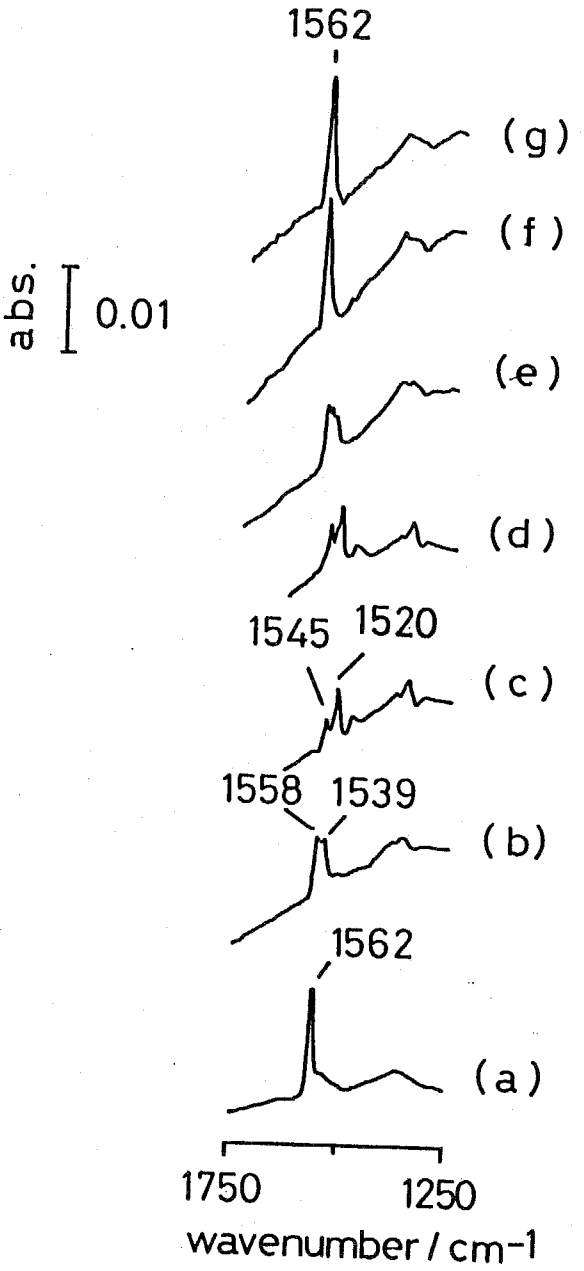

• 2-10 Effect of H_2 in gas phase on ZrH band at low temperature: (a) under H_2 existence at 268 K, (b) at 173 K, (c) at 113 K; (d) evacuated at 113 K, (e) at 153 K, (f) at 188 K and (g) at 153 K. H_2 gas exists in (a)-(c) and (d)-(g) were taken under evacuated condition.

[fig. 2-9(c)]. Above the temperature the bandshape recovered to its original shape [fig. 2-9(d)]. In fig. 2-10, the effect of H_2 in gas phase on ZrH species is shown. The system was cooled down to 113 K after production of ZrH species at room temperature. Meanwhile continuous change of the ZrH band was observed [(a)-(c)]. The distorted shape of the ZrH band was retained after evacuation of H_2 at 213 K as in case of D_2. The recovery process during warming procedure under vacuum condition was continuously observed [(d)-(f)]. It should be noted that as shown in fig. 2-10(g) peak shifting and splitting of ZrH absorption band does not occur without presence of H_2 or D_2 in gas phase even at low temperature. To infer whether this phenomena is ascribable to: 1) physical collision effect of any molecule in gas phase; or 2) chemical electronic effect of dipole coupled with the same molecule in gas phase (i.e. H_2 or D_2), the effect of He was examined. The exactly the same results were observed by He introduction, which suggests that the observed phenomena was attributed to the physical collision effect. The transformation is irreversible below 183 K.

2-4-3 The Effect of Catalyst Treatment by O_2, H_2O and H_2 on Heterolytic Dissociative Adsorption.

To obtain information on the site for heterolytic dissociative adsorption, the effect of several pretreatments was studied. First, O_2 was introduced over ZrO_2-1003 at 773 K and cooled to room temperature. Then H_2

was introduced to the O_2-treated surface after O_2 evacuation at room temperature heterolytic dissociative adsorption of H_2 was observed.

In other words, O_2 has no effect on the activated pair site. It is mentioned above that the activated site cannot be produced until the surface OH is removed to some extent. To form surface OH species, H_2O (1 Torr) was introduced at room temperature to the sample ZrO_2-1003. The sample then was evacuated followed by heating to 523 K. Due to this treatment the active sites were completely blocked and the formation of ZrH and OH were not observed after introduction of H_2 at room temperature. However, the H_2O-treated surface was reactivated by evacuation at 1003 K. It is known, as will be discussed in detail in the following section, that H_2 adsorption above room temperature produces only two kinds of OH species, which are not removed by evacuation at 773 K[8]. To examine the differences between OH species produced by H_2O and those by H_2 on hydrogen adsorption, the following experiment was performed. After OH species were produced by H_2 at adsorption 353 K, H_2 was introduced again at room temperature. Heterolytic dissociative adsorption occurred on the surface with OH produced from H_2 treatment. Thus it is inferred that, as far as H_2 adsorption is concerned, the surface OH produced from H_2O has quite a different nature from that produced from H_2, although their bands appear at the same wavenumbers. Moreover, residual OH species after evacuation below 920 K are regarded to be

the same as those OH derived from H_2O. These species are considered to poison the heterolytic dissociative adsorption sites.

2-4-4 Dissociative Adsorption at High Temperature

Two OH species with bands at 3772 and 3668 cm^{-1} are formed slowly from H_2 at room temperature while the band at 1562 cm^{-1} due to the ZrH is formed rapidly. When hydrogen was passed over ZrO_2 at higher temperatures, the OH bands at 3780 and 3668 cm^{-1} increased in intensity while ZrH band was reduced, and at 525 K the latter band disappeared as shown in fig. 2-11. The bands at 3780 and 3668 cm^{-1} due to OH groups on the ZrO_2 have been studied in detail by Yamaguchi et al.[18] and these bands were assigned to the terminal and bridged OH species, respectively.

The mechanism of dissociative adsorption above room temperature seems to be as follows: (1) homolytic dissociative adsorption to produce two OH species, (2) heterolytic dissociative adsorption to form the OH and IR inactive ZrH species. In mechanism (1), an electron is transferred

$$2O^{2-} + H_2 \longrightarrow 2OH^- + 2e^-.$$

Reduction of the catalyst proceeds by production of OH^- species. When H_2 was introduced over ZnO, slow adsorption which forms IR inactive species was observed accompanied by reduction of the catalyst[10]. This means that conduction electrons are produced,

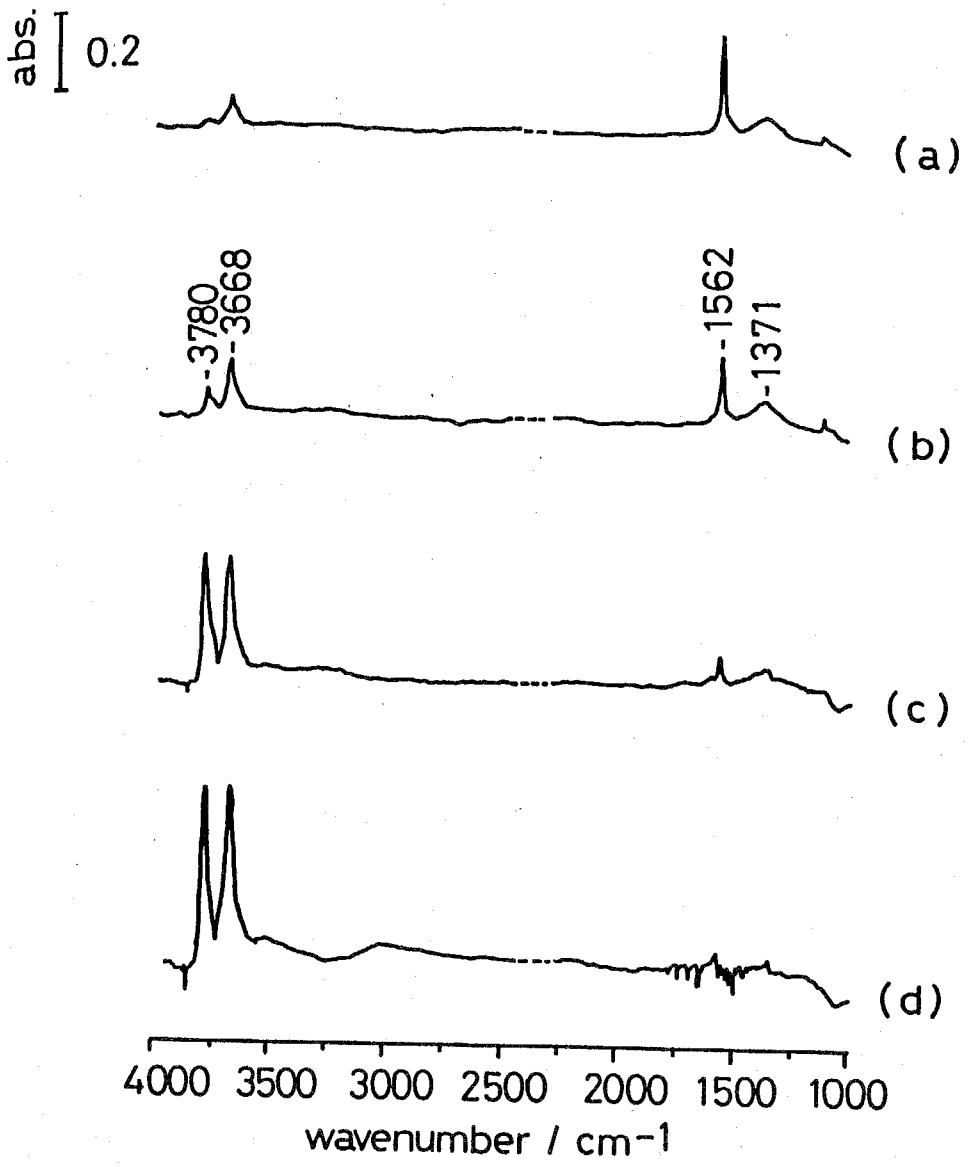

g. 2-11 IR spectra of H_2 adsorption at higher temperature. (a) At room temperature; (b) at 373 K; (c) at 473 K; (d) at 523 K.

H_2 ---> $2H^+ + 2e^-$ (conduction band).

Whereas, in the case of ZrO_2, the reduction of the catalyst was not observed in the IR spectra and the electrons produced do not become conduction electrons. Therefore if mechanism (1) is assumed, the electrons produced are supposed to be localized in such place as on Zr^{3+} and/or on a defect of oxygen of the surface. By mechanism (2), hydride-type species are produced, which are not considered to be stable above 373 K at which temperature more stable OH species are produced rapidly. Hence, it would be reasonable to regard the adsorption mechanism as the formation of OH and IR inactive H^+-type species rather than that of H^--type species. In this case two electrons are produced. For the whereabout of the produced electrons, the same discussion is made as in the case of mechanism (1).

2-4-5 Bridged ZrHZr Species

Hydrogen (or Deuterium) adsorbed on various oxides is summarized in table 2-1. In this table all the observed hydrogen species on ZrO_2 in the temperature range of 173-523 K are assigned to several species. Among these species, the band at 1371 cm^{-1} in fig. 2-11 is tentatively assigned to the bridged hydrogen. The similar hydrogen band observed at 1475 cm^{-1} on ZnO[14] was also assigned to ZnHZn (type 2).

The assignment on ZnO is in agreement with the literature of homogeneous complex containing hydrogen in

Table 2-1 Infrared bands due to hydrogen (or deuterium) adsorbed on various oxides / cm^{-1}

assignments	ZrO_2	ZnO	ThO_2	MgO
OH str.	3780 (2760)	3498 (2585)	3660 (2700)	3750
OH str.	3668 (2706)	3400 (2500)	3640 (2685)	
^{a}M-H str.	1562 (1124)	1708 (1233)		
MHM str.	1371 (995)	1475 (1075)	1115 (800)	1326
-----	1116 (--)	850	860	1130
-----		817		

^{a}M = metal atom

bridged site[19,20]. According to the literature, on ZnO, two types of heterolytic adsorption were found; 1) adsorption which produced ZnH and OH; 2) adsorption which resulted in ZnHZn and hydrogen bonded OH--O species. It was mentioned that the adsorption center for type two adsorption is consequently more complex with respect to that involved in type 1 chemisorption. The bridged nature of type 2 hydrogen adsorption, implying extended interaction of the hydrogen atoms with more than one oxygen and zinc ion, seemed to support the hypothesis[21] that this type of hydrogen is located in substrate cavities.

On the other hand, the observed peak position at 1371 cm^{-1} on ZrO_2 seems to be close enough to give an assignment of this species to ZrHZr. The corresponding OH--O species, however, were not observed in IR spectra. Also the band at 1371 cm^{-1} was disappeared by evacuation at room temperature, which is different from ZnHZn species. Therefore, those species were tentatively assigned to ZrHZr species.

2-4-6 Homolytic Dissociative Adsorption

IR spectra resulted from H_2 adsorption at low temperature are shown in fig. 2-12. These spectra were taken by procedures as follows ; H_2 was admitted at 140 K and warmed gradually. Below 223 K a broad band at about 1540 cm^{-1} is observed. This band shifts to 1100 cm^{-1} (at 263 K) when D_2 was used, so the band at 1540 cm^{-1} is

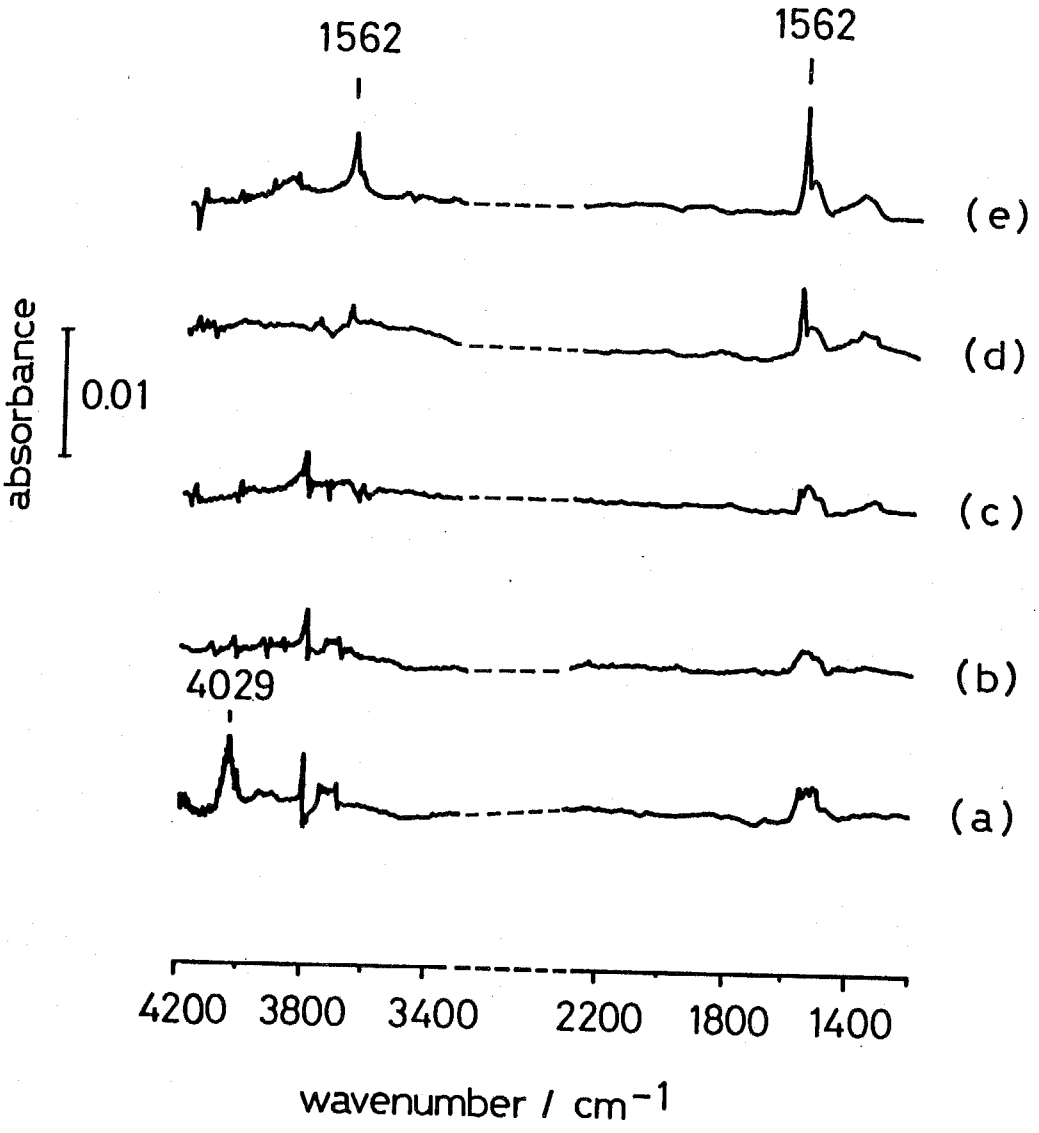

Fig. 2-12 IR spectra of H_2 adsorption at low temperatures, (a) at 173 K, (b) at 203 K, (c) at 223 K, (d) at 243 K and (e) at 273 K.

Table 2-2 Observed IR bands due to hydrogen species / cm^{-1}

	band	separation	band on ZrO2	separation	assignment
$^{a}L_2Zr(OCH3)(H)$	1580		1562		Zr-H str.
		25		22	
$L_2Zr(H)_2$	1555		1540		$Zr(H)_2$ str.

$^{a}L = \eta^{5}\text{-}C_5Me_5$

certainly derived from adsorbed H_2. In a Zr coordinated complex species[22] besides a sharp band of ZrH at 1680 cm^{-1} appears at 1580 cm^{-1}, a broad band at 1555 cm^{-1} was attributed to $Zr<^{H}_{H}$ species. On the ZrO_2 surface, a sharp band due to dissociatively adsorbed ZrH was observed at 1562 cm^{-1} as discussed in the former paragraph, and a broad band exists at 1540 cm^{-1}. The band at 1540 cm^{-1} due to adsorbed hydrogen can be assigned to the $Zr<^{H}_{H}$ species on the basis of reference zirconium complex, as shown in table 2-2. This species has not been observed on other oxides including ZnO. The broad band of the $Zr<^{H}_{H}$ species was hard to detected above room temperature because it appears at a shoulder of conspicuous band of ZrH. Homolytic dissociative adsorption occurs below room temperature and rapidly even at 100 K. The species is removed by evacuation above 173 K. Therefore, the $Zr<^{H}_{H}$ species can be separated from the ZrH species by introducing H_2 below 223 K followed by evacuation below 100 K. On the other hand, the ZrH species can be separated from the $Zr<^{H}_{H}$ species by introducing H_2 above 223 K followed by evacuation between 173 and 223 K.

Isotherms of homolytic dissociative adsorption at 183 K are shown in fig. 2-13, which was obtained with reducing the pressure. The amount of $Zr<^{H}_{H}$ is expressed by integrated absorbance. It is apparent that the site is saturated at ca. 2 Torr of H_2 gas. From all these facts, both activation energy for adsorption and heat of

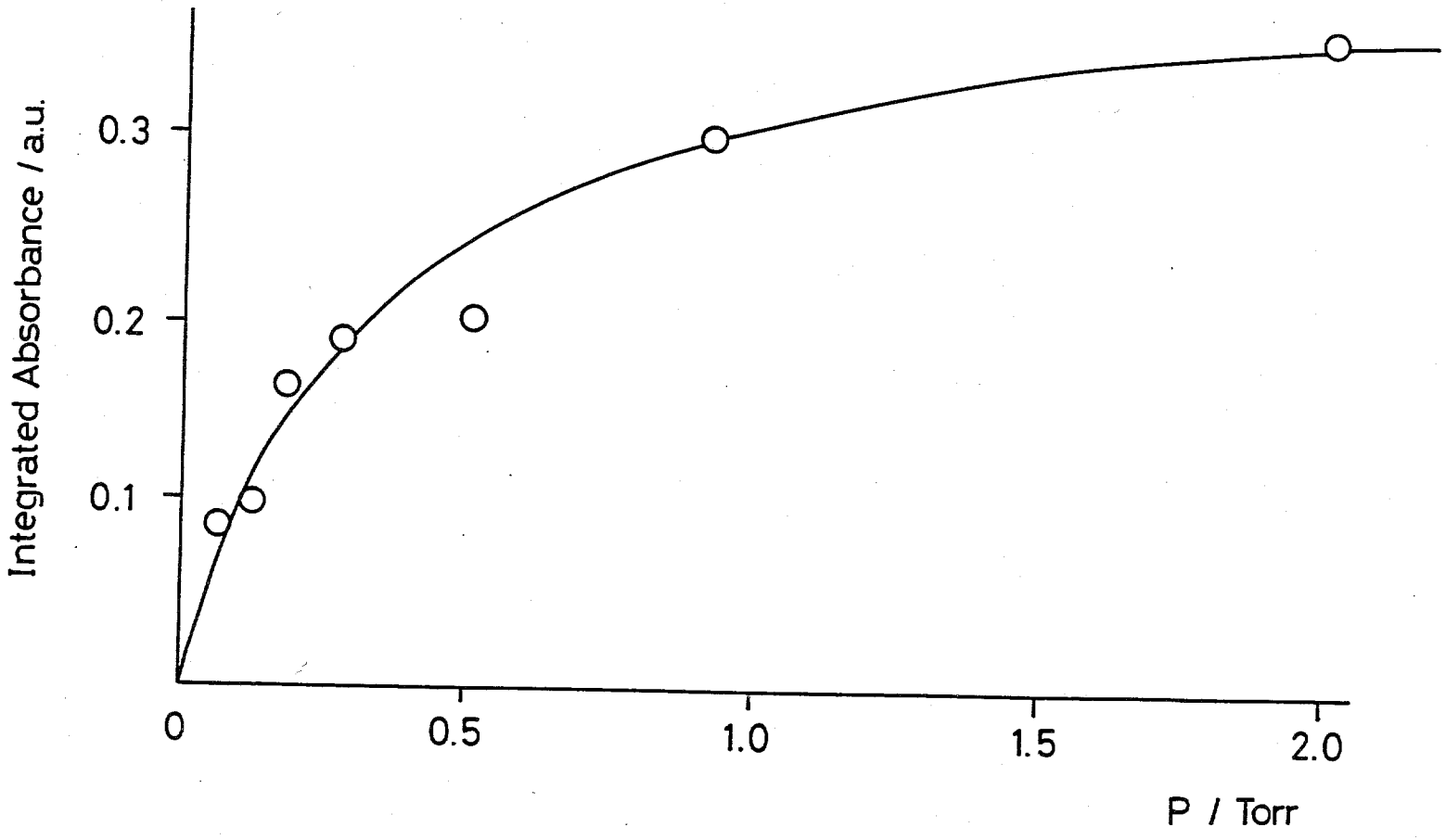

Fig. 2-13 Isotherm of homolytic dissociative adsorption at 183 K.

adsorption for this homolytic dissociative adsorption are expected to be small compared to that of the heterolytic dissociative adsorption, which will be shown later.

2-4-7 Associative Adsorption

In fig. 2-12, a band at 4029 cm^{-1} was observed only when the sample was cooled below 173 K. This species is removed by evacuation even at 173 K. On ZnO, a similar band was observed at 4019 cm^{-1}[11]. The band at 4019 cm^{-1} shifted to 2887 cm^{-1} by D_2 and is assigned to the H-H (D-D) stretching vibration of molecular adsorbed H_2 (D_2). The species at 4029 cm^{-1} on ZrO_2 is also assigned to the molecularly adsorbed H_2. However, no D_2 band was detected under our experimental condition. The reason of missing the band of D_2(a) might be the result of an isotope effect which is stronger on ZrO_2 than on ZnO.

In relation to the isotope effect and the structure of the associative adsorption, HD adsorption below 193 K is noticeable. IR spectra of adsorbed HD below 193 K are shown in fig. 2-14. The main band appears at 3516 cm^{-1} with a shoulder at 3483 (3485) cm^{-1} at lower temperatures. This shoulder appeared below ca. 163 K during a cooling procedure and reversibly disappeared above the same temperature during warming procedure. To compare this with the result of the corresponding H_2 species which appears at 4029 cm^{-1} (fig. 2-12), it is noticed that the shoulder is a characteristic of the HD species and not observed for the H_2 species. Also the absorption intensity is much

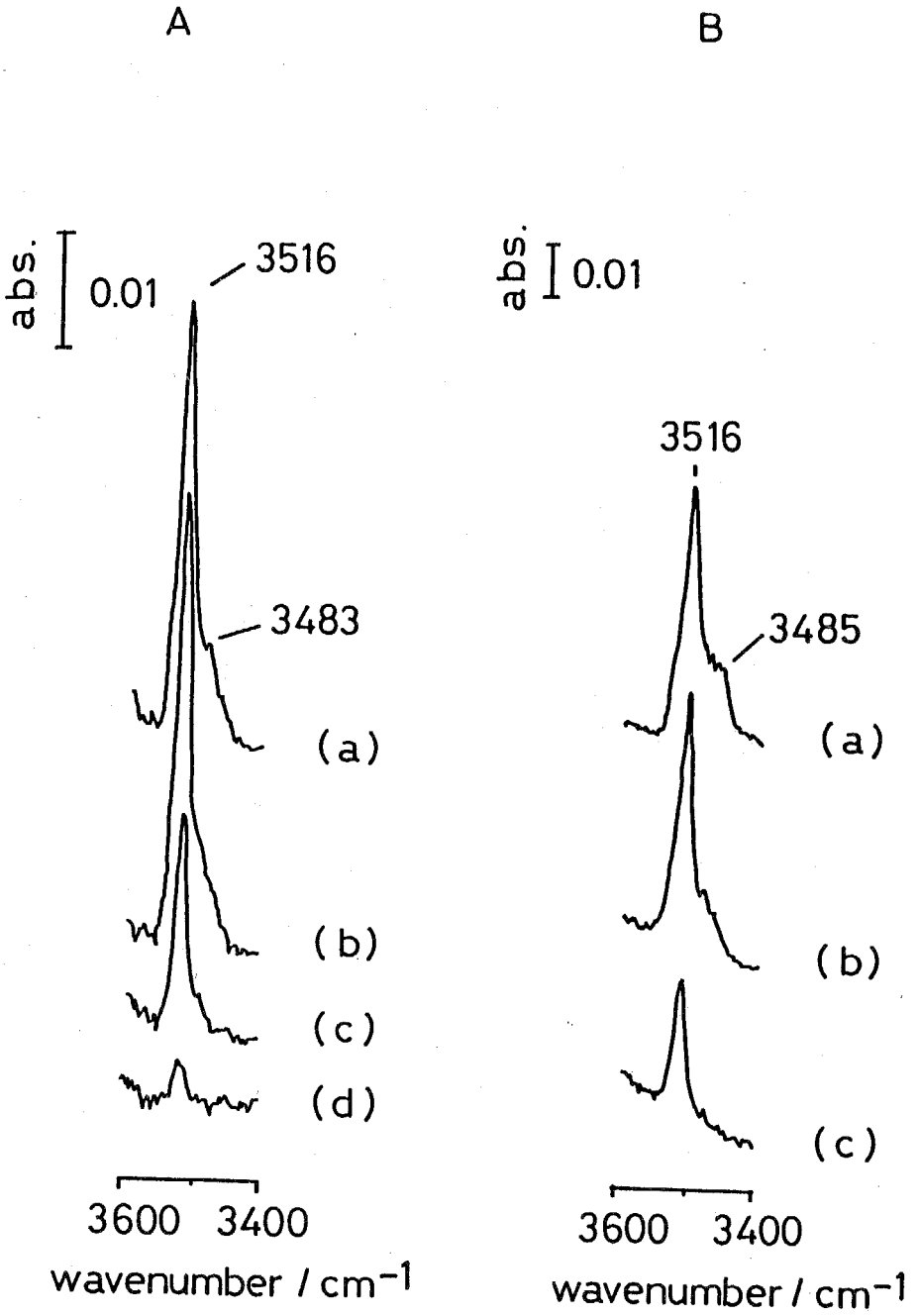

g. 2-14 IR spectra of associative adsorption of HD.
Spectra in A were taken at the HD pressure of 15 Torr, (a) at 143 K, (b) 158 K, (c) 173 K and (d) 193 K.
Spectra in B were taken at the HD pressure of 20 Torr, (a) at 123 K, (b) at 153 K and (c) at 173 K.

On the other hand, in the case of O-H and O-D stretching modes, it is

$$O\text{-}H < O\text{-}D \ .$$

Therefore, there seems to be no general and simple rule for molar absorption coefficient of isotopes, even for free molecules. At present, it looks to be too complicated to interpret precisely the results obtained here including three isotopes (H_2, HD and D_2). Further systematic study will be necessary to understand this somewhat strange phenomenon.

From the result that the H-H (D-D) stretching vibration on oxides shifts to wavenumbers much lower than that in the gas phase (4140 cm^{-1}), it is expected that the H-H bond is weakened over the oxide catalysts. The pressure dependence of the amount of the associated adsorption is described in fig. 2-15. It kept constant above 150 Torr, which indicates that there are specific "sites" for this adsorption. The associated adsorption, therefore, is well distinguished from physisorption.

2-4-8 Isotope Effect of H_2 and D_2 for heterolytic Dissociated Adsorption

In fig. 2-12 heterolytic dissociated adsorption was observed below 223 K on ZrO_2, whereas the same type of adsorption occurs rapidly on ZnO even at 73 K. It is expected that there will be a higher activation energy for adsorption on ZrO_2 than on ZnO[14]. The relative amounts

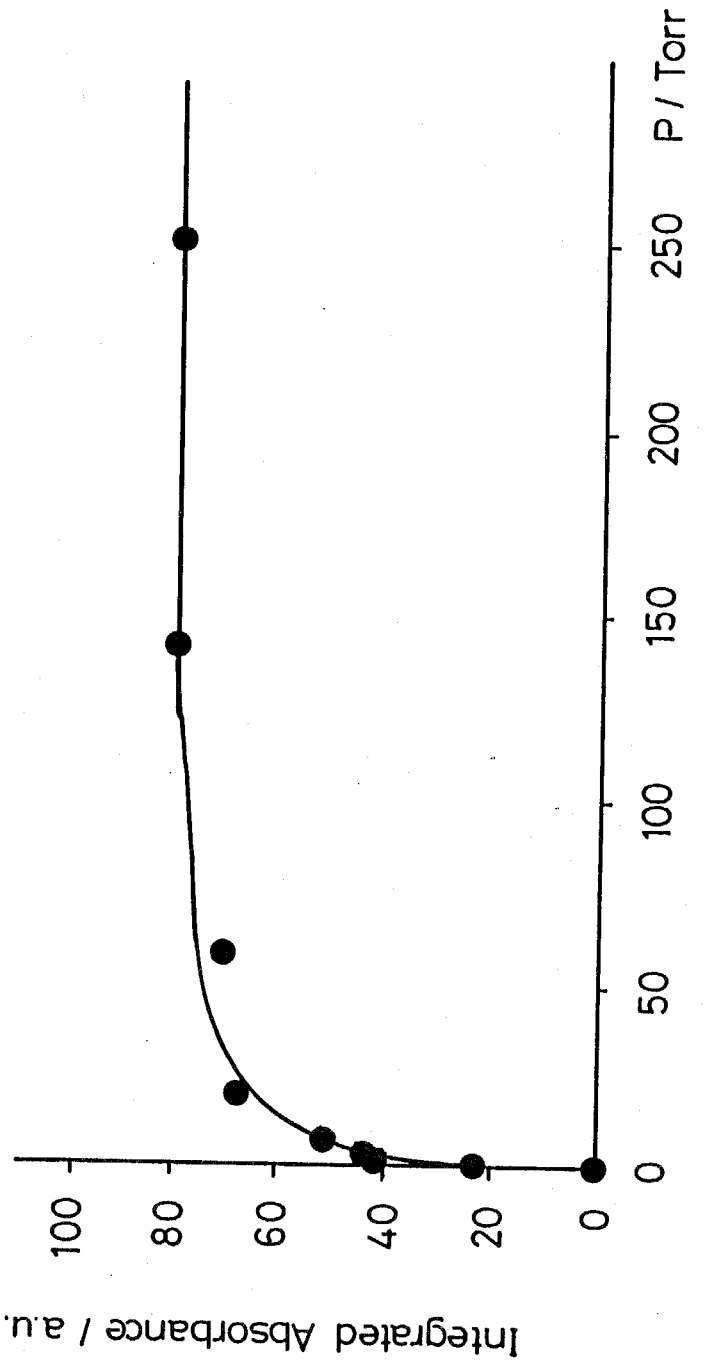

Fig. 2-15 Isotherm of associative adsorption of H_2 at 143 K.

of adsorbed species were estimated for both H_2 and D_2 by the integrated absorbance of the ZrH and ZrD bands, respectively. In fig. 2-16, these were plotted versus adsorption temperature. It was found that there is about 20 K difference for adsorption temperature between H_2 and D_2 to give the same degree of adsorption, presumably due to an isotope effect for adsorption between H_2 and D_2. Activation energies for adsorption of H_2 and D_2 were determined by measuring the initial rate of adsorption at every 10 K between 233 to 273 K. The amount of adsorption was determined by calculating the integrated absorbance of ZrH and ZrD bands. Each integrated absorbance for both bands was measured in the upper half of the wavenumber range so as not to involve the $Zr<^{H}_{H}$ species. The activation energies of H_2 and D_2 for heterolytic dissociative adsorption were obtained to be 10 ± 0.5 and 11 ± 0.5 kcal/mol, respectively. The heat of adsorption for heterolytic dissociative adsorption was obtained by isotherms between 343 and 373 K. The values obtained were 8 ± 1 kcal/mol for both H_2 and D_2

The activation energy deference between the adsorption of H_2 and D_2 was also calculated simply from the observed IR bands. Although activation energies depend very much on the nature of the assumed transition state, we estimated the energies based on same assumptions for the activated complex made previously by Kokes et al.[10] and Griffin and Yates[15]. The obtained activation energy for H_2 adsorption was ca. 10 kcal/mol, while the bond energy of H-H is

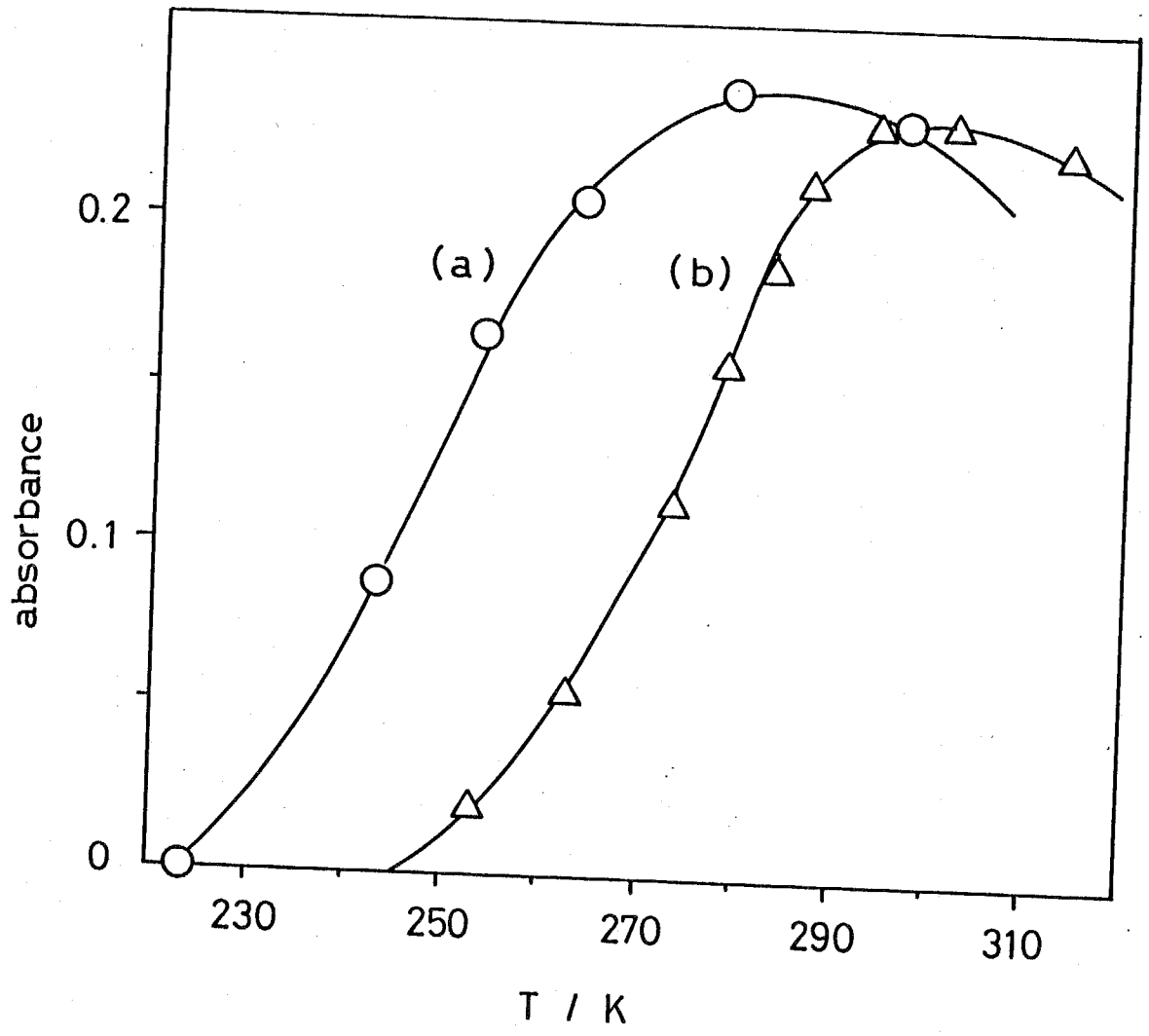

Fig. 2-16 Relative amount of heterolytic dissociative adsorption for H_2 and D_2 as a function of adsorption temperature. (a) H_2 and (b) D_2.

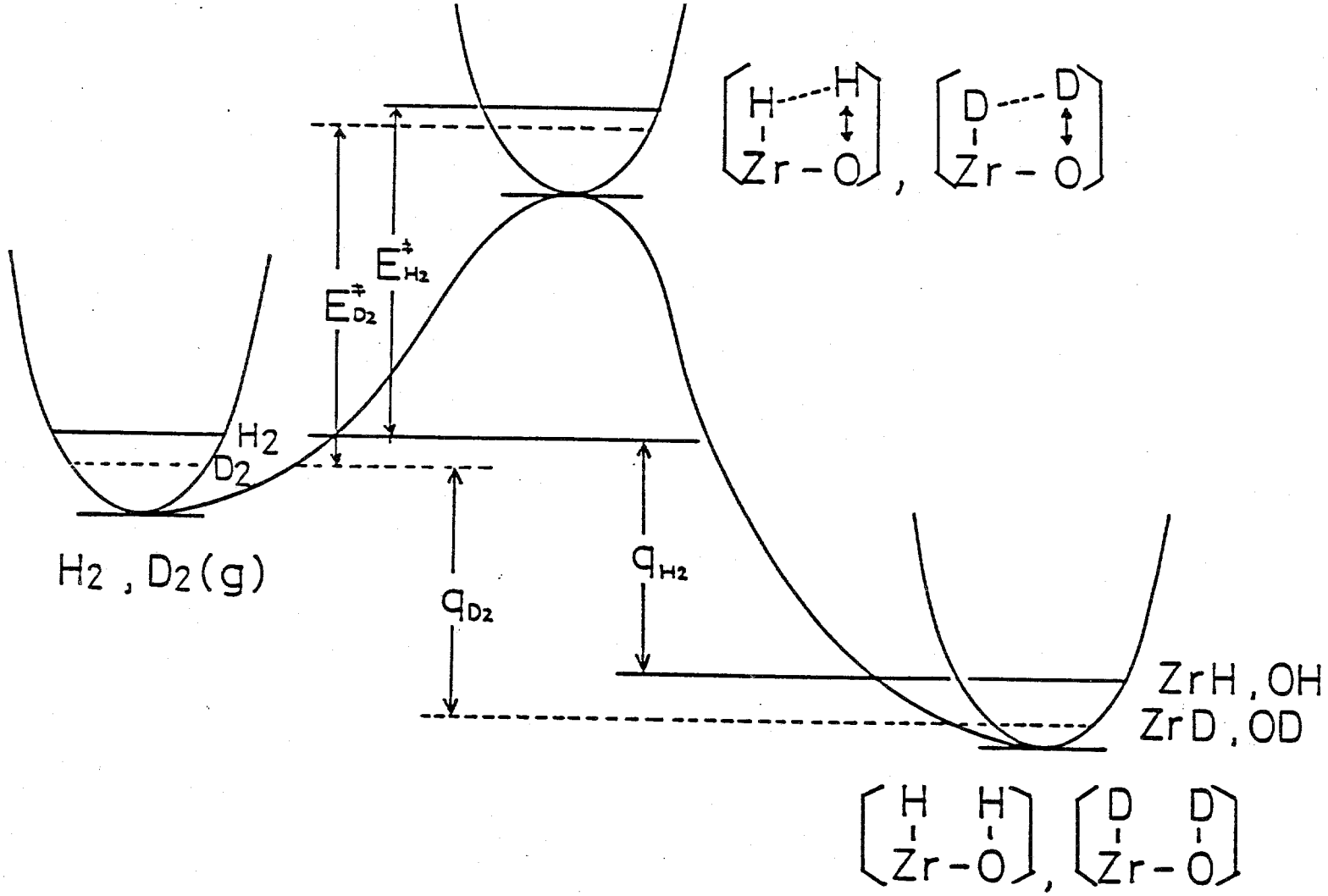

Fig. 2-17 Energy diagram of adsorption of H_2 and D_2.

about 100 kcal/mol. This fact suggests that H_2 in an activated complex is already weakened on a Zr-O pair site. If one assumes that surface atoms have infinite mass and immobile, there are six normal modes in the activated complex. Limits of both a strong and weak H-H bond can be considered for the activated complex. In the limit of strong H-H bond, the six normal modes are distributed between three translations, two liberations and one stretching. In this case the use of HD for adsorption should make no difference to the resulting species, ZrH-OD and ZrD-OH. However a strong isotope effect of HD adsorption between ZnH-OD type and ZnD-OH type was observed[10,15]. The H-H bond in the transition state was therefore considered to be weak on ZnO. On the ZrO_2 the H-H bond would be regarded to be weak because the same type of adsorption behavior appears both ZnO and ZrO_2. In the limit of a weak H-H bond the six normal modes are distributed between the stretching of ZrH and OH, and two types of bending each for OH and ZrH. All of these six modes are IR active and the OH stretching mode has the highest energy among them. Thus the OH stretching is the most likely to the reaction coordinate which attributes the whole energy of an activated complex. An energy diagram for adsorption of molar hydrogen and deuterium over ZrO_2 is shown in fig. 2-17. The activation energy for adsorption, E^*, are given by

$$E^*_{H_2} = E^*_0 + \frac{1}{2}(h\nu_{ZrH} + h\delta_{ZrH} + h\delta'_{ZrH}$$

$$+ h\delta_{OH} + h\delta'_{OH}) - \tfrac{1}{2} h\nu_{H_2} \quad (1)$$

$$E^*_{D_2} = E^*_0 + \tfrac{1}{2}(h\nu_{ZrD} + h\delta_{ZrD} + h\delta'_{ZrD} + h\delta_{OD} + h\delta'_{OD}) - \tfrac{1}{2} h\nu_{D_2} \quad (2)$$

where E^*_0 represents the activation energy from well-bottom to well-bottom in fig. 2-17, and δ and δ' represent two types of bending modes for ZrH and OH. Here in these equations ν_{OH} is omitted, which is the reaction coordinate. From these equations the difference of activated energies between H_2 and D_2 is derived to

$$E^*_{H_2} - E^*_{D_2} = \tfrac{1}{2}[(h\nu_{ZrH} - h\nu_{ZrD}) + (h\delta_{ZrH} - h\delta_{ZrD}) + (h\delta'_{ZrH} - h\delta'_{ZrD}) + (h\delta_{OH} - h\delta_{OD}) + (h\delta'_{OH} - h\delta'_{OD}) - (h\nu_{H_2} - h\nu_{D_2})] \quad (3)$$

If one assumes that the contribution of the difference between H and D in low-energy modes is small, equation (3) will be calculated utilizing the observed bands above 800 cm^{-1}. Our rough calculation gives

$$E^*_{H_2} - E^*_{D_2} = -0.6 \pm 0.2 \text{ kcal/mol.}$$

The calculated and experimental values are in good agreement within the error range. The assumptions made for the activated complex are therefore reasonable; the H-H bond is weakened in the activated complex and the OH stretching is the reaction coordinate. These assumptions are recently proved for the heterolytic dissociative adsorption on ZnO by calculation using extended Huckel method. The activation energy for H_2 adsorption on ZnO is ca. 5 kcal/mol whereas that on ZrO_2 is ca. 10 kcal/mol. The greater activation barrier on ZrO_2 is obviously consistent with the experimental fact that heterolytic

dissociative adsorption was observed only above 223 K on ZrO_2 whereas it occurs rapidly on ZnO even at 83 K.

The difference in heat of adsorption of H_2 and D_2 was also calculated using the observed frequencies. The heat of adsorption, q, for H_2 and D_2 are given by

$$q_{H_2} = q_0 - \tfrac{1}{2}(h\nu_{ZrH} + h\nu_{OH} + h\delta_{ZrH} + h\delta_{OH} - h\nu_{H}) \quad (4)$$

$$q_{D_2} = q_0 - \tfrac{1}{2}(h\nu_{ZrD} + h\nu_{OD} + h\delta_{ZrD} + h\delta_{OD} - h\nu_{D}) \quad (5)$$

Here q_0 represents the energy difference between the bottom of the potential-energy curves for gaseous H_2 and D_2 and those for adsorbed species. The energy difference is derived as

$$q_{H_2} - q_{D_2} = \tfrac{1}{2}[(h\nu_{H_2} - h\nu_{D_2}) - (h\nu_{ZrH} - h\nu_{ZrD}) - (h\nu_{OH} - h\nu_{OD}) - (h\delta_{ZrH} - h\delta_{ZrD}) - (h\delta_{OH} - h\delta_{OD})]. \quad (6)$$

Using observed frequencies above 800 cm^{-1} and the same assumption as for activation energy, the difference between the heats of adsorption of H_2 and D_2 is calculated as

$$q_{H_2} - q_{D_2} = -0.8 \pm 0.2 \text{ kcal/mol}.$$

From this calculation, the heat of adsorption for D_2 is greater than that for H_2. This difference was not obtained from present experiments because the indicated experimental errors for the method used here were not sufficiently precise.

Based on these results for hydrogen adsorption, the mechanistic studies on alkene hydrogenation is described in chapter 5.

2-5 Conclusion

The main results obtained regarding hydrogen adsorption on ZrO_2 are summarized as follows: (1) there are five different types of hydrogen adsorption on ZrO_2: molecular adsorption, homolytic dissociative adsorption, heterolytic dissociative adsorption, the adsorption resulted in bridged ZrHZr species and another dissociative adsorption; (2) for heterolytic dissociative adsorption, an isotope effect was observed between H_2 and D_2; (3) the resulting species of homolytic dissociative adsorption was identified for the first time on a solid surface.

2-6 References

1 W.A. Pliskin and R.P. Kokes, Z. Phys. Chem N.F., 1960, 24, 60.

2 H. Ibach and D.L. Mills, Electron Energy Loss Spectroscopy and Surface Vibration (Academic Press, London, 1982).

3 D.M. Riffe, L.M. Hanssen and A.J. Sievers, Surf. Sci., 1985, 161, L559.

4 J.J. Arrecis, Y.J. Chabal and S.B. Christmas, Phys. Rev. B, 1986, 33, 7906.

5 R.P. Eischens, W.A. Pliskin and M.J. Low, J. Catal., 1962, 1, 180.

6 L.A. Denisenko, A.A.Tsiganeko and V.N. Filiminof, React. Kinet. Catal. Lett., 1983, 22, 265.

7 J. Lamotte and J-C. Lavalley, J. Chem. Soc., Faraday Trans. 1, 1985, 81, 215.

8 T. Onishi, H. Abe, K. Maruya and K. Domen., J. Chem. Soc., Chem. Commun., 1985, 617.

9 S. Naito, H. Shimizu, E. Hagiwara, T. Onishi and K. Tamaru, Trans. Faraday Soc., 1971, 56, 1519

10 R.J. Kokes, A.L. Dent, C.C.Chang and L.T. Dixon, J. Amer. Chem. Soc., 1972, 94, 4429.

11 C.C.Chang, L.T. Dixon and R.J. Kokes, J. Phys. Chem., 1973, 77, 2634.

12 W.C. Conner Jr and R.J. Kokes, J. Catal., 1975, 36, 199.

13 A. Baranski and K. Galuszka, J. Catal., 1976, 44, 256.

14 F. Boccuzzi, E. Barello, A. Zecchina, A. Bossi and M. Camia, J. Catal., 1978, 51, 150.

15 G.L. Griffin and J.T. Yates Jr, Chem. Phys. Lett., 1982, 87, 201.

16 G.L. Griffin and J.T. Yates Jr, 1982, 73, 396.

17 J. Howard and I.J. Braid, J. Chem. Soc., Faraday Trans. 1, 1984, 80, 225.

18 T. Yamaguchi, Y. Nakano and K. Tanabe, Bull. Chem. Soc., Jpn., 1978, 21, 2482.

19 R.J. Kokes and A.L. Dent, Advan. Catal., 1972, 22, 1.

20 S. Naito, H. Shimizu, E. Hagiwara, T. Onishi and K. Tamaru, Trans. Faraday. Soc., 1971, 67, 1519.

21 A.L. Dent and R.J. Kokes, J. Phys. Chem., 1969, 73, 3781.

22 J.M. Mangrigues, D.R. McAlister, R.D. Sanner and J.E. Bercaw, J. Amer. Chem. Soc., 1976, 98, 6733.

Chapter 3

Infrared Studies of Ethene Adsorption on ZrO_2

3-1 Summary

Adsorption species of ethene over ZrO_2 have been observed by FT-IR. Three different species were identified from IR spectroscopic analysis; physically adsorbed, π-bonded and strongly π-bonded (s-π-bonded) ethene. s-π-bonded ethene is adsorbed more stably then π-bonded ethene. The physically adsorbed ethene was observed below 173 K with strong bands of IR active modes and very weak bands of IR inactive ones for free molecules. Both π-bonded and s-π-bonded ethene show common bands at 1446 ($=CH_2$ asym. scissoring) and 993-1007 cm^{-1} (CH out-of-plane bend), and are produced below 275 and 373 K, respectively. s-π-bonded ethene is characterized by four bands in CH stretching region (3091, 3079, 2989 and 2962 cm^{-1}) and additional bands at 1606 cm^{-1} (C=C stretching) and 1338 cm^{-1} ($=CH_2$ sym. scissoring). The adsorption and desorption behavior of these two species were examined with use of bands at 1446 and 1338 cm^{-1}. The dependence on temperature of the amount of both species adsorbed and on the amounts of surface OH species were studied in detail.

3-2 Introduction

The adsorption and hydrogenation mechanism of ethene have attracted a great deal of interest and have been investigated by a large number of researchers for several decades. In the early stage of the research of the catalysis, the volumetric method was applied to study this reaction[1-26], followed by IR study of supported metal catalysts[27,28] and oxide catalysts[22-26]. In recent years progress in ultra-high vacuum (UHV) systems and spectroscopic technique has led to vibrational study of adsorbed species on clean metal surfaces by means of high-resolution electron energy loss spectroscopy (HREELS) and IR reflection absorption spectroscopy (IRAS). Ethene adsorbed on clean metal surfaces has been examined by HREELS coupled with low-energy electron diffraction (LEED)[29] and supported metal surfaces has been examined by IR transmission spectroscopy[30-36].

The observed species are π-bonded, di-σ-bonded ethene and ethylidyne[37]. Although ethylidyne is the most stable species on many metal surfaces, it is concluded that ethylidyne is not the direct intermediate during ethene hydrogenation[33,38-40]. The real intermediate for ethene hydrogenation on metals has not yet been identified and the mechanism for it is still a matter of controversy.

While this reaction seems to be complicated over metals because of their high reactivity, ethene hydrogenation over metal oxides is known to proceed rather slowly with less complexity. However, studies of ethene hydrogenation

over metal oxides are scarcer than those over metals. It was first shown by Burwell and co-workers over Cr_2O_3[9-13] that hydrogenation was simpler over oxides than over metals. For instance, only $C_2H_4D_2$ is produced from the $C_2H_4 + D_2$ reaction, which means that the reaction scheme is irreversible and that self-hydrogenation does not occur. The same results were obtained over ZnO by intensive examination by Kokes and co-workers[18-23]. They combined a study of the IR active species of both hydrogen and ethene, and also observed IR spectra during ethene hydrogenation in situ, which led them to the following reaction mechanism[20]:

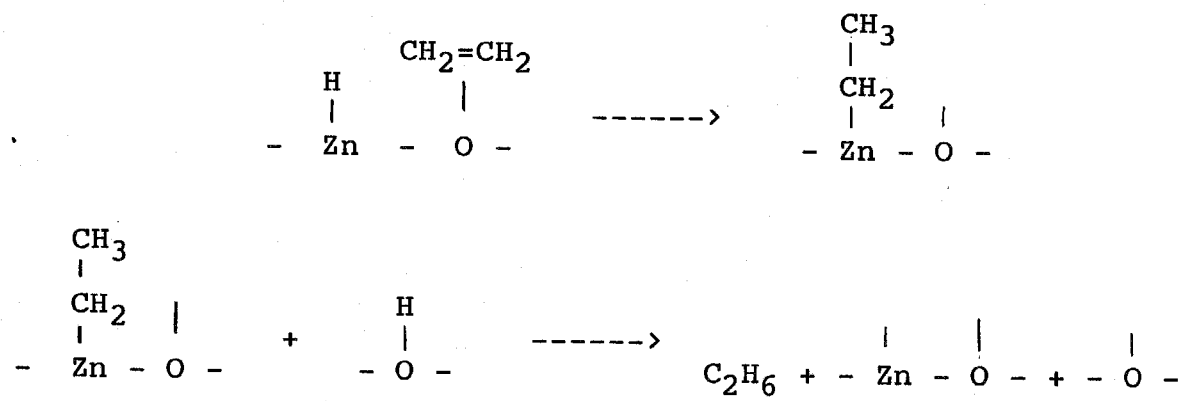

On the other hands, it was found that the ZrO_2 used in this study has high selectivity for the CO hydrogenation reaction to produce methanol, dimethyl ether and isobutene depending on the reaction temperature[41,42]. IR observation has already performed for the ZrO_2 as for hydrogen adsorption[43,44] as well as the in situ CH hydrogenation reaction[45,46]. Hydrogen is activated on ZrO_2 by four different methods of adsorption below room temperature

which are described in detail in chapter 2 and are summarized as follows[44]: (1) molecularly adsorbed hydrogen, $H_2(a)$, is observed below 173 K with an IR band at 4029 cm^{-1}; (2) homolytic dissociative adsorption which produces $Zr<^{H}_{H}$ species, is formed below 373 K and is adsorbed irreversibly below 178 K; (3) heterolytic dissociative adsorption, which forms ZrH (1562 cm^{-1}) and OH (3668 cm^{-1}), is observed between 223 and 373 K, and showed a noticeable isotope effect for adsorption between H_2 and D_2; (4) an adsorption which generates two OH bands at 3778 and 3668 cm^{-1}.

Ethene hydrogenation was chosen to consider the hydrogenation reaction and also to give general idea for alkene hydrogenation reaction mechanism of ethene hydrogenation over metal oxides. To elucidate the total mechanism of ethene hydrogenation, adsorption of both ethene and ethane were first examined in detail by IR. The reaction mechanism is to be overviewed by IR and volumetric study in chapter 5.

3-3 Experimental

The preparation method of ZrO_2 catalyst, the used system, the temperature control, the pretreatment and the measurement condition are the same as described in chapters 2-3. Ethene (Takachiho, 99.9 % pure) was refined by vacuum distillation and was introduced to the cell at 3-5 Torr. Then gas-phase ethene was trapped or evacuated to obtain spectra of adsorbed species only. Control of the amount of surface OH species was performed by either the H_2 exposure time at 573 K or by H_2O exposure at 673 K.

3-4 Results and Discussion

3-4-1 Assignment of Ethene Adsorbed over ZrO_2

IR spectra of adsorbed ethene at various temperatures are shown in fig. 3-1. Ca. 5 Torr of ethene was introduced to ZrO_2 in each experiment. In a warming procedure ZrO_2 was exposed to ethene at 153 K for ca. 1 min and the gas phase was evacuated before and during IR measurement. The use of liquid N_2 trap for removal of ethene in the gas phase instead of evacuation resulted in the same spectra as those in fig. 3-1. In a cooling procedure, ethene was introduced at room temperature and the ZrO_2 was cooled in an atmosphere of ethene. The gas phase was trapped only when spectra were taken at each temperature. When warming and cooling procedures were cycled the same spectra were obtained at the same temperature for all procedures of this series, implying that the adsorption of ethene is fully reversible on this ZrO_2 surface. Each spectrum in fig. 3-1 was taken during a procedures of gradual warming (ca. 2 K/s). In fig. 3-1(a), four bands in the CH stretching region and several bands below 2000 cm^{-1} were observed. All these bands decreased in intensity with increasing temperature, i.e. the amount of adsorbed ethene decreased monotonically. Reverse peaks in the OH stretching region around 3700 cm^{-1} changed reversibly for adsorption of ethene. If there was only one adsorbed species, the ratios of bands would remain constant in the course of increase and/or decrease in the amount of adsorbed, in so far as the adsorption coefficient of each

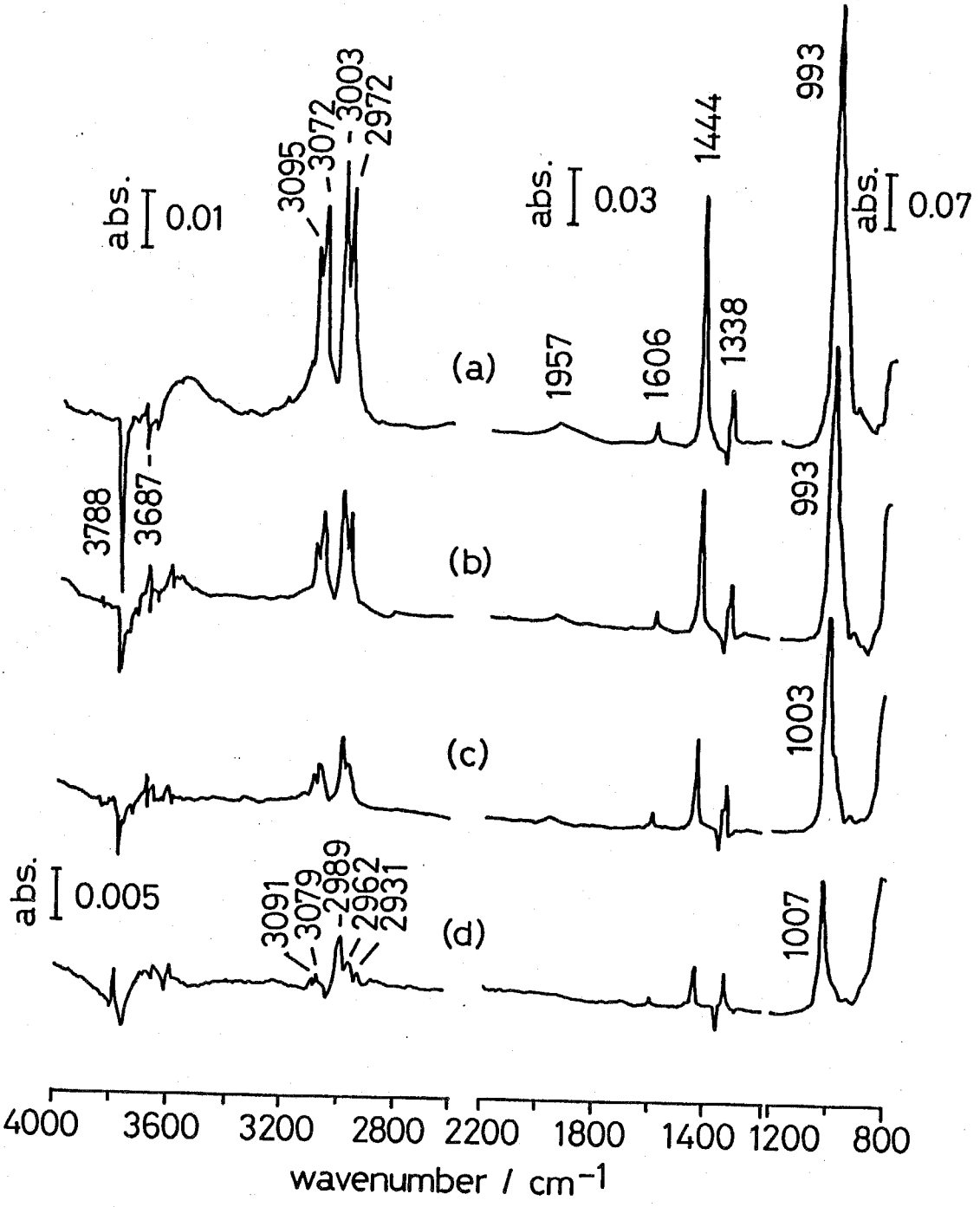

Fig. 3-1 IR spectra of ethene adsorbed on ZrO_2: (a) 173 K, (b) 208 K, (c) 238 K and (d) 298 K.

band is regarded to be constant. However the ratio of the band at 1444 and 1338 cm^{-1}, for instance, was not always the same as that observed in fig. 3-1. The peak intensities of the bands at 1444 and 1338 cm^{-1} are plotted in fig. 3-2 as a function of the adsorption temperature. The band at 1444 cm^{-1} increased in intensity with decreasing temperature while that at 1338 cm^{-1} remained constant below ca. 210 K. The different behavior of these bands suggests the existence of two different species at least, which involve the bands at 1444 and 1338 cm^{-1}.

An attempt to subtract fig. 3-1(d) from (b) was carried out to separate spectra of different species so as to cancel the band at 1338 cm^{-1} (b), described in fig. 3-3. The species in fig. 3-3 shows four bands in the CH stretching region and other bands at 1443 and 993 cm^{-1}.

On the other hand, the subtracted species, which is characterized by the band at 1338 cm^{-1}, includes bands at 3091, 3072, 2989 and 2962 cm^{-1} in the CH stretching region, and around 1608-1603, 1443 and 1000 cm^{-1}. The band at 2931 cm^{-1} was perhaps from 1606 + 1338 cm^{-1} in Fermi resonance with one of the other CH stretching modes. Those four CH stretching bands can be assigned to the same species as that with the band at 1338 cm^{-1} as shown in fig. 3-1(d). The other bands at 1608-1603, 1443 and 1000 cm^{-1} were inferred from the peak shifting and narrowing in fig. 3-3 compared with the original fig. 3-1(b). Therefore, Typical IR spectra of two different types of adsorbed ethene are considered to be

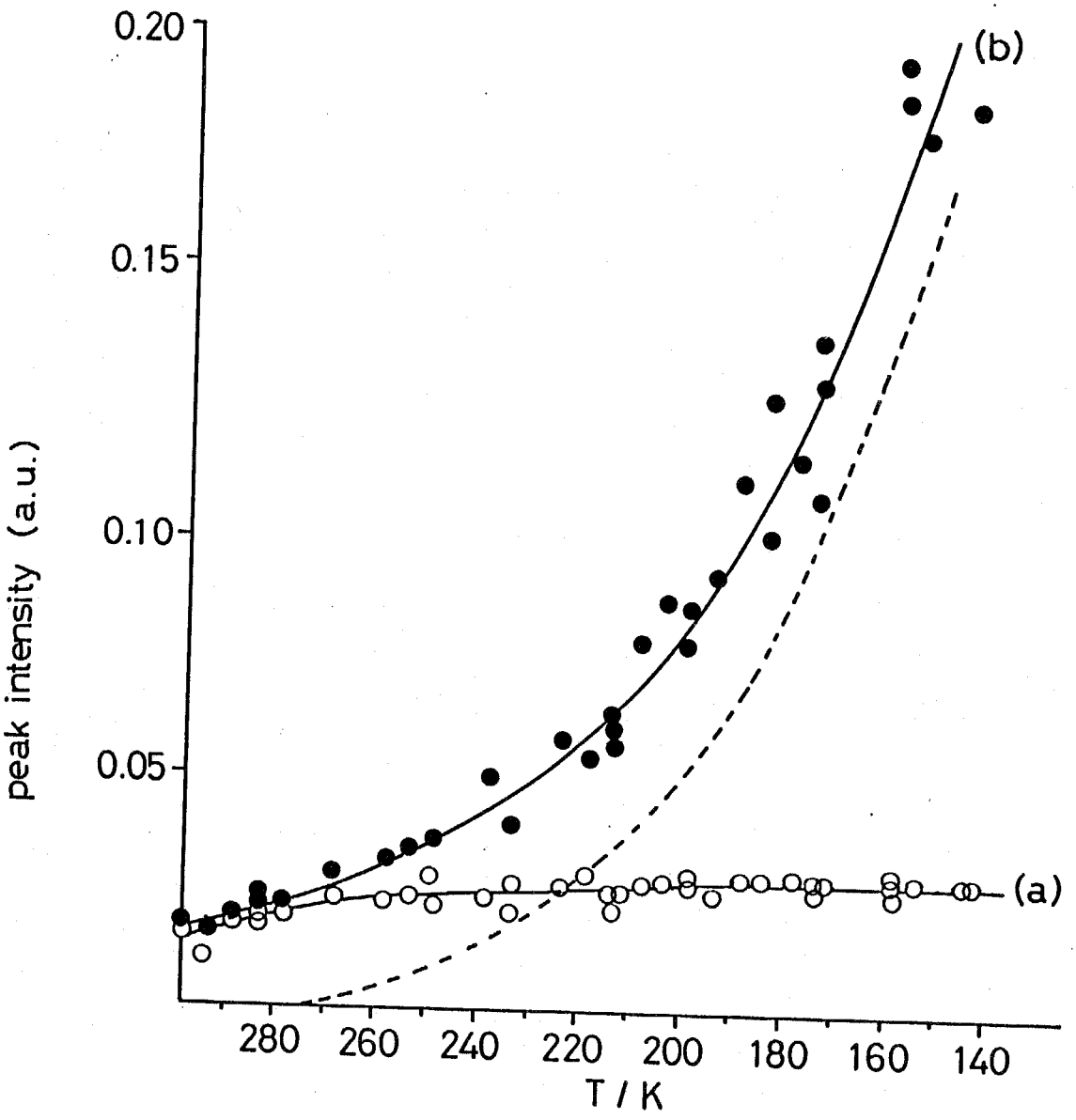

Fig. 3-2 Changes of peak intensities at (a) 1338 and (b) 1444 cm^{-1} in spectra of adsorbed ethene as a function of temperature; (---) the estimated amount of π-bonded ethene.

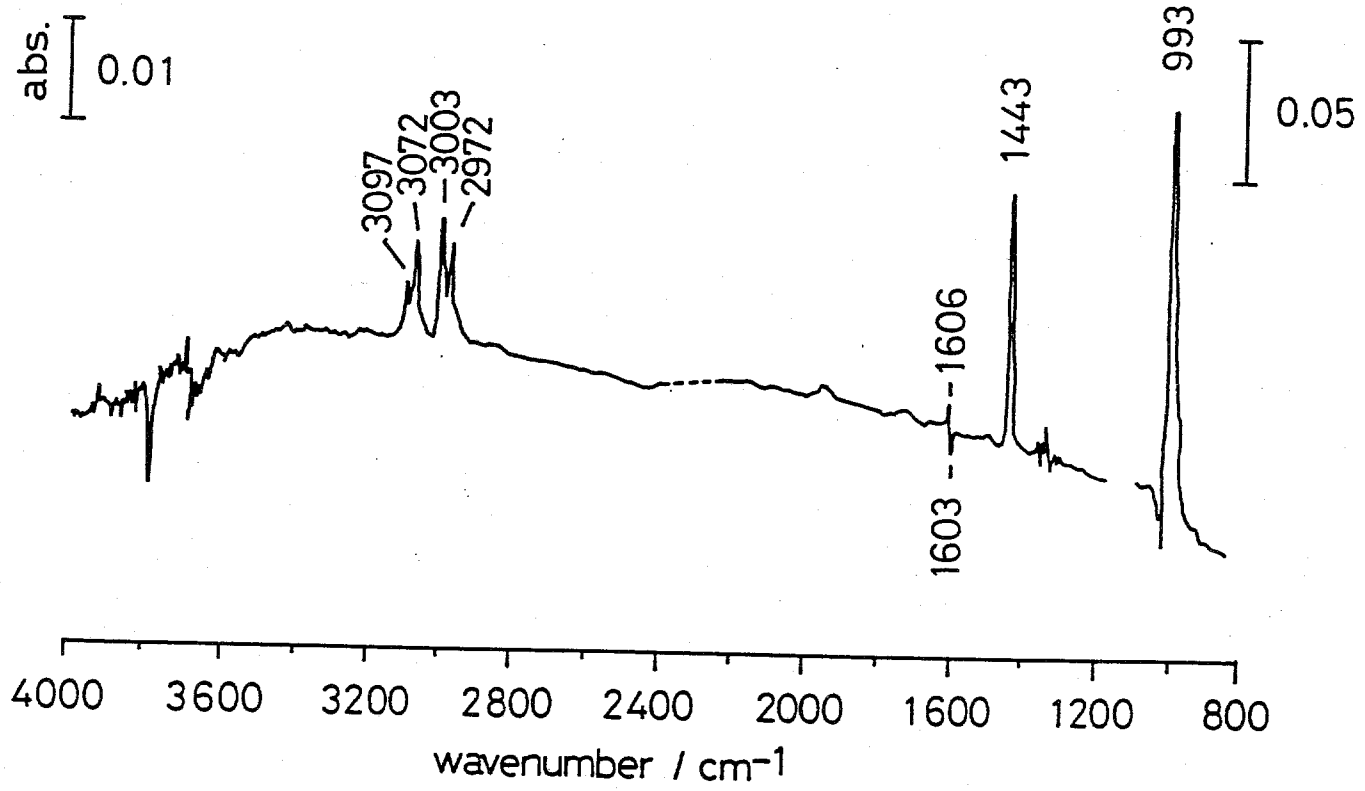

Fig. 3-3 IR spectrum of π-bonded ethene obtained by subtraction of fig. 3-1 (d) from (b).

these of fig. 3-1(d) and of fig. 3-3.

Two results were obtained for C_2D_4 adsorption which was performed to assign all these bands in those two spectra: (1) when C_2D_4 was adsorbed over ZrO_2, neither the OD nor the ZrD bands that were expected to appear at around 2700 and 1120 cm^{-1}, respectively, were observed below 300 K; (2) in each case when the adsorption and desorption cycle was carried out several times, identical spectra were obtained. From these results, the formation of adsorbed species such as ethylidyne accompanied by the C-H bond breaking, as observed on many metal surfaces, is unlikely. The possibility of the existence of di- -bonded ethene is also excluded because the di- -species is expected to give two CH stretching bands between 2900 and 3000 cm^{-1} , and because two Zr^{4+} ions are considered to be too far from each other in ZrO_2 to form a di- -bonded species. Above all, both observed species possess a very strong band around 1000 cm^{-1} which is characteristic of an olefin species (CH out-of-plane bend). Hence, it is concluded that adsorbed ethene maintains its original form, i.e. ethene is adsorbed via -bonding to the ZrO_2.

The observed bands of the species in fig. 3-3 are listed on the left-hand side of table 3-1. This species shows four CH stretching bands and other bands at 1444 and 993 cm^{-1}, implying ordinary -bonding for its adsorption. The bands of the other species, four CH stretching bands and other bands at 1606, 1444, 1338 and 1007 cm^{-1}, are

Table 3-1 Assignments for adsorbed ethene on ZrO_2

C_2H_4 [47] (free molecule)	assignment	w_H/w_D	C_2H_4(a) π	C_2H_4(a) s-π	C_2D_4(a) π	C_2D_4(a) s-π	w_H/w_D
3106	CH a-str.	1.32	3095	3091	2233		1.33
3103[a]	CH a-str.	1.35	3072	3079	2308		1.33
3026[a]	CH s-str.	1.34	3003	2962	2247		1.34
2989	CH s-str.	1.36	2972	2962 (2931)	2191		1.36
	overtone		1957		1541		1.27
1623[a]	C=C str.	1.07		1606		1495	1.07
1444	CH2 sci.	1.34	1444	1444	1076	1076	1.34
1342[a]	CH2 sci.	1.36		1338		982	1.36
1236[a]	CH2 rock	1.22					
826	CH2 rock	1.41					
1023[a]	CH2 twist	1.41					
949	CH2 wag.	1.32	993	1007			
943[a]	CH2 wag.	1.21		922			

[a] IR-inactive

listed on the right-hand side of table 3-1. For this species it is noted that CH stretching bands appear at very low frequencies for an olefin, and that two IR inactive modes in the gas phase are observed at 1606 cm^{-1} (C=C stretching) and 1338 cm^{-1} (CH_2 scissoring). From the adsorption and desorption behavior this species is considered to be more stable than π-bonded ethene, i.e. it is regarded that this species is adsorbed with a stronger interaction with the surface that is ordinary π-bonded ethene, as suggested from the low CH stretching bands. Here, this species is referred to as "strongly-π-bonded (s-π-bonded) ethene", s-π-bonded ethene is considered to involve an interaction with the ZrO_2 surface additional to that of π-bonded ethene, resulting in the observation of IR inactive modes for a free ethene molecule and in band shifting of the CH stretching modes. These assignments are also confirmed by a comparison of the isotope ratio (w_H/w_D) of the adsorbed species and free molecule as shown in table 3-1.

In fig. 3-2, if one assumes that the molar coefficient is constant with change in the amount of adsorption, the peak intensity of the band at 1338 cm^{-1} expresses the relative amount of s-π-bonded ethene and the other at 1444 cm^{-1} involves both s-π-bonded and π-bonded ethene. On the assumption that only s-π-bonded ethene exists in fig. 3-1(d), an estimated value, 1:1.1, between peak intensities of the bands at 1338 and 1444 cm^{-1} for s-π-bonded ethene is obtained. Using this value, the amount of

π-bonded ethene is estimated as described by the dotted line in fig. 3-2. π-bonded ethene seems to be adsorbed below ca. 275 K.

3-4-2 Effect of Surface OH Species on Adsorbed Ethene

When ethene is adsorbed on ZrO_2 reverse peaks in the OH stretching region are observed in the ratio spectra as shown in fig. 3-1. This suggests interaction between surface OH groups and adsorbed ethene. We estimated the amount of interacting OH species with adsorbed ethene by measuring the intensity of the reverse band at 3788 cm^{-1}. These amounts are plotted in fig. 3-4 against the total amount of π-bonded and s-π-bonded ethene measured from the peak intensity at 1444 cm^{-1}. Two spectra in the OH stretching region are also shown in the inset of fig. 3-4. The spectrum (a) is the reverse peak when ethene is adsorbed at 160 K and (b) is a spectrum of the remaining OH species even after pretreatment (evacuation at 1023 K) which was obtained by ratioing the spectrum of ZrO_2 with that after D_2 treatment where no OH species was expected to exist. D_2 treatment was performed with 100 Torr of D_2 at 673 K for 10 min while monitoring the time course of OH-OD exchange reaction, which is usually completed in ca. 5 min. Through this treatment there were finally no OH species on the surface. By comparison of the amount of OH species in spectra (a) and (b), it is noted that almost 100 % of the remaining OH species interact with adsorbed ethene at 160 K. OH species seem to shift to hydrogen-

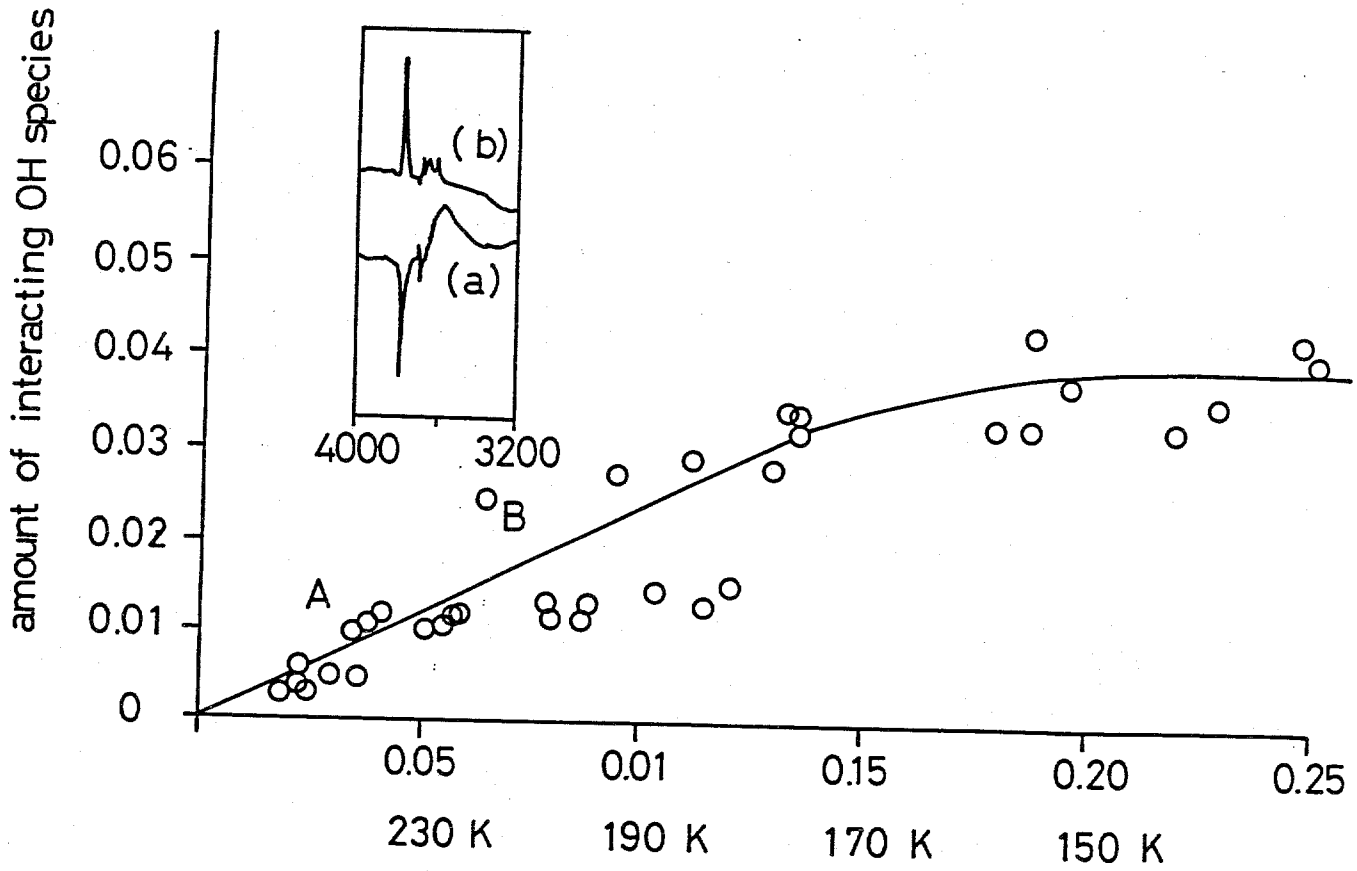

Fig. 3-4 Interaction of OH with adsorbed ethene: (a) OH interacted with adsorbed ethene at 160 K obtained by a ratio of the spectra after/before ethene adsorption and (b) remaining OH species after pretreatment described as a ratio of spectra after/before D_2 Treatment.

bonded ones by interaction with adsorbed ethene as shown in (a). In fig. 3-4, the adsorption temperature is also given for a unit of abscissa estimated from fig. 3-2. Fig. 3-4 shows a linear relation between the amount of interacting OH species and adsorbed ethene up to 0.15 a.u. of adsorbed ethene (170 K). Here it is noted that interaction of OH species still increase with the increase in adsorbed ethene after saturation of s-π-bonded ethene (described as the point B in fig. 3-4), and that the interaction is observed before π-bonded ethene begins to be adsorbed (described as the point A). Both the points were also estimated from fig. 3-2. Thus the interaction of OH with adsorbed ethene is considered to be due to both π-bonded and s-π-bonded species. As for the region where the curve in fig. 3-4 leaves off (above 0.15 a.u., below 170 K) another species begins to be adsorbed as described below. It would be interesting to use a fully dehydroxylated surface for ethene adsorption. However only a small amount of OH species compared to a fully hydroxylated surface could not be removed by any means within this study, as mentioned in chapter 2.

It is reported in chapter 2 that two OH species are produced on ZrO_2 surface by H_2 adsorption above room temperature and also by H_2O treatment. To examine the effect of surface OH species on ethene adsorption in more detail, a series of ZrO_2 surfaces with various amounts of OH species were prepared for ethene adsorption below

300 K. The amounts of OH species were controlled by an exposure time of H_2 at 627 K to pretreated ZrO_2, and H_2O was exposed at 573 K to form a much greater amount of OH species on the ZrO_2 surface. In each case, H_2 or H_2O gas phase was evacuated at the same temperature as those of exposure. Here, the amounts of OH were estimated by the integrated absorbance of OH peaks in the spectra ratioed by that of D_2-treated ZrO_2. The results are shown in fig. 3-5. The total amount of adsorbed ethene estimated by the band intensity at 1444 cm^{-1} is shown on the left and the amount of s-π-bonded ethene calculated by the band at 1338 cm^{-1} on the right. Fig. 3-2 is reproduced in fig. 3-5 (a) and all the lines in fig. 3-5 have the same scattering of experimental data as those of fig. 3-2. It is obvious that the amount of s-π-bonded ethene decreased with increasing amount of OH, although the behavior of -bonded species itself was not observed clearly from fig. 3-5 because it contains the both changes of π-bonded and s-π-bonded ethene. The same data were plotted vs. the amount of OH in fig. 3-6, where the temperature was the same for each line. In the top of fig. 3-6, the amount of s-π-bonded species was subtracted from the total amount of adsorbed ethene calculated by the band at 1444 cm^{-1} based on the same assumption as those for the dotted line in fig. 3-2. It became clear also that the amount of π-bonded ethene decreased with increasing amount of OH at each temperature similarly to the s-π-bonded one.

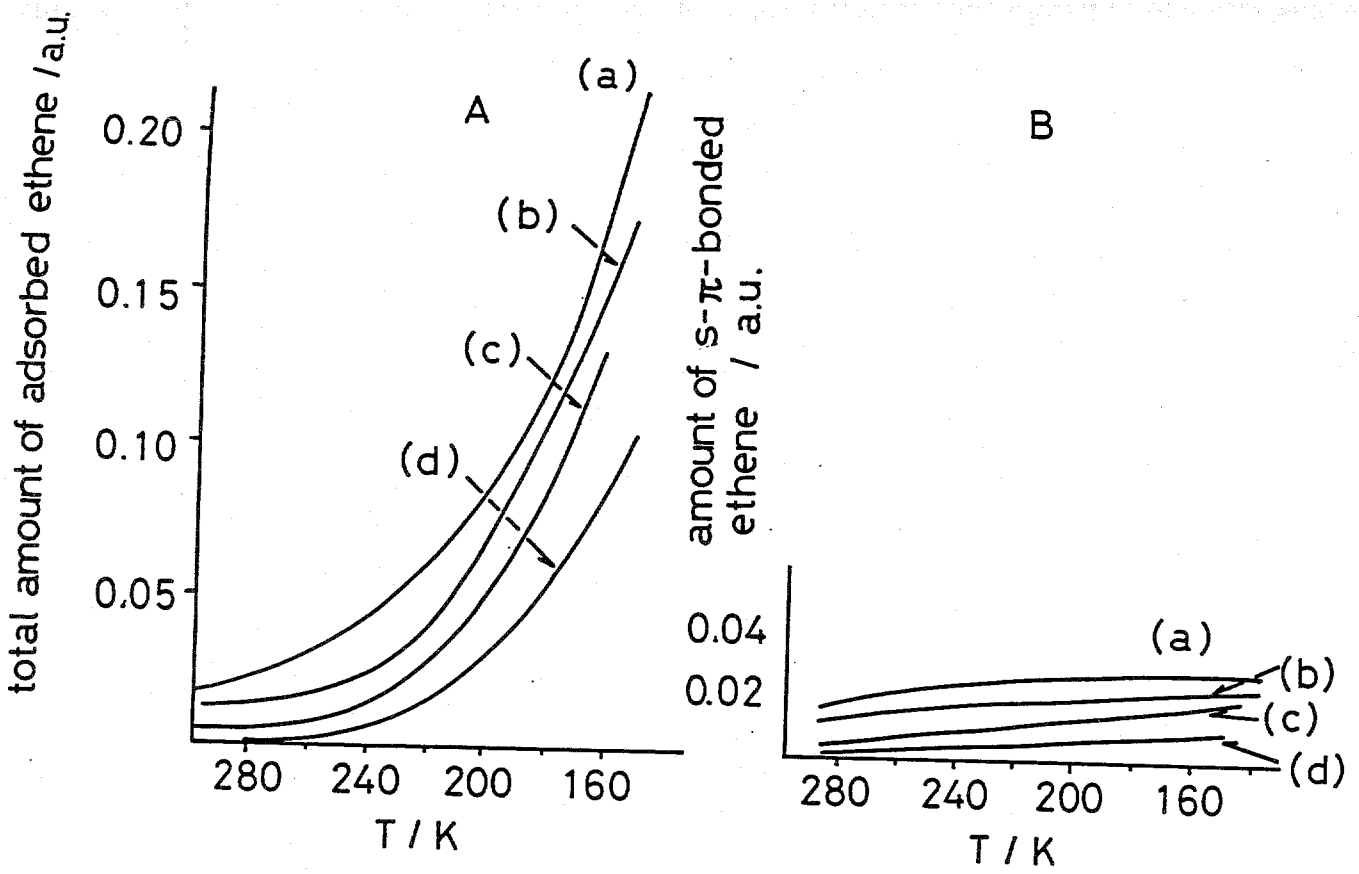

Fig. 3-5 Effect of surface OH species on ethene adsorption: left, total amount of adsorbed ethene measured by the band at 1444 cm^{-1}, and right, amount of s-π-bonded ethene measured by the band at 1338 cm^{-1}, (a) 1.5 a.u. of OH species after pretreatment, (b) 3.7 a.u. of OH species produced by H_2, (c) 9.2 a.u. of OH species produced by H_2 and (d) 10.2 a.u. of OH species produced by H_2O.

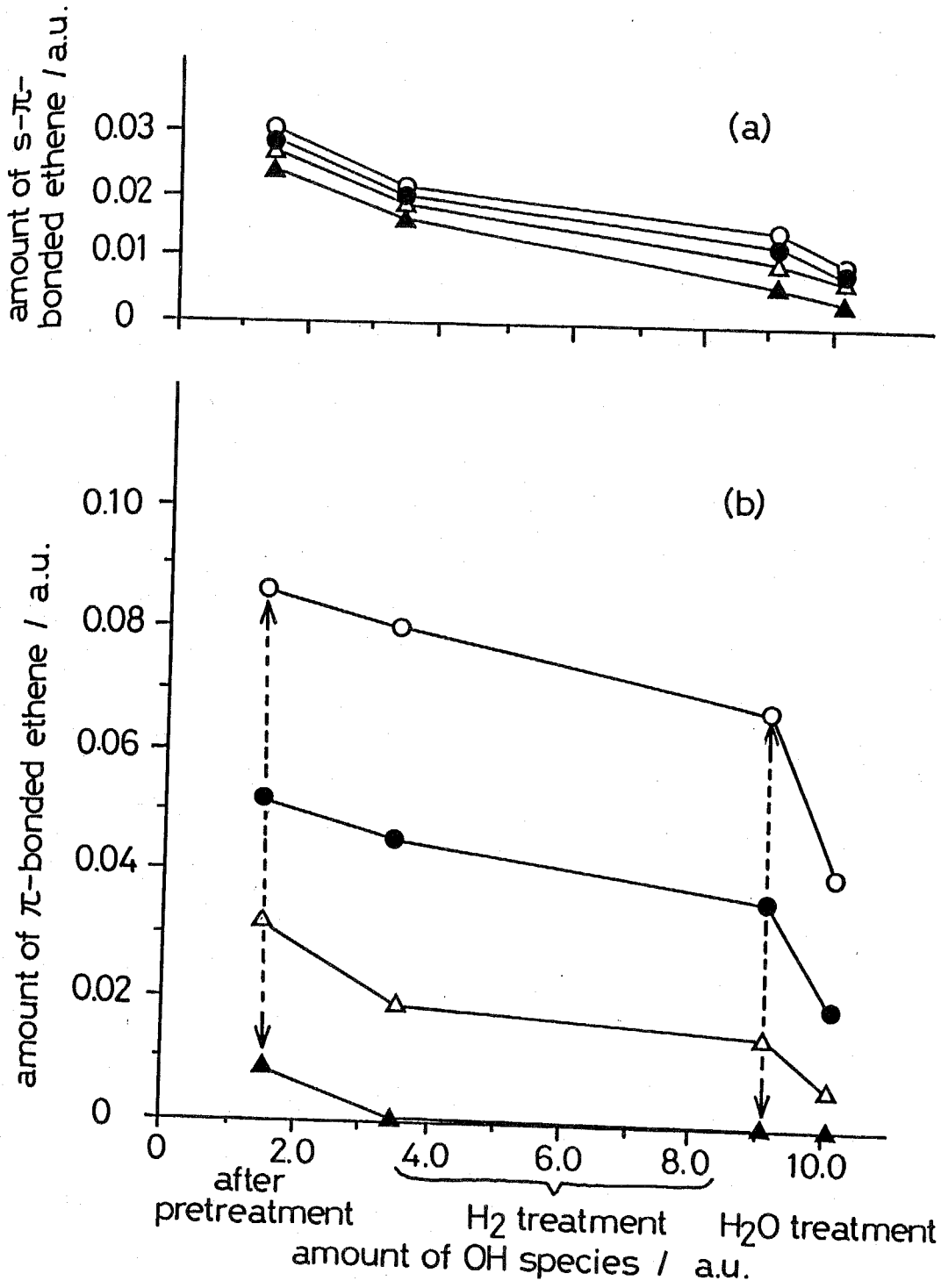

Fig. 3-6 Effect of surface OH on ethene adsorption: (a) amount of s-π-bonded ethene, (b) amount of π-bonded ethene; ▲, 260 K; △, 220 K; ●, 200 K; ○, 180 K.

Focusing on the effect of OH species on π-adsorbed ethene described at the bottom of fig. 3-6 where the s-π-bonded species is canceled, the increase in amount adsorbed from 260 to 180 K [(---) in fig. 3-6] is not affected by the production of OH species except when it is produced by H_2O. This means that there two types of π-bonded species as well as the s-π-bonded species, which cannot easily be discriminated from their IR spectra. The one whose site is blocked by surface OH species produced by H_2 is adsorbed rather strongly at the higher temperature. The other [indicated by (---) in fig. 3-6], which is adsorbed below 260 K, shows no significant effect of surface OH species by produced H_2. However, the site for weakly adsorbed π-bonded species (the latter) is blocked by OH species produced by H_2O as seen in fig. 3-6. In other words, surface OH species preferentially inhibit both kinds of site where ethene is adsorbed stably.

3-4-3 Physically Adsorbed Ethene below 173 K

Besides two types of π-bonded ethene identified above 180 K and the s-π-bonded one, another type of adsorbed ethene was observed below 173 K. The IR spectrum of adsorbed ethene at 133 K is shown in fig. 3-7(b) in comparison of that of adsorbed species at 173 K in fig. 3-7(a). There is a difference of intensity ratio among the four peaks in CH stretching region between the species at 173 and 133 K. Fig. 3-7(c) was obtained by subtraction of spectrum (a) from (b), where a shifted peak

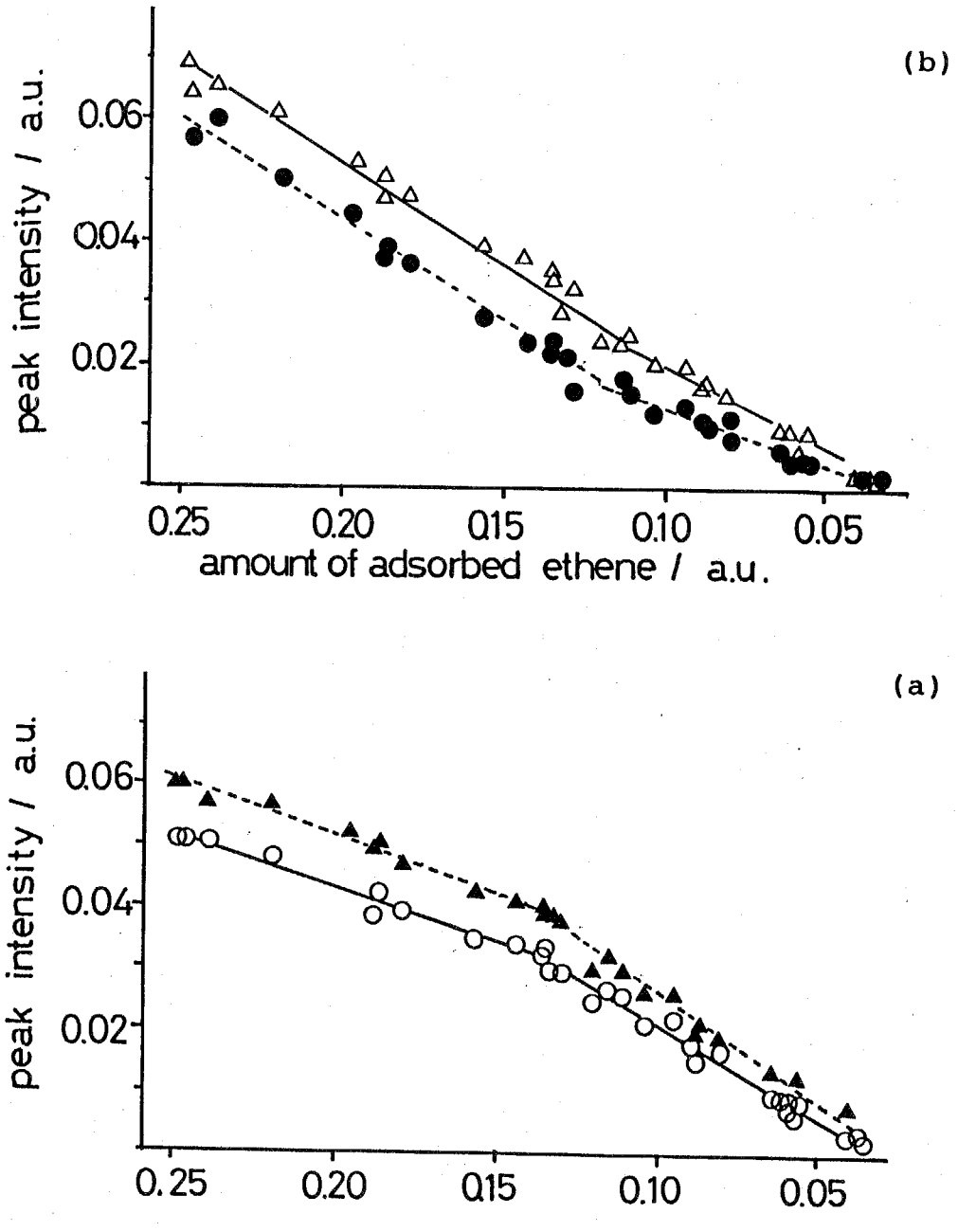

Fig. 3-8 Peak intensities of four CH stretching bands of adsorbed ethene as a function of amount of adsorbed :
(a) ▲, 3064 cm^{-1}; ○, 3004 cm^{-1};
(b) △, 3089 cm^{-1}; ●, 2976 cm^{-1}.

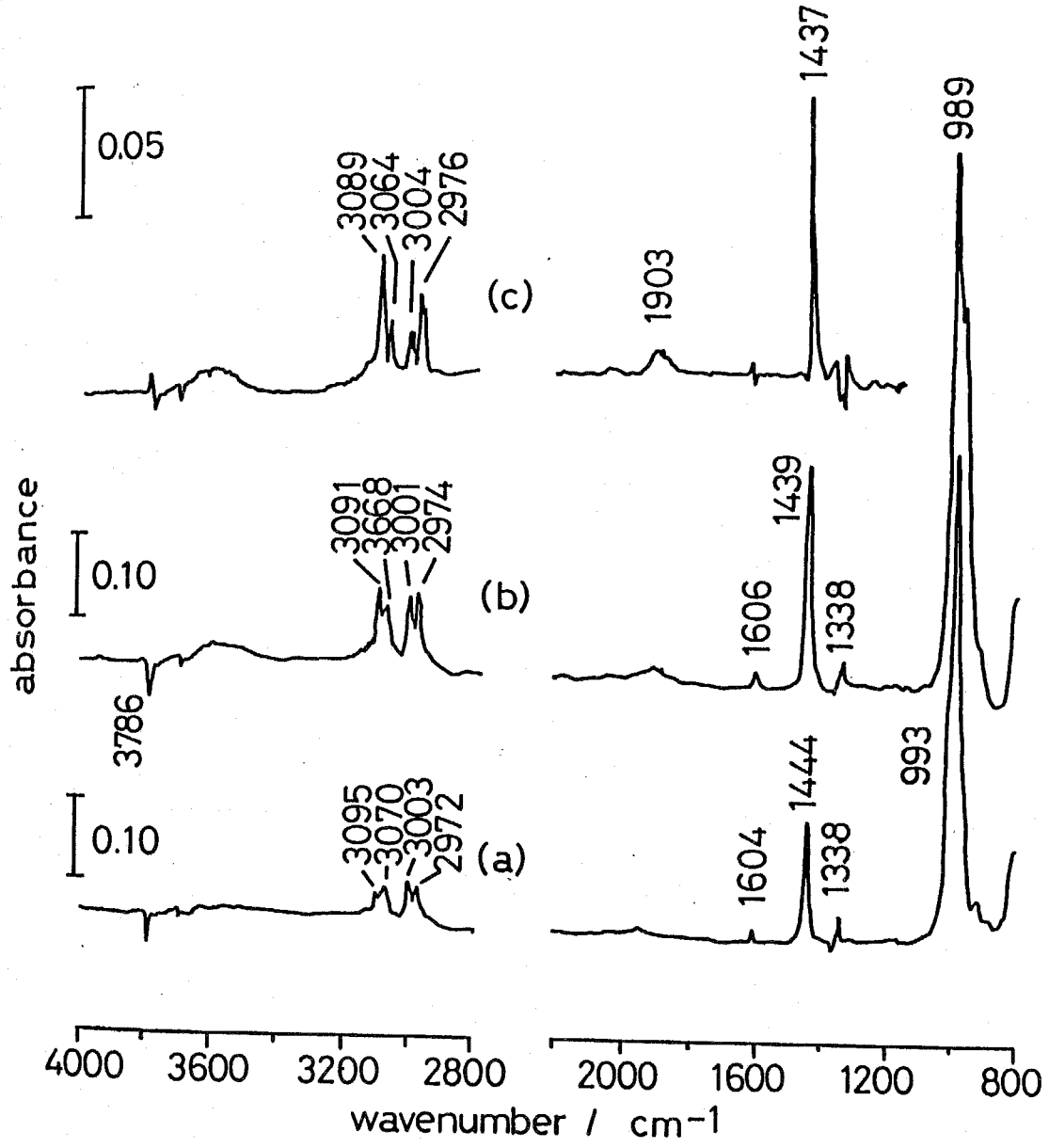

Fig. 3-7 IR spectra of adsorbed ethene, (a) π-bonded and s-π -bonded ethene at 173 K, (b) π-bonded, s-π-bonded and physically adsorbed ethene at 133 K and (c) physically adsorbed ethene obtained by subtraction of (a) from (b).

between 800 and 1000 cm^{-1} is omitted. In (c), note that two peaks at 3064 and 3004 cm^{-1} are very weak compared with the other peaks and that the band at 1604 cm^{-1} , which is IR inactive in the gas phase, is not observed. This means that the species observed below 173 K is in a state which is similar to that of a free molecule and is adsorbed less strongly than the π-adsorbed ethene observed above 173 K. This species, therefore considered to be physically adsorbed ethene.

Peak intensities of the four CH stretching bands in spectra of various amounts of adsorbed ethene were measured. The intensities of the two bands at 3072 and 3003 cm^{-1}, which are originally IR inactive, are plotted in fig. 3-8(a) vs. the total amount of adsorbed ethene measured by the peak intensity of the band at 1444 cm^{-1} and those of the other two at 3097 and 2972 cm^{-1} in fig. 3-8(b), respectively. Two peaks shown if fig. 3-8(b) increased with increasing amount of adsorbed ethene almost linearly while the other two bands shown in (a) changed their rate of increase at ca. 180 K (estimated by fig. 3-2). From this result, it is concluded that physically adsorbed ethene is produced below 173 K, with its spectrum as shown in fig. 3-7(c). This species has less interaction with surface OH species, which is supported by the decrease of the slope in fig. 3-4 below 170 K.

3-5 Conclusion

Three adsorbed ethene species over ZrO_2 were observed and identified by IR: (1) physically adsorbed ethene, which was observed below 173 K, showed almost the same IR spectrum as that of the gas phase; (2) π-bonded ethene, which was observed below room temperature, was more prominent as the temperature decreased, showing two IR inactive modes at 3072 and 3003 cm^{-1}; (3) s-π-bonded ethene, which was identified by the band at 1338 cm^{-1}, showed several IR inactive modes at 1604 and 1338 cm^{-1} in addition to those of π-bonded one and saturated at 210 K.

The reactivity of those species for hydrogenation is discussed in chapter 5.

3-6 References

1 J. Horiuti and K. Miyahara, "Hydrogenation of Ethylene on Metallic Catalysts", NSRDS-NBS, 1968, No. 13.

2 A. Farkas and L. Farhas, J. Chem. Soc., 1938, 60, 22.

3 O. Beeck, Rev. Mod. Phys., 1945, 17, 61.

4 V.B. Kazanski and V.P. Strunin, Kinet. Catal. (Engl. Transl.), 1960, 1, 517.

5 T.A. Dorling, M.J. Eastlake and R.J. Moss, J. Catal., 1969, 14, 23.

6 J.C. Schlatter and M. Boudart, J. Catal., 1972, 24, 482.

7 G.C. Bond, J.C. Phillipson, P.B. Wells and J.M. Winterbottom, Trans. Faraday. Soc., 1964, 60, 1847.

8 D.L. Harrison, D. Nicholls and H. Steiner, J. Catal., 1967, 7, 359.

9 R.L. Burwell Jr, A.B. Littlewood, N. Cadew, G. Pass and C.T.L. Stoddart, J. Amer. Chem. Soc., 1960, 82, 6272.

10 G. Pass A.B. Littlewood and R.L. burwell Jr, J. Amer. Chem. Soc., 1960, 82, 6281.

11 C.T.H. Stoddart, G. Pass and R.L. Burwell Jr, J. Amer. Chem. Soc. 1960, 82, 6284.

12 A.B. Littlewood and R.L. Burwell Jr, J. Amer. Chem. Soc., 1960, 82, 6287.

13 M. Cardew and R.L. Burwell Jr, J. Amer. Chem. Soc., 1960, 82, 6289.

14 J.L. Carter, P.J. Lucchesi, J.H. Sinfelt and D.J.C. Yates, Proc. 3rd Int. Congr. Catal., (North Holland, Amsterdam, 1964), vol.1, p.644.

15 J.H. Sinfelt, J. Phys. Chem., 1964, 68, 232.

16 Y. Amenomiya, H.H.B. Chenier and R.J. Cvetanovic, J. Catal., 1967, 9, 28.

17 D. Narayana, J. Lal and V. Kesavulu, J. Phys. Chem., 1970, 74, 4150.

18 W.C. Conner, R.A. Innes and R.J. Kokes, J. Amer. Chem. Soc., 1968, 90, 6858.

19 A.L. Dent and R.J. Kokes, J. Phys. Chem., 1969, 73, 3772.

20 A.L. Dent and R.J. Kokes, J. Phys. Chem., 1969, 73, 3781.

21 W.C. Conner and R.J. Kokes, J. Phys. Chem., 1969, 73, 2439.

22 A.L. Dent and R.J. Kokes, J. Amer. Chem. Soc., 1969, 91, 7207.

23 A.L. Dent and R.J. Kokes, J. Phys. Chem., 1970, 74, 3653.

24 A.A. Efremov and A.A. Davydov, React. Kinet. Catal. Lett., 1980, 15, 327.

25 R. Grabowski, A.A. Efremov, A.A. Davydov and E. Haber, Kinet. Catal. (Engl. Transl.), 1981, 22, 294 (Russian edition p.1014).

26 T.A. Gordymona and A.A. Davydov, Dolk. Akad. Nauk. SSSR. 1979, 245, 635.

27 G.C. Bond, Trans. Faraday Soc., 1956, 52, 1235.

28 W.A. Pliskin and R.P. Eischens, J. Phys. Chem., 1956, 24, 482.

29 E.g., R.J. Koestner, M.A. Van Hove and G.A. Somorjai, J. Phys. Chem., 1983, 87, 203, and references therein.

30 Y. Soma, J. Chem. Soc., Chem. Commun., 1976, 1004.

31 T.P. Beebe Jr, M.A. Albert and J.T. Yates Jr, J. Catal.,

1985, 96, 1.

32 T.P. Beebe Jr and J.T. Yates Jr, Surf. Sci., 1986, 173, L606.

33 T.P. Beebe Jr and J.T. Yates Jr, J. Amer. Chem. Soc., 1986, 108, 663.

34 T.P. Beebe Jr and J.T. Yates Jr, J. Phys. Chem., 1987, 91, 254.

35 M.P. Lapinski and J.G. Ekerdt, J. Phys. Chem., 1988, 92, 1708.

36 S.B. Mohsin, M. Trenary and H.J. Roboto, J. Phys. Chem., 1988, 91, 254.

37 E.g., C. de la Cruz and N. Sheppard, J. Chem. Soc., Chem. Commun., 1987, 1854; G.A. Somorjai, M.A. Van Hove and B.E. Bent, J. Phys. Chem., 1988, 92, 973, and references therein.

38 F. Zaera and G.A Somorjai, J. Amer. Chem. Soc., 1984, 106, 2288.

39 D. Godbey, F. Zaera, R. Yates and G.A. Somorjai, Surf. Sci., 1986, 167, 150.

40 A.B. Anderson and S.J. Choe, J. Phys. Chem., 1989, 93, 6145.

41 K. Maruya, T. Maehashi, T. Haraoka, S. Narui, K. Domen and T. Onishi, J. Chem. Soc., Chem. Commun., 1985, 617.

42 T. Onishi, K. Maruya, K. Domen, T. Fujisawa and T. Arai, Colloids Surf., 1989, 38, 93.

43 T. Onishi, H. Abe, K. Maruya and K. Domen, J. Chem. Soc., Chem. Commun, 1985, 617.

44 J. Kondo, Y. Sakata, K. Domen, K. Maruya and T. Onishi, J. Chem. Soc., Faraday Trans., 1990, 86, 397.

45 J. Kondo, H. Abe, Y. Sakata, K. Maruya, K. Domen and T. Onishi, J. Chem. Soc., Faraday Trans. 1, 1988, 84, 511.

46 T. Onishi, K. Maruya, K. Domen, H. Abe and J. Kondo, Proc. 9th Int. Congr. Catal., (The Chemical Institute of Canada, Calgary, 1988), vol.2, p.507.

47 T. Shimanouchi, Tables of Molecular Vibrational Frequencies, NSRDS-NBS, 1972, No. 39.

Chapter 4

Infrared Studies of Ethane adsored on ZrO_2

4-1 Summary

IR spectra of adsorbed ethane have been examined following on from those of ethene determined in chapter 3 which deals with ethene adsorption. Two types of adsorbed ethane were identified by IR spectra. A strongly adsorbed "end-on" species has its C-C bond inclined to the ZrO_2 surface with one methyl interacting with the surface and showed a softened CH stretching band at 2798 cm^{-1} (2119 cm^{-1} in the case of CD stretching band of C_2H_5D). This species irreversibly adsorbs up to 253 K. Another weakly adsorbed "side-on" species of ethane was observed below 193 K. This species seems to adsorb with its two methyls equivalent to the ZrO_2 surface, which was concluded from its observed Ch stretching bands almost in the same region as those of the free molecule.

The interaction of of adsorbed ethane with the surface OH species has also been studies as in the case of ethene adsorption. This interaction was observed as reverse peaks of OH species (shifted to hydrogen-bonded peaks). About 30 % of the remaining OH species even after evacuation at 1023 K was observed to interact with adsorbed ethane while 100 % interacted in the case of ethene adsorption. It has also become clear that the intentionally produced OH species obstruct the adsorption sites of ethane, especially that of the strongly adsorbed end-on species.

4-2 Introduction

From early on, adsorbed species of unsaturated hydrocarbons attracted considerable attention and have been frequently studied[1-11]. Adsorption on saturated hydrocarbons has only just become a subject of interest in regard to the C-H bond activation[12-26]. Recent studies of adsorbed cyclic alkane have studied by ultraviolet photoelectron spectroscopy (UPS)[13-16], low energy electron diffraction (LEED)[15,16], thermal desorption (TDS)[15-19], electron stimulated angular distribution (ESDIAD)[17], high resolution electron energy loss spectroscopy (HREELS)[18-25] and infrared reflection absorption spectroscopy (IRAS)[12,22]. Vibrational spectroscopic studies among these investigations showed that there exists a C-H---metal interaction which results in a "softened C-H" stretching broad band of lower frequency than typical C-H bands of saturated hydrocarbons. Subsequently, Chesters' group extended these studies on adsorption of saturated hydrocarbons from cyclic alkane to n-alkane by means of IRAS in reference to the C-H bond vibration[12].

In this chapter the adsorption of ethane over ZrO_2 is described, which follows the observation of alkane adsorption without any bond breaking over TiO_2, in the context of the C-H bond softening. The main object of the study in this chapter is to give some important information on the adsorbed products in order to interpret the mechanism of ethene hydrogenation over ZrO_2, following

on from the IR study of ethene adsorption which is shown in chapter 3.

4-3 Experimental

The system used for IR study here is already described in chapter 2. The same pretreatment and temperature control were performed in this study as those in previous chapters. The condition for IR measurements such as resolution and scan times is also demonstrated in chapter 2.

C_2H_6 (Takachiho, 99.9 % pure) and C_2H_4 (Takachiho, 99.9 % pure) were refined by vacuum distillation. H_2 was purified through "Deoxo" and liquid N_2 trap. D_2 was refined only with liquid N_2trap, and C_2D_4 (MSD isotopes, 98.9 % atom D) and HD (MSD isotopes, 98.9 atom D) were used without further purification. Isotopes of ethane CH_2CH_2D, CH_2DCH_2D, CHD_2CHD_2, CHD_2CD_3 and C_2D_6 were obtained by hydrogenation at 213 K of either C_2H_4 or C_2D_4 with either H_2, D_2 or HD. The possibility of self-hydrogenation or exchange reaction at this low temperature was disregarded by analysis of the product of the C_2H_4 + D_2 reaction to produce only CH_2DCH_2D by NMR as initially reported by Burwell and his co-workers over Cr_2O_3[19-33]. Ethane was introduced to the sample at ca. 5 Torr and was either evacuated or trapped by liquid N_2 before and during the measurement of spectra.

4-4 Results and Discussion

4-4-1 Infrared Spectra of Adsorbed Ethane

IR spectra of adsorbed ethane were taken in both warming and cooling procedures. In former case, ethane was introduced to the sample at 113 K and the gas phase was trapped or evacuated (the same result) during warming. Adsorbed ethane was observed to be completely desorbed at 253 K. In the latter case, ethane was introduced at 253 K followed by cooling the sample, and the sample was exposed to ethane gas except while the spectra were taken. The spectra in fig. 4-1 obtained in the cooling procedure are the same as those as observed in the warming one. Above 193 K, up to 253 K, all the bands decreased keeping their intensity ratios constant as the temperature increased. This means that only one type of adsorbed ethane exists over ZrO_2 between 193 and 253 K. However, at 183 K and below, the feature of the spectra of adsorbed ethane appeared differently from fig. 4-1(a). For example, it is noted from the comparison of (a) and (b) in fig. 4-1 that peak intensity ratios between 2987 and 2798 cm^{-1} and between 1464 and 1340 cm^{-1} changed or even appeared inverted. These tendencies were observed more strongly in fig. 4-1(c). This indicates the existence of another species which is dominant at lower temperatures. So it is suggested that fig. 4-1 (c) is the mixed spectrum of two different species. To obtain a spectrum of lower-temperature species, spectrum (a) of higher-temperature species was subtracted from spectrum (c) so that the

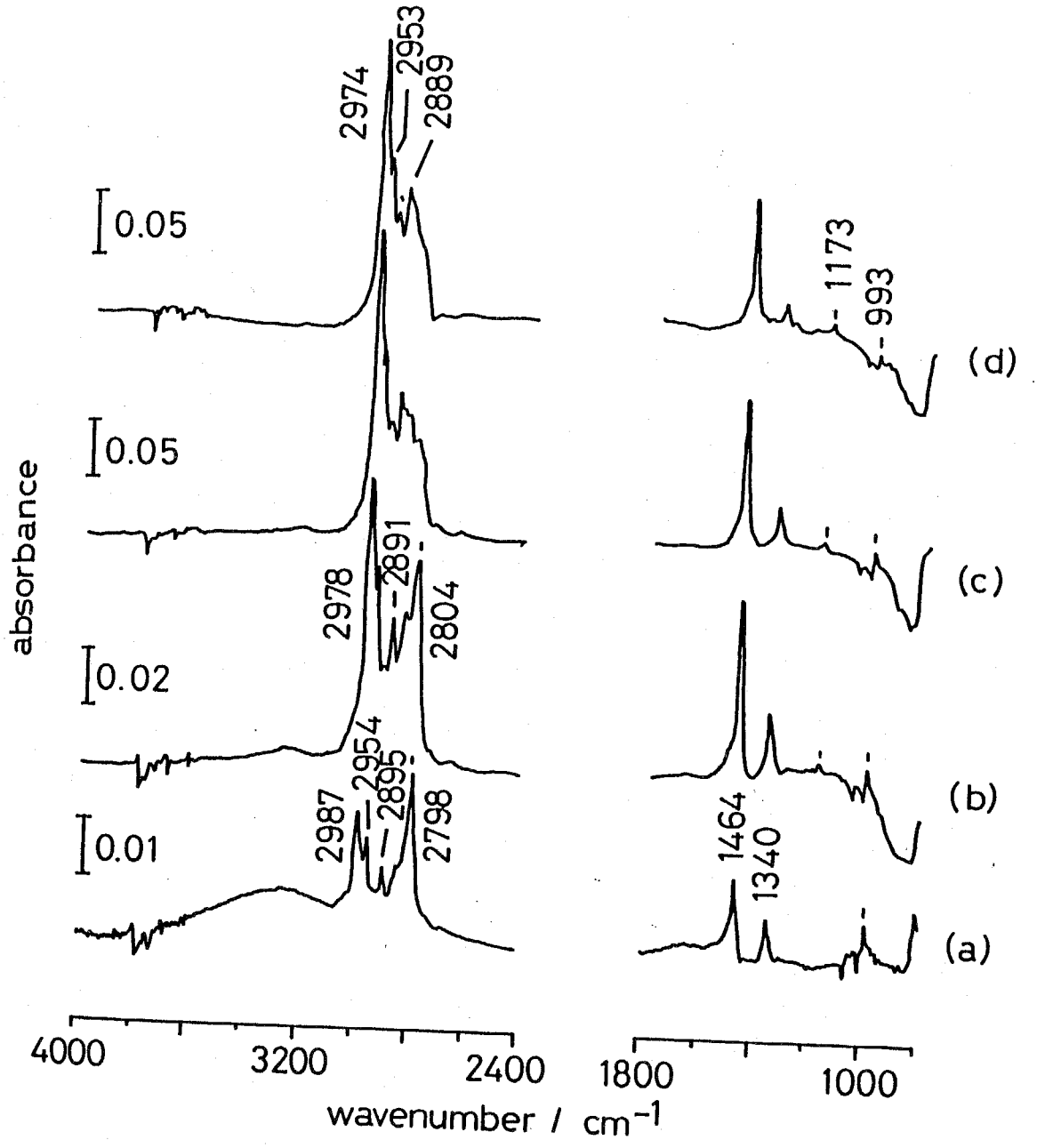

Fig. 4-1 Infrared spectra of adsorbed ethane on ZrO_2; (a) 193 K, (b) 163 K, (c) 143 K and (d) subtracted spectrum of (c) from (a), obtained to reduce the main band at 2798 cm^{-1} from (c).

characteristic band at 2798 cm^{-1} of this specie would be canceled without any reverse bands [fig. 4-1(d)]. From the spectra in fig. 4-1, it is concluded that ethane is adsorbed in two forms on ZrO_2 below 193 K: higher-temperature species [fig. 4-1(a)] and lower-temperature species [fig. 4-1(d)]. The assignments of these species are presented in table 4-1 in terms of "end-on" and "side-on" for higher-temperature and lower-temperature species, respectively. For structural determination, results of the isotope study are to be discussed in the next part.

The CH stretching region of side-on ethane was observed in the same region as those of the gas phase[34] and condensed phase[35] (Table 4-1). This suggests that the side-on species results from the weak adsorption of ethane, keeping a similar form to a free molecule. This side-on species is considered not to be a part of physisorbed ice because above 2 Torr adsorption of the species is independent of pressure. On the other hand, the end-on species has its CH stretching bands over a wider region (ca. 200 cm^{-1}) and at lower frequency for alkanes, which implies that all C-H bonds do not undergo the same adsorption process, i.e. the interaction of each C-H bond with the ZrO_2 surface is not the same. From the fact that end-on species were observed at higher temperature, it is considered that end-on species adsorb on ZrO_2 with a stronger interaction with the surface than do side-on species. It is therefore proposed that the stronger

Table 4-1 Assignments of adsorbed ethane on ZrO_2

assignments	C2H6(g)[34]	condensed phase	ZrO_2 side-on	ZrO_2 end-on	Pt(111) by Chesters[12] monolayer	Pt(111) by Chesters[12] multilayer
CH_3 a-str.	2985	(2959)	2974 s	2987 s	----	----
CH_3 a-str.	[a]2969	2972 s	2953	2954 m	2958	2973
CH_3 s-str.	[a]2954	(2877)	2916		2853	----
CH_3 s-str.	2896	2880 m	2889 m	2895 m	----	2884
				2845 sh		
				2798 s		
CH_3 a-def.	1469	(1447-62)	1464 s	1464 s	----	----
CH_3 a-def.	[a]1468	1450-65 m-s	1514 sh	1514 sh	1457	1462
CH_3 s-def.	[a]1338	(1402)	----	----		
CH_3 s-def.	1379	1368-71 m	1340 m	1340 m		
CH_3 rock	1190	813-25 m-s	1173 w	----		
CH_3 rock	[a]882	(1185-1200)	----	----		
C-C str.	[a]995	(993-6)	993 w	993 w		
tort.	289	----	----	----		

[a] IR-inactive. s,strong; m, medium; w, weak; sh, shoulder.

interaction of end-on species gave rise to C-H stretching band shifting. This phenomenon has already been interpreted by investigations of cyclohexane adsorption in terms of "C-H---metal interaction" and resulted in "softened C-H" observed shifted to lower frequency[18-25]. Recently, Chesters et al tried to observe this phenomenon in n-alkane adsorption and obtained IRAS spectra of ethane adsorption on Pt(111) at 95 K (Table 4-1)[12]. They concluded that observed ethane adsorb with its C-C bond parallel to the surface without any C-H---metal hydrogen bonding even for a monolayer. This type of adsorption seems to correspond reasonably to the side-on species of ethane on ZrO_2 at lower temperatures. The end-on species seems to involve the C-H---metal (Zr) hydrogen bonding which was not observed on Pt(111).

4-4-2 Determination of Structure of Adsorbed Ethane by an Isotope Study

In fig. 4-2 IR spectra of adsorbed CH_3CH_2D and CH_2DCH_2D are shown for species (a) at higher temperatures and (b) at lower temperatures. First in regard to the higher temperature species (a) two CD stretching bands are observed for both CH_3CH_2D and CH_2DCH_2D. This result is well expected for CH_2DCH_2D because it has two C-D bonds in a molecule. However, two CD bands were also observed in the spectrum of CH_3CH_2D where only one C-D band exist, which led us to the adsorption models as illustrated beside each spectrum in fig. 4-2(a). In this "end-on"

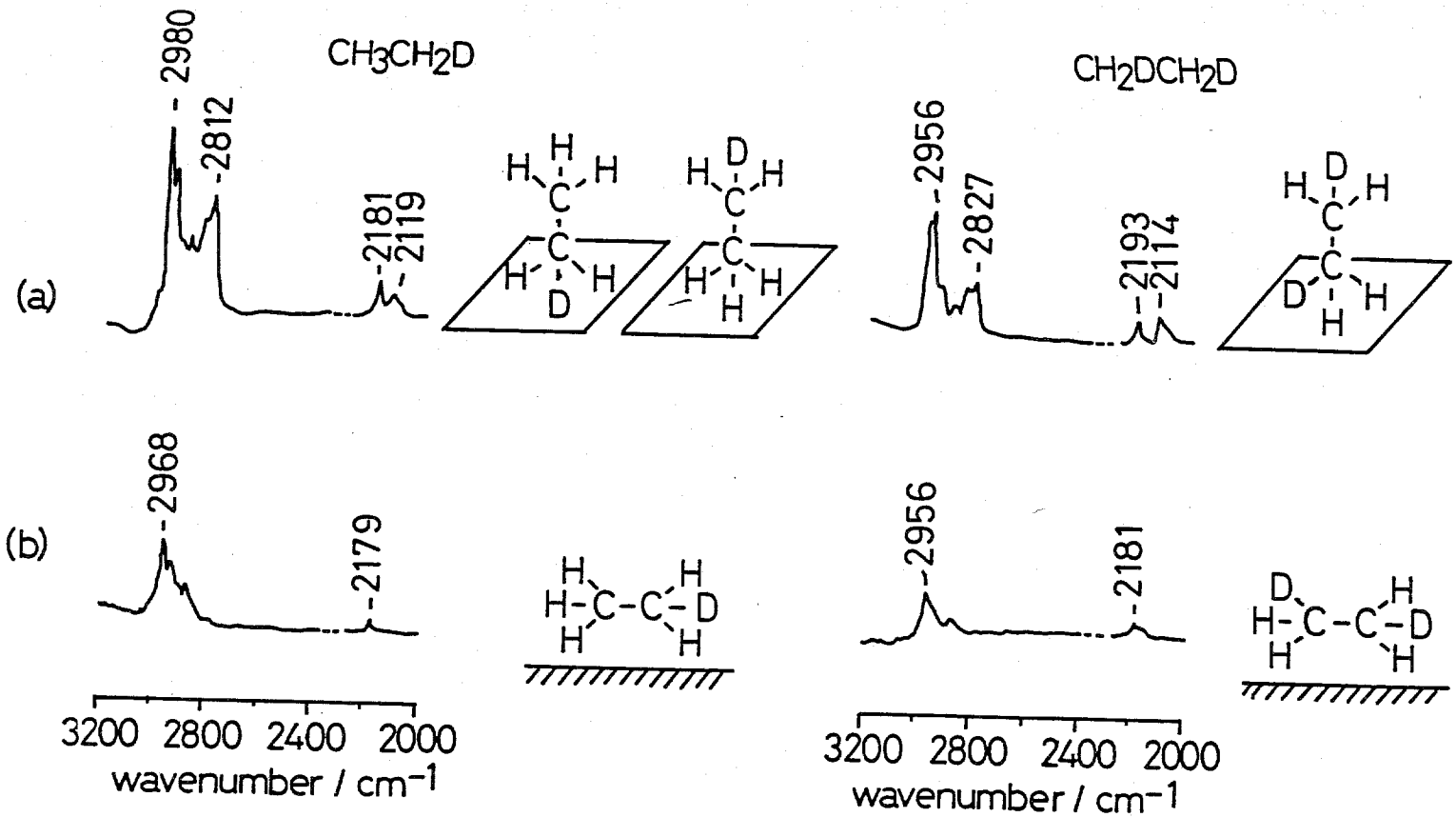

Fig. 4-2 Infrared spectra of adsorbed CH_3CH_2D and CH_2DCH_2D over ZrO_2;
(a) higher temperature "end-on" species and (b) lower temperature "side-on" species.

form, two CD stretching bands appear both for CH_3CH_2D and CH_2DCH_2D. So it is concluded that the CH and CD stretching bands in lower frequency region are attributed to the methyl interacting with the surface and that those in the higher-frequency region are attributed to the methyl without any interaction withe the ZrO_2 surface. The C-C bond of end-on species is not necessarily perpendicular to the surface as depicted in fig. 4-2 but is expected somewhat inclined to the surface. This is supported by the IR band of CC stretching band at 993 cm^{-1}, which was observed more strongly for the end-on species than the side-on one. The Zr^{4+} could be the interacting atom with the methyl of the adsorbed ethane although the surface is illustrated as a flat square surface. In the spectra (b) of the lower-temperature species, only one CD stretching band was observed for both CH_3CH_2D and CH_2DCH_2D dominantly. The appearance of only one CD stretching band for CH_2DCH_2D is explained by the fact that two methyls in a molecule are equivalent on the surface. The shoulder observed in the case of CH_2DCH_2D adsorption is derived from symmetric and asymmetric stretching due to two C-D bands and is not observed for CH_3CH_2D. Therefore, the adsorption form of the lower-temperature species is considered to be as illustrated in fig. 4-2(b).

Now, the attention would be focused on the observed spectrum for the end-on species of CHD_2CHD_2. In the case of CH_2DCH_2D, CD stretching bands are too weak to examine the band shape although they are simpler than that of CH

stretching bands. However, CH stretching bands in CHD_2CHD_2 are strong and clear enough for discussion (fig. 4-3). exactly the same spectra of the CH stretching region were observed for non-dissociatively adsorbed cyclohexane[16, 20-25] and cyclopentane[18,19] monolayers and n-alkane[12]. The appearance of a sharp bands in the high-frequency region and a broad band in the low-frequency region is in good agreement with the assignment of these bands at 2958 and 2807 cm^{-1} to free methyl and interacting methyl in CHD_2CHD_2, respectively.

4-4-3 Effect of Surface OH Species on Ethane Adsorption

In fig. 4-1 reverse bands in OH stretching region (4000-3600 cm^{-1}) were observed, which were due to remaining OH species on the surface evacuate at 1023 K. To obtain the amount of OH on the surface the following experimental procedure was performed. After removing all the adsorbed ethane at room temperature by evacuation the OH-OD exchange reaction was carried out at 673 K for 10 min by introducing 100 Torr of D_2. All the surface OH species can be exchanged to OD species by this treatment. Comparing spectra before and after D_2 treatment, the absolute intensity of the remaining OH species on the surface evacuated at 1023 K was obtained. Then the amount of interacting OH species observed as reverse peaks was ratioed by the initially remaining OH species the absolute intensity of which was already obtained by a comparison with OD exchanged surface. This indicates clearly that ca.

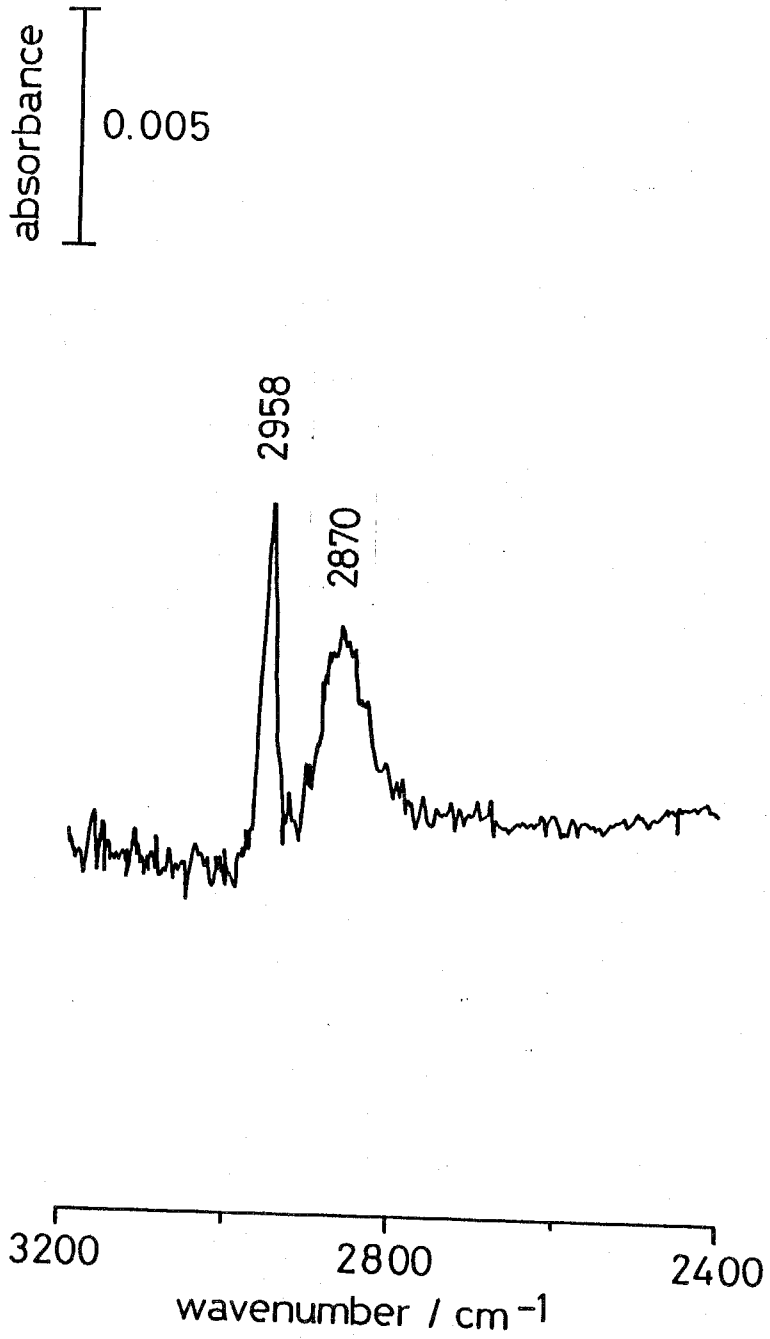

Fig. 4-3 Observed CH bands of adsorbed CHD_2CHD_2 for end-on species.

30 % of remaining OH species had interacted with the adsorbed ethane. In the case of ethene, 100 % of the OH species was found to interact and this interaction was not the necessary condition but was the inhibiting factor for ethene adsorption[27]. The surface OH was again intentionally produced by H_2 and H_2O. The detailed procedure for producing OH species was described in chapter 3. The relative amount of adsorbed ethane was measured by peak intensity of the band at 1464 cm^{-1}, so both the side-on and end-on species were included in the amount. The results are shown in fig. 4-4. The total amount of adsorbed ethane decreased with the increase of the amount of OH species on the surface as has already been observed for ethene adsorption. In fig. 4-5 the amount of ethane adsorbed is presented as a function of OH amount at constant temperature. The obvious conclusion is made that adsorption sites of ethane were gradually blocked as the OH species increased. Unfortunately, it was difficult to examine the adsorbed sites separately for the side-on and end-on species quantitatively because neither of the two species possesses any characteristic bands that could clearly separate them from the other species. However, from the spectra corresponding to the adsorbed species in fig. 4-4(d), which are shown in fig. 4-6, the adsorbed species, which possibly exist with a large amount of OH species, are found to be the side-on species alone. Therefore, it is confirmed that OH species were primarily

formed on such sites, providing stronger interaction with the adsorbate.

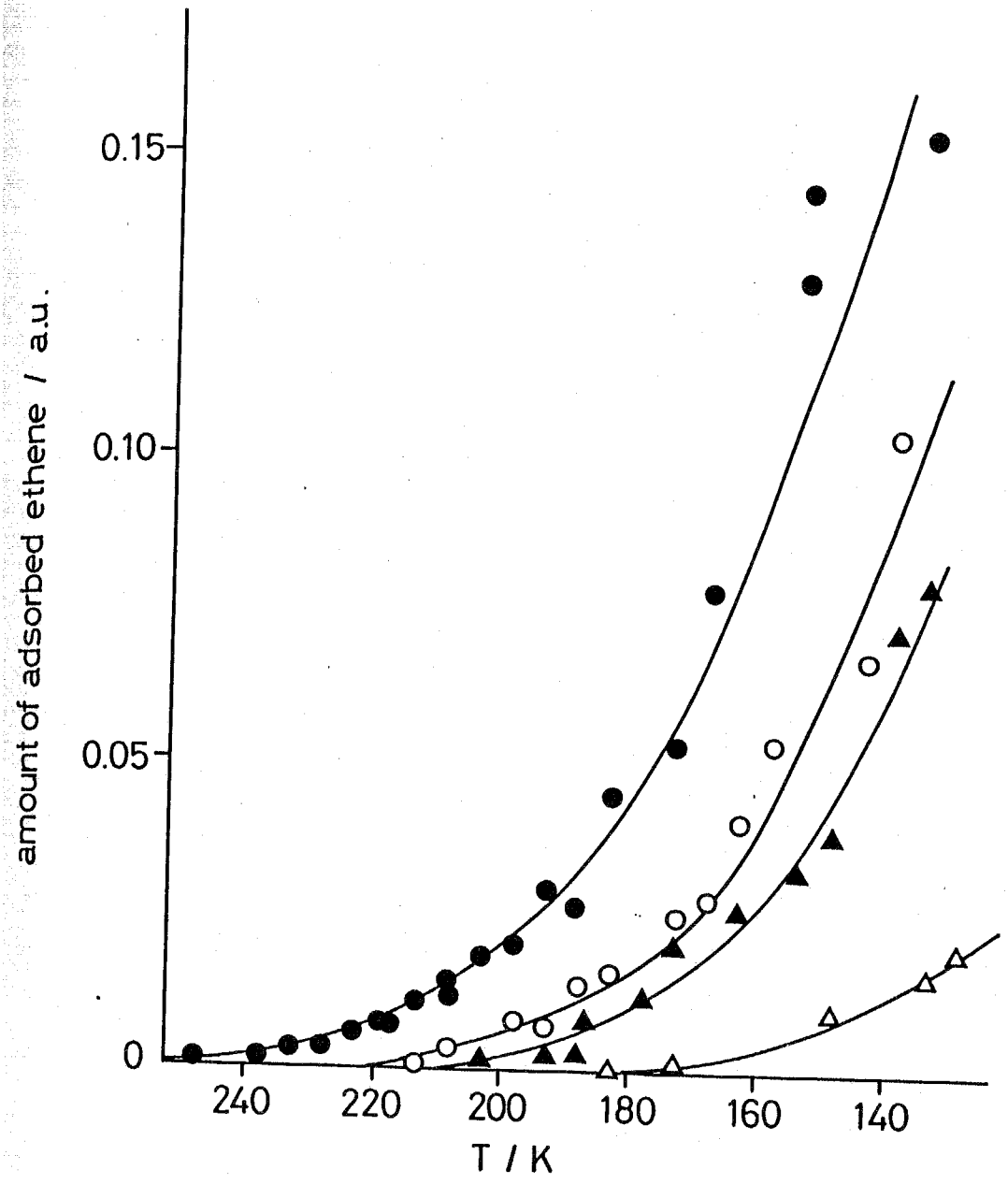

Fig. 4-4 The effect of OH species on total amount of adsorbed ethane: ● , 2.2 a.u. of OH species after pretreatment; O , 5.2 a.u. of OH species produced by H_2; ▲ , 8.4 a.u. of OH species produced by H_2; △ , 9.8 a.u. of OH species produced by H_2O.

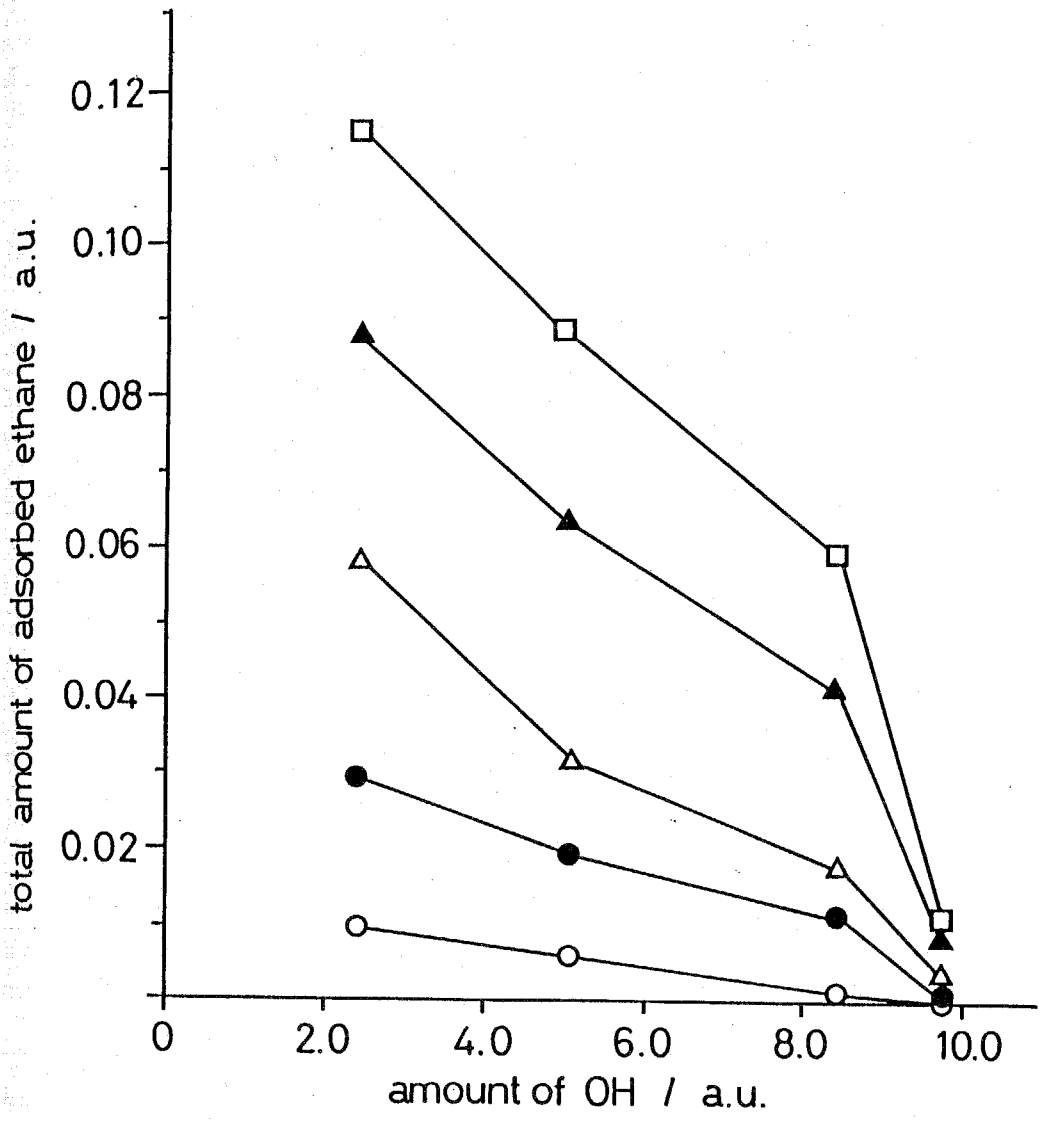

Fig. 4-5 Dependence of total amount of adsorbed ethane on OH species; the data in fig. 4-4 were used, see text: □, 140 K; ▲, 150 K; △, 160 K; ●, 180 K; ○, 200 K.

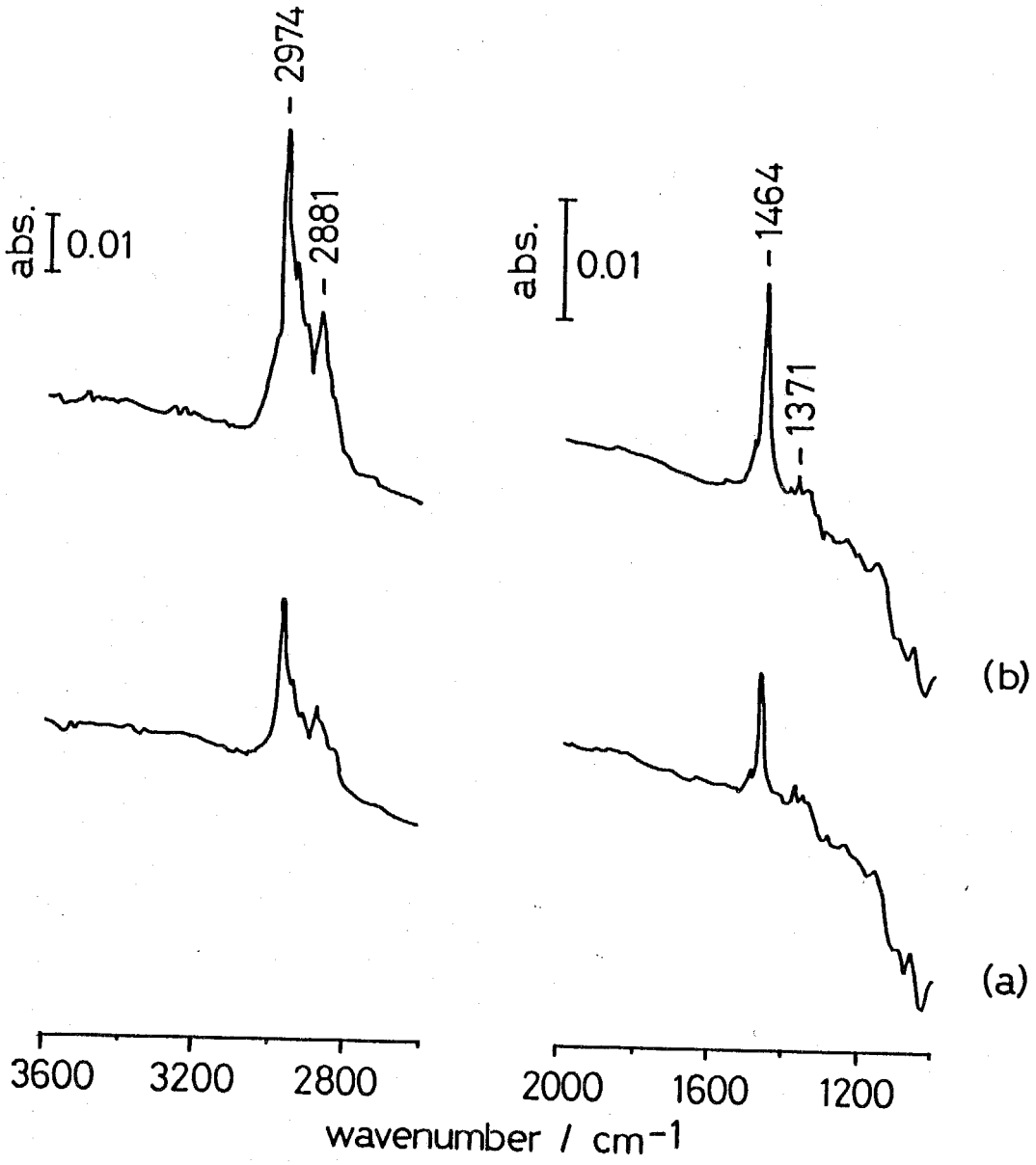

Fig. 4-6 Infrared spectra of adsorbed ethane on the ZrO_2 covered with 9.8 a.u. of OH species produced by H_2O: (a) 148 K and (b) 133 K.

4-5 Conclusion

Two adsorbed species of ethane adsorption were identified by an IR study: the side-on and end-on species. The side-on species was observed below 183 K and adsorbed with its two carbon atoms almost equivalent to the surface. The end-on species was found to have a strong interaction with the surface which is interpreted in terms of C-H---metal hydrogen bonding and was observed below 253 K. As in the case of ethene adsorption, the existence of OH species obstructs the adsorption site of ethane.

The discussion of the ethene hydrogenation mechanism over ZrO_2 is shown in the next chapter.

4-6 References

1 L.H. Little, Infrared Spectra of Adsorbed Species (Academic Press, London, 1966).

2 R.P. Eischens and W.A. Pliskin, Adv. Catal., 1958, 10, 1

3 J. Horiuti and K. Miyahara, Hydrogenatuin of Ethylene on Metallic Catalysts, 1968, NSRDS-NBS No. 13.

4 J. Horiuti and M. Polanyi, Trans. Faraday Soc., 1934, 30, 1164.

5 A. Farkas and L. Farkas, J. Amer. Chem. Soc., 1938, 60, 22.

6 R.J. Koestner, M.A. Van Hove and G.A. Somorjai, J. Phys. Chem., 1983, 87, 203, and references therein.

7 G.A. Somorjai, M.A. Van Hove and B.E. Bent, J. Phys. Chem., 1988, 92, 973,

8 F. Zaera and G.A. Somorjai, J. Amer. Chem. Soc., 1984, 106, 2288.

9 D. Godbey, F. Zaera, R. Yates and G.A. Somorjai, Surf. Sci., 1986, 167, 150.

10 T.P. Beebe Jr and J.T. Yates Jr, J. Amer. Chem. Soc., 1986, 108, 663.

11 A.B. Anerson and S.J. Choe, J. Phys. Chem., 1989, 93, 6145.

12 M.A. Chesters, P. Gardner and E.M. McCash, Surf. Sci., 1989, 209, 89.

13 G.W. Rubloff, H. Luth, J.E. Demuth and W.D. Grobman, J. Catal., 1978, 53, 423.

14 J.E. Demuth and D.E. Eastman, Phys. Rev. Lett., 1974, 32, 1132; Phys, Rev., 1976, B13, 1523.

15 T.E. Felter, F.M. Hoffmann, P.E. Thiel and W.H. Weinberg, Surf. Sci., 1983, 130, 163.

16 F.M. Hoffmann, T.E. Felter, P.A. Thiel and W.H. Weinberg, Surf. Sci., 1983, 130, 173.

17 T.E. Madey and J.T. Yates Jr, Surf. Sci., 1978, 76, 397.

18 F.M. Hoffmann, E.V. O'Brien, J. Hrbek and R.A. de Paola, J. Electron Spectrosc. Related Phenemena, 1983, 29, 301.

19 N.A. Avery, Surf. Sci., 1985, 163, 357.

20 J.E. Demuth, H. Ibach and S. Lehwald, Phys. Rev. Lett., 1986, 128, 208.

21 S. Lehwald and H. Ibach, Surf. Sci., 1979, 89, 425.

22 M.A. Chesters, S.F. Parker and R. Raval, J. Electron Spectrosc. Related Phenomena, 1986, 39, 155.

23 G.D. Waddill and L.L. Kesmodel, Chem. Phys. Lett., 1986, 128, 208.

24 R. Raval and M.A. Chesters, Surf. Sci., 1989, 219, L505.

25 R. Raval, M.A. Pemble and M.A. Chesters, Surf. Sci., 1989, 210, 187.

26 F. Al-Mashta, C.U. Davanzo and N. Sheppard, J. Chem. Soc., Chem. Commun., 1983, 1258.

27 J. Kondo, K. Domen, K. Maruya and T. Onishi, J. Chem. Soc., Faraday Trans., 1990, 86, 3021.

28 Y. Maehashi, K. Maruya, K. Domen, K. Aika and T. Onishi, Chem. Lett., 1984, 747.

29 R.L. Burwell Jr, A.B. Littlewood, M. Cardew, G. Pass and C.T.H. Stoddart, J. Amer. Chem. Soc., 1960, 82, 6272.

30 G. Pass A.B. Littlewood and R.L. Burwell Jr, J. Amer. Chem. Soc., 1960, 82, 6281.

31 C.T.H. Stoddart, G. Pass and R.L. Burwell Jr, J. Amer. Chem. Soc., 1960, 82, 6284.

32 A.B. Littlewood and R.L. Burwell Jr, J. Amer. Chem. Soc., 1960, 82, 6287.

33 M. Cardew and R.L. Burwell Jr. J. Amer. Chem. Soc., 1960, 82, 6289.

34 M.G. Wisnosky, D.F. Eggers, L.R. Fredrickson and J.C. Decius, J. Chem. Soc., 1983, 79, 3505.

35 T. Shimanouchi, "Tables of Molecular Vibrationam Frequencies", NSRDS-NBS, 1972, No. 39.

Chapter 5

Infrared Studies of Ethene Hydrogenation over ZrO_2

5-1 Abstract

The reaction mechanism of ethene hydrogenation over ZrO_2 was examined through detailed analysis of IR spectra as well as with volumetric experiment results at the temperature between 197 and 370 K. From the infrared studies it was found that hydrogen is activated on the site where ethene is preadsorbed and that dissociatively adsorbed hydrogen species are not reactive with ethene in gas phase. The intermediate species such as an ethyl group was not identified. Instead, ethene was found to be first hydrogenated to form "side-on" adsorbed ethane followed by a transformation into "end-on" ethane. Kinetic studies supported the idea that the reaction scheme observed by IR spectroscopy is certainly the main route of the catalytic ethene hydrogenation over ZrO_2 at the investigated temperatures.

5-2 Introduction

Studies of hydrogenation of unsaturated hydrocarbons, especially ethene which is the simplest alkene, have been carried out over many metal catalysts as one of the fundamental catalytic reactions[1,2]. At the beginning of this century, several mechanisms for ethene hydrogenation were proposed by researchers like Horiuti and Polanyi[3], Farkas and Farkas[4], and Twigg and Rideal[5]. These mechanisms were examined by the observation of the adsorbed species during the reaction over supported metals with infrared (IR) spectroscopy. IR spectroscopy was the only method to observe the adsorbed species directly in that period.

Recently accompanied with the ultra high vacuum (UHV) technique, it has become possible to observe the adsorbed species on clean and well-defined metal surfaces by means of electron spectroscopies such as low energy electron diffraction (LEED) and high resolution electron energy loss spectroscopy (HREELS) as well as other methods which do not need the UHV system as temperature programmed desorption (TPD), infrared reflection absorption spectroscopy (IRAS) and conventional IR transmission spectroscopy. The adsorbed ethene species have been found by numerous investigations to exist as π-bonded[6], di-σ-bonded[3] ones and/or ethylidyne[7].

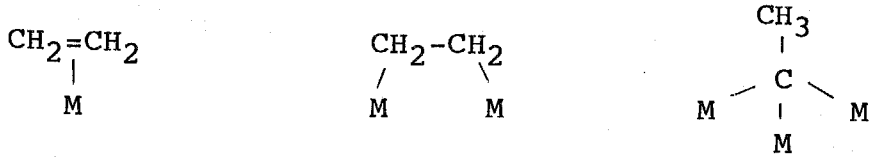

π-bonded ethene, di-σ-bonded ethene, ethylinyne.

Although ethylidyne is the most stable species derived from ethene adsorption[8], it was not observed during in situ hydrogenation[9] and its hydrogenation rate was about 1/3 to 1/2 of that of the steady state value of the reaction[9]. Godbey et al.[10] first suggested a reaction mechanism in which ethylidyne is employed as a transporter of the hydrogen species over Pt(111) surface. On the other hand, Beebe et al.[9] suggested that ethylidyne is only a spectator for ethene hydrogenation over Pt/Al_2O_3. In this way, the real mechanism and the intermediate during steady state of this reaction over metals still seems to be obscure.

The activity of metal oxides for ethene hydrogenation was first found by Burwell et al. over Cr_2O_3[11-15] followed by that over Al_2O_3[16-18], ZnO[19-25] and others[27]. In these early researches several proposals were made; 1) the reaction mechanism might be simpler on metal oxides than on metals[11,18,20,24]; 2) H_2 might be supplied from gas phase[17]; and 3) there are at least two activated sites: the stronger site where the polymerization takes place and the weaker site which is effective for hydrogenation[18]. Kokes et al. obtained corresponding results to those described above and they combined the IR active adsorbed hydrogen species to ethene hydrogenation reaction[24]. They found the behaviour of the ZnH and the OH species derived from hydrogen adsorption and adsorbed ethene during ethene hydrogenation at room temperature. Their conclusion is

that a hydrogen atom is captured and first forms the ethyl species, and then it is finally hydrogenated to produce ethane. This mechanism was based on their observation of the ethyl species by IR.

Among the metal oxides ZrO_2 is shown to be a suitable material for IR studies of adsorbed species[28-33]. The in situ FT-IR studies have been performed as well as conventional volumetric studies in our laboratory. So far the IR studies of adsorption of hydrogen[30,31], ethene[32] and ethane[33] are presented in chapter 2, 3 and 4, respectively. In this chapter a coherent mechanism of ethene hydrogenation over ZrO_2 is proposed by means of IR study coupled with conventional kinetic studies.

5-3 Experimental

The ZrO_2, the system, the temperature control device and the pretreatment method used in this chapter are the same as those described in chapter 2. C_2H_4 and C_2H_6 (Takachiho, 99.9 % for both) was refined by vacuum distillation. C_2H_4 was introduced to the IR cell at a pressure of 5 Torr (666.6 kPa). Then the IR cell was evacuated to observe the reaction of adsorbed ethene and hydrogen in gas phase. H_2 was purified by passing it through a "Deoxo" and a liquid N_2 trap. D_2 was refined only with a liquid N_2 trap. The spectra were taken under the same condition as shown in the previous chapters.

The activation energies for the catalytic hydrogenation of ethene were obtained with a conventional closed gas circulation system with either 0.2 or 2.0 g of ZrO_2. 2.0 g of the catalyst was used for the reaction over the OH modified ZrO_2 because the reaction rate was very slow. The same pretreatment of the catalyst were performed as those for IR study for consistent comparison of the obtained values.

5-4 Results

5-4-1 Ethene Adsorption

The details of the behaviour of adsorbed ethene species are described in chapter 3. Briefly, two different species, π-bonded and s(strongly)-π-bonded ethene were identified with IR spectroscopic analysis. In fig. 5-1(a) the spectrum of s-π-bonded ethene at room temperature is shown with its characteristic bands at 2987, 2960 (CH stretch.), 1604 (C=C stretch.) and 1338 cm^{-1} (CH_2 asy. scis.) Also the common bands with ordinary π-bonded species at 1446 (CH_2 sym. scis.) and 1009 cm^{-1} (CH_2 out of plane bend.) were observed.

As the temperature decreases π-bonded ethene becomes dominant because its amount increased, while the amount of the s-π-bonded one keeps its amount constant below 240 K. A mixed spectrum of both π-bonded and s-π-bonded species taken at 203 K is described in fig.(b). Here π-bonded ethene is observed with bands at 3097, 3072, 3003, 2972 (CH stretch.), 1961 (overtone of the band at 995 cm^{-1}), 1446 (CH_2 scis.) and 995 cm^{-1} (CH_2 out of plane bend.). Quantitative analysis from the IR data in this study was performed with use of the band at 1446 cm^{-1} for total amount of adsorbed ethylene and that at 1338 cm^{-1} for the amount of s-π-bonded ethene. The amount of π-bonded species was estimated from both peaks as previously described.

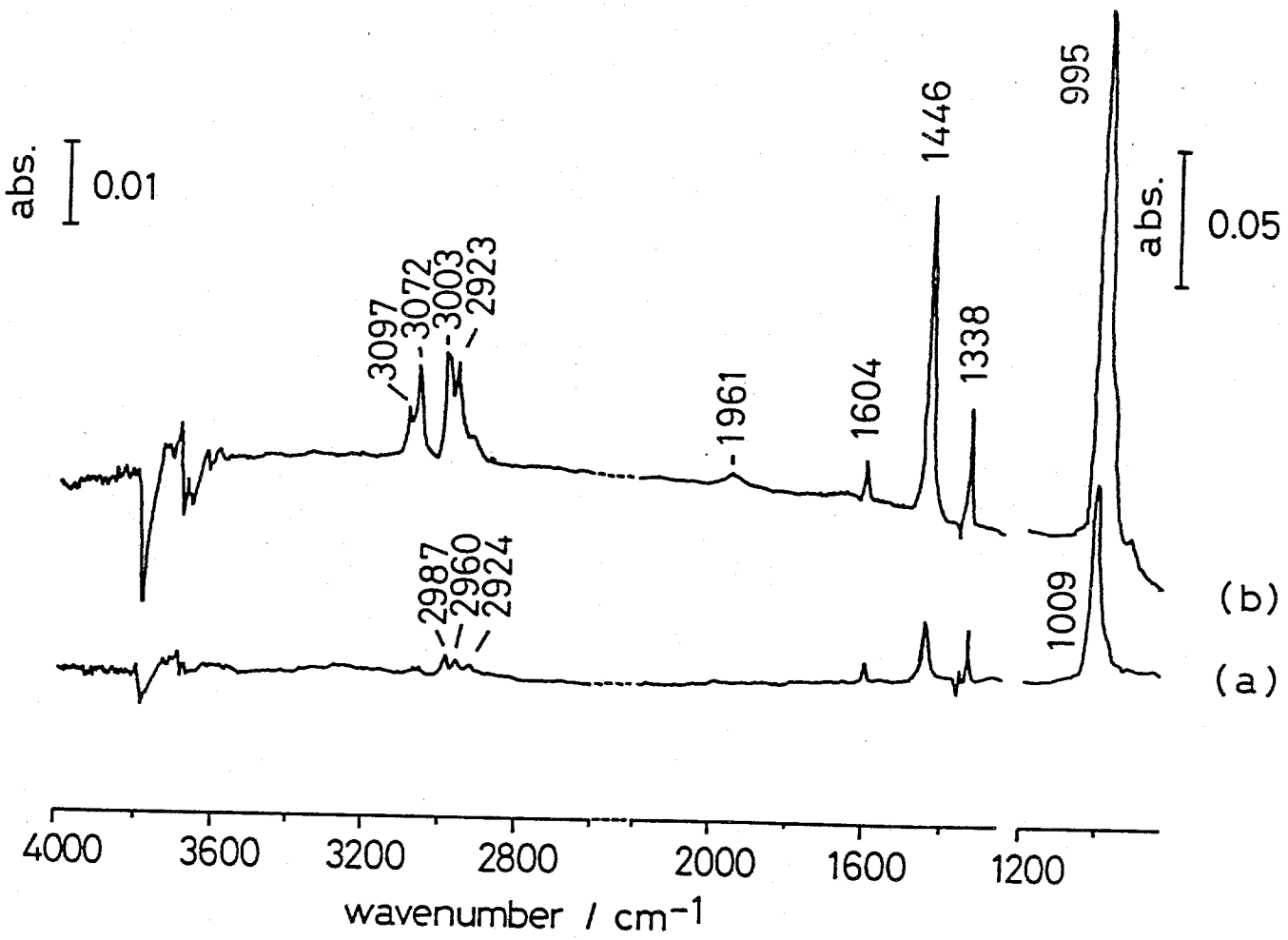

Fig. 5-1 IR spectra of adsorbed ethene on ZrO_2:(a) 298 K and (b) 203 K.

5-4-2 Reaction of Adsorbed Hydrogen with Ethene Gas

As it is already presented in chapter 2, hydrogen molecules are adsorbed on ZrO_2 in five different ways:

1) associative adsorption below 173 K (4029 cm^{-1});

2) homolytic dissociative adsorption to produce $Zr<^{H}_{H}$ species (1540 cm^{-1}) observed below 373 K;

3) heterolytic dissocistive adsorption which forms ZrH (1562 cm^{-1}) and OH (3668 cm^{-1}) species between 223 and 373 K;

4) bridged ZrHZr species (1371 cm^{-1}); and

5) the adsorption which generates two OH species above room temperature (3778 and 3668 cm^{-1}).

On metal oxides metal-H species due to the heterolytic dissociative adsorption ($\begin{matrix} H & H \\ | & | \\ M-O \end{matrix}$ species) could well be considered to be the most reactive species for hydrogenation. To monitor the reactivity of ZrH-OH species, the reaction of adsorbed ZrH-OH species and ethene in the gas phase was observed. This was done by diluting ethene with He so that the absorption bands of gas phase ethene would not be mixed with the spectra of adsorbed species. Then this was introduced to ZrH-OH species at 193 K. At this temperature an overall ethene hydrogenation proceeds. No bands suggesting newly produced species were observed, instead, ethene adsorption was observed suggesting hydrogen replacement. The change of peak intensities of ZrH species (1562 cm^{-1}), s-π-bonded ethene (1338 cm^{-1}) and π-bonded ethene (estimated by the bands at 1446 and 1338 cm^{-1}) are plotted in fig. 5-2.

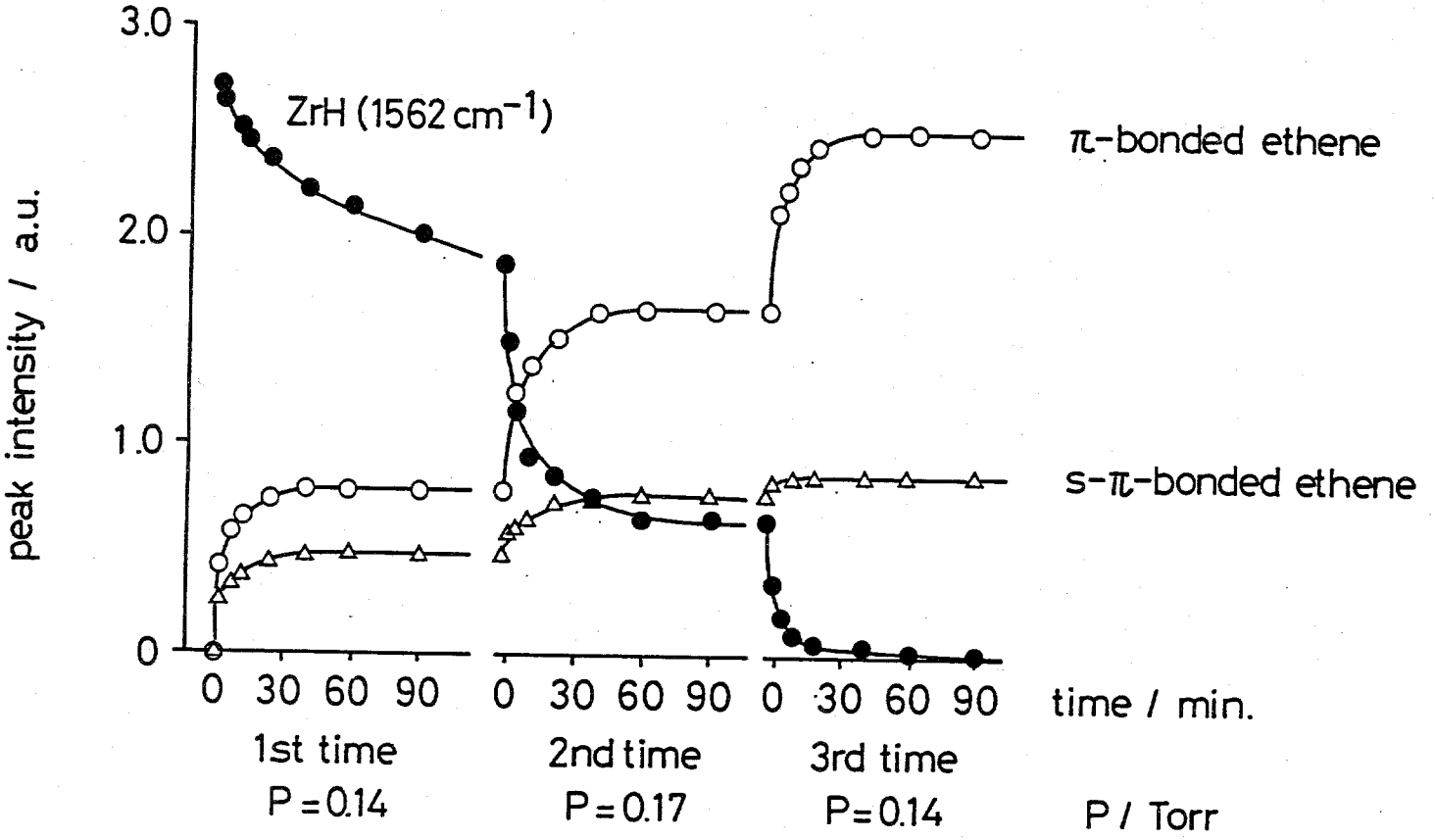

Fig. 5-2 The time course of the adsorbed species during ZrH-OH + C_2H_4(g), see text.

A good correspondence of decrease of ZrH and increase between both π- and s-π-bonded ethene indicates that ethene in the gas phase does not react with the ZrH species but just adsorbs on the sites by removing the adsorbed hydrogen. If intermediate species such as ethyl species ($-C_2H_5$) or the product (C_2H_6) had been produced, it should have had concentration high enough to be observed with IR spectroscopy, and ethane remains on the surface at this temperature, as will be shown below. Nonreactivity of dissociatively adsorbed hydrogen is also suggested by the fact that ethene adsorption on the surface without hydrogen species at the same condition gave the same adsorption behaviour as those shown in fig. 5-2. Therefore, it must be concluded that ZrH-OH species are not the intermediate nor the reactive species for ethene hydrogenation over ZrO_2.

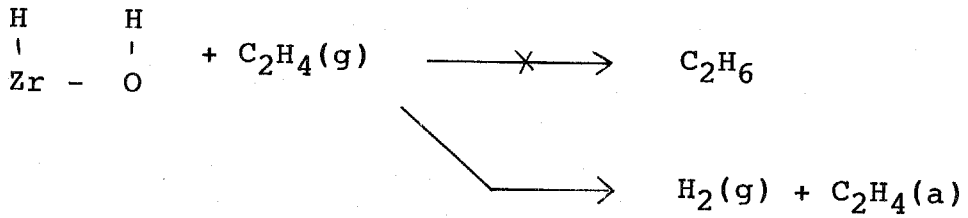

Moreover, several supporting evidences for this conclusion based on some kinetic data are presented in the next section.

5-4-3 Reaction of Adsorbed Ethene and Hydrogen Gas

The transformation of spectra taken during hydrogenation of adsorbed ethene at 183 K with 100 Torr of H_2 are shown in fig. 5-3. All absorption bands attributed to adsorbed ethene [spectrum (a)] decreased as the reaction proceeded,

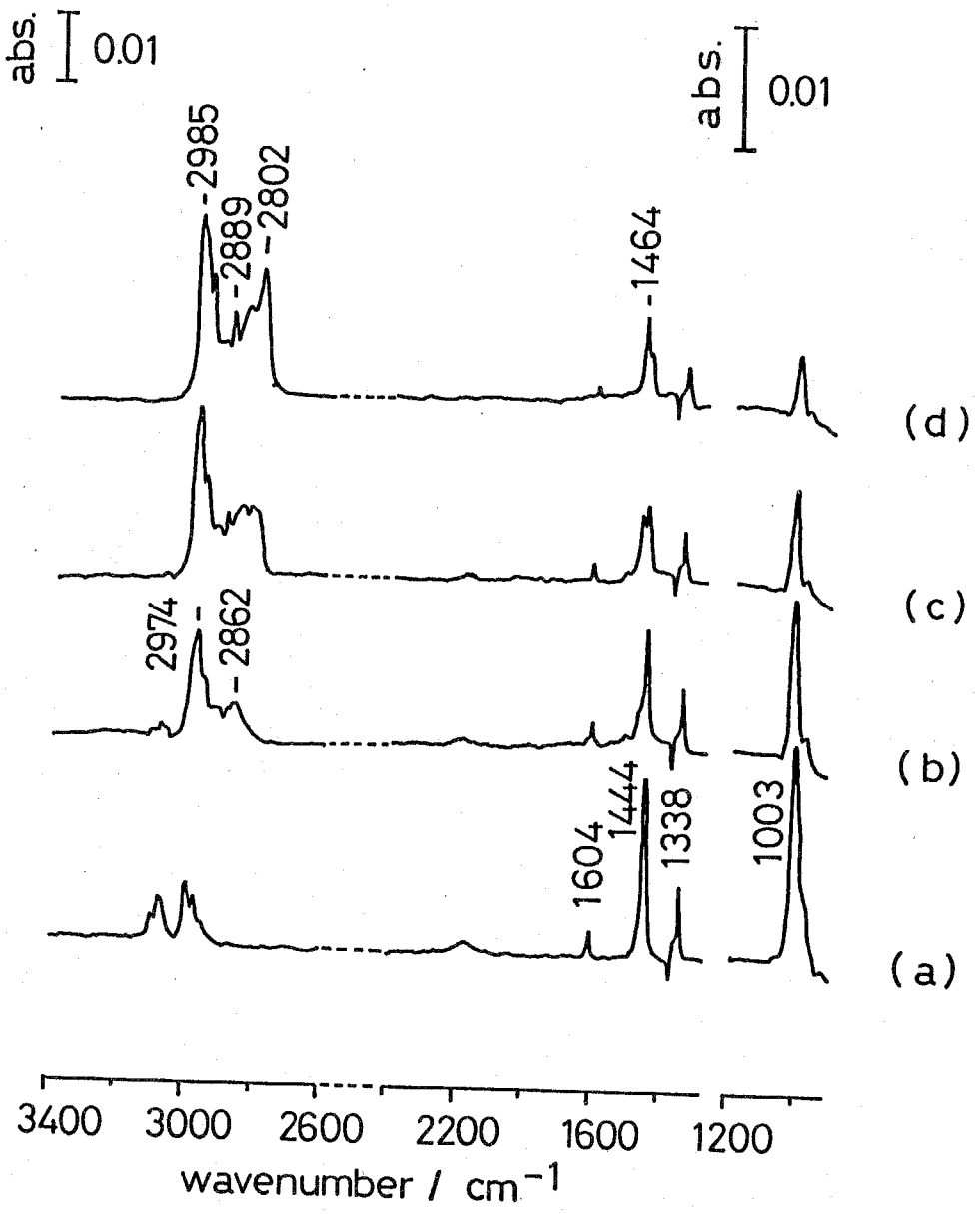

Fig. 5-3 IR spectra of adsorbed species during the reaction of C_2H_4(a) + H_2(g) at 183 K: (a) before introduction of H_2, (b) 2 h, (c) 6 h and (d) 9h.

i.e. both the π-bonded and the s-π-bonded ethenes species were hydrogenated together although the reaction rate of π-bonded species is much faster. Within two hours as observed in fig. 5-3(b), new bands appeared at 2974 and 2862 cm^{-1} in CH stretch. region and a shoulder of the band at 1444 cm^{-1}. As the hydrogenation proceeded [spectra (c) and (d)], several new bands appeared at 2985 and 2802 cm^{-1}. The shoulder on the band at 1446 cm^{-1} grew up to be the band at 1464 cm^{-1}. From these results, it is thought that the adsorbed ethene is finally transformed to a species of the spectrum (d) via that of the spectrum (b). It should be also noted that no Zr-H species were observed during the reaction. The IR bands of these species are expected to appear between 1560 and 1540 cm^{-1}.

In fig. 5-4 spectra of adsorbed CH_3CH_3 and CH_2DCH_2D are illustrated; the end-on species above and the side on species below. Details of the structure of adsorbed ethane have been presented in chapter 4. The end-on species is the only adsorbed species between 243 and 193 K at which the side-on species is not formed. Below 193 K, however, the side-on species is observed and becomes the dominant one as the temperature decreases. At ca. 190 K mixed spectra of the side-on and the end-on ethane are observed. It was also observed that the end-on species gave band shifting of the CH stretch. modes due to stronger interaction of the the end-on species with the surface. The observed band and its shoulder in the CD stretch. for

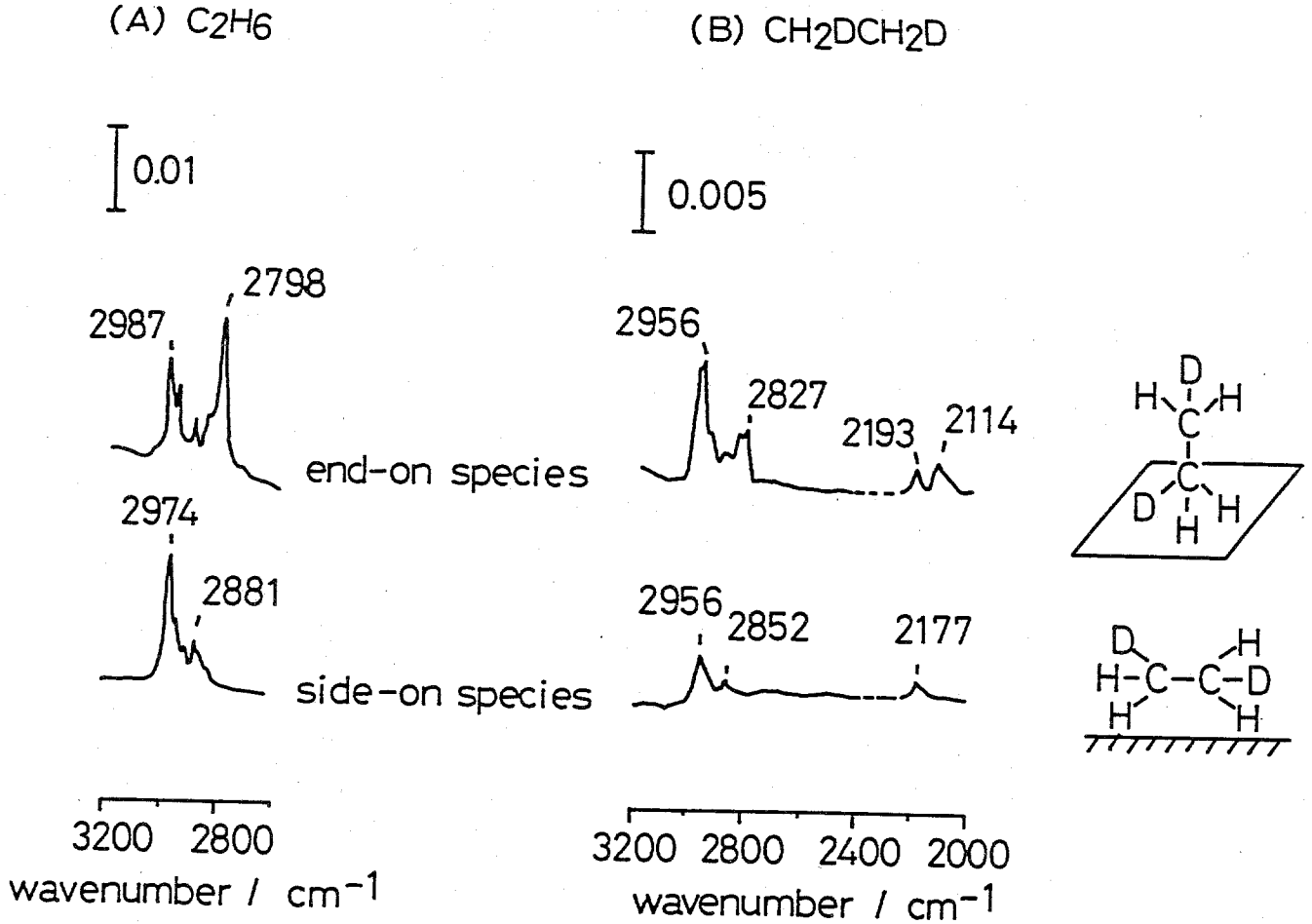

Fig. 5-4 IR spectra of adsorbed ethane on ZrO_2 together with adsorption models.

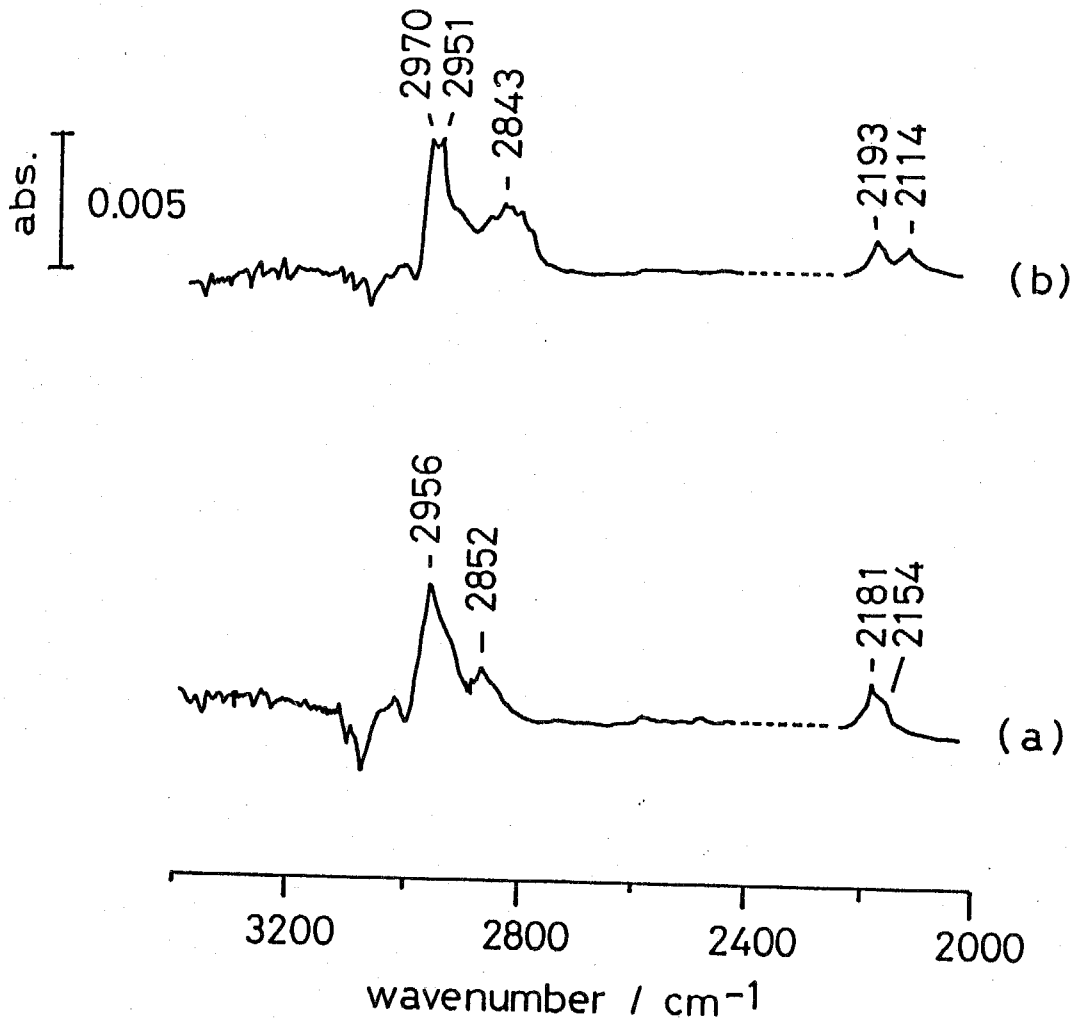

5-5 IR spectra of adsorbed species during the reaction of C_2H_4(a) + D_2(g) at 193 K: (a) initial change of the spectra, reaction of 1 h / before D_2 introduction and
(b) final change of the spectra, reaction of 4 h / 3 h.

the side-on species in fig. 5-4(B) could be attributed to both symmetric and asymmetric stretch. which appear to be quite different from the CD stretch. bands of the end-on species. To compare the spectra of adsorbed CH_2DCH_2D in fig. 5-4(B), spectra were taken during deuterization of adsorbed ethene (fig. 5-5). The deuterization was performed at 193 K with a 100 Torr of D_2. The spectra in fig. 5-5 are described in ratio spectra; (a), [after 1 hr of reaction]/[before D_2 introduction] and (b), [after 4 hr]/[after 3 hr]. The inverted bands are due to a decreased species in progress of the reaction and the upward species are the formed products. At the initial stage whose change is exhibited by fig. 5-5(a), only one CD band with a shoulder band was observed. On the other hand, as the reaction proceeded two distinct CD bands were observed at 2193 and 2114 cm^{-1} with the CH band shifting to lower frequency. From the spectra taken during the reaction, which are shown in figs. 5-3 and 5-5, it might be regarded that two hydrogen atoms become involved stepwise. However, these spectra in fig. 5-5 should be compared with those of the adsorbed CH_2DCH_2D in fig. 5-4(B). One can easily notice that fig. 5-5(a) is very similar to the spectrum of the side-on ethane in fig. 5-4(B) and fig. 5-5(b) to the end-on species. Therefore, it should be concluded from these observations of IR spectra that adsorbed ethene is first hydrogenated to the side-on adsorbed ethane and then transformed to the stabler end-on species (scheme 5-1). The stepwise

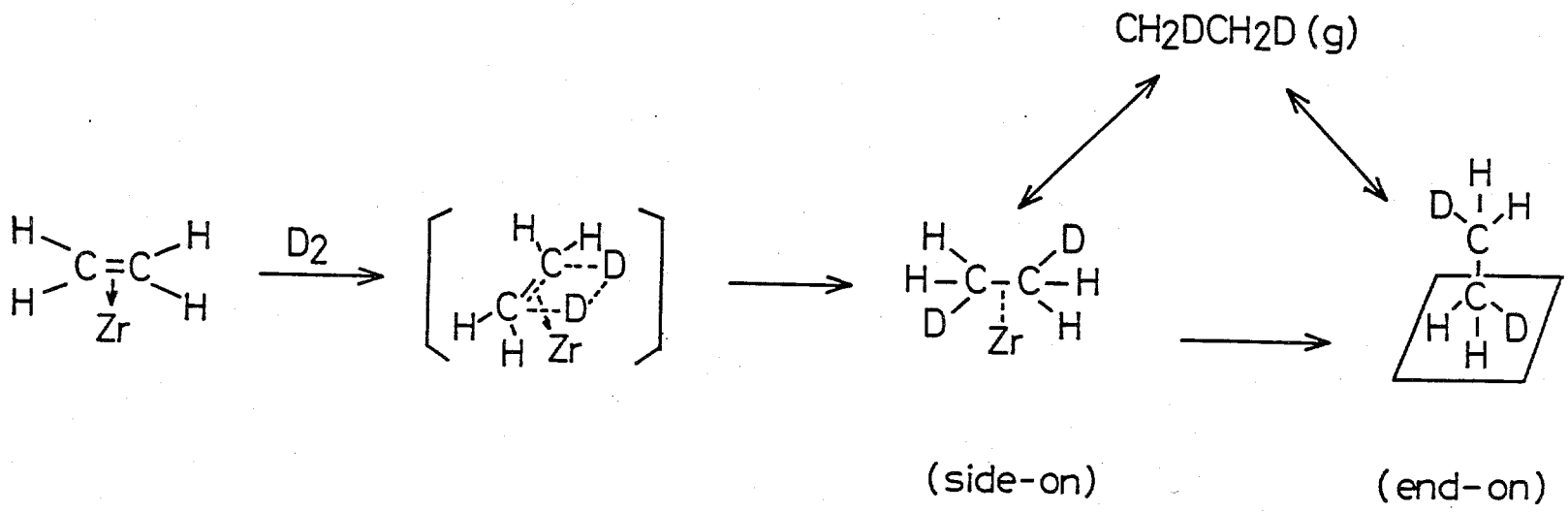

Scheme 5-1 The proposed mechanism of ethene hydrogenation over ZrO_2.

conversion from the side-on species to the end-on one during the hydrogenation is supported by the fact that the end-on species were constantly produced even when adsorbed ethene scarcely remained at the final stage of the reaction.

5-4-4 Activation Energy of Adsorbed Ethene Hydrogenation

Activation energies for hydrogenation of adsorbed ethene over ZrO_2 were obtained by measuring the decrease rate of the peak intensity of the band at 1446 cm^{-1} at various temperatures. The data for the s-π-bonded and π-bonded ethene are preferred to being separately acquired with use of both bands at 1446 and 1338 cm^{-1}. Unfortunately, however, the error in the activation energy obtained from the band at 1338 cm^{-1} was too large to estimate precisely because of the interference of the reverse band close to it. Therefore, activation energies of hydrogenation of adsorbed ethene were obtained from the band at 1446 cm^{-1} which includes both species. Two measurements were carried out for irreversibly adsorbed species at 273 and 223 K, respectively. The obtained value for the species adsorbed irreversibly at 273 K is 7.3 $\pm$ 0.3 kcal/mol, while the value for irreversible species at 223 K is 5.4 $\pm$ 0.3 kcal/mol. This means that the ethene species adsorbed below 273 K may have a smaller activation energy than that of 273 K. In fig. 5-6, amounts of irreversibly adsorbed ethene at various temperatures are shown with and without pretreatment with H_2O at 673 K. From fig. 5-6, as has

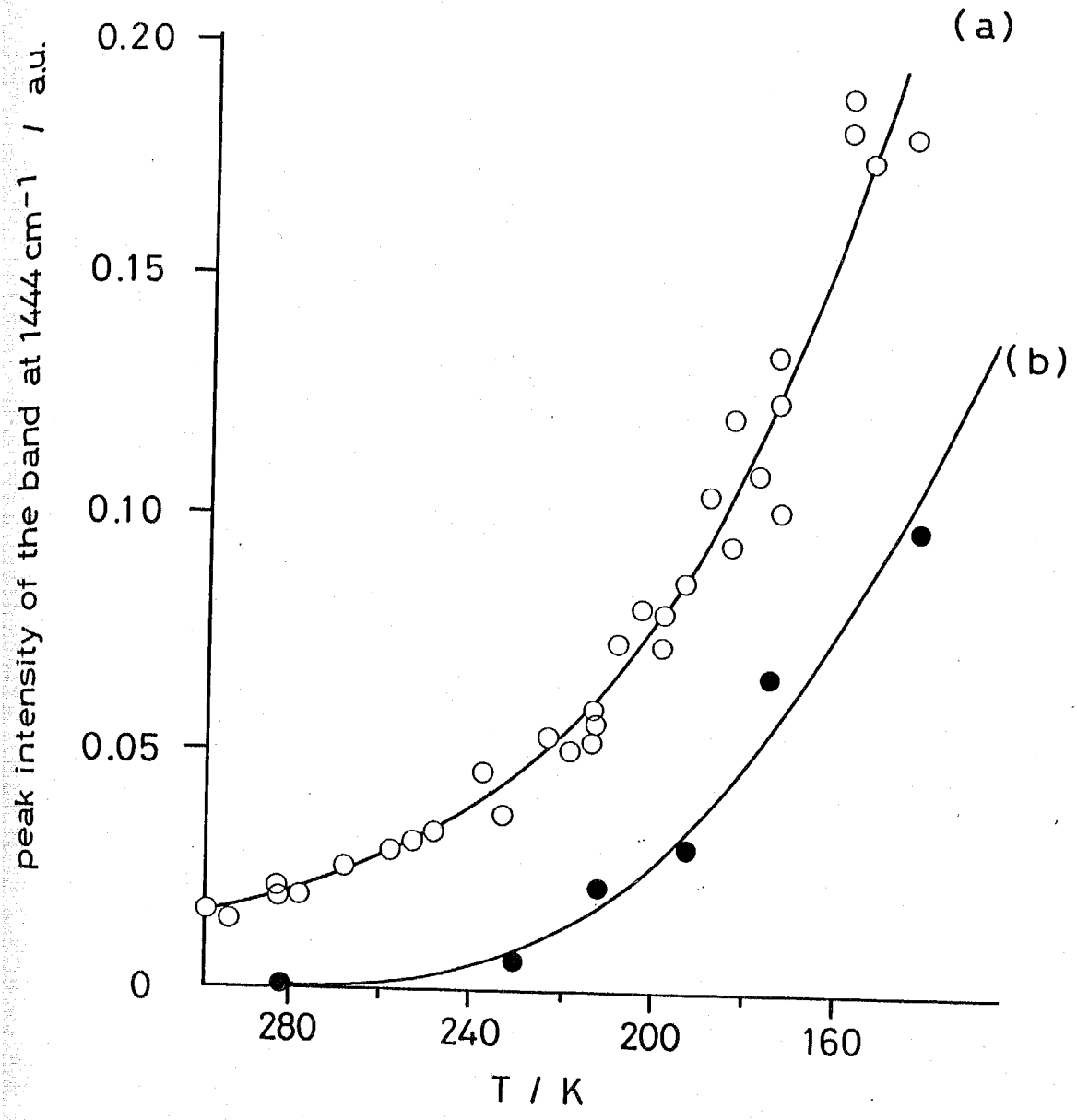

Fig. 5-6 Temperature dependence of the adsorbed amount of ethene and the effect of surface OH:
(a) adsorption on ZrO_2 after usual pretreatment and
(b) adsorption on ZrO_2 with surface OH species produced by H_2O at 673 K.

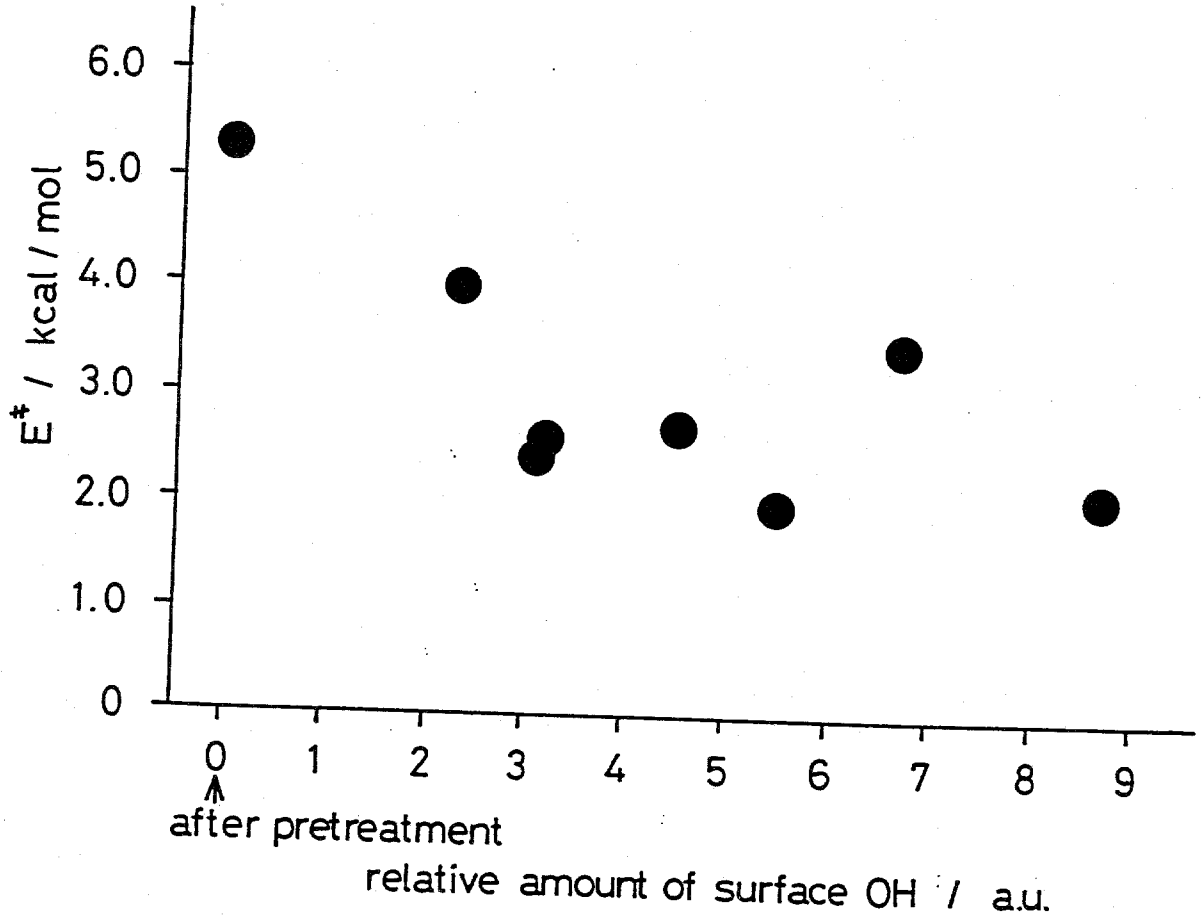

Fig. 5-7 Changes of activation energies for hydrogenation of adsorbed ethene as a function of the amount of surface OH species.

already been described in chapter 3, the adsorption sites blocked by OH species produced by H_2O treatment is mainly for ethene stable at higher temperature (>270 K). The activation energies for hydrogenation of adsorbed ethene were obtained on the ZrO_2 with various amounts of surface OH. The results are given in fig. 5-7. When the amount of surface OH increased, the reaction rate and the activation energy decreased. Therefore it is concluded that the more strongly the ethene adsorbs, the larger the activation energy for hydrogenation it has. No detectable isotope effect was observed between hydrogenation of adsorbed ethene with H_2 and D_2.

5-4-5 Catalytic Hydrogenation of Ethene

Kinetic data of the catalytic cycle were obtained to assess the kinetics of adsorbed ethene hydrogenation as observed by IR. Pressure dependence of the amount of adsorbed ethene at 300 K is shown in fig. 5-8, where the amount of irreversibly adsorbed ethene is also indicated. The amounts of various kinds of adsorbed ethene at 300 and 200 K are summarized in table 5-1. The irreversible species correspond to the species observed by IR spectroscopy after evacuation. The difference from species which exist under equilibrium state indicates reversible species. The adsorbed amounts were also measured for OH preadsorbed-ZrO_2. Surface OH groups were produced by H_2O at 673 K, which gave the same surface as seen in fig. 5-6 (b). The different amounts of irreversible species on as

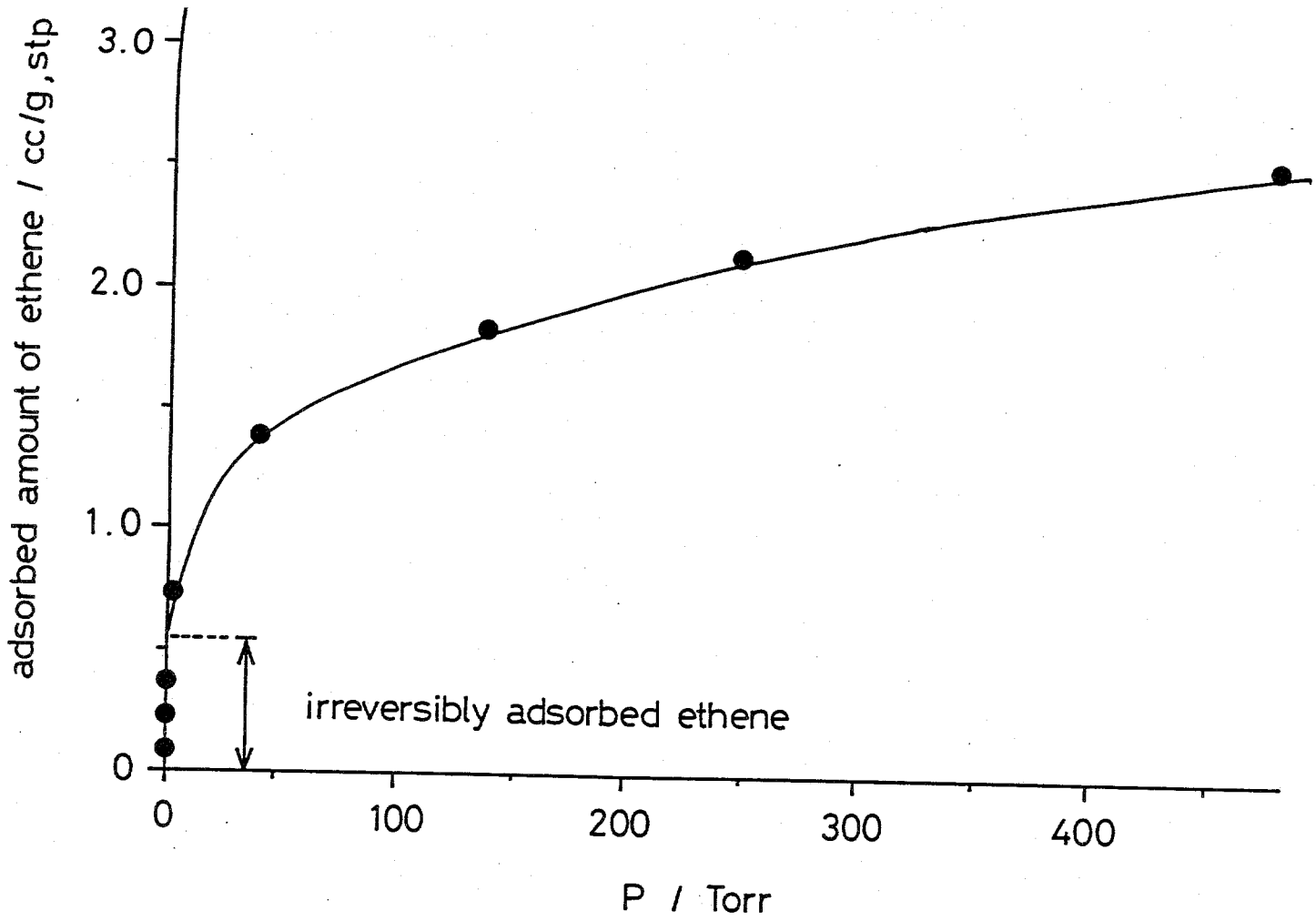

Fig. 5-8 Isotherm of ethene at 300 K.

Table 5-1 Adsorbed amount of ethene on ZrO_2 (cc/g, stp)

	equilibrium species at 100 Torr		irreversible species		irreversible species on OH preadsorbed surface
200 K	4.60	2.56	2.04	1.08	0.98
300 K	1.62	1.07	0.55	0.51	0.04

	reversible species	blocked species by surface OH species	
strength of adsorption	3	1	2

ordinary-treated-ZrO_2 and OH-preadsorbed-ZrO_2 indicate the amount of the blocked species by surface OH groups and which should correspond to the difference between (a) and (b) in fig. 5-6. From comparison of the results shown in both fig. 5-6 (obtained by IR spectra) and table 1 (obtained by volumetric measurements), it is noticed that those data for irreversibly adsorbed species show good quantitative agreement in the ratio of the amounts at 200 and 300 K.

Pressure dependence of this reaction was 1st order for H_2 and 0th order for C_2H_4 below 300 K. The result that the reaction does not depend on the pressure of ethene means that mainly hydrogenated species during the steady state of the reaction are irreversibly adsorbed. Also the 1st order for H_2 pressure in this reaction means that the rate determining step is the activation of hydrogen.

The activation energies for the overall ethene hydrogenation were also obtained. The values both for ordinary-preatreated-ZrO_2 and that for the OH-preadsorbed-ZrO_2 were 5.7 $\pm$ 0.4 and 5.8 $\pm$ 0.4 kcal/mol, respectively. Although there was no difference in these activation energies (obtained over OH-preadsorbed-ZrO_2 and the ordinary-treated-ZrO_2), the former reaction rate was about 2-6 % of the latter. The reaction rate, r, may be expressed as

$$r = A\ P_{H_2}\ \theta_{et} \exp(-\frac{E^*}{RT})$$

where A : pre-exponential factor

P_{H_2} : pressure of H_2

θ_{et} : coverage of ethene

R : gas constant

T : temperature

$E^{\ddagger}$: activation energy

The activation energies for the catalytic ethene hydrogenation presented above were measured at the same partial pressures of hydrogen and ethene. However, the irreversibly adsorbed amount of ethene which is catalytically hydrogenated during the reaction, θ_{et}, is dependent on the temperature as shown in fig. 5-6. Therefore, the activation energy for hydrogenation of adsorbed ethene was normalized with θ_{et} and gave the value of 8.1 $\pm$ 0.5 kcal/mol.

These values fairly well correspond to those obtained by IR spectroscopy for the irreversibly adsorbed ethene hydrogenation within the experimental accuracy. Therefore, the irreversibly adsorbed ethene hydrogenation studied in this work is regarded as a main route of the catalytic hydrogenation process, at least below room temperature.

5-5 Discussion

From the observation of IR spectroscopy we propose a mechanism of hydrogenation of adsorbed ethene over ZrO_2 as shown in scheme 5-1. In scheme 5-1 adsorbed ethene and both side-on and end-on ethane were directly observed in IR spectra. Then, how is hydrogen activated? Heterolytic dissociative adsorption of hydrogen which results in ZrH-OH pair species seems to be the most probably, as proposed on ZnO by Kokes et al[24]. The experimental results as mentioned and shown in fig. 5-2, the reaction between ZrH-OH pair species and gaseous C_2H_4 resulted in small amount of C_2H_6 formation. Instesd, just the replacement between adsorbed hydrogen and gaseous ethene was observed. In addition to this, the other characteristics of the heterolytic dissociative adsorption should be mentioned. The activation energies for this adsorption of H_2 and D_2 are 9 ± 0.5 and 10 ± 0.5 kcal/mol, respectively[31]. If ethene was hydrogenated by ZrH-OH species the activation energy is expected to be larger than 9 kcal/mol and an isotope effect should be observed between H_2 and D_2. However, the experimental values obtained in the present work were obviously less than 9 kcal/mol. Actually, at lower temperatures, e.g. 180 K, adsorbed ethene hydrogenation proceeds much faster than the heterolytic H_2 adsorption. These facts lead to a reaction mechanism without heterolytic dissociative adsorption of hydrogen.

The activation pathway of hydrogen is further inferred as follows:

1) No hydrogen species was observed during the adsorbed ethene hydrogenation. This suggests that even if ethyl species do exist, their life time should be too short to be observed by IR spectroscopy, otherwise the remaining hydrogen species, ZrH or OH species, would be observed.
2) Hydrogenation by D_2 generates only CH_2DCH_2D below 300 K, which implies that the first step of hydrogen insertion, if exists, is irreversible or that two hydrogen atoms are associatively involved.
3) If ethyl species are produced, the circumstances of two carbon "atoms" in ethyl group would be rather different, and hydrogenated product, ethane, is also expected to be the "end-on" form because it is unlikely that "end-on" ethane transforms to unstable "side-on" species. The experimental fact is that initially produced ethane was a "side-on" one. This means that hydrogenation is speculated to proceed with adsorbed ethene keeping its C-C axis parallel to the surface. Therefore, it is reasonable to conclude that hydrogen molecules are activated on the sites which are modified by preadsorbed ethene, and both hydrogen atoms are instantaneously involved in the products, ethane. It is not clear whether two hydrogen atoms during this step work in an equivalent manner or not, and the activated complex described in scheme 5-1 is only a speculation.

The strongest support for this mechanism (scheme 5-1) is that the amount of adsorbed ethene is much larger than

that of dissociatively adsorbed hydrogen on a naked ZrO_2 surface and all of those adsorbed ethene have the possibility to be hydrogenated at low temperature where dissociative adsorption of H_2 does not actually proceed as observed by IR spectroscopy. A similar mechanism has been already proposed in early study of ethene hydrogenation over Al_2O_3 by Sinfelt[17]. He suggested that hydrogen would be supplied directly from gas phase without hydrogen activation on the surface as the first step.

The mechanism mentioned above differs from the proposed mechanism by Kokes et al. over ZnO[24] which is described as follows:

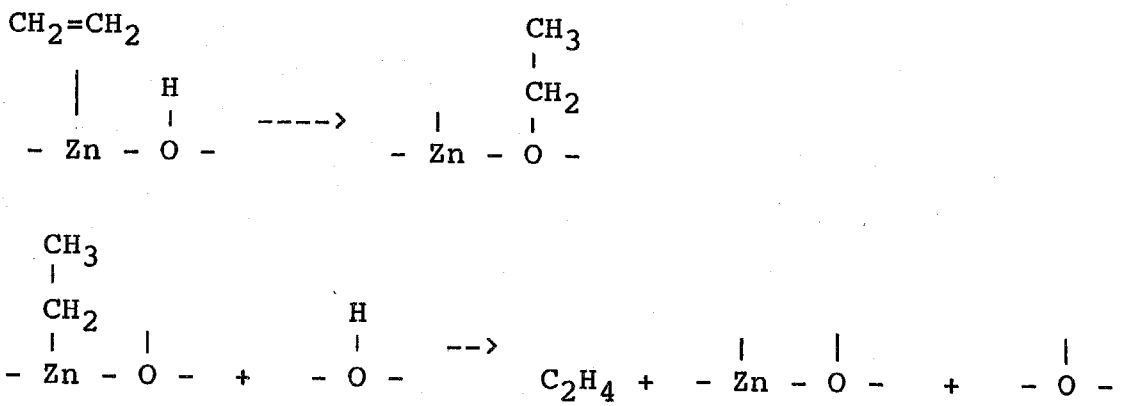

Since the nature of heterolytic dissociative adsorption of H_2 gives rise to the metal-H, and the O-H species is not the same on ZnO and ZrO_2, the two mechanism cannot easily be compared. For instance, hydrogen species were observed during ethene hydrogenation over ZnO while not over ZrO_2. However, the IR spectrum of the intermediate species which they assigned to ethyl species[24] looks very similar to that of side-on ethane over ZrO_2. It should be noted that in case of propene hydrogenation over ZnO, heterolytic

adsorbed hydrogen is not involved in the reaction pathway, which was proposed by Tanaka et al. by means of isotope study[25,27]. Detailed IR analysis of adsorbed ethane on ZnO will be necessary to directly compare the two mechanisms.

Finally, it would be emphasized that in this series of studies a new route of activation process of hydrogen appears to be induced by ethene adsorption, which cannot be expected only by adsorption study of hydrogen.

5-6 References

1 J. Horiuti and K. Miyahara, "Hydrogenation of Ethylene on Metallic Catalysts", 1968, NBS-NSRDS, No. 13.

2 L.H. Little, "Infrared Spectra of Adsorbed Species", Academic Press, London, 1966.

3 J. Horiuti and M. Polanyi, Trans. Faraday Soc., 1934, 30, 1164.

4 A. Farkas and L. Farkas, J. Amer. Chem. Soc., 1938, 60, 22.

5 C.H. Twigg and E.K. Rideal, Proc. Roy. Soc., 1939, A171, 55., Proc. Roy. Soc., 1941, A178, 106., Trans. Faraday Soc., 1939, 35, 934.

6 J.J. Rooney and G. Webb, J. Catal., 1964, 3, 488.

7 L.L. Kesmodel, L.H. Dubois and G.A. Somorjai, Chem. Phys. Lett., 1978, 56, 267.

8 R.J. Koestner, M.A. Van Hove and G.A. Somorjai, J. Phys. Chem., 1983, 87, 203, and the references therein.

9 T.P. Beebe and J.T. Yates, Jr., J. Amer. Chem. Soc., 1986, 108, 663.

10 D. Godbey, F. Zaere, R. Yates and G.A. Somorjai, Surf. Sci., 1986, 167, 150.

11 R.L. Burwell, Jr., A.B. Littlewood, M. Cardew, G. Pass and C.T.H. Stoddard, J. Amer. Chem. Soc., 1960, 82, 6272.

12 G. Pass, A.B. Littlewood and R.L. Burwell, J. Amer. Chem. Soc., 1960, 82, 6281.

13 C.T.H. Stoddard, G. Pass and R.L. Burwell, J. Amer. Chem. Soc., 1960, 82, 6284.

14 A.B. Littlewood and R.L. Burwell, J. Amer. Chem. Soc., 1960, 82, 6287.

15 M. Cardew and R.L. Burwell, J. Amer. Chem. Soc., 1960, 82, 6289.

16 J.L. Carter, P.J. Lucchesi, J.H. Sinfelt and D.J.C. Yates, Proc. 3rd Intern. Congr. Catal., (North Holland, Amsterdam), 1964, vol. 1, p. 644.

17 J.H. Sinfelt, J. Phys. Chem., 1964, 68, 232.

18 Y. Amenomiya, J.H.B. Chenier and R.J. Cvetanovic, J. Catal., 1967, 9, 28.

19 D. Narayana, Jagdih Lal and V. Kesavulu, J. Phys. Chem., 1970, 74, 4150.

20 W.C. Conner, R.A. Innes and R.J. Kokes, J. Phys. Chem., 1968, 72, 6858.

21 A.L. Dent and R.J. Kokes, J. Phys. Chem., 1969, 73, 3772.

22 A.L. Dent and R.J.Kokes, J. Phys. Chem., 1969, 73, 3781.

23 A.L. Dent and R.J. Kokes, J. Amer. Chem. Soc., 1969, 91, 7207.

24 A.L. Dent and R.J. Kokes, J. Phys. Chem., 1970, 74, 3653.

25 T. Okuhara, T. Kondo and K. Tanaka, J. Phys. Chem., 1977, 81, 808.

26 D.L. Harrison, D. Nichollas and H. Steiner, J. Catal., 1967, 7, 359.

27 K. Tanaka, Adv. Catal., 1985, 23, 99.

28 J. Kondo, H. Abe, Y. Sakata, K. Maruya, K. Domen and

T. Onishi, J. Chem. Soc., Faraday Trans. 1, 1988, 84, 511.

29 T. Onishi, K. Maruya, K. Domen, H. Abe and J. Kondo, Proc. 9th Intern. Congr. Catal., (The Chemical Institute of Canada, Calgary, 1988), vol. 2, p. 507.

30 T. Onishi, H. Abe, K. Maruya and K. Domen, J. Chem. Soc., Chem. Commun., 1985, 617.

31 J. Kondo, Y. Sakata, K. Domen, K. Maruya and T. Onishi, J. Chem. Soc., Faraday Trans., 1990, 86, 397.

32 J. Kondo, K. Domen, K. Maruya and T. Onishi, J. Chem. Soc., Faraday Trans., 1990, 86, 3021.

33 J. Kondo, K. Domen, K. Maruya and T. Onishi, J. Chem. Soc., Faraday Trans., 1990, 86, 3665.

34 N. Kinoshita, K. Kido, K. Domen, K. Aika and T. Onishi, J. Chem. Soc., Faraday Trans. 1, 1986, 82, 2269.

Chapter 6

CO Hydrogenation over ZrO_2.

6-1 Summary

A reaction mechanism for catalytic hydrogenation of CO to produce methanol over ZrO_2 is proposed. To consider the reaction mechanism, adsorption studies of methanol, dimethylether and formic acid were performed. These basic studies were then combined with the study of adsorbed species during in situ CO hydrogenation. The evidence for the mechanism of CO hydrogenation over ZrO_2 comes from the observation by IR spectroscopy at low temperature (203-300 K), in addition to a possible mechanism at high temperature. The catalytic mechanism was found to proceed via formyl and dioxymethylene species. The unstable formyl species were identified in this study directly by FT-IR. The proposed mechanism to produce methanol over ZrO_2 via formate species was not found. Moreover, the rate determining step for methanol synthesis is thought to be the reaction pathway from dioxymethylene to the methoxide species.

6-2 Introduction

Methanol synthesis is a process of major industrial importance. It consists of hydrogenation of carbon monoxide or carbon dioxide according to the equations

$$CO + 2H_2 \Longleftrightarrow CH_3OH$$

where $\Delta H_{600\ K} = -100.46$ kJ/mol and $\Delta G_{600\ K} = +45.36$ kJ/mol;

$$CO_2 + 3H_2 \Longleftrightarrow CH_3OH + H_2O$$

where $\Delta H_{600\ K} = -61.59$ kJ/mol and $\Delta G_{600\ K} = +61.80$ kJ/mol. Methyl alcohol is one of the least thermodynamically favorable products of CO and CO_2 hydrogenation, since the formation of higher alcohols and hydrocarbons is accompanied with a more negative free-energy change. Dimethylether (DME) may also be produced by the dehydrogenation

$$2CH_3OH \Longleftrightarrow CH_3OCH_3 + H_2O$$

where $\Delta H_{600\ K} = -20.59$ kJ/mol and $\Delta G_{600\ K} = -10.71$ kJ/mol[1].

To avoid the formation of DME, higher alcohols and hydrocarbons, methanol synthesis requires a selective catalyst that rapidly executes the hydrogenation of CO or CO_2 to methyl alcohol but at the same time does not allow the reaction to proceed any further downhill on the thermodynamic free-energy scale. Based on general experience with catalysts in other hydrogenation reactions, this appears to be a formidable if not an impossible task. However, the industry now does have a catalyst which selectively steers the hydrogenation of the

synthesis gas, CO + CO_2 + H_2 in various proportions, to almost pure methanol. The activity, and consequently, the pressure and temperature range at which the methanol synthesis catalysts operate have undergone dramatic changes in the last two decades, which culminated in the commercialization of the so-called low-pressure processes operating at pressures less than 100 atm. The low-pressure catalysts invariably contain copper and a mixture of oxides such as ZnO-Al_2O_3 or ZnO-Cr_2O_3. Oxides V_2O_5, V_2O_3, ThO_2 and others have also been claimed as effective components of the low-pressure copper-based catalysts[2].

Investigations of synthesizing hydrocarbons and oxygenated hydrocarbons from CO and H_2 started with methane synthesis over Ni catalysts by Sabatier. Soon after, Fischer and Tropsch attracted a great deal of attention by discovering effective catalysts to produce higher hydrocarbons[3].

The process of synthesizing methanol from CO and H_2 can be regarded as an already established technique. CuO-ZnO catalysts are used for industrial purpose, under the condition of 473-573 K and 40-250 atm. Many catalysts are reported to be active for methanol synthesis[4-11]. However, the mechanism and the reaction intermediates are still a matter of controversy.

Several methods have been applied to reveal the mechanism of CO hydrogenation[12-15]. Infrared spectroscopy is considered to be an excellent technique to observe the

adsorbed species on the catalysts under the reaction conditions. In this chapter, IR analysis of probable adsorbed species during CO hydrogenation are presented first. Then, in situ studies both at high and low temperature are compared with the results of adsorption studies. Finally a probable mechanism of CO hydrogenation to produce methanol over ZrO_2 is proposed.

6-3 Experimental

The preparation of the catalyst and the experimental conditions are described in the chapter 2.

H_2 gas was refined through a Deoxo and a liquid-N_2 trap. D_2 was used without further purification. CO (Takachiho) and ^{13}CO (B.O.C. 99.7 %) were refined by passing them through a liquid-N_2 trap for 30 min. The CO_2 was prepared from the decomposition of $NaHCO_3$.

6-4 Results

6-4-1 Adsorption of CO and CO_2

CO Adsorption

IR spectra of adsorbed ^{12}CO and ^{13}CO on ZrO_2 below room temperature are shown in fig. 6-1,2,3 and 4. Both ^{12}CO and ^{13}CO were exposed to the catalyst at about 148 K. Subsequently evacuation was carried out in order to eliminate the IR absorption of gaseous CO. Then the sample was heated gradually.

The change of appearance in main ^{12}CO stretching bands depending on temperature is presented in fig. 6-1. Assuming that the molar absorption coefficient does not change, the adsorbed amount is considered to decrease upon heating. It must also be noted that the peak position shifted to higher wavenumber and that two bands were observed at intermediate temperatures (fig. 6-5). These two bands are at much higher frequencies compared with that of the gas phase CO (2143 cm^{-1}). They are assigned to the C=O stretching mode of adsorbed CO on the cationic surface sites. The shift to higher wavenumbers can be explained very well in terms of adsorption on Lewis acid sites (M^{x+}), because CO is expected to coordinate to cationic sites via a σ-donor bond. The σ-donor bond typically leads to positive CO stretching frequency shifts relative to the gas phase frequency, unless the coordination site is a low valent transition metal ion having significant d-electron density[16]. Recently, an attempt to correlate the carbonyl frequency shifts with

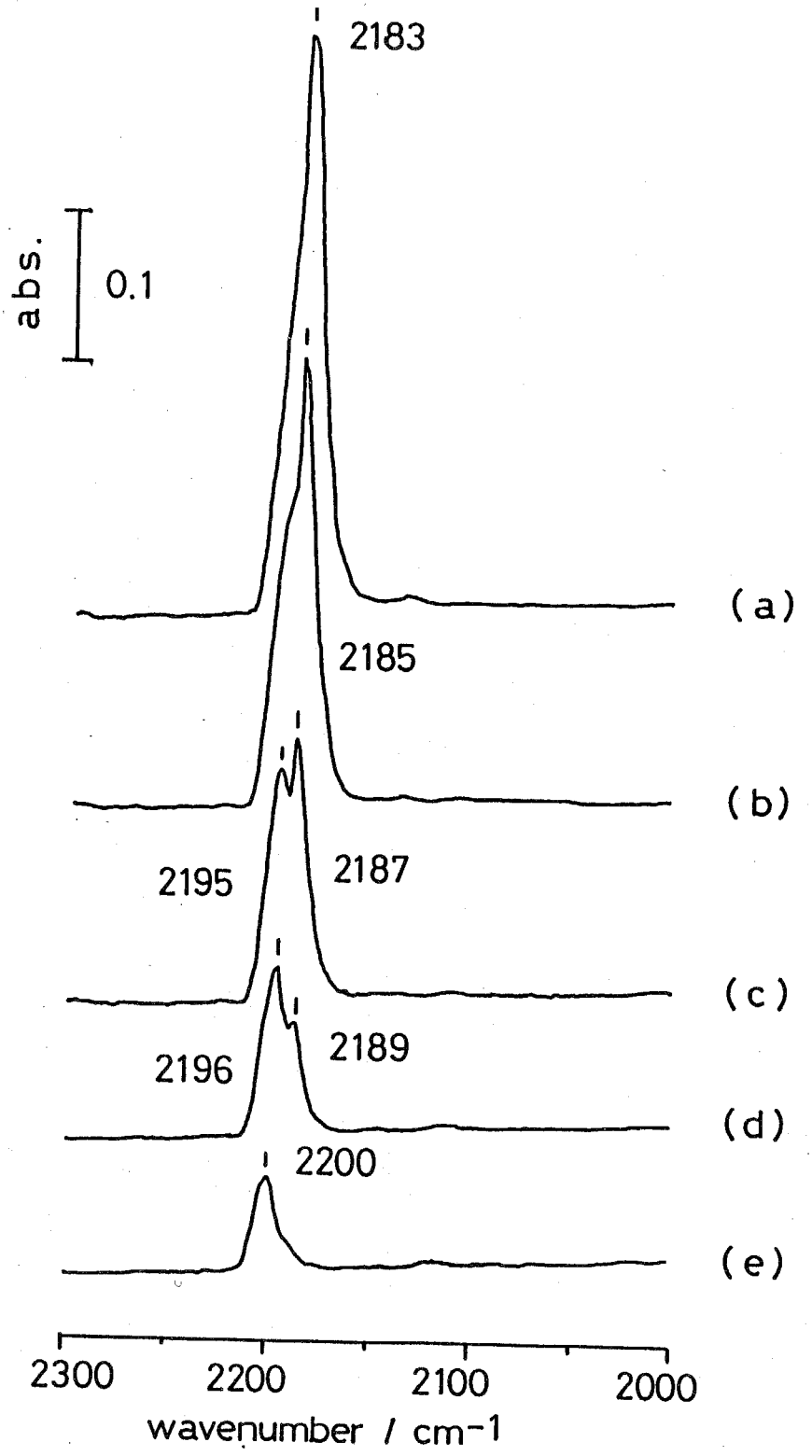

Fig. 6-1 IR spectra of adsorbed ^{12}CO at various temperatures, (a) 183 K, (b) 198 K, (c) 213 K, (d) 225 K and (e) 243 K.

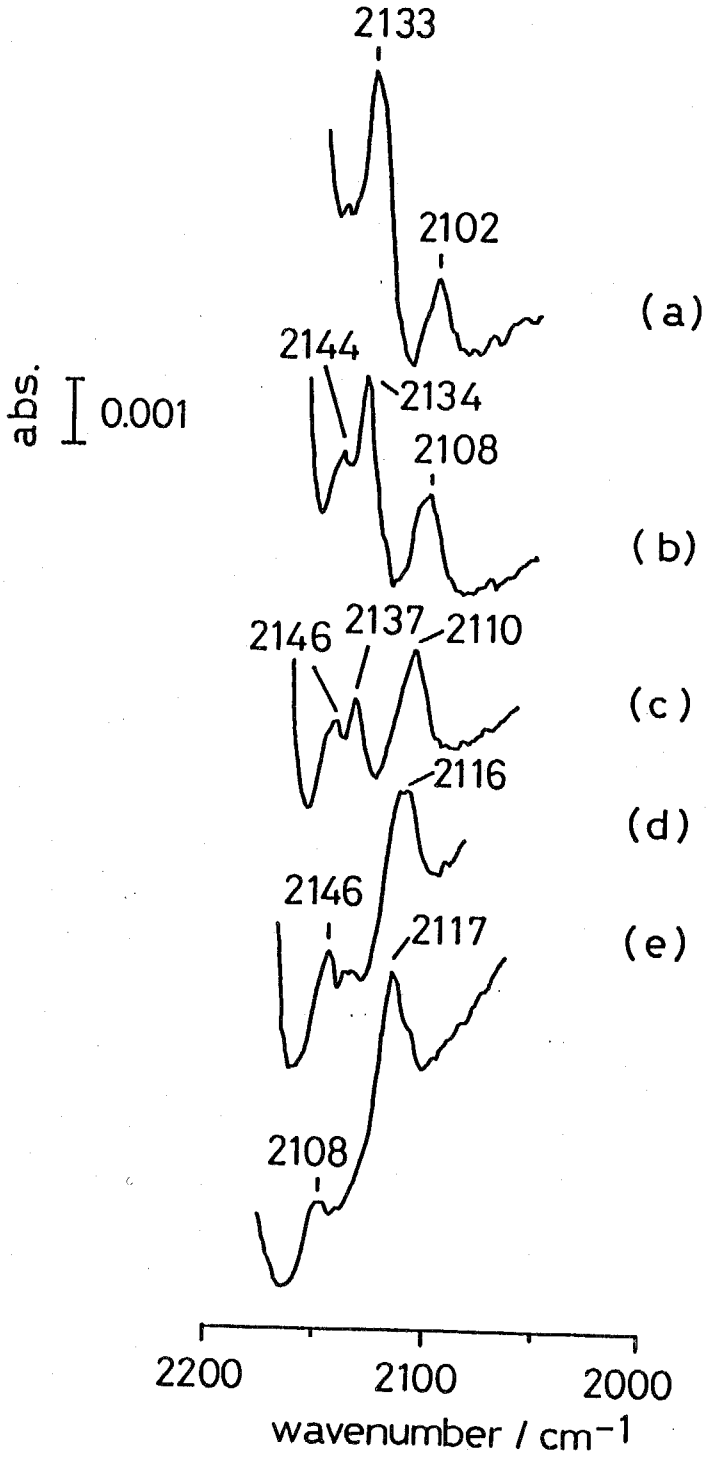

Fig. 6-2 IR bands due to ^{12}CO adsorption, (a) 183 K, (b) 198 K, (c) 213 K, (d) 225 and (e) 243 K.

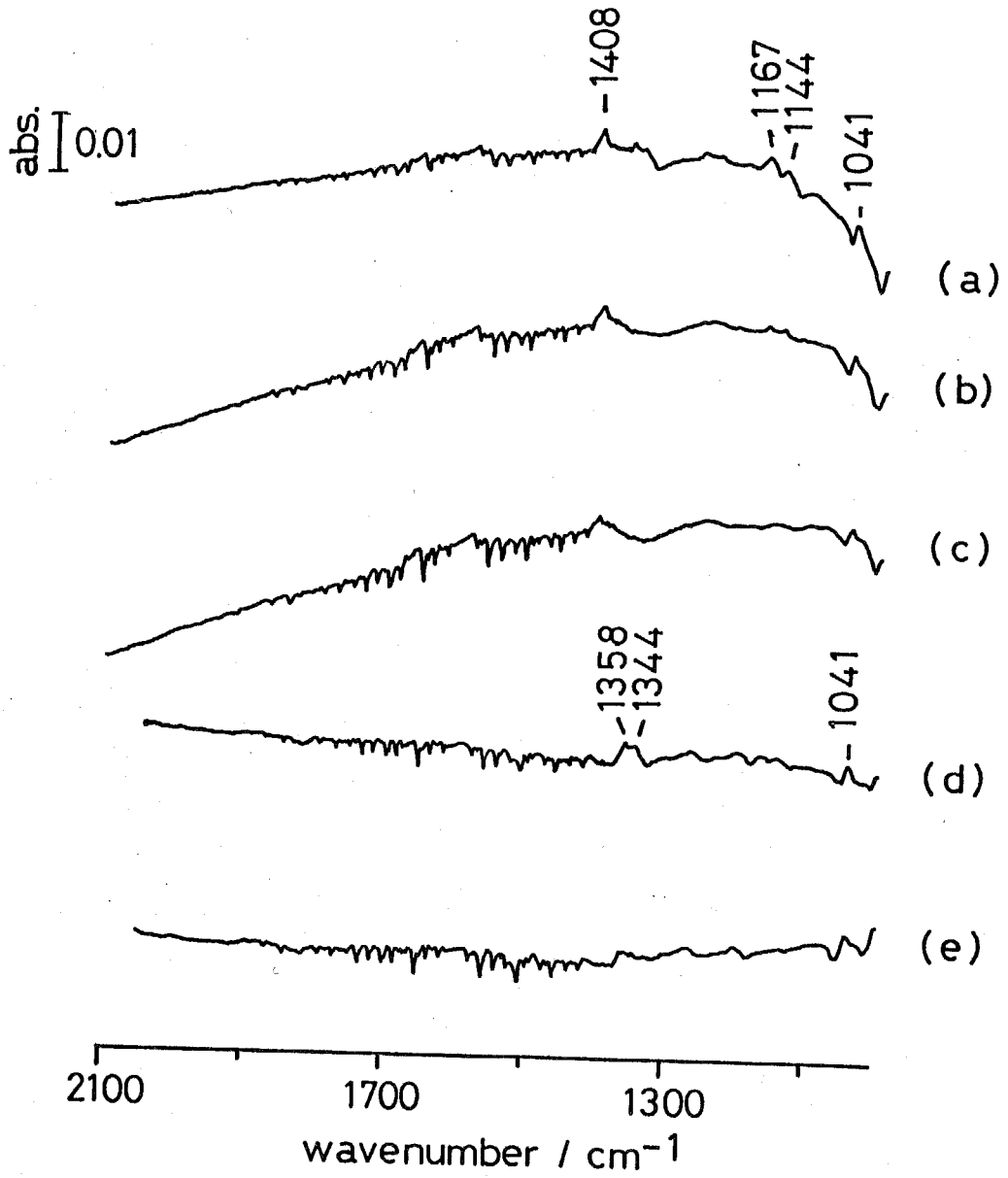

Fig. 6-3 IR spectra of ^{12}CO and ^{13}CO adsorption in low frequency region, (a) ^{12}CO at 183 K, (b) ^{12}CO at 198 K, (c) ^{12}CO at 213 K, (d) ^{13}CO at 193 K and (e) ^{13}CO at 213 K.

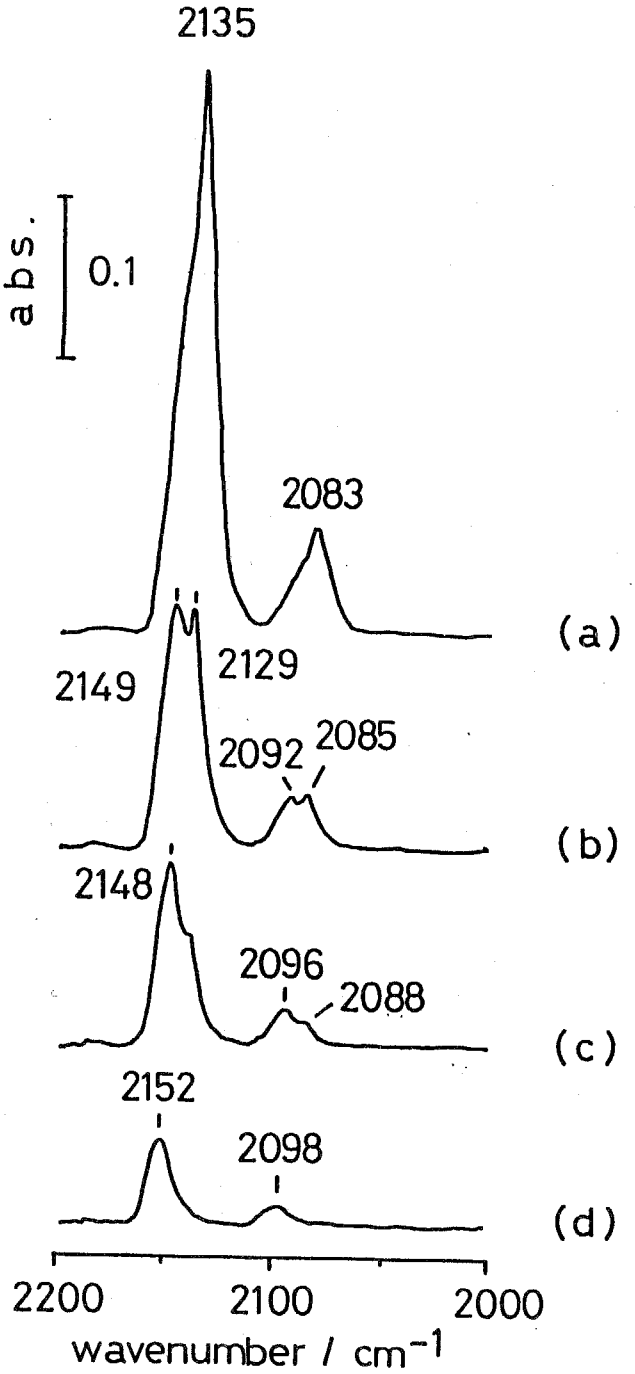

Fig. 6-4 IR spectra of adsorbed ^{13}CO at various temperatures, (a) 193 K, (b) 213 K, (c) 233 K and (d) 248 K.

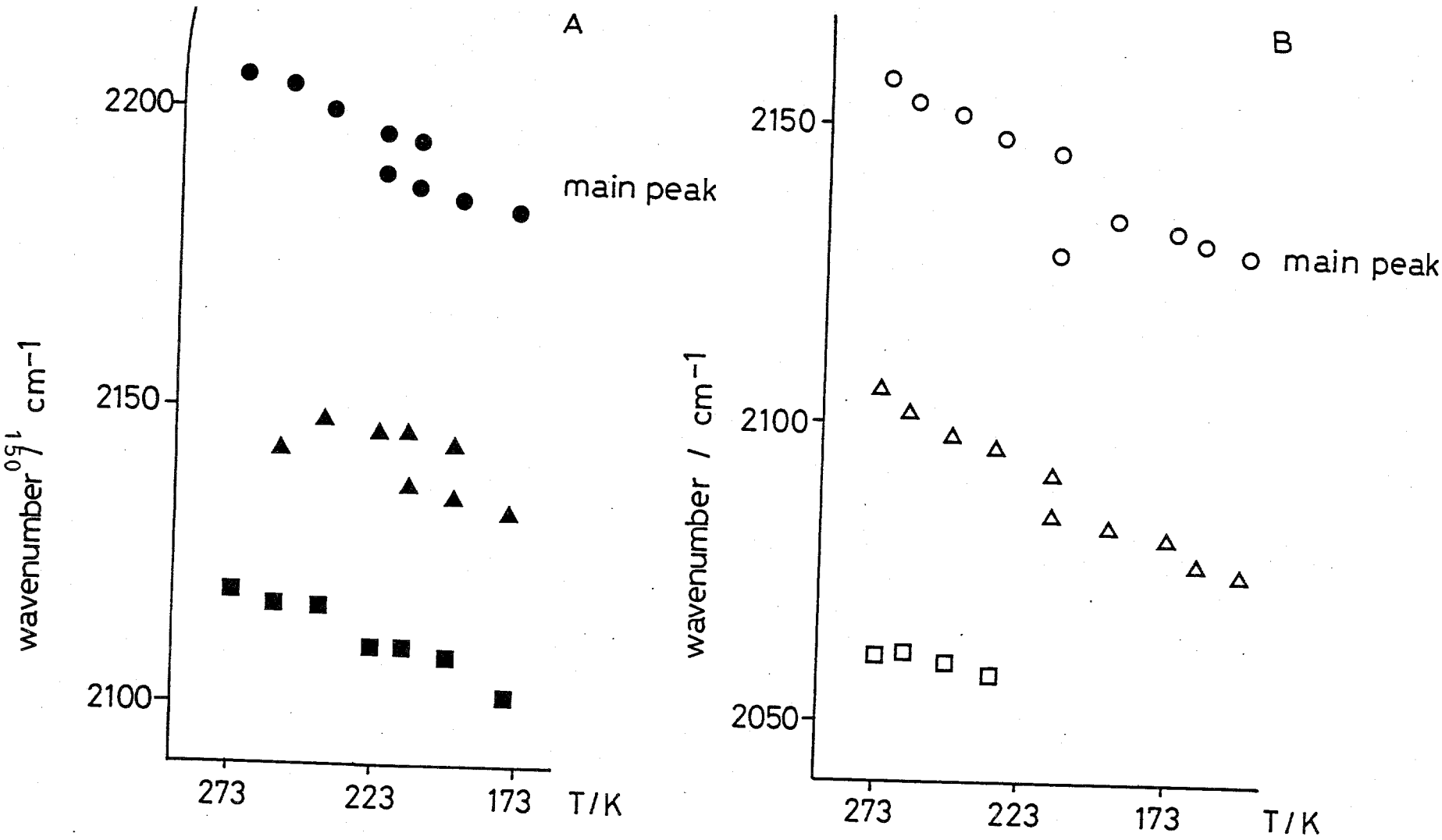

Fig. 6-5 Dependence of observed IR bands frequency due to ^{12}CO (A) and ^{13}CO (B) adsorption on temperature or coverage. The coverage decreases with increasing temperature.

the electric field strength of the cation centers of catalysts has been made in order to obtain a information on the nature of the surface coordination site with the use of CO as a probe[17,18]. A brief conclusion is that an intensive CO stretching shift to a higher wavenumber reflects a strong acidic site of adsorption with a considerable heat of adsorption. Based on this and the thermal stability of adsorbed species in fig. 6-1, the band at higher frequency (2200 cm^{-1} at 243 K) is assigned to CO adsorbed on stronger acidic site. And the band at lower frequency (2183 cm^{-1} at 183 K) is considered to be due to weaker acidic site.

Weak bands which are also attributed to adsorbed ^{12}CO were observed at lower frequencies as can be seen in fig. 6-2. The band observed below 2120 cm^{-1}, which shifts to lower frequency, is assigned to CO being bonded to a reduced center (basic site) where back donation involving d-electrons may take place. This assignment is supported by basicity of ZrO_2[19] and the strong adsorption of this species upto a considerably high temperature. A cause of backdonation from metal atoms of a metal oxide upon CO adsorption is reported for TiO_2 by Busca et al.[20] and for ZrO_2 by Morterra et al.[21] They ascribed the reduced sites to Ti^{3+} and Zr^{3+}, as detected by ESR spectroscopy. Therefore the site for CO adsorption generating an adsorbed species at 2102-2117 cm^{-1} could be regarded as reduced Zr^{3+} sites.

Two Other species were also observed at 2146 and 2137 cm^{-1} (at 213 K). The adsorbed CO on TiO_2[22] and La_2O_3[23] which show bands between 2130 and 2150 cm^{-1} were assigned to physisorbed or hydrogen bonded CO because the IR bands did not shift very much from that of gaseous CO. However two bands at 2146 and 2137 cm^{-1} (at 213 K) in fig. 6-2 cannot be assigned to such weakly adsorbed species because these species in fig. 6-2 existed under evacuation. The sites which provide this adsorption would rather be regarded as Zr^{x+} $(3<x<4)$. On these sites weak backdonation of the d-electrons of Zr^{x+} to empty antibonding $2p\pi^*$ orbital of CO occurs to compensate for high frequency shift resulted from the formation of σ-bond.

Spectra made during ^{12}CO and ^{13}CO adsorption at lower frequency are also shown in fig. 6-3. A weak band was observed at 1408 cm^{-1} which reduced with increasing temperature. When ^{13}CO was adsorbed it shifted to 1358 and 1344 cm^{-1}. Therefore the appearance of this band is well ascribed to adsorbed CO on ZrO_2. However, the assignment of this species and the reason for band splitting when ^{13}CO was adsorbed are not clear.

Spectra taken for ^{13}CO adsorption are presented in fig. 6-4. Here, the bands at the highest frequencies are considered to behave in the same way as the corresponding bands of ^{12}CO adsorption in the context of band shifting and peak splitting. Although these spectra are not expanded in the lower frequency region, a weak

corresponding band at 2102 cm^{-1} to the one at 2117 cm^{-1} (at 243 K) for ^{12}CO in fig. 6-2(a) existed in all the spectra in fig. 6-4 for ^{13}CO adsorption. The ^{13}CO species showed the same behavior as the ^{12}CO one. The only difference between ^{12}CO and ^{13}CO is peak intensity of adsorbed CO on Zr^{x+} ($3<x<4$) sites. This is regarded as an isotope effect in intensity.

It has been already shown in fig. 6-1,2,3 and 4 that all the observed bands during CO adsorption shifted to higher wavenumbers with heating the sample and/or with decreasing the coverage. This result is summarized in fig. 6-5, where band positions are presented as a function of temperature. The main causes for bandshifting could possibly be the change in adsorption amount or the change in temperature. This question was checked by an experiment to change the temperature maintaining the same amount of adsorbed CO species. The result showed that the temperature change has no effect on the bandshift. Therefore the observed bandshift is resulted from the change in the amount of CO adsorbed.

Hoffmann summarized[24] the effect of coverage on frequency shift. When CO is adsorbed on metal single crystal surfaces its adsorption band shifts to higher frequency as its coverage increases. This is first found to result from "through space dipole-dipole coupling" and via "through metal electrons". However, the observed frequency shift here is unlikely to be involved in one of

these because through-metal interactions is only expected to proceed via metal free electrons. Also dipole-dipole coupling takes only place when the dipole-images of adsorbed species are homogenous and close. But, adsorbed CO on ZrO_2 cannot be considered to have enough density in order to give rise to dipole-dipole coupling with neighboring adsorbed species giving the same direction. On ZrO_2, the bandshift shows the opposite trend from what is expected by those interpretations. The band shifting in the present case could be explained by the change of the σ-bonding from CO to the surface. When the concentration of CO on the surface becomes large enough, the degree of σ-bonding of each CO molecule to a coordinated center of ZrO_2 surface becomes small. As a result a small degree of σ-bonding (low concentration of CO) causes a small bandshift to higher frequency, where backdonation does not occur.

Above room temperature new peaks appeared (423 K) at 1550 and 1300 cm^{-1} in the presence of gaseous CO (fig. 6-6). This species is assigned to carbonate species. They will be described in the next paragraph.

CO_2 Adsorption

After gaseous CO_2 (10 Torr) had been introduced on to ZrO_2 at 373 K and then was evacuated, the IR bands of adsorbed species were observed at 373 and 523 K as shown in fig. 6-7. Three main bands appear at ca. 1550, 1310 and 1060 cm^{-1}. In addition to these bands, several

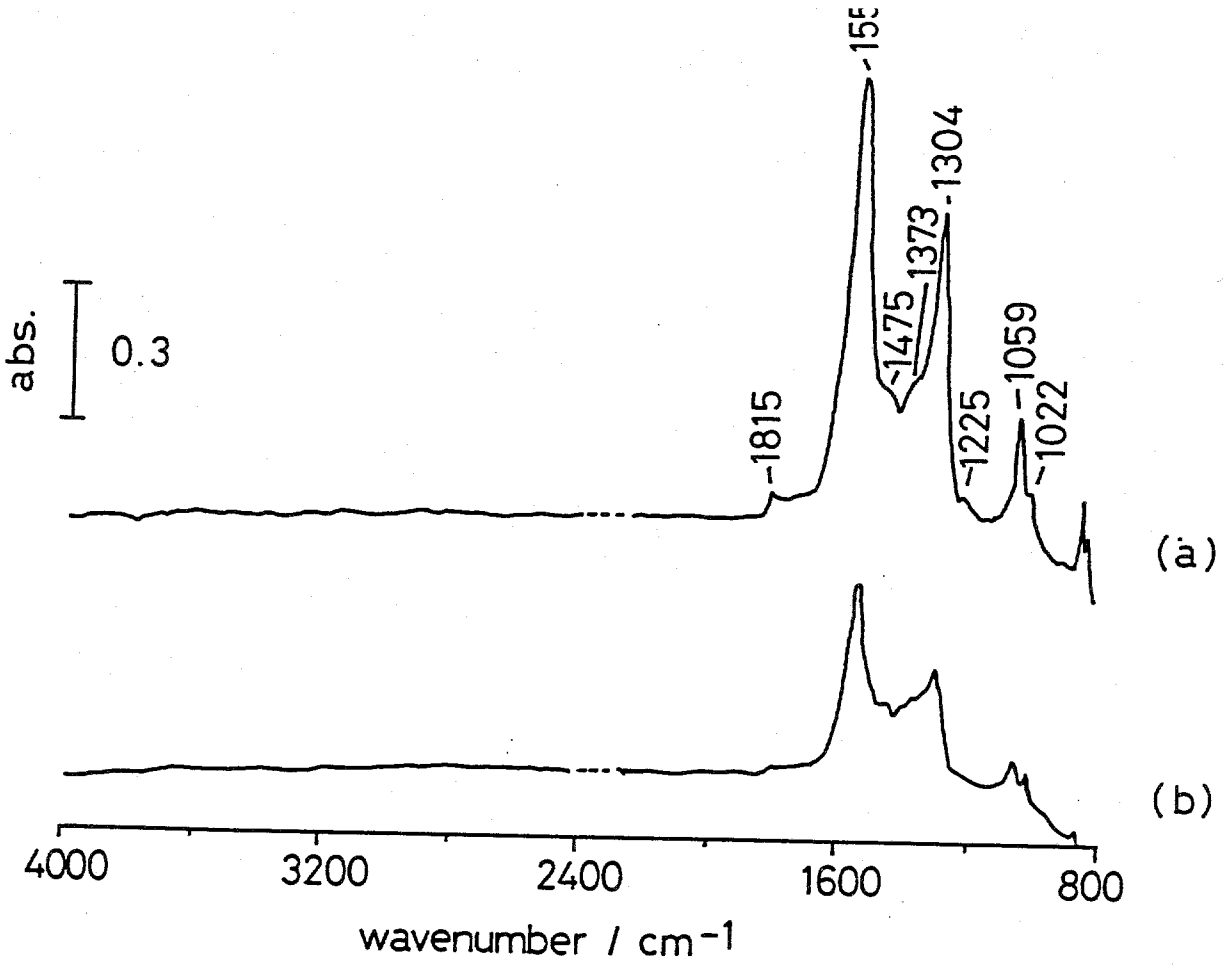

Fig. 6-7 IR spectra of CO_2 adsorption on ZrO_2, (a) At 373 K after contact for 30 min in the presence of 10 Torr CO_2, (b) at 523 K after degassing.

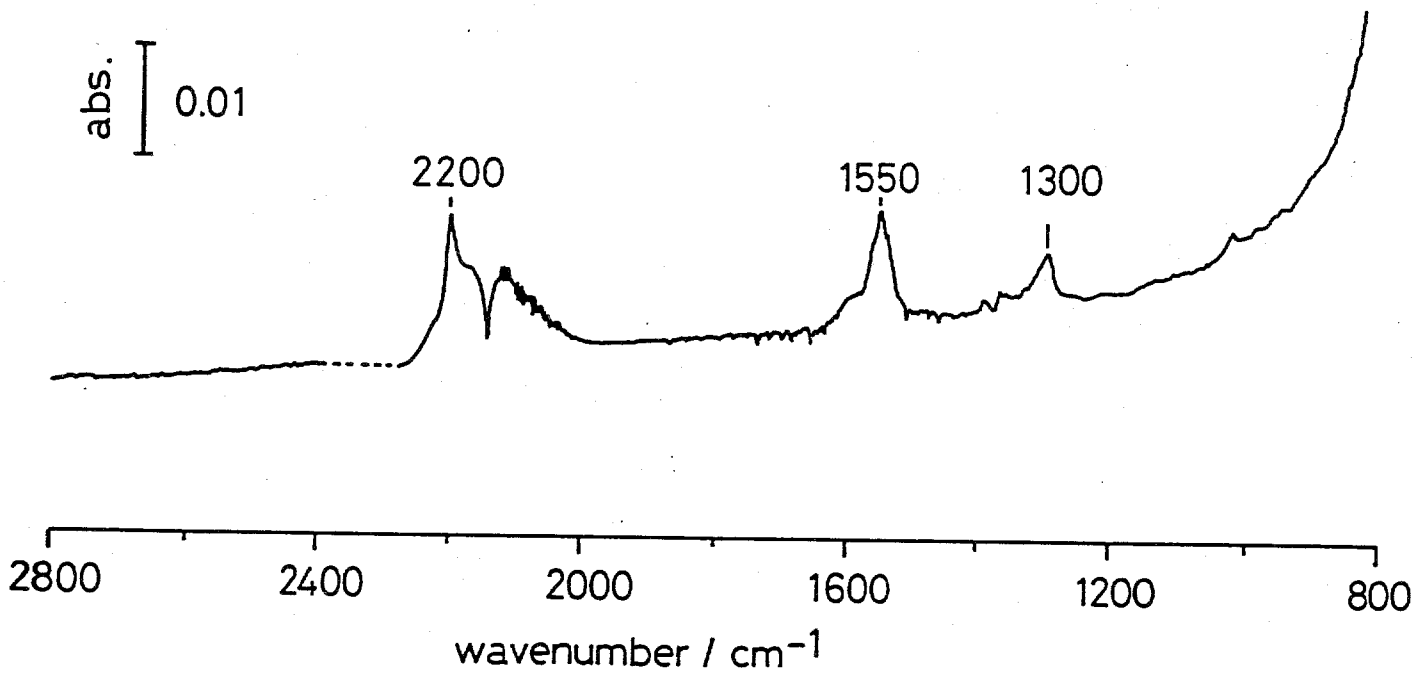

Fig. 6-6 An IR spectrum of CO adsorption on ZrO_2 at 423 K.

weak bands were observed. These bands gradually disappeared as described previously after outgassing above 523 K. Filimonov et al.[25] observed two IR bands at 1560 and 1300 cm^{-1} due to CO_2 adsorption on ZrO_2 and they tentatively assigned the bands to bidentate carbonate species. According to theoretical calculations, Fujita et al.[26] have found that in the IR spectra of Co^{III} carbonate complexes, three main bands due to unidentate and bidentate carbonates appear in the range 1600-1000 cm^{-1} as shown in table 6-1. In the case of the unidentate carbonate, the separation of the first two bands is ca. 100 cm^{-1} while for the bidentate one it is ca. 300 cm^{-1}. Blyholder[27], Evans et al.[28] and Fukuda et al.[28] applied this rule to assign the IR bands of adsorbed surface carbonate species over oxide catalysts. Using these considerations, the adsorbed species of CO_2 over ZrO_2 can be assigned to the bidentate species as shown in table 6-2.

The C=O group frequencies of organic carbonates are seen at ca. 1750 cm^{-1} while those of the covalently bound carbonate group appear at ca. 1550 cm^{-1},[30]. The large difference in frequency between these two species is to be expected if one assumes that there is more ionic character in the carbonate complexes than in the organic carbonates.

In the case of CO adsorption onto ZrO_2, at high temperature (above 523 K) the two weak bands at 1550 and 1300 cm^{-1} appear as stated above. These bands may correspond to the bidentate carbonate species over ZrO_2.

Table 6-1 Calculated frequencies due to carbonate species of Co^{III} complex / cm^{-1},[26]

unidentate carbonate[a]	separation	assignment[b]	bidentate carbonate[c]	separation	assignment[b]
1483		OCO a-str.	1595		C=O str.
	110			312	
1373		OCO s-str.	1282		OCO a-str.
	334			244	
1039		C-O str.	1038		OCO s-str.

a 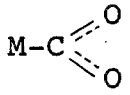

b a, antisymmetric; s, symmetric.

c 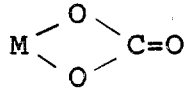

Table 6-2 Observed IR bands due to carbonate species on oxides

$NiO-(CO+O_2)$[27]	separation	ZrO_2-CO_2	separation	assignment
1560	230	1556	250	C=O str.
1330	290	1304	240	OCO a-str.
1040		1061		OCO s-str.

a, antisymmetric; s, symmetric.

Weak bands at 1600, 1470 and 1225 cm^{-1} in fig. 6-7 can be assigned to the bicarbonate species 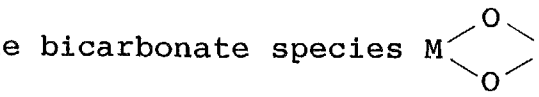 - OH, which were also assigned by Filimonov et al.[25]

6-4-2 Adsorption of CH_3OH, HCOOH and CH_3OCH_3

Methanol adsorption on metal oxides is well known to result in formation of methoxide species. The assignments of methoxide species on different metal oxides are summarized in table 6-3. ZrO_2, whose spectra are shown in fig. 6-8 at various temperatures, is included. In fig. 6-8 two strong bands in the range 1000-1200 cm^{-1} are possible to be assigned to CH_3 rock and C-O stretching of methoxide species. However in the spectra taken for CD_3OD adsorption (fig. 6-9), both of these bands did not shift, which lead to assigning both bands to the C-O stretching mode. This implies the existence of two different types of methoxide species on ZrO_2, as is also observed on MgO[38]. This is also expected by the shoulders in CH stretching bands (fig. 6-8) and the appearance of a corresponding strong band at 2206 cm^{-1} (CD stretching, fig. 6-9). Following the assignments of Lamotte et al.[39] on ThO_2 and CeO_2, the two different methoxide species are regarded to be monodentate and bidentate methoxides (table 6-3). Hereafter the methoxide involving the band at 1157 and 1059 cm^{-1} are called type 1 and type 2 methoxide species, respectively, as Bensitel et al.[40] first proposed.

Table 6-3 Observed methoxide species on oxides

assignment	Al_2O_3[32]	Al_2O_3[33]	MoO_3[34]	MgO[35]	ZnO[36]	SiO_2[37]	ThO_2[39]	CeO_2[39]	ZrO_2
CH_3 a-str.	2960(2255)	2950	2925(2185)	2920	2938	3000(2252) 2958(2118)			2924(2127)
CH_3 s-str.	2849(2089)	2840	2825(2065)	2860	2823	2858(2081)			2818(2056)
CH_3 a-def.	1475(1119)					1472			1468(1084)
CH_3 s-def.	1420(1086)		1440(1098)			1464			
CH_3 rock	1081(--)	1190a 1100a 1030a							
C-O str.	1055(1067)		1065(1050)	1080			1124b 1061c 1045c 1013d	1104b 1057c 1042c 1013d	1157(1157)b 1059(1026)c

a, not assigned; b, monodentate species; c, bidentate species; d, tridentate species.

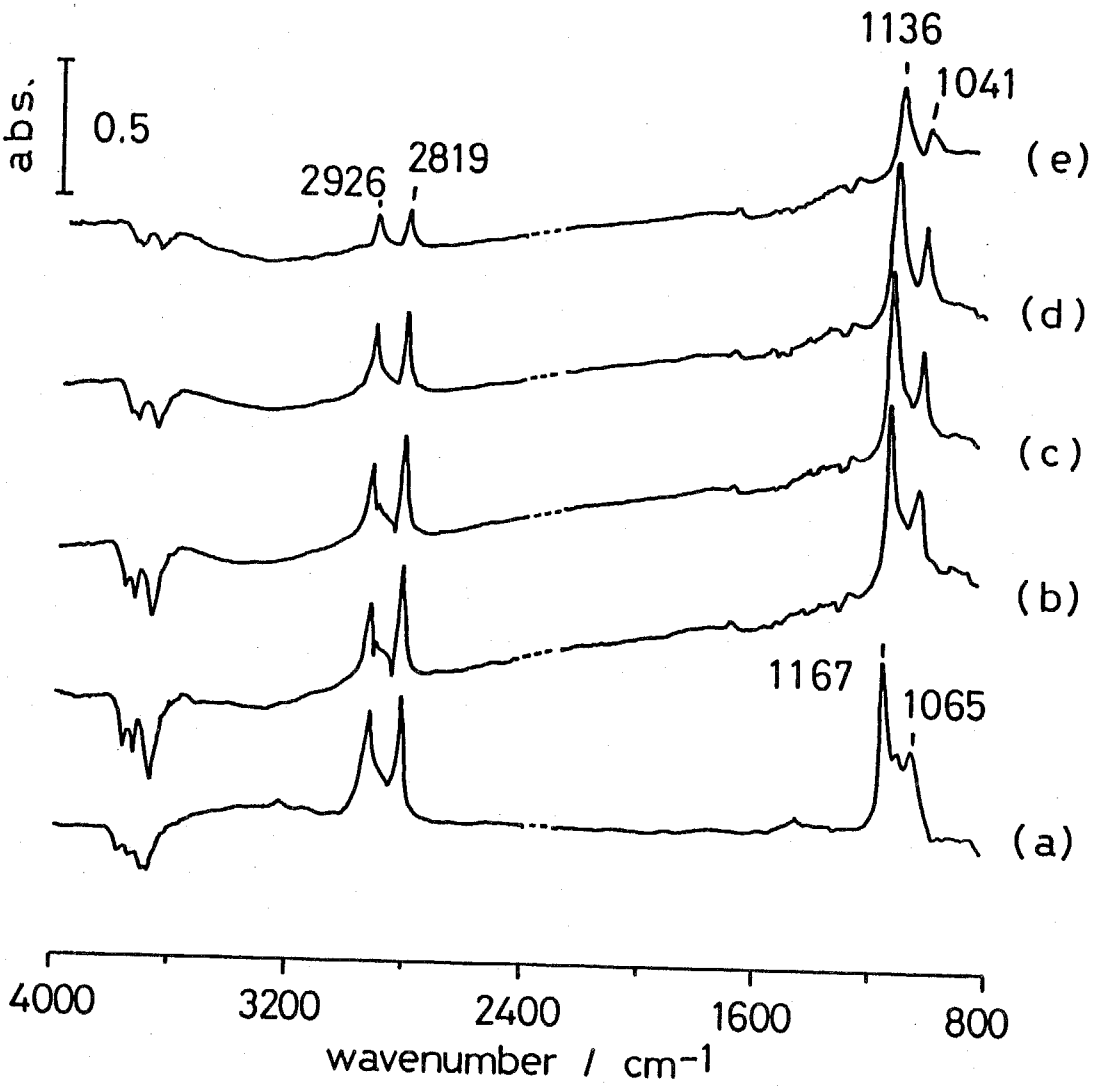

Fig. 6-8 IR spectra of methanol adsorption on ZrO_2, (a) room temperature, (b) 373 K, (c) 473 K, (d) 573 K and (e) 673 K.

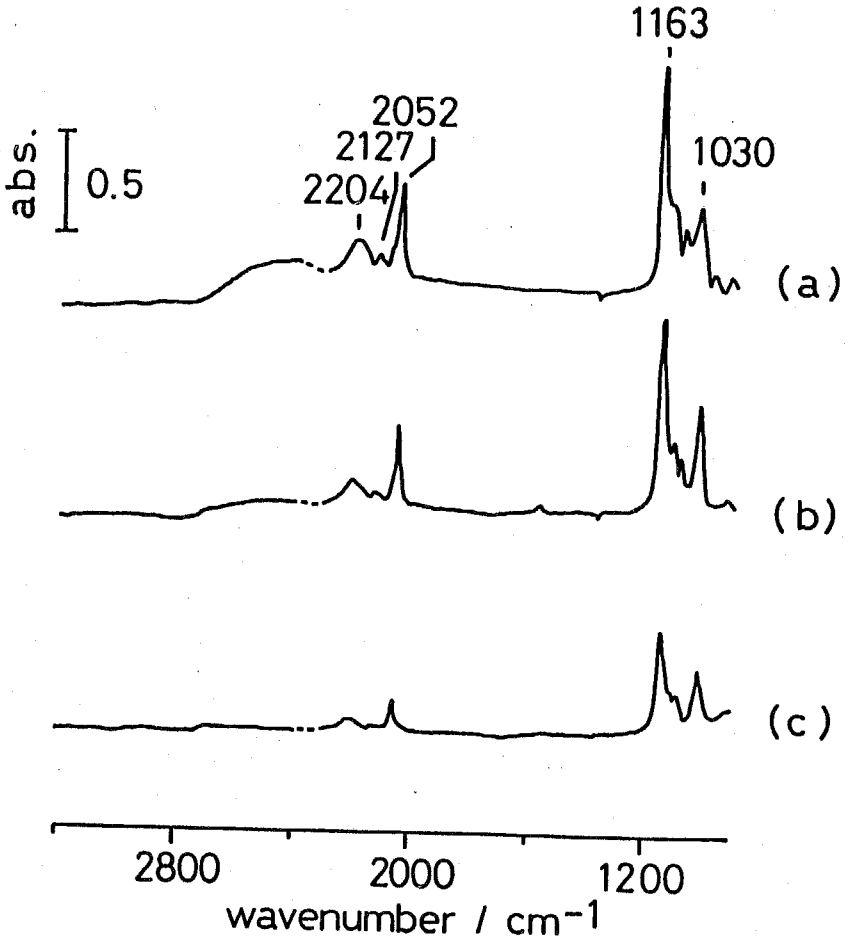

Fig. 6-9 IR spectra of CD_3OD adsorption on ZrO_2, (a) 373 K, (b) 523 K and (c) 673 K.

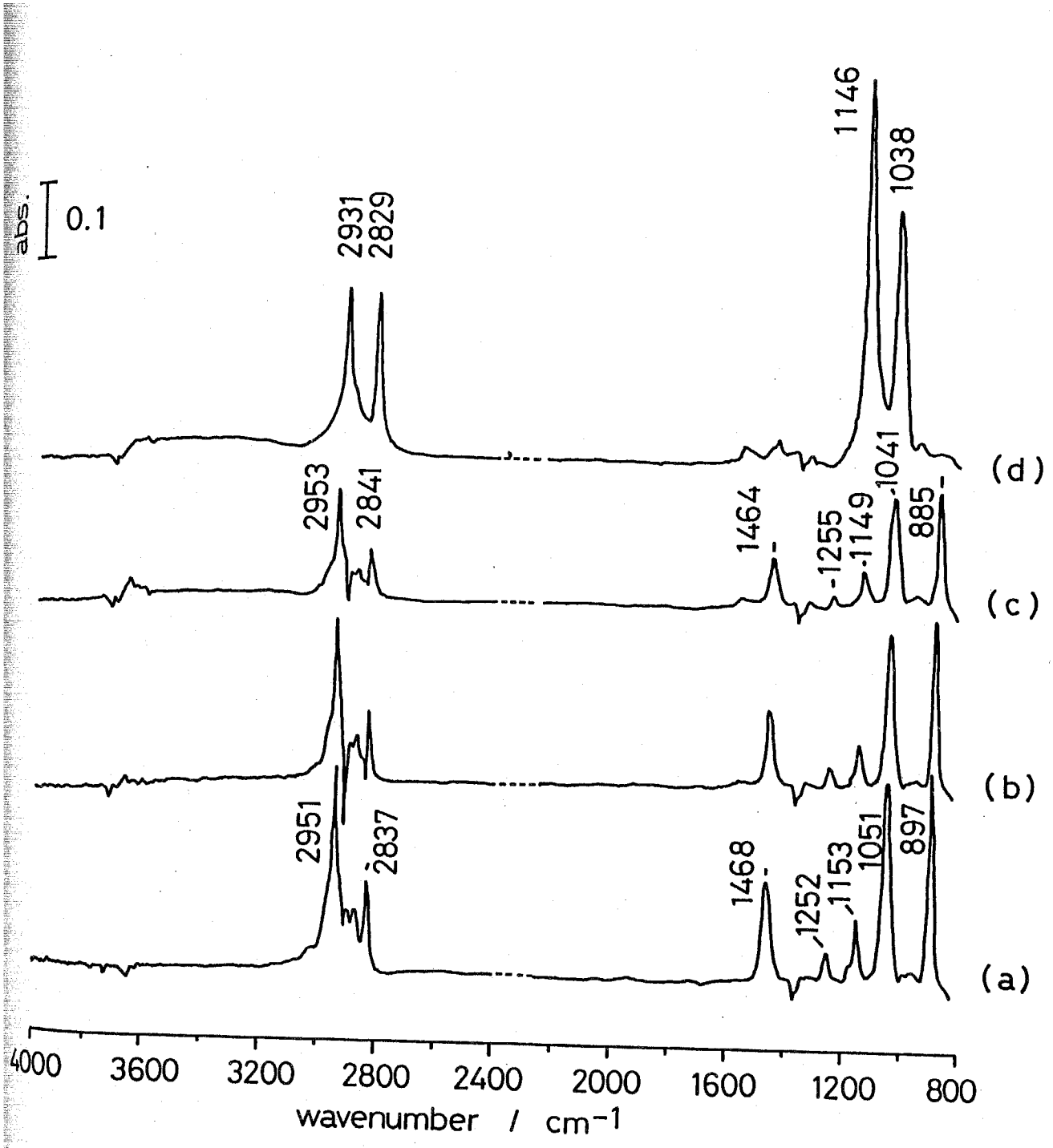

Fig. 6-10 IR spectra of DME adsorption on ZrO_2, (a) 373 K, (b) 423 K, (c) 473 K and (d) 573 K.

Adsorption of dimethylether (DME) gives the spectra presented in fig. 6-10. DME was exposed to the sample at each temperature and gaseous DME was trapped during IR measurement in the procedure from (a) to (d). DME is considered to adsorb while maintaining its molecular shape upto 473 K because the ratios among all bands are constant in (a)-(c) though the adsorbed amount is different. At 573 K, however, both type 1 and 2 methoxide species are produced by DME adsorption resulted from C-O bond breaking. This spectrum looked similar to the one of methanol adsorption. Possible assignments of molecularly adsorbed DME are listed in table 6-4 with a comparison of those with DME in the gas phase.

Adsorption studies of formic acid on oxide catalysts have been performed for many years and assignments of formate species resulted from formic acid adsorption on several oxides are given in table 6-5. The appearance of two CH stretching mode is so far explained by existence of two different types of formate species. However, the exact distinction of two species cannot correctly be made with only reactivity and stability analysis.

During the series of experiments on CO hydrogenation, one fact stood out regarding the adsorption sites of methoxide and formate species. Since site study is considered to be important to elucidate a mechanism of CO hydrogenation over ZrO_2 to produce methanol, coadsorption experiments of methanol (methoxide) and formic acid (formate) were carried out. The resulting spectra of

Table 6-4 Observed species due to DME adsorption / cm^{-1}

assignment	selected value of frequency[16]		adsorbed species on ZrO_2 at 375 K	
CH_3 d-str.	2996	s	2951	s
CH_3 d-str.	2952	ia	2908	m
CH_3 d-str.	2925	s	2877	m
CH_3 s-str.	2817	s	2837	s
CH_3 d-def.	1464	m	1468	m
CH_3 s-def.	1452	m		
CH_3 rock	1244	w	1252	w
CH_3 rock	1227	w	1173	sh
CH_3 rock	1179	vs	1051	s
CH_3 rock	1150	ia	1153	m
C-O str.	928	s	897	s
COC str.	418	m		
tort.	242	w		
tort.	203	ia		

ia, IR-inactive; vs, very strong; s, strong; m, medium; w, weak; sh, shoulder.

Table 6-5 Observed formate species on oxides / cm^{-1}

assignment	MgO[41]	MgO[12]	MgO[38]	La_2O_3[12]	ZnO[36]	ZrO_2(this work)
CH str.	2907	2804	2866	2850	2880	2962 2872
CO a-str.	1603	1604 1635	1593	1578 1630	1580	1566
CO s-str.	1385 1376 1366	1370	1398 1381	1372	1380	1381
CH def.	1404 1391					1369
CH def.	1081					

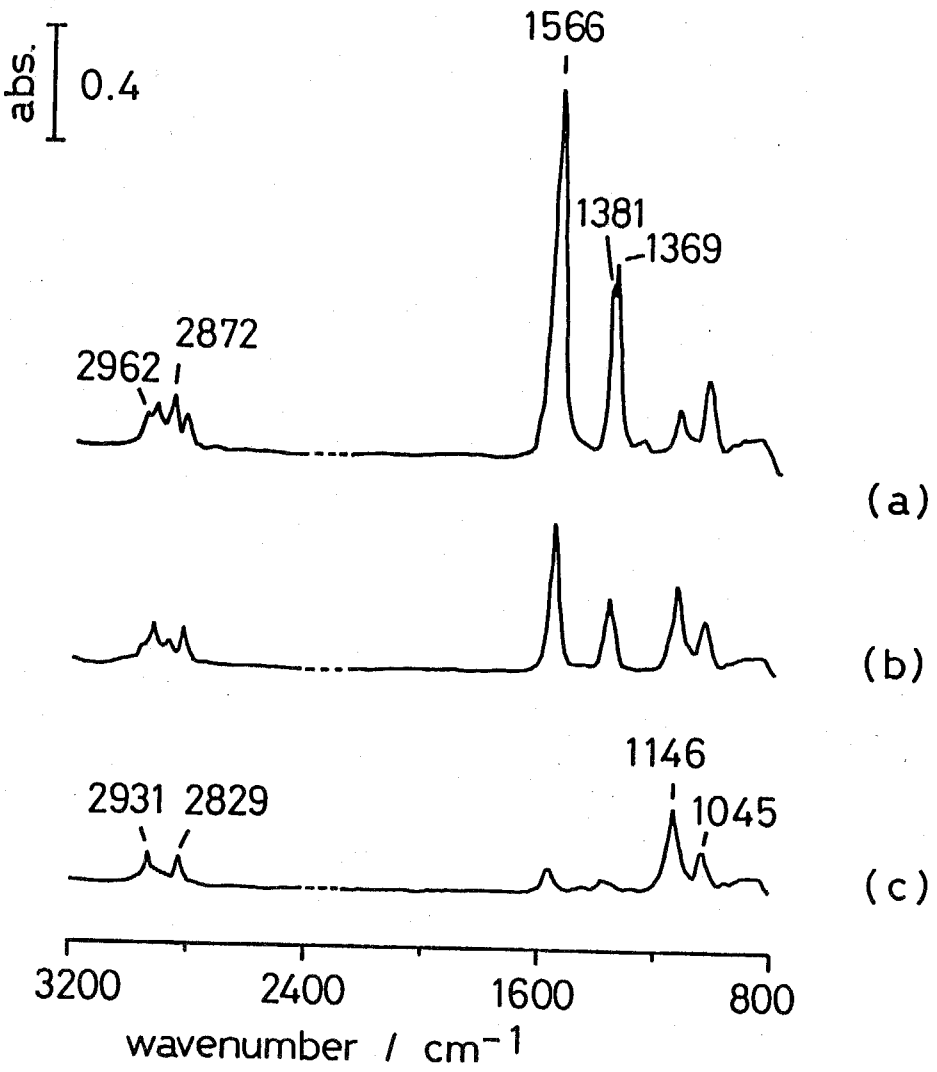

Fig. 6-11 IR spectra of co-adsorption study of formate and methoxide species, (a) 523 K, (b) 623 K soon and (c) 623 K for 30 min.

coadsorption are shown in fig. 6-11. Fig. 6-11(a) is the spectrum when 4 Torr of formic acid and 20 Torr of methanol were mixed and exposed to the ZrO_2 surface at 523 K. It is apparent that the band at 1045 cm^{-1} (type 2) is stronger than that at 1147 cm^{-1} (type 1) when methoxide species coadsorb with formate species at 523 K. At 623 K when formate species was decomposed the intensity ratio of these bands reversed. The ratio spectrum of fig. 6-11 (a)/(c) is presented in fig. 6-12. The same result was obtained by the addition of formic acid to methoxide species on a ZrO_2 surface; the band at 1045 cm^{-1} (type 2) decreased while the one at 1145 cm^{-1} (type 1) increased with formation of formate species. Fig. 6-13 represent the ratio of the relative amount of two methoxide species versus the relative amount of formate species which was calculated with use of the band of OCO^- stretching mode. The ratio of CO stretching mode was calculated using the integrated absorbance of the bands at 1146 cm^{-1} (type 1)/1045 cm^{-1} (type 2) both for coadsorption experiment and formate addition experiment. The ratio of CH stretching mode was also calculated from integrated absorbance of the bands at 2829 cm^{-1} (type 1)/2931 cm^{-1} (type 2). Both the CO- and CH-ratio (type 1 methoxide/type 2 methoxide) linearly decreased with the increase of the amount of adsorbed formate species. From all these results, there seems to be alteration between two types of methoxide species. This is caused by

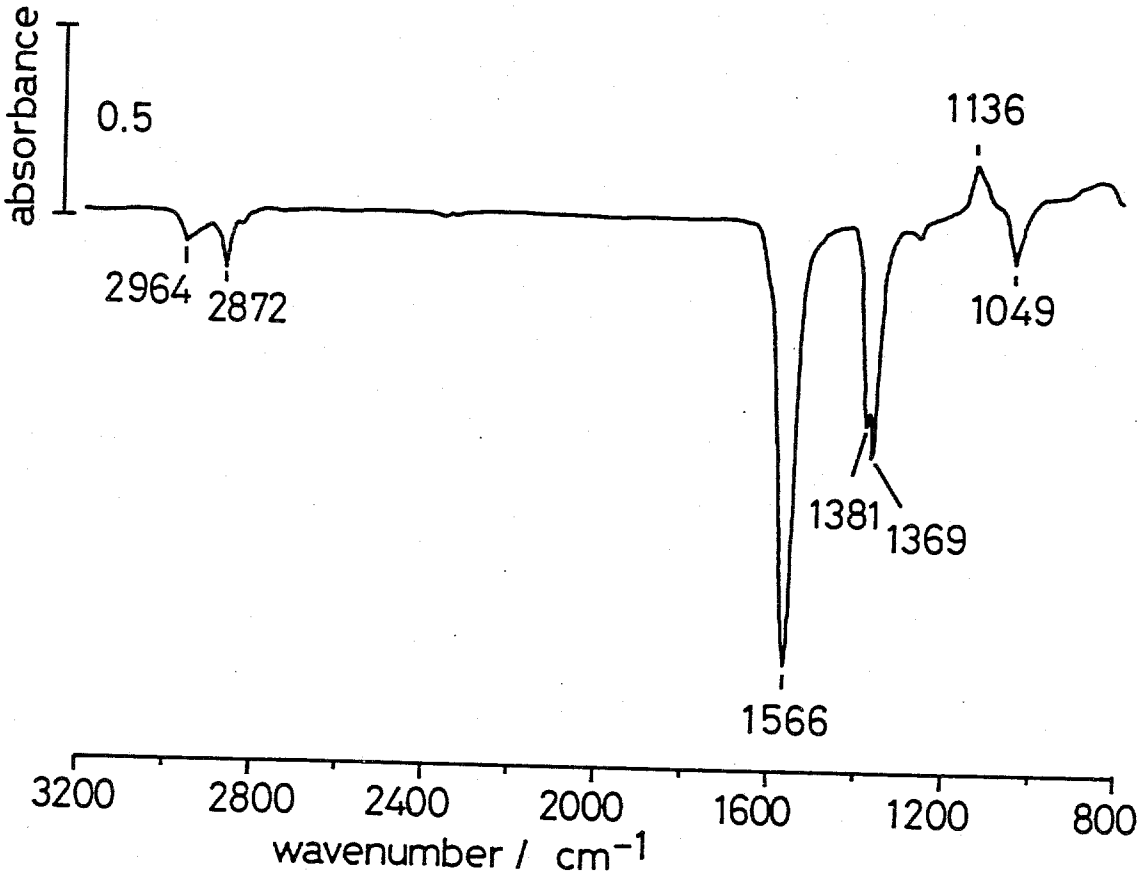

Fig. 6-12 A ratio spectrum of (c)/(a) in fig. 6-11.

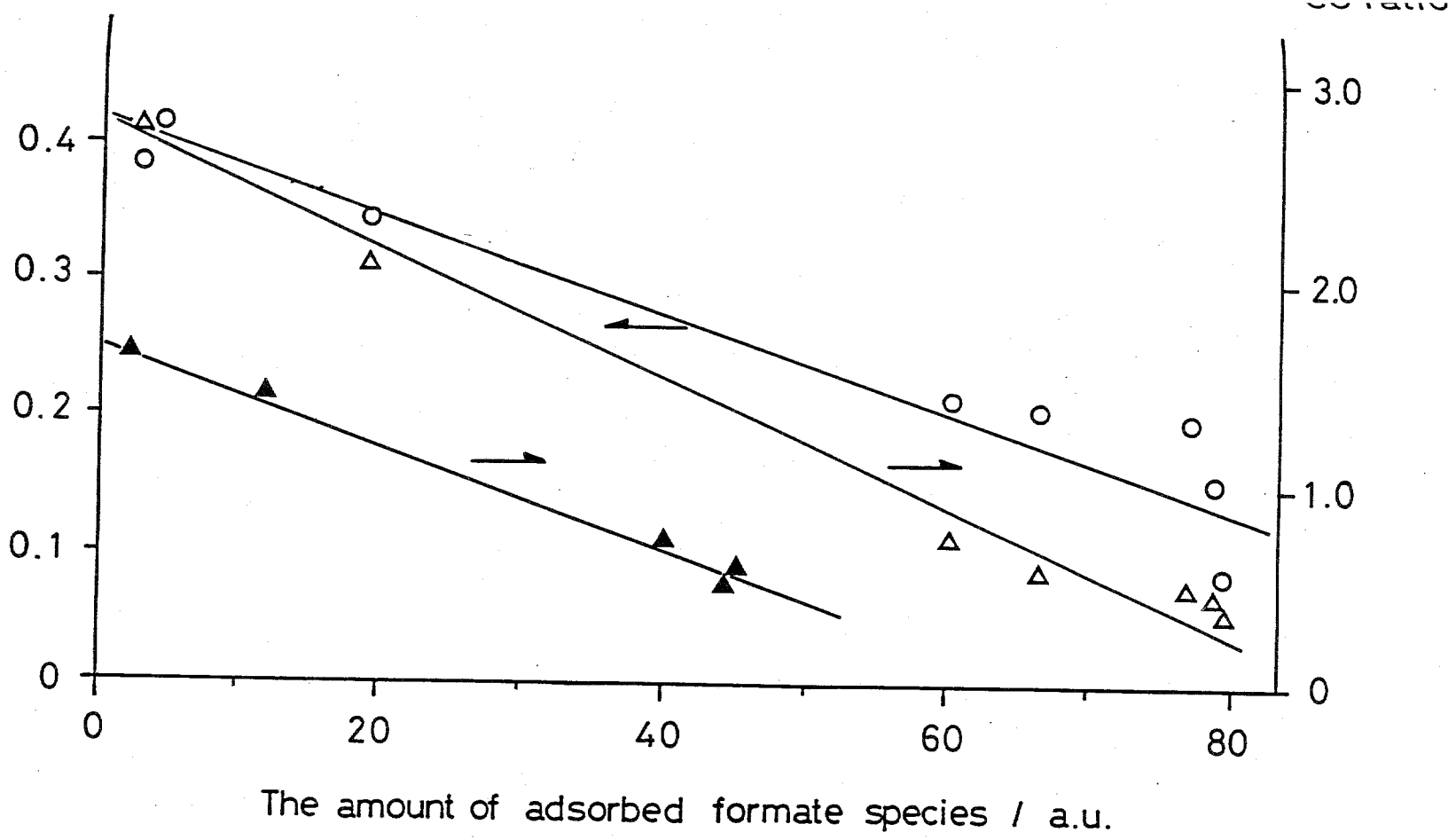

Fig. 6-13 CH str. and CO str. intensity ratios of two types of methoxide species, the effect of the existence of formate species, ○ and △ : from co-adsorption experiment, ▲ : from addition effect of formate species on methoxide preadsorbed ZrO_2.

adsorption and desorption of formate species. Furthermore, it is considered that type 1 methoxide species adsorbs on the same sites as the formate species. Also, type 1 methoxide is removed by formate adsorption to type 2 species, and their exchange seems to be reversible.

6-4-3 In Situ CO Hydrogenation at Synthesis Temperature

Methanol is produced from CO and H_2 from ZrO_2 at 523 K with high selectivity. Adsorbed species produced during the reaction were observed by IR spectroscopy at the same temperature. The resulting spectra are shown in fig. 6-14, which were taken 10 min (a) and 2 hr (b) after starting the reaction. In spectrum (a) carbonate, formate and methoxide species are shown. When reaction proceeded (b), the carbonate species disappeared and only the formate and methoxide species remained. 2 hr after the steady state was reached, no other species than formate and methoxide species were observed. After 25 hr the product mixture of reaction consisted of 85 % methanol, 12 % DME and small amount of C2 and C3 compounds.

6-4-4 Reactivity of Adsorbed Species

OH(a) + CO(g) on ZrO_2

As stated in chapter 2 two strong adsorption bands due to the OH species on ZrO_2 appeared at 3780 and 3668 cm^{-1} when ZrO_2 was treated with H_2 at 473 K. The IR spectra of surface species are shown in fig. 6-15(a) recorded when gaseous CO (30 Torr) was passed over the OH-covered ZrO_2 at 373 K. It was found that the OH species at 3780 cm^{-1} is

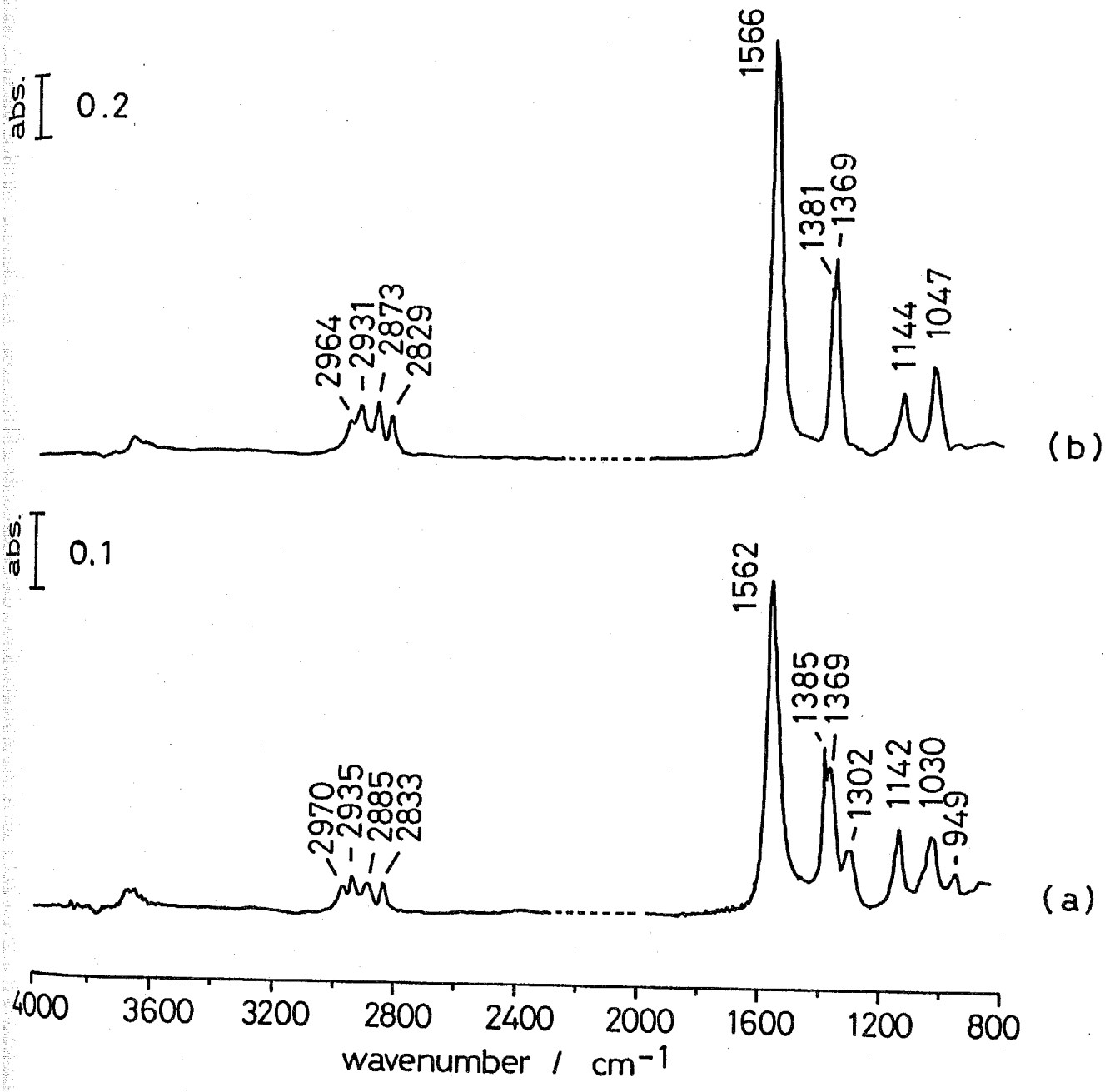

Fig. 6-14 IR spectra of in-situ CO hydrogenation at 523 K over ZrO_2, (a) for 10 min and (b) for 2 hr.

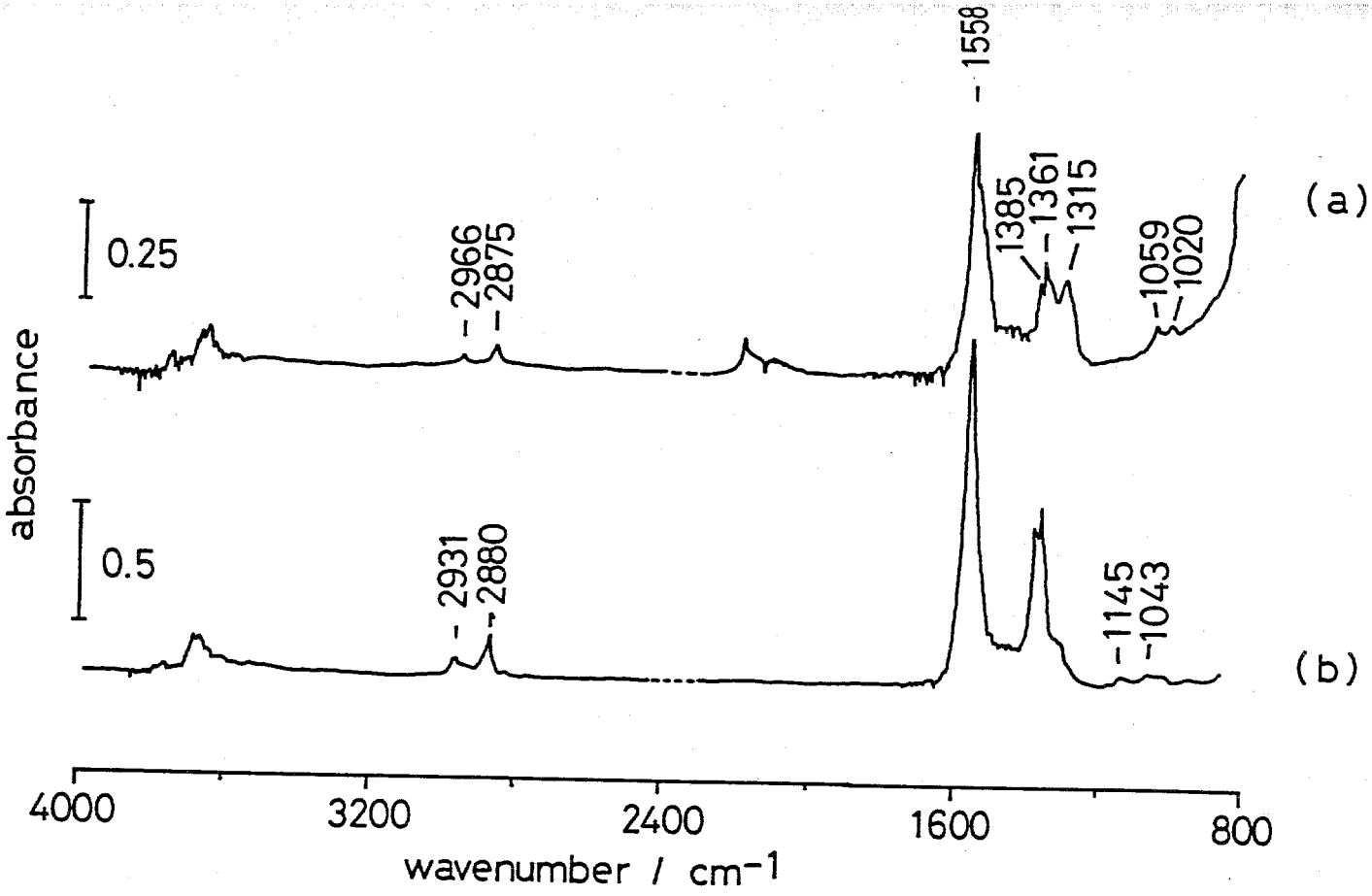

Fig. 6-15 IR spectra of adsorbed species formed from the OH(a)+CO(g) reaction, (a) at 373 K in the presence of 15 Torr CO after contact for 10 hr, and (b) at 473 K, CO was degassed after contact for 1 hr and then in the presence of H_2 (30 Torr) for 2 hr.

more reactive towards CO than the species at 3670 cm^{-1}, as reported by Yamaguchi et al.[42]

In fig. 6-15(a) the band at 2966 and 2875 cm^{-1} due to the CH stretching, at 1586, 1385 and 1361 cm^{-1} due to the antisymmetric stretching CO_2, the CH in-plane deformation and symmetric stretching of CO_2 for the formate ion can be assigned[31]. The bands at ca. 1550, 1310 and 1060 cm^{-1} are due to the bidentate carbonate species which were discussed in the adsorption of CO_2 an ZrO_2. At 523 K, essentially a similar spectrum was observed, although the amount of formate species had increased. Fig. 6-15(b) shows an IR spectrum of adsorbed species which was found from the OH(a)-CO reaction at 473 K for 1 hr and then H_2 (30 Torr) was introduced at the same temperature for 2 hr after evacuation of gaseous CO. Very weak bands appeared at 1145 and 1043 cm^{-1}. In order to clarify the change in the spectra the ratio spectrum (a)/(b) due to the species formed from H_2 treatment (a) at 473 K for 2 hr and (b) at 473 K for 1 hr after the OH(a) + CO reaction at 473 K for 1 hr, is shown in fig. 6-16. It was found that the formate bands increased and new bands at 2931, 2880, 1146 and 1041 cm^{-1} appeared while those at 1550, 1351 and 1060 cm^{-1} due to the bidentate carbonate species decreased markedly. The new bands can be assigned to the CH_3O species formed on the surface.

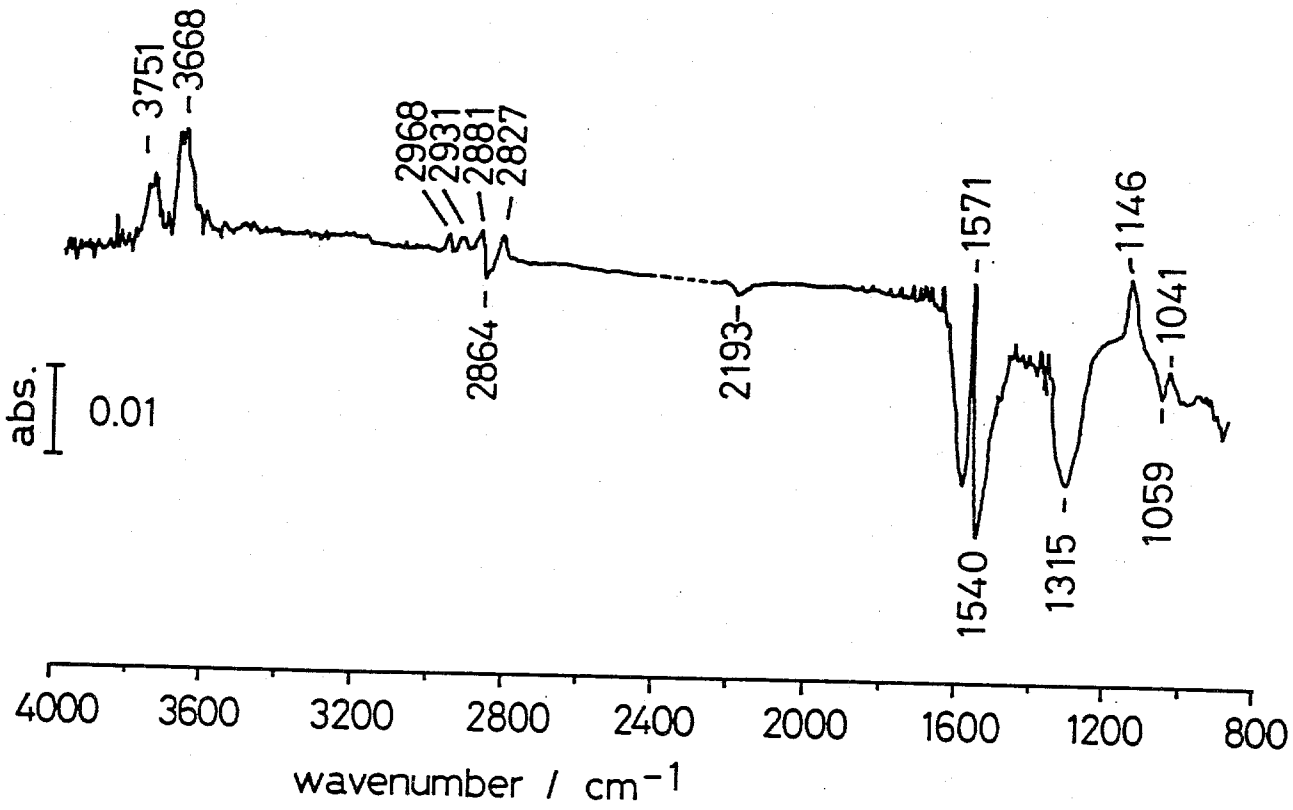

Fig. 6-16 The ratio spectrum of (a)/(b) of adsorbed species formed from the OH(a)+CO(g) reaction for 1 hr at 473 K. (a) At 473 K for 2 hr in the presence of 30 Torr H_2 and (b) at 473 K for 1 hr.

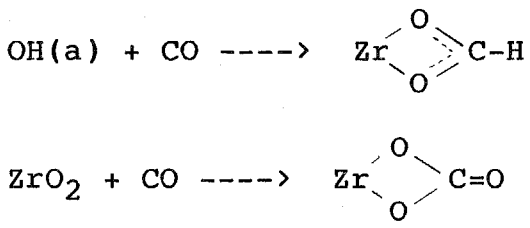

OH(a) + CO_2(g) an ZrO_2

When CO_2 was admitted over the OH-covered ZrO_2 surface, similar results to those in fig. 6-7 were obtained except in the OH regions.

CO_2(a) + H_2(g) on ZrO_2

When gaseous hydrogen (60 Torr) was introduced onto CO_2-preadsorbed ZrO_2 at 298 K [fig. 6-7(a)], and then the system was heated at 523 K, the formation of the formate species was observed by IR, as shown in fig. 6-17. After the reaction had proceeded for 30 min., an additional methoxide species appeared [fig. 6-17(b)]. The ratio spectrum [fig. 6-17(c)] of (b)/(a) clearly shows that the formate bands at 2962, 2879 and 1570 cm^{-1} and the methoxide species at 2931, 2827, 1144 and 1038 cm^{-1} increased, while the bidentate species at 1533, 1311 and 1062 cm^{-1} decreased markedly. Note that the ratio spectrum in fig. 6-17(c) was very close to that in fig. 6-16. It is concluded that hydrogenation of the bidentate carbonate species produces the formate and methoxide species.

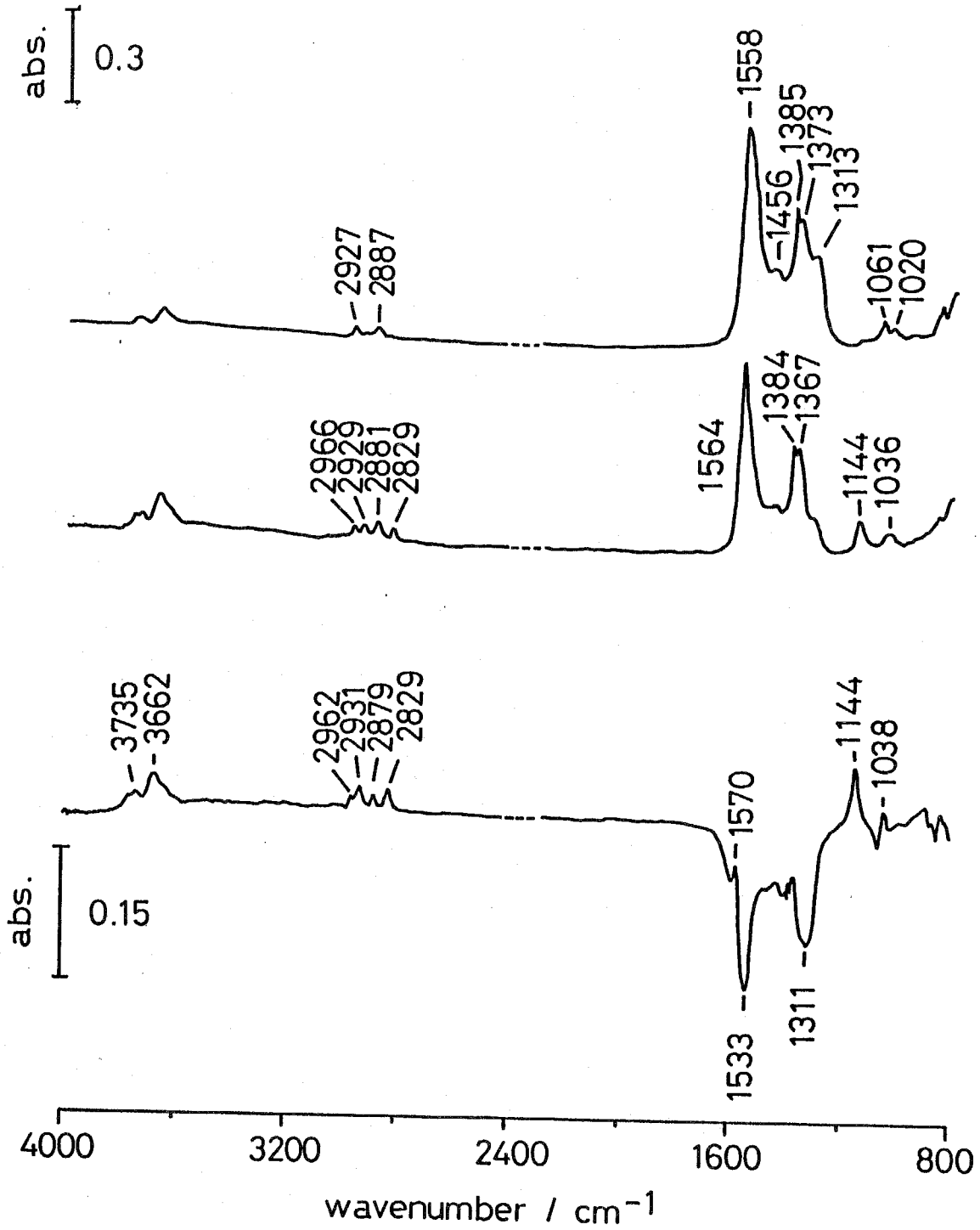

Fig. 6-17 IR spectra of adsorbed species from CO_2(a)+H_2(g) reaction: (a) at 523 K for 5 min in the presence of 60 Torr H_2; (b) at 523 K after 3 hr; (c) ratio spectrum of (b)/(a).

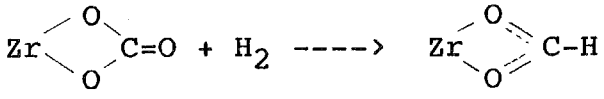

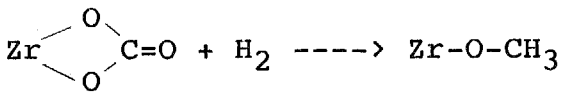

Reactivity of Methoxide Species

When the CO-H_2 reaction was carried out over the methoxide-preadsorbed-ZrO_2 at 643 K (at this temperature isobutene is selectively produced), initial activity for production of C4 compounds were observed to be 20 times more than that by CO-H_2 reaction. This suggests the methoxide species to be an effective intermediate of isobutene synthesis. After 10 Torr of O_2 was introduced to methoxide preadsorbed-ZrO_2 at room temperature the system was heated gradually (fig. 6-18). The formate species appeared when methoxide species were oxidized at 523 K. It should be noted that the type 1 methoxide species (1147 cm^{-1}) reacted faster than the type 2 methoxide (1047 cm^{-1}).

Reaction of methoxide species with 10 Torr of H_2 gave no change in the IR spectra from room temperature to 573 K. CO gave the same result as in case of CO and H_2 mixed gas. The IR spectra of the reacted methoxide species with CO gas at 523 K are shown in fig. 6-19 and the calculated ratio spectrum after/before the reaction in fig. 6-19(c). Formate species was formed with the bands at 1572 and

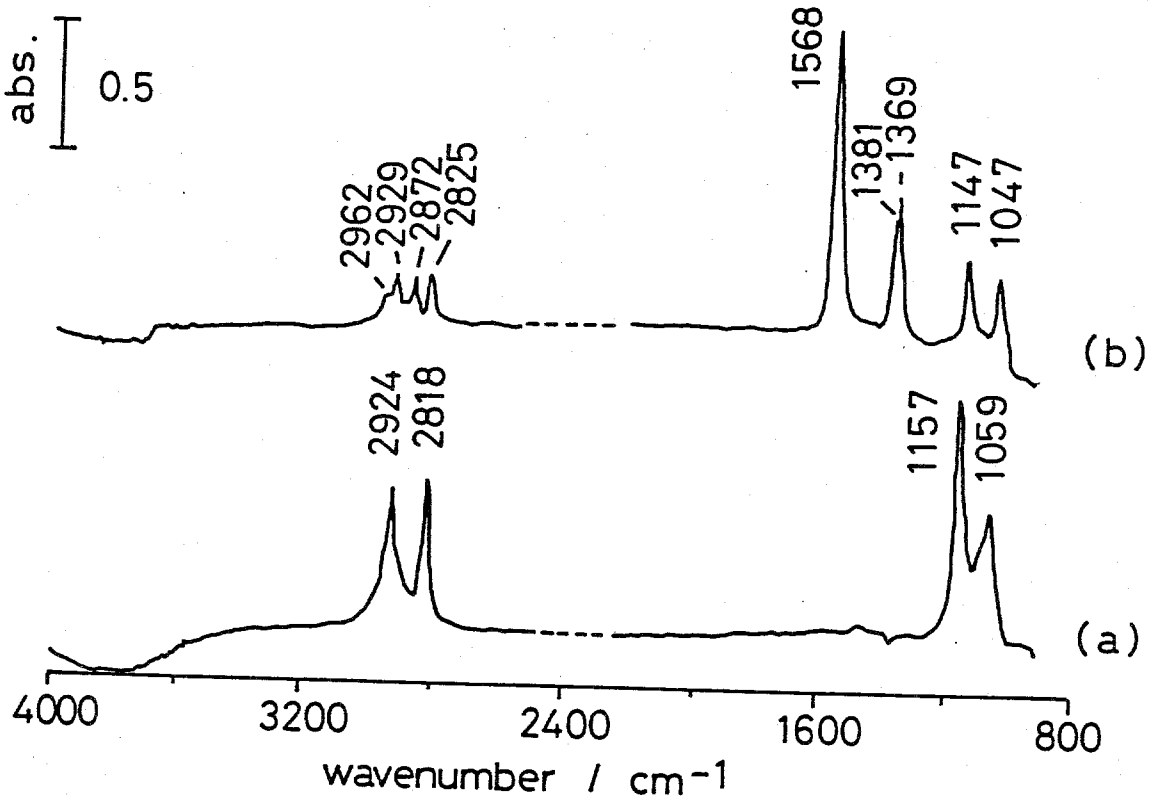

Fig. 6-18 IR spectra taken during the oxidation of methoxide species by O_2(g); (a) methoxide species at 453 K and (b) after O_2 introduction at 523 K for 3 hr.

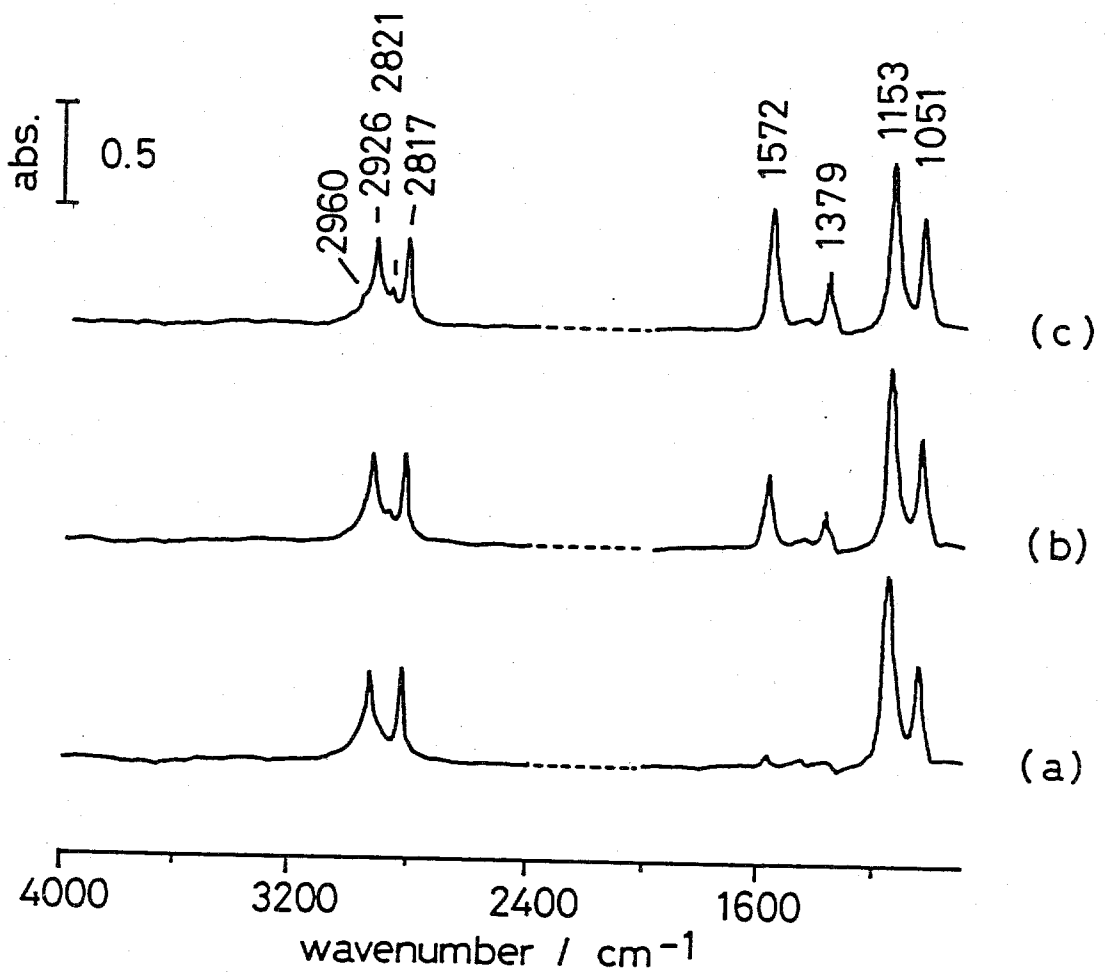

Fig. 6-19 The effect of CO introduction on methoxide species preadsorbed ZrO_2, (a) methoxide species at 523 k, (b) after CO admission at 523 K for 10 min. and (c) for 1 hr.

1379 cm^{-1} in OCO^- stretching region and at 2964 and 2870 cm^{-1} in CH stretching region. In case of reaction with synthesis gas, formation of formate was much faster than the usual reaction. This may be considered to be caused not from the adsorbed methoxide species but directly from the synthesis gas.

Reactivity of Formate Species

The $CO-H_2$ reaction over formate-preadsorbed-ZrO_2 showed low selectivity towards C4 products (less than the 80 % of usual the reaction) and high CO_2 formation rate (by about 700 times) at the initial stage of the reaction. So the adsorbed formate species can be regarded as an inhibitor rather than an intermediate for the synthesis reaction. From the IR results of formate hydrogenation it is considered that the formate species was not hydrogenated to produce methoxide species but only to desorb or decompose in the atmosphere of H_2. This supports the fact that the formate species is not a useful intermediate for synthesis of methanol.

Exchange reactions of DCOO and CD_3O species with gaseous H_2 were also carried out. DCOO and CD_3O species were prepared by the reaction of CO and D_2 at 523 K for 14 hr. Their spectrum is shown in fig. 6-20(a). H_2 was introduced to the ZrO_2 surface after the surface was covered with DCOO and CD_3O species. After 4 hr of exchange reaction an IR spectrum was given as presented in fig. 6-20(b). All the bands due to d-formate species (2173, 2065, 1560 and

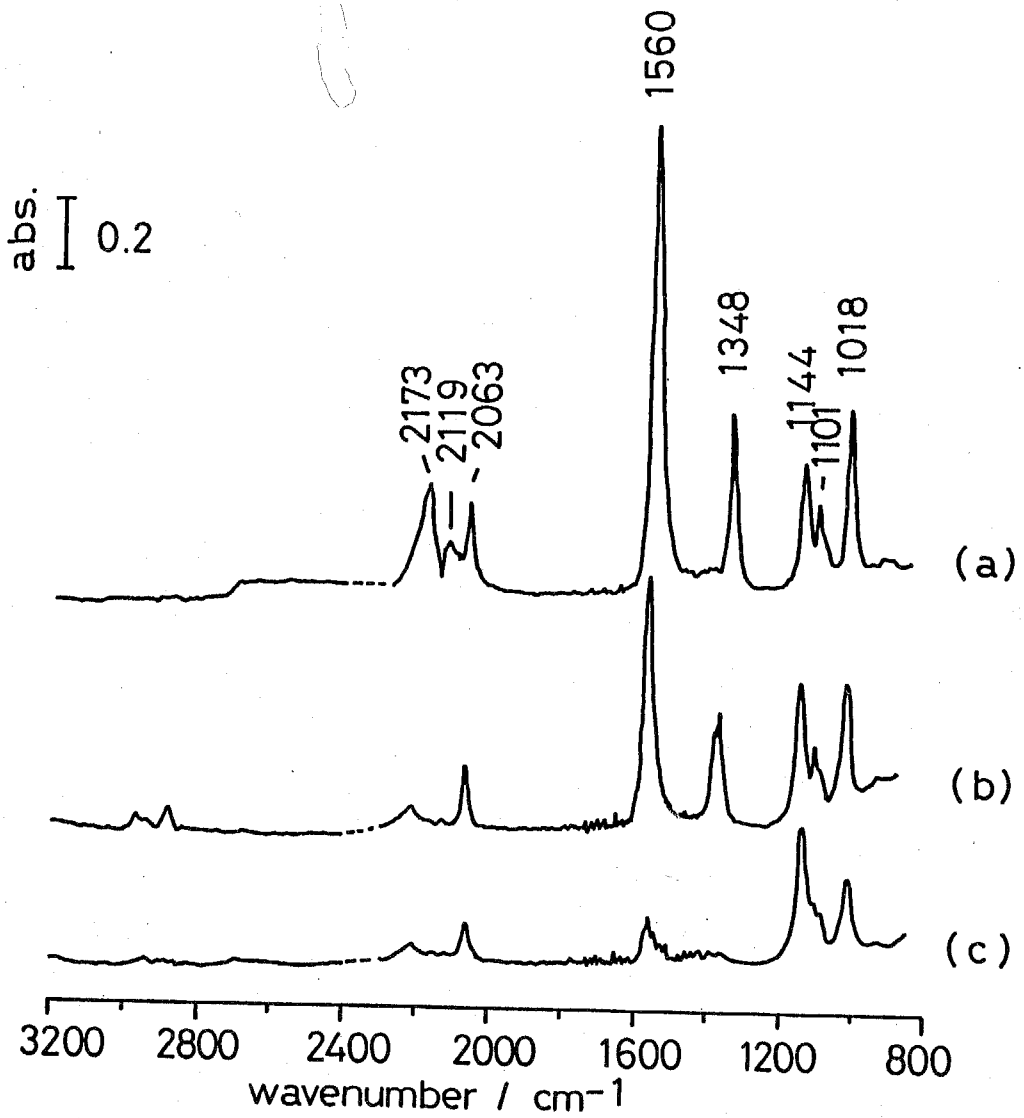

Fig. 6-20 Exchange reaction of methoxide and formate species with H_2, (a) surface CD_2O and DCOO species at 523 K, (b) after addition of H_2 at 523 k for 4 hr and (c) after evacuation at 623 K.

1348 cm^{-1}) were exchanged to HCOO species, while those of CD_3O species remained unchanged. Furthermore, the produced formate species are either desorbed or decomposed when the system was evacuated at 673 K. This result makes it clear that the CH bond of methoxide species is much stabler than the bond of formate species, which may be interpreted by the fact that CH bond of methoxide species is further away from activated hydrogen atoms on the surface than the one of the formate species.

6-4-5 CO Hydrogenation at Low Temperature

IR band analysis

At synthesis the temperature, only formate and methoxide species were observed. It is shown in 6-4-4, the formate species was not the reaction intermediate for CO hydrogenation to produce methanol. It is clear that methanol is formed by hydrogenation of methoxide species. Then how does the initial insertion of hydrogen atoms occur and/or what is the reaction intermediate to methoxide? To acquire information for these questions above, CO hydrogenation were observed at lower temperatures.

When 140 Torr of synthesis gas (mixture of CO and H_2, ca. 5 % CO in this study) was admitted at room temperature, IR spectra as shown in fig. 6-21 were observed. It is in good agreement with one of our previous reports[42]. Mainly two species were formed: formate species

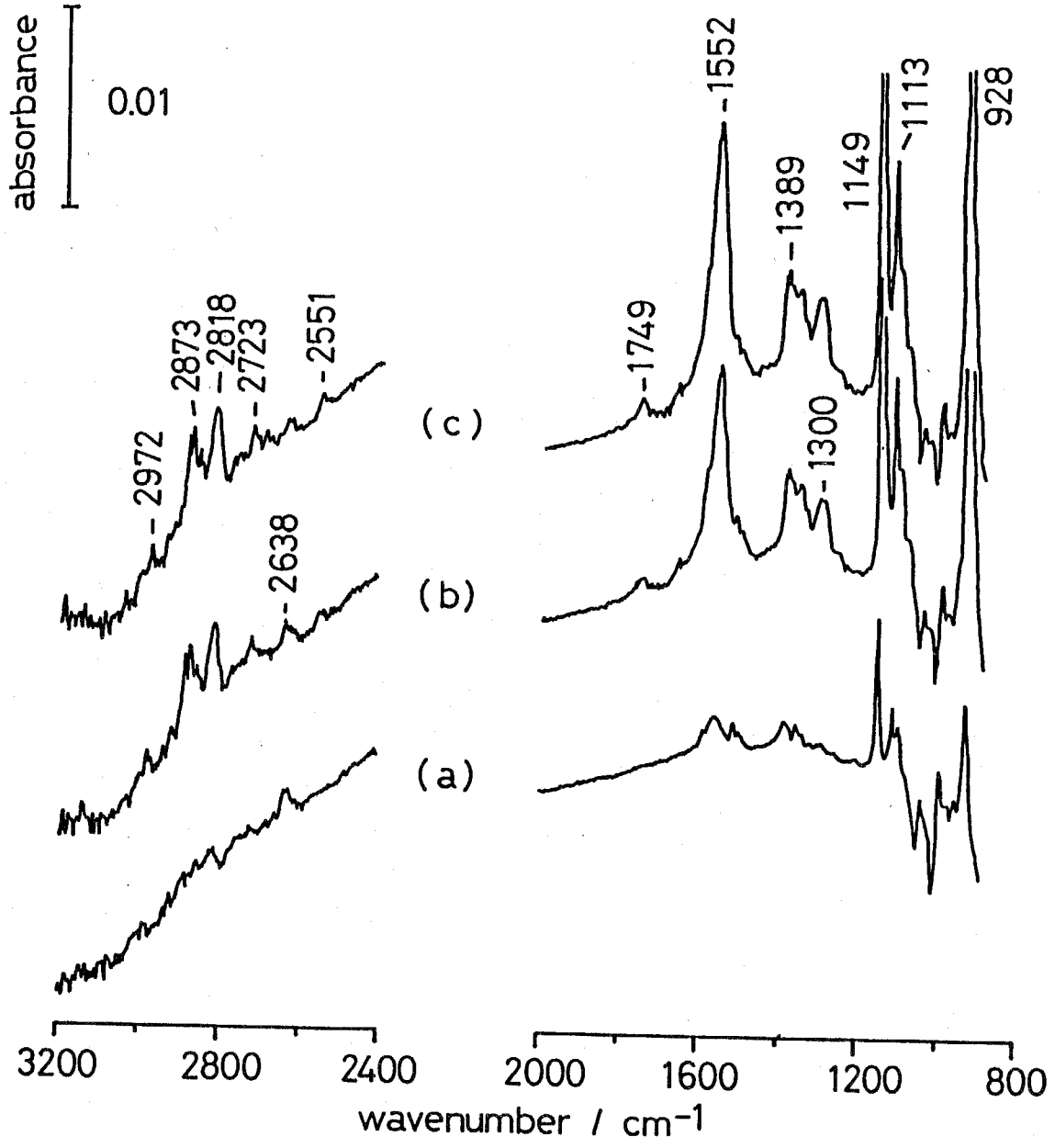

Fig. 6-21 CO hydrogenation at room temperature, (a) soon, (b) 20 min and (c) 1 hr.

Table 6-6 Assignment of oxymethylene species

assignment	$H_2C(OCD_3)_2$ [44]	TiO_2 [45]	ZrO_2 [45]	ThO_2 [45]	this work
CH_2 a-str.	2945	2950	2970	2960	
CH_2 s-str.	2882	2882	2868	2870	2840
CH_2 sci.	1473	1482,1464	1490,1470	1495	
CH_2 wag.	1401	1418-1408	1410	1405	1350 w
CH_2 tort.	1302	1300	1315	1280	1300 w
	1186	1251	1255		
	1138	1172,1156	1180,1157	1180,1150	1149 vs
CH_2 rock	1114	1113	1117	1112	1113 s
C-O str.	1086	1070	1070	1070	
			965	948	928 vs
			890	920	
	858				

w, weak; s, strong; vs, very strong.

(2972, 2873, 1552 and 1389 cm^{-1}) and oxymethylene species (2818, 1300, 1149, 1113 and 928 cm^{-1}). The assignment of oxymethylene species are presented in table 6-6. Other bands were also found at 2638, 2551, 1749 and 1097 (shoulder of this band at 1113) cm^{-1}. The bands at 2638 and 2551 cm^{-1} are assigned to CH str. modes because they shifted by the isotope ratio when CO-D_2 reaction at the same temperature was performed. It is noted that the band at 2638 cm^{-1} appeared soon after starting the reaction, while the two bands at 2551 and 1749 cm^{-1} appeared about 20 min later.

Also at 268 K (fig. 6-22), formate and oxymethylene species were produced but in a less amount. Then new bands at 1514, 1350 and 1097 cm^{-1} became observable. Spectra (a) and (b) contain the vibration-rotation absorption bands of gas phase water between 1800 and 1400 cm^{-1} which make the analysis difficult in this region. Therefore, the change from 20 min to 1 hr is also shown in fig. 6-21 (c). The feature of the band at 2636 cm^{-1} as well as the paired bands at 2559 and 1755 cm^{-1} was observed in the same way as that at room temperature.

Below 268 K weak bands which are normally hidden by strong formate and oxymethylene bands became detectable. IR spectra of the initial stage of the reaction at 258, 253, 248 and 233 K are shown in fig. 6-23, 24, 25 and 26, respectively. As is seen in fig. 6-25 and 26, formate species was hardly produced at the initial stage at 248 K and even after 1 hr at 233 K, while oxymethylene species

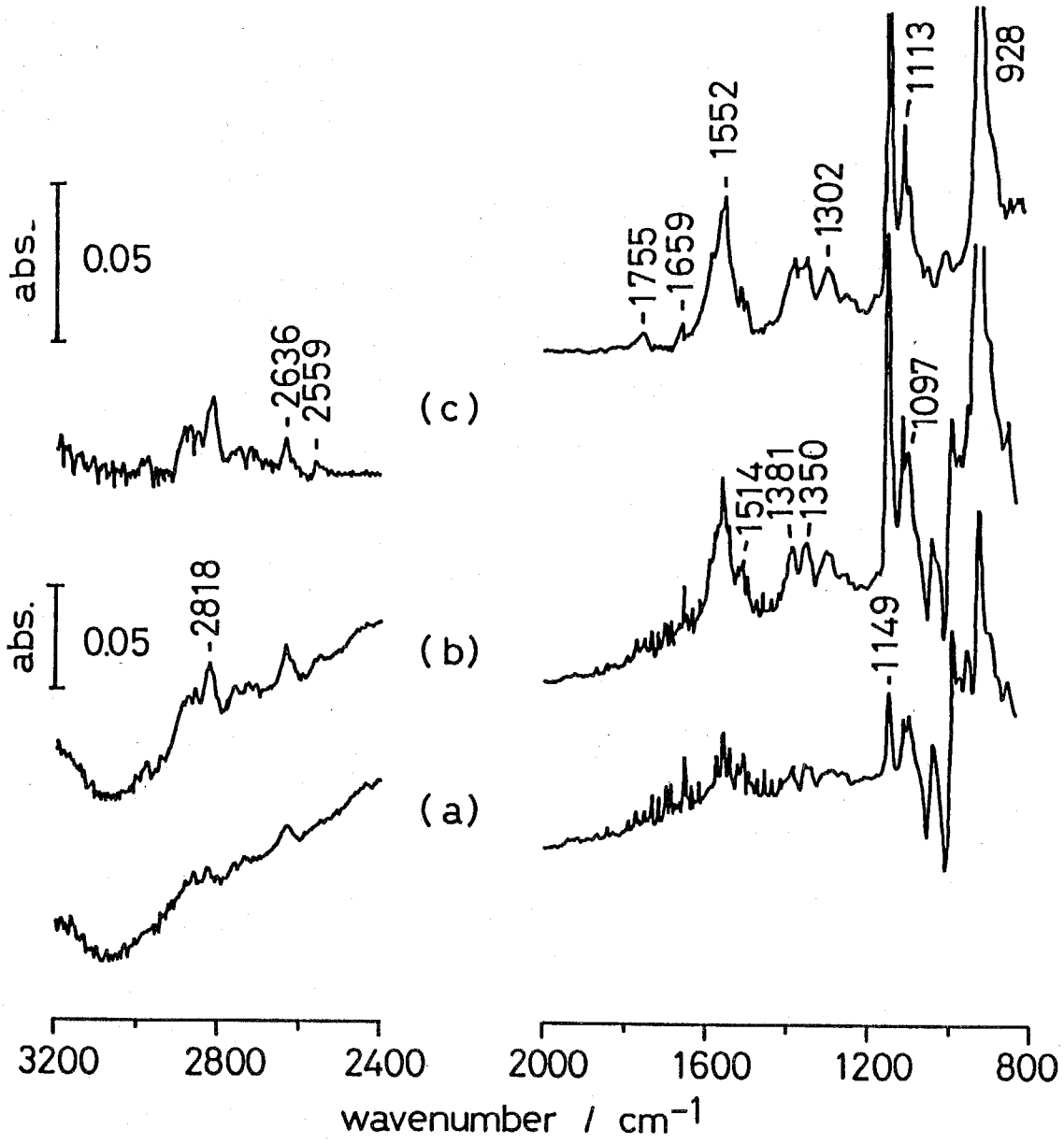

Fig. 6-22 CO hydrogenation at 268 K, (a) soon, (b) 20 min and (c) 1 hr / 20 min.

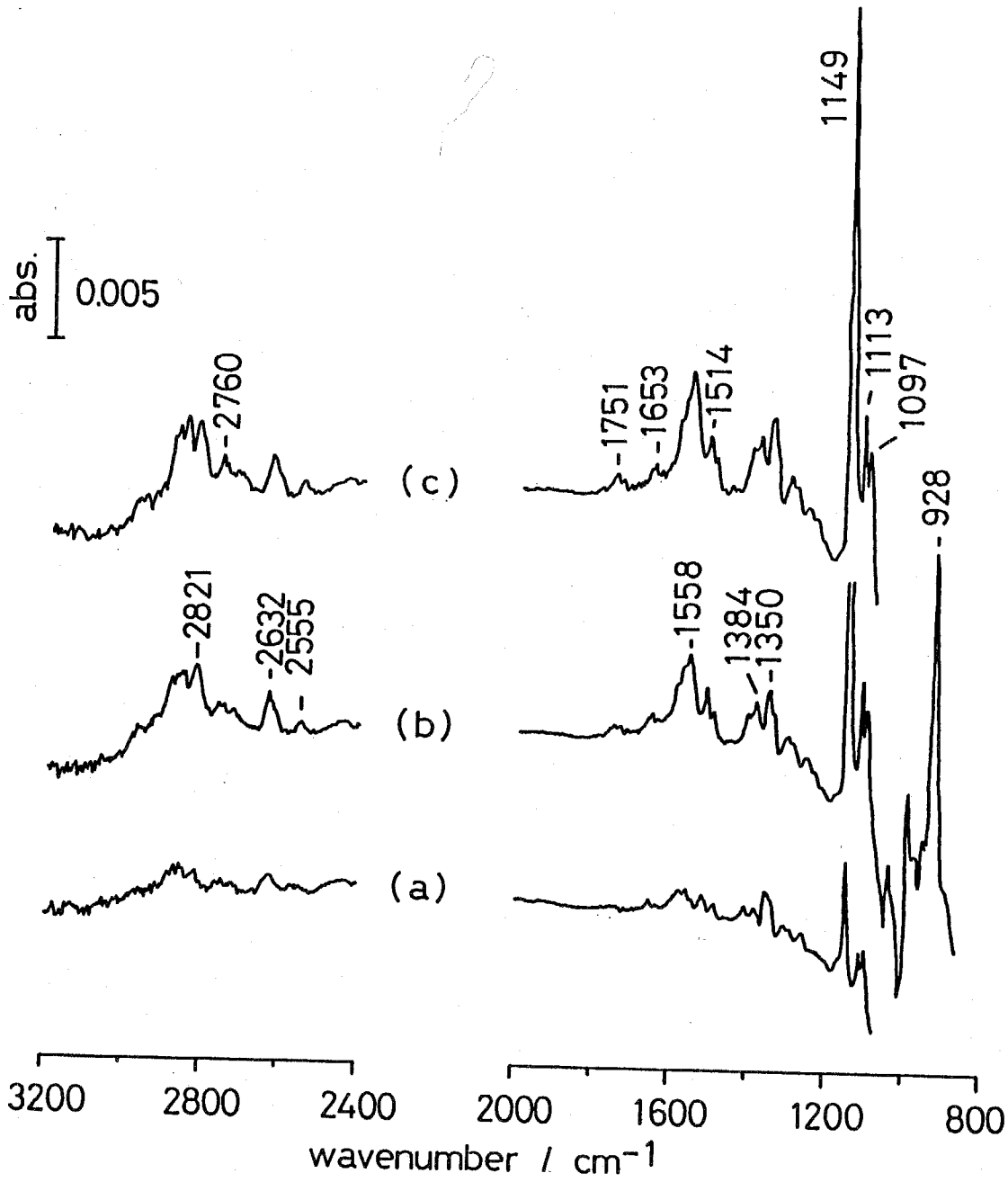

Fig. 6-23 CO hydrogenation at 258 K, (a) soon, (b) 10 min and (c) 30 min.

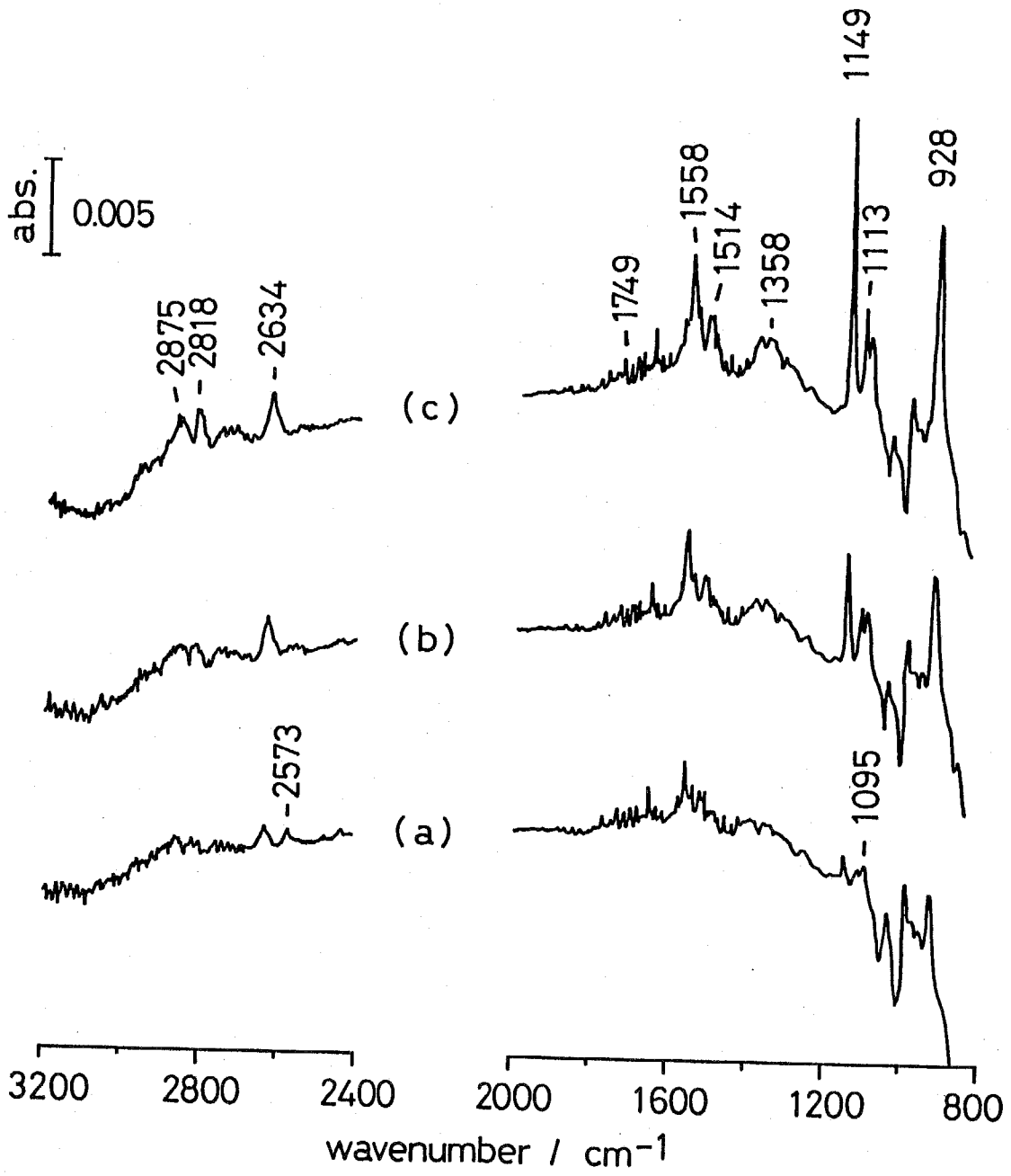

Fig. 6-24 CO hydrogenation at 253 K, (a) soon, (b) 5 min and (c) 20 min.

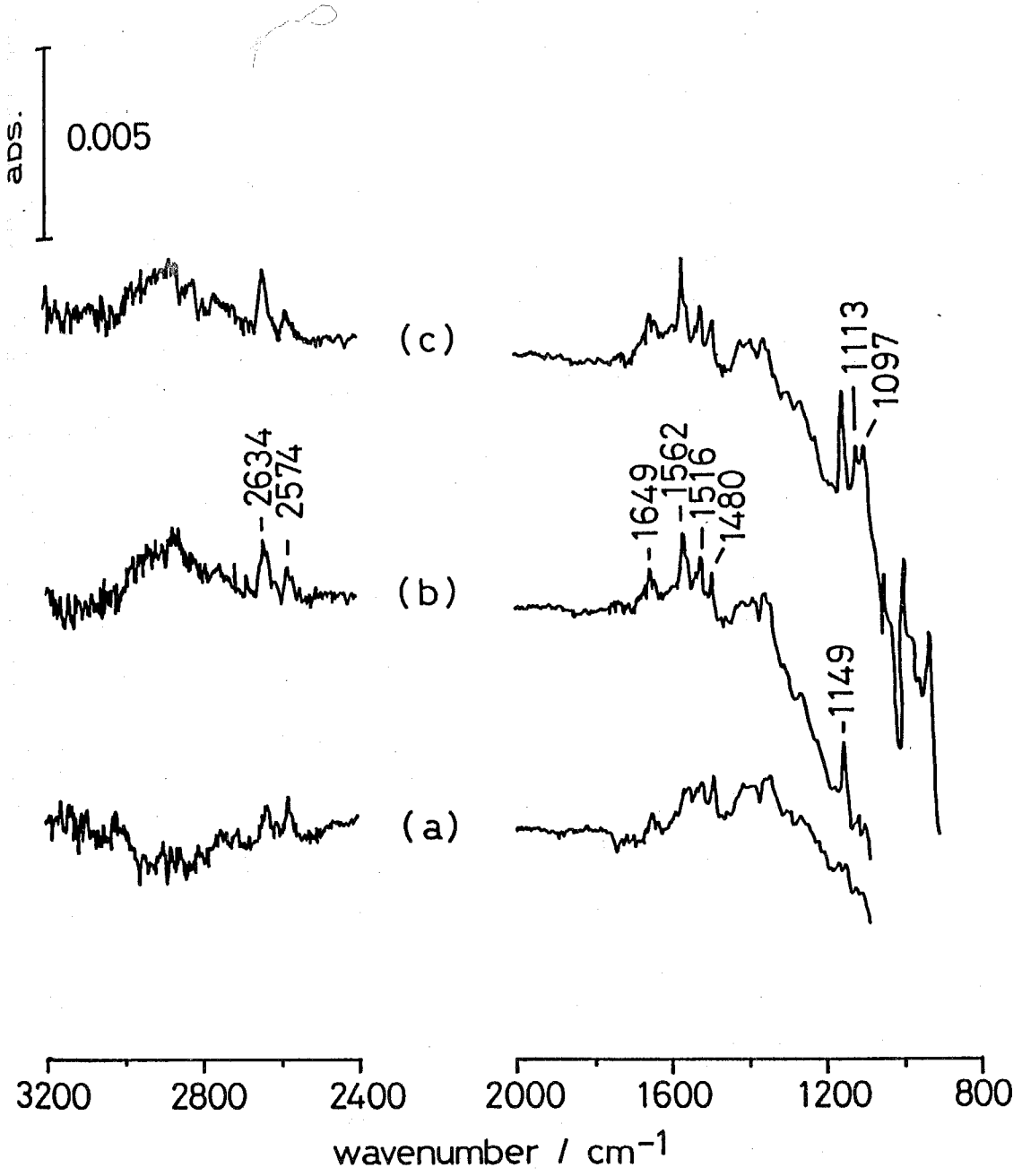

Fig. 6-25 CO hydrogenation at 248 K, (a) soon, (b) 8 min and (c) 15 min.

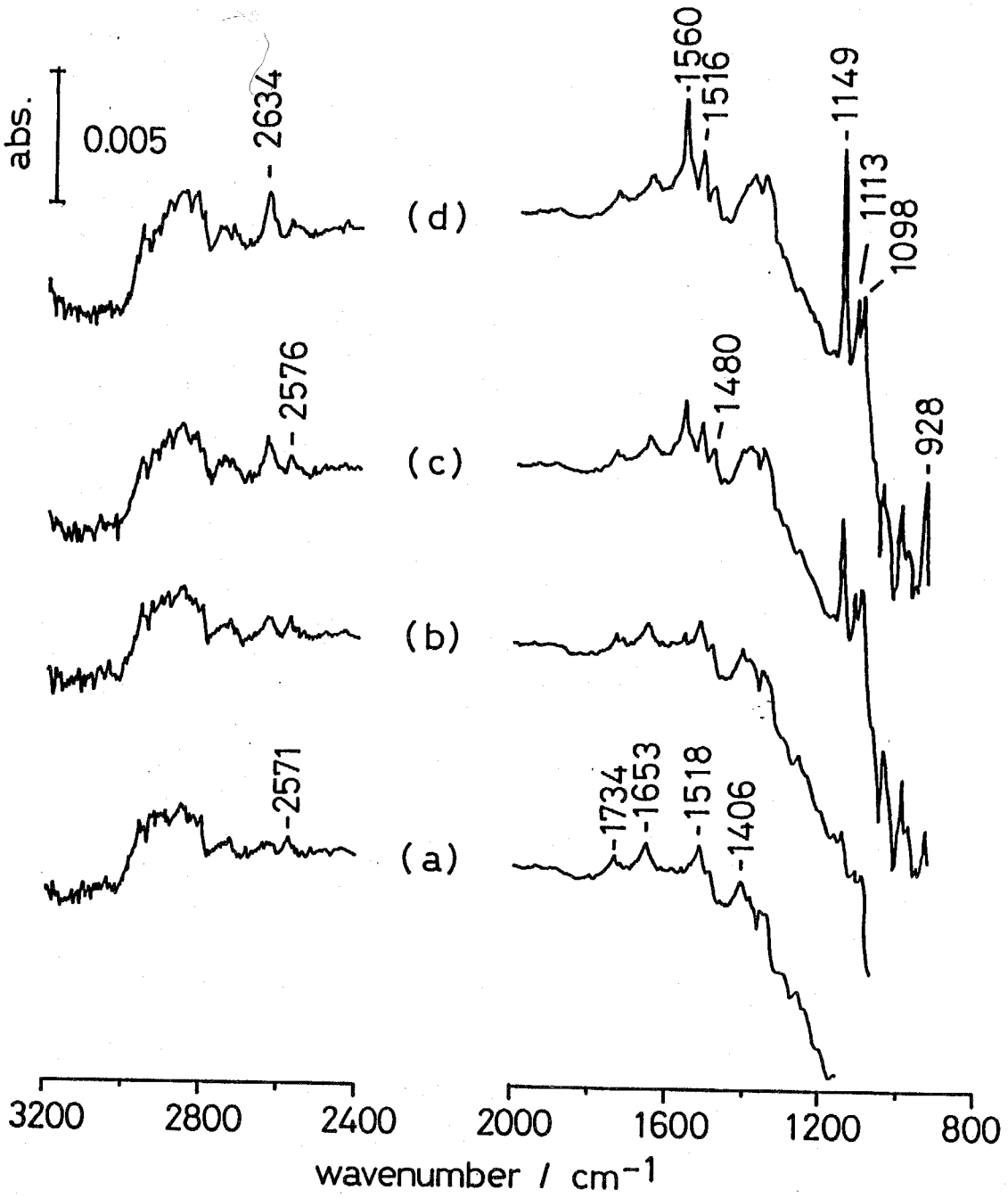

Fig. 6-26 CO hydrogenation at 233 K, (a) 5 min, (b) 10 min, (c) 30 min and (d) 1 hr.

was still formed quite rapidly. Between 1800 and 1400 cm^{-1}, five bands appeared at 1743, 1653, 1560, 1516 and 1480 cm^{-1}. The band at 1560 cm^{-1} is assigned to ZrH species from its peak position and behavior, i.e. slow formation rate at 233 K. The band at 1734 cm^{-1} is paired with the band at 2571 cm^{-1}, as mentioned already, accompanied by another band at 1480 cm^{-1}. These three bands were always observed in the same way through all the of experiments. The band at 2634 cm^{-1} was also found to be paired with those at 1516 and 1097 cm^{-1}. The band at 1653 cm^{-1} was not related to any other bands.

The observed bands, except those due to formate and oxymethylene species, are classified as follows (fig. 6-26 is to be referred for band frequencies):

1) the bands at 2634, 1516 and 1098 cm^{-1},
2) the bands at 2571, 1734 and 1480 cm^{-1},
3) the band at 1560 cm^{-1} due to ZrH species,
4) the band at 1653 cm^{-1},
5) several bands between 2700 and 2800 cm^{-1},
6) the band at 1350 cm^{-1}.

The species 1) and 2) are expected to be intermediate species from adsorbed CO to produce oxymethylene, methoxide and formate species because they were observed only below room temperature and before production of other stable species. The most probable form of these species is monohydrogenated CO, i.e. formyl species.

The existence of formyl species during CO hydrogenation

Table 6-7 Assignment of formyl species

assignment	$\begin{matrix}H\\ \diagdown\\ H\end{matrix}C=O^{16}$	$\begin{matrix}H\\ \diagdown\\ CH_3\end{matrix}C=O^{16}$	$\begin{matrix}H\\ \diagdown\\ CH_3O\end{matrix}C=O^{16}$	complex[46]	$\begin{matrix}H\\ \diagdown\\ Zn\end{matrix}C=O$[47,48]	this work[a]	
						H-bonded	O-bonded
CH str.	2843 vs 2783 s	2822 m	2943 s	2760	2770	2571	2634
C=O str.	1746 vs	1743 vs	1754 vs	1601	1650 1550	1743	1516
CH bend		1400 s	1371 w			1480	
CH bend		763 w	1032 m				1098

vs, very strong; s, strong; m, medium; w, weak.
a, band frequencies are referred to fig. 6-26.

as an intermediate has been expected it was actually detected only on ZnO by Saussey et al.[47,48] They observed the bands at 2770, 1650 and 1550 cm^{-1} during CO hydrogenation over ZnO at room temperature, and compared these with those of an Os coordinated complex[46]. IR bands attributed to formyl in various compounds and the surface species are listed in table 6-7.

On ZrO_2, there seems to be two different species whose bands were observed at quite different positions. They exhibited a different behavior. The one species with the bands at 2571, 1743 and 1480 cm^{-1} shows its CH str. mode at an extremely low frequency and its CO str. at usual frequency for formyl species. The other species presented on the right side in table 6-7, show a very softened CO stretching mode. The bands which shifted to low frequency are expected to have additional interaction with the ZrO_2 surface. Therefore, from the band positions of these species, the adsorbed forms are regarded as "H-interacted" (2571, 1743 and 1480 cm^{-1}) and "O-interacted" (2634, 1516 and 1098 cm^{-1}) formyl species.

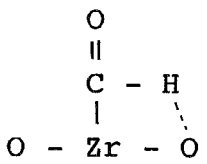

H-interacted formyl

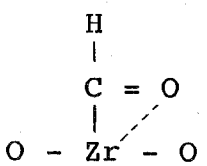

O-interacted formyl

All the observed IR bands during CO hydrogenation below room temperature are summarized in table 6-8. Several

Table 6-8 Observed bands during CO hydrogenation below room temperature.

frequency/cm-1	assignment	surface species
2972	CH str.	formate
2873	CH str.	formate
2818	CH str.	oxymethylene
a2760	CH str.	
2723	CH str.	
2638	CH str.	O-interacted formyl
2551	CH str.	H-interacted formyl
1749	C=O str.	H-interacted formyl
b1653		
b1560	Zr-H str.	ZrH
1552	OCO a-str.	formate
b1516	C=O str.	O-interacted formyl
b1480	CH bend.	H-interacted formyl
1389	OCO s-str.	formate
a1350		
1300		formate
1149		oxymethylene
1113		oxymethylene
b1098	CH bend	O-interacted formyl
928		oxymethylene

All band frequencies are from fig. 6-21 except a and b. a, from fig. 6-23; b, from fig. 6-26

bands could however, not be identified.

The behavior of observed species

The methoxide species were observed only above 473 K. Formate species was not produced at 233 K even after 5 hr but was observed at 253 K. Even at 203 K, oxymethylene and two types of formyl species were formed. Those three species were produced at 203 K much faster than the production rate of the ZrH species. When the oxymethylene species was heated to 453 K (under evacuation condition), formate and OH species were generated with a decreasing amount of oxymethylene species. This is confirmed by heating that there is a reaction pathway from oxymethylene species to formate species by heating (above ca. 400 K).

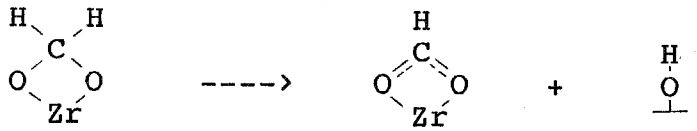

An OH band was observed at 3670-3675 cm^{-1} in the spectra taken during CO hydrogenation at low temperature although some were very obscure because of the low SN ratio.

To see the reactivity of ZrH-OH species for CO hydrogenation, CO was introduced to hydrogen preadsorbed-ZrO_2 at room temperature. ZrH-OH species were produced at room temperature with 400 Torr of H_2 and evacuated. Then, 20 Torr of CO was admitted. Although the reaction was slower than that from synthesis gas, the same species (formyl, oxymethylene and formate species) were observed.

6-5 Discussion

6-5-1 CO hydrogenation mechanism at high temperature

At the synthesis temperature (523 K) CO is adsorbed to form bidentate carbonate species.

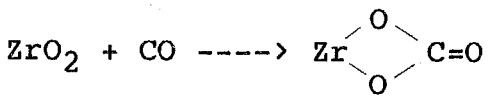

The bidentate species is also produced from CO_2 adsorption. Hydrogenation of bidentate carbonate formed from CO_2 adsorption results in the production of formate and methoxide species:

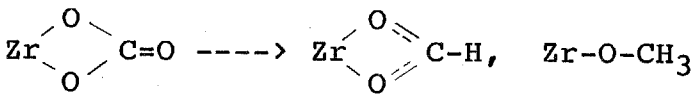

The methoxide species is not formed from the hydrogenation of the formate species, while oxidation of methoxide to form formate species occurs:

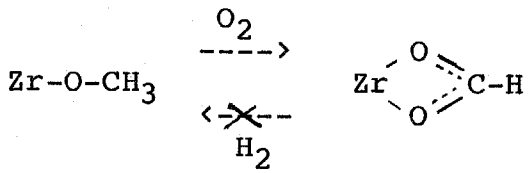

Therefore, it is suggested that at high temperature the following path way is working:

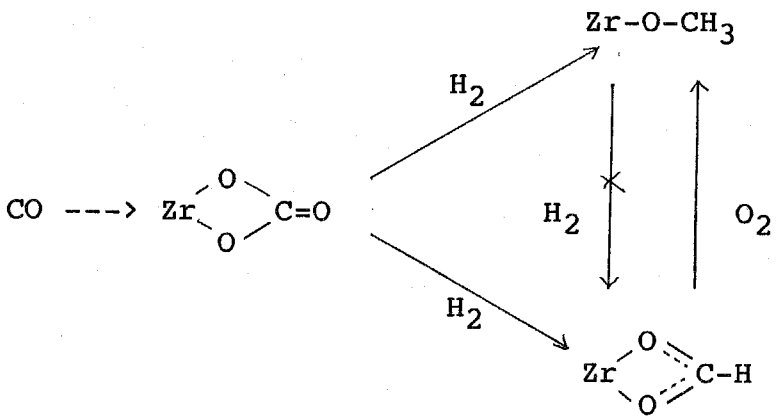

The main difference of this mechanism compared with the one proposed by other workers[13-15,52] is that the intermediate species is the bidentate carbonate. This difference is derived from the different site of CO adsorption. Generally CO is considered to be adsorbed on the metal site (Metal-C≡O), while in this mechanism oxygen is regarded as an adsorption site. This reaction path way is reasonably supported to take place by the presented results. However, if this mechanism is the main process, then it should be noted that CO_2 is better than CO as a reactant. Therefore another reaction mechanism which was observed at low temperature is discussed in the next paragraph.

6-5-2 CO hydrogenation mechanism at low temperature

Formation of formyl species

At low temperature CO is adsorbed on Zr metal through a Zr-C bond. The first product of CO hydrogenation is O-bonded and H-bonded formyl species:

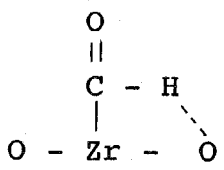

H-interacted formyl

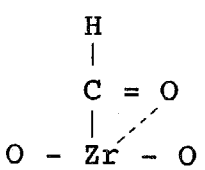

O-interacted formyl

The O-interacted formyl species is also proposed on ZnO[47,48]. They attribute the observed C=O str. at 1520 cm^{-1}-1 which appeared at very low frequency for a formyl species to Zn-interacted C=O str. The C=O str. band at 1516 cm^{-1} due to formyl species on ZrO_2 is then considered

to be Zr-interacted C=O str. On the other hand the C-H bond for H-interacted formate species on ZrO_2 appearing at low frequency (2557 cm^{-1}) seems to interact with the surface oxygen next to the Zr atom.

The source of the hydrogen, which is involved in the formyl species is now considered. The formyl, formate and oxymethylene species were observed when CO was introduced to the ZrH-OH preadsorbed ZrO_2 surface. This result supports that the ZrH-OH species are the reaction intermediate for CO hydrogenation on ZrO_2. In other words, formyl species is formed via ZrH-OH species. As presented in chapter 2, ZrH-OH species are produced above 223 K. CO hydrogenation however, proceeds at 223 K. This fact suggests that H_2 molecule reacts before the actual cleavage of H-H bond to form ZrH-OH. The existence of OH species after the formation of formyl species supports that ZrH species is included into formyl species.

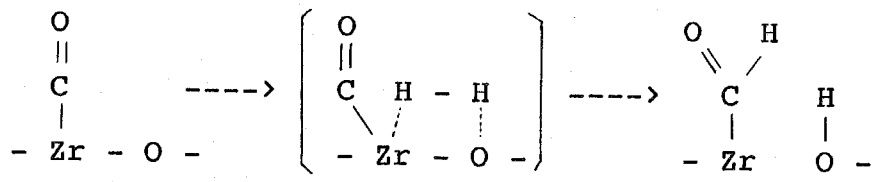

Formation of oxymethylene and formate species

Oxymethylene and formate species are regarded to be produced from the formyl species. For both cases, Zr-C bond has to be transformed to a 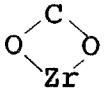 bond. OH species is also a reactive hydrogen source because OH bands were not accumulated during the reaction. Accordingly, formyl

species might migration to the OH site and react to form oxymethylene species.

In case of O-bonded formyl species, both formate and oxymethylene species could possibly be produced as follows:

1.1) The hydrogen of OH interact with carbon of the formyl species maintaining the interaction of =O and Zr.
Then two new bonds are formed, C-H and C-O, which give rise to breaking the Zr-C bond:

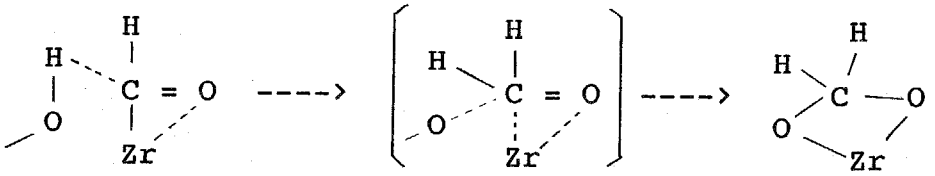

oxymethylene

1.2) If the carbon in the formyl species does not react with the hydrogen of the OH species but interacts with the lattice oxygen located at the opposite side of the OH species, a formate species is formed.

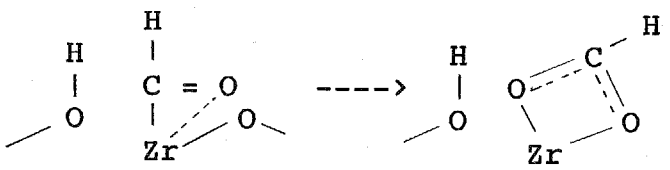

formate species

This H-bonded formyl species also seems to have the possibility to produce both oxymethylene and formate species:

2.1) In case the carbon interacts with both oxygen and hydrogen atoms of OH species and results in OH bond cleavage, and new Zr-O-C bond is formed from inversion of

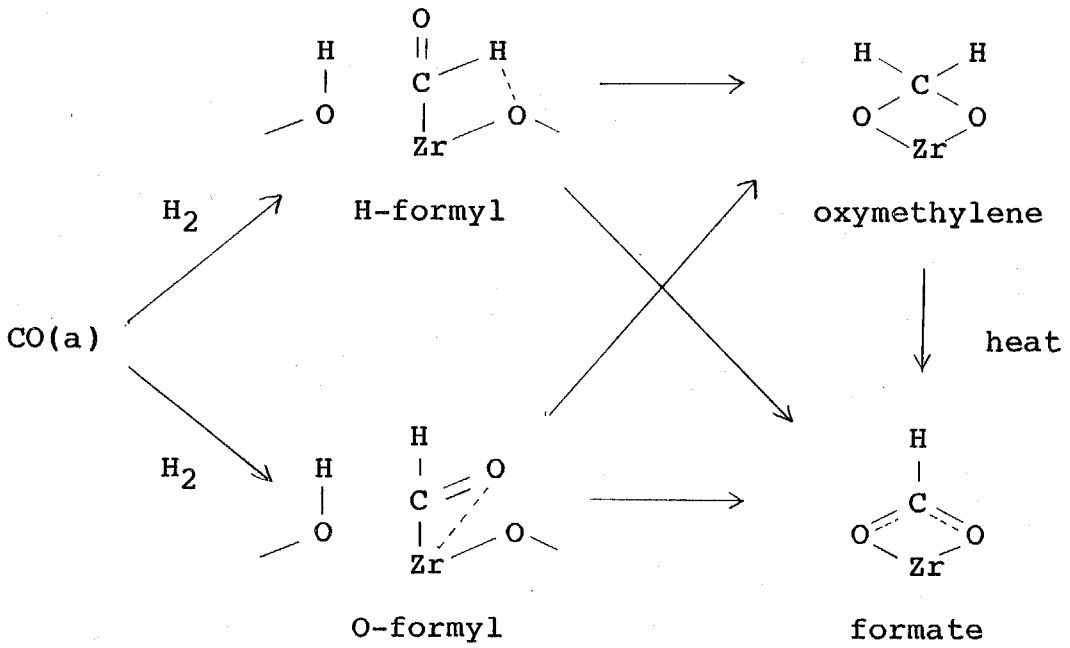

Formation of methoxide species

For methanol production from CO hydrogenation mainly three probable mechanisms have been proposed. These mechanisms are schematically given below.

1) formate-to-methoxide mechanism[2,13,49-51]

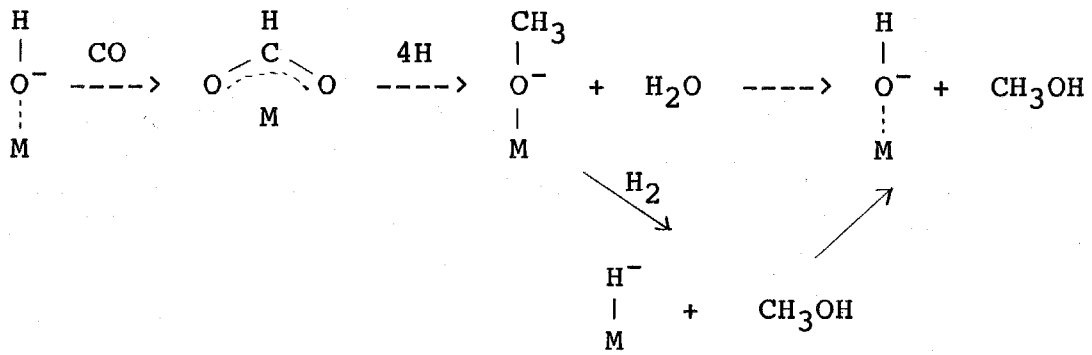

or

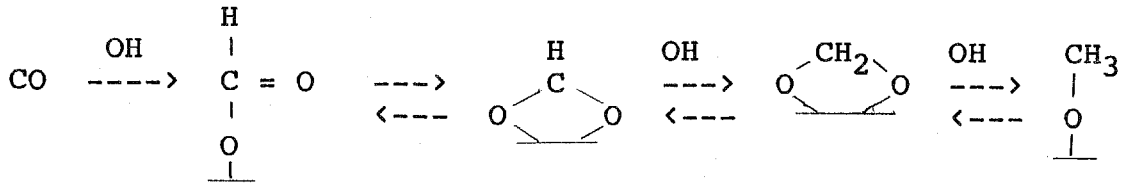

2) formyl-to-enol mechanism[2,11]

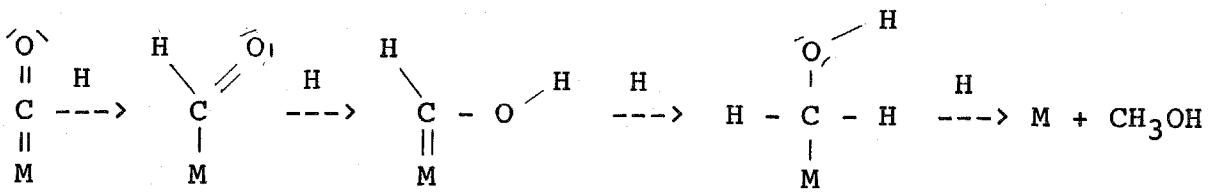

(enol)

3) side-on hydrogenation mechanism[2]

(adsorbed formaldehyde mechanism)

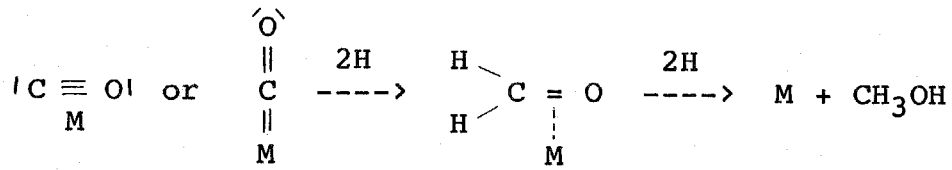

Manriques et al. supported the adsorbed formaldehyde species as an intermediate by a study of Zr homogeneous complex.

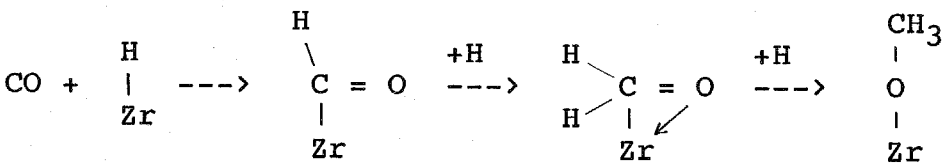

The intermediate involved a Zr atom bonded to both the carbon and oxygen of a formyl, in a sort of three-sided cyclic resonance structure.

On ZrO_2, Ekerdt and his co-workers supported the "formyl mechanism" over ZrO_2 since formate species has never been satisfactorily shown to convert directly to the methoxide species.

In the present study, the formate-to-methoxide mechanism (1) is not considered likely because formate was not hydrogenated to methoxide species. The formyl-to-enol mechanism (2) is also thought to be unlikely. If an enol species which possesses a C-O-H bond existed, another type of C-O str. mode could be observed in the IR spectra. The side-on hydrogenation mechanism (3) is considered to be possible. In the observed spectra there were still several bands remaining unassigned which might be attributed to adsorbed formaldehyde species. However, when a part of the formate-to-methoxide mechanism is applied, the oxymethylene species would be expected to be a precursor of the methoxide species. Although the proposers of this mechanism did not directly detect the oxymethylene species during the reaction, in this study this species was observed. Therefore the most probable reaction mechanism is regarded as to be the one described in scheme 6-1. Methoxide species are produced by hydrogenation of oxymethylene species.

To generate methoxide species, a reaction temperature of above 473 K is needed, while oxymethylene species is produced even at 203 K. This indicates that the formation of the third C-H bond requires a higher activation energy than those for the first and the second C-H bond formation. Consequently, it is concluded that the insertion of the third hydrogen is the rate determining step for methanol synthesis from CO hydrogenation over ZrO_2.

Scheme 6-1 Proposed CO hydrogenation over ZrO_2 at low temperature

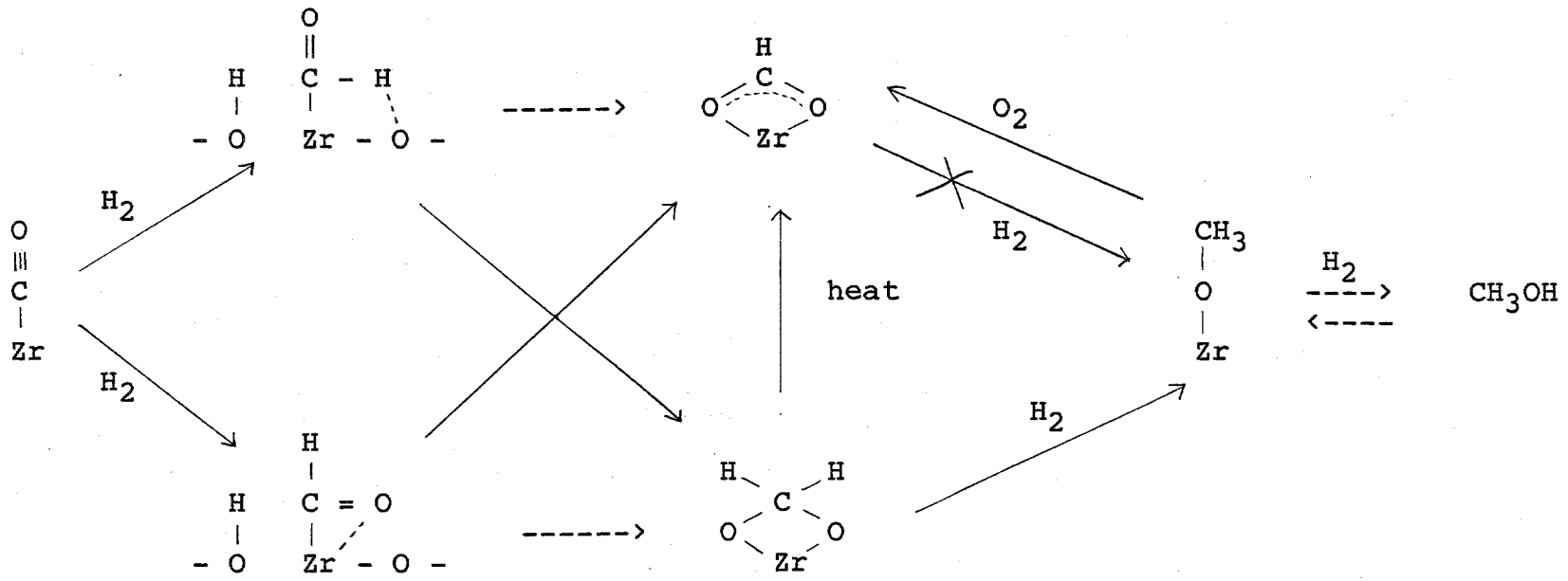

6-6 Conclusion

A reaction mechanism of CO hydrogenation over ZrO_2 to produce methanol is proposed. This mechanism is based on adsorption and in situ studies by FT-IR. In the in situ study below room temperature two types of formyl species were identified as precursor of oxymethylene and formate species. The formate species did not transform to methoxide species by H_2. This indicates that the oxymethylene species is hydrogenated to methoxide species. The fact that the methoxide species were not formed below 527 K might mean that the rate determining step for methanol production is the insertion of the third hydrogen atom to the carbon.

6-7 References

1 Energetic values are refered to, D.R. Stull, E.F. Westrum and G.C. Sinke, "The Chemical Thermodynamics of Organic Compounds", Wiley, New York, 1969.58

2 K. Klier, "Mthanol Synthesis", Adv. Catal., 1982, 31, 243.

3 W. Kein, "Catalysis ion C1 Chemistry", D Reidel Publishing Co., 1983.

4 U.S. Patent, 1978, 4, 110 (IFP).

5 M. Ichikawa, Bull. Chem. Soc. Jpn., 1978, 51, 2268.

6 German Offen., 2, 503, 204 (Unuon Carbide).

7 Y. Kikuzono, S. Kagami, S. Naito, T. Onishi and K. Tamaru, Chem. Lett., 1981, 9, 1219.

8 J.W. Rathke and H.M. Feder, J. Amer. Chem. Soc., 1978, 100, 3023.

9 W. Kein, M. Berger and J. Schlupp, J. Catal., 1980, 61, 359.

10 D.R. Fahey, J. Amer. Chem. Soc., 1981, 103, 136.

11 H.H. Kung, Cat. Rev. Sci. Eng., 1980, 22, 235.

12 H. Hattori and G-W. Wang, Proc. 8th Intern. Congr. Catal., Berlin, 1984, 3, 219.

13 Y-M. He and J.G. Ekerdt, J. Catal., 1984, 87, 238.

14 Y-M. He and J.G. Ekerdt, J. Catal., 1984, 87, 381.

15 Y-M- He and J.G. Ekerdt, J. Catal., 1984, 90, 17.

16 K. Nakamoto, "Infrared and Raman Spectra of Inorganic and Coordination Compounds", 4th Edn., ISBN 0-471-01066-9, 1986, A. Wiley-Interscience Publication.

17 C. Moterra, E. Carrone, V. Bolis and B. Fubini, Spectrochim. Acta, 1987, 43A, 1577.

18 M.I. Zaki and H. Knozinger, Spectrochim. Acta, 1987, 43A, 1455.

19 B-Q. Xu, T. Yamaguchi and K. Tanabe, Chem. Lett., 1988, 1663.

20 L. Morterra, E.Giamello, L. Orio and M. Volante, J. Phys. Chem., 1990, 94, 3111.

21 G. Busca, H. Saussey, O. Saur, J.C. Lavalley and V. Lorenzelli, Appl. Catal., 1985, 14, 245.

22 M.I. Zaki, B. Vielhaber and H. Knozinger, J. Phys. Chem., 1986, 90, 3176.

23 A.A. Tsyganenko, J. Lamotte, J.P. Gallas and J.C> Lavalley, J. Phys. Chem., 1989, 93, 4179, 23

24 F.M. Hoffman, Surf. Sci. Report, 1983, 3.

25 N.E. Tretyakov, D. Pondnyakov, O.M. Orankaya and V.N. Filimonov, Russ. J. Phys. Chem., 1970, 44, 596.

26 J. Fujita, A.E. Martell and K. Nakamoto, J. Chem. Phys., 1962, 36, 339.

27 C. Blyholder, Proc. Inte n. Congr., Elsevier, Amsterdam, 1964, p. 657.

28 J.V. Evans and T.L. Whateley, J. Chem. Soc., Faraday Trans. 1, 1967, 63, 2769.

29 Y. Fukuda and K. Tanabe, Bull Chem. Soc. Jpn., 1973, 46, 1616.

30 B.M. Gatehouse, S.B. Livingston and R.S. Nyholm, J. Chem. Soc., 1958, 3137.

31 A. Ueno, T. Onishi and K. Tamaru, J. Chem. Soc., Faraday Trans. 1, 1971, 67, 3585.

32 T.P. Beebe, Jr., J.E. Crowell, Jr. and J.T. Yates, Jr., J. Phys. Chem., 1988, 92, 1296.

33 R.G. Greenler, J. Chem. Phys., 1962, 37, 2094.

34 R.P. Groff, J. Catal., 1984, 86, 215.

35 A.J. Tech, D. Giles and J.F. Kibblewhite, J. Trans. Faraday Soc., 1967, 67,854.

36 G. Hussain and N. Sheppard, Spectrochim. Acta, 1987, 43A, 1631.

37 B.A. Morrow, J. Chem. Soc., Faraday Trans. 1, 1974, 70, 1527.

38 J. Kondo, Y. Sakata, K. Maruya, K. Tamaru and T. Onishi, Appl. Surf. Sci., 2987, 28, 475.

39 J. Lamotte, V. Moravek, M. Bensitel and J.C. Lavalley, React. Kinet. Catal., 1988, 36, 113.

40 M. Bensitel, V. Moravek, J. Lamotte, O. Saur and J.C. Lavalley, Spectrochim. Acta, 1987, 43A, 147.

41 R.O. Kogel and R.G. Green, J. Chem. Phys., 1986, 49, 1638.

42 T. Yamaguchi, Y. Nakano and K. Tanabe, Bull. Chem. Soc. Jpn., 1978, 21, 2482.

43 T. Onishi, H. Abe, K. Maruya and K. Domen, J. Chem. Soc., Chem. Commun., 1986, 103.

44 K. Nukaba, Spectrochim. Acta, 1983, 18, 745.

45 G. Busca, J. Lamotte, J.C. Lavalley, V. Lorenzelli, J. Amer. Chem. Soc., 1987, 109, 5197.

46 $OS(CHO)H(CO)_2(PPh_3)_2$,
K.L. Brown, G.R. Clark, C.E.L. Headford, K. Marden and W.R. Roper, J. Amer. Chem. Soc., 1979, 101, 503.

47 J. Saussey, J.C. Lavalley, J.C. Lamotte and T. Rais, J. Chem. Soc., Chem. Commun., 1982, 278.

48 J. Saussey, J.C. Lavalley and T. Rais, J. Mol. Catal., 1984, 26, 159.

49 P.J. Fagan, K.G. Moloy and T.J. Marks, J. Amer. Chem. Soc., 1981, 103, 6959.

50 B. Denise, R.P.A. Cheeden and C. Hamon, J. Mol. Catal., 1982, 17, 359.

51 R.S. Sapienza, M.J. Sansone, L.D. Spaulding and J.F. Lynch, "Fundamental Research in Homogeneous Catalysis", vol.3, Plenum, New York, 1979.

52 N.B. Jackson and J.G. Ekerdt, J. Catal., 1986, 101, 90.

Chapter 7

Infrared Studies of Methanol Adsorbed on MgO

7-1 Summary

Two kinds of methoxide species formed from methanol adsorbed on MgO were observed by infrared spectroscopy.

7-2 Introduction

Infrared spectra of methanol adsorbed on magnesium oxide to form methoxide species have been studied by Kagel and Greenler[1], and they found that the methoxide species changes into the formate species at 438 K. Similar results were observed on Al_2O_3[2], ZnO[3], TiO_2[4], MoO_3[5] and ZrO_2[6]. In this chapter the adsorption of methanol on the highly degassed MgO surface was studied in detail by means of Fourier-transform infrared spectroscopy.

7-3 Experimental

The magnesia (99.92 %) powder used in this chapter was obtained from Kamishima Co. Ltd. No impurities were found by XPS measurement. About 60 mg of the powder was pressed into a self-supporting disc of 20 mm in diameter. The sample was placed in an IR quartz cell which was connected to a closed circulation reaction system with a vacuum line. The sample in the cell was heated in O_2 at 773 K overnight, followed by evacuation at 973 K for 10 min.

FT-IR spectra were recorded on a JEOL-100 Fourier-transform infrared spectrometer using a liquid N_2 cooled HgCdTe detector, in the region 400-800 cm^{-1}. Usually 256 scans with a resolution of 4 cm^{-1} were collected. Spectra of adsorbed species were obtained by ratioing the background spectrum of magnesia at the adsorption temperatures to those of the adsorbed gases.

Methanol (ca. 10 torr) was exposed to the magnesia disc after pretreatment. After removing the gas phase with a liquid N_2 trap, IR spectra of the surface species were obtained.

7-4 Results and Discussion

IR spectra of methanol adsorbed on MgO at various temperatures are shown in fog. 7-1. Here, the bands observed around 2700 cm^{-1} and at 1200-1000 cm^{-1} are assigned respectively to C-H and C-O stretching vibrations due to the methoxide species.

Fig. 7-2 shows the ratio spectrum of (b)/(a) in fig. 7-1. It shows clearly that when the temperature increased from 373 to 473 K (figs. 1a and 1b) the intensities of the bands at 2779 and 1120 cm^{-1} decreased while the bands at 2798 and 1098 cm^{-1} increased. In the temperature range of 473-573 K, the former bands decreased and the latter remained almost unchanged. These facts suggest that the bands at 2779 and 1120 cm^{-1}, and the bands at 2798 and 1092 cm^{-1} are paired respectively; in the other words, two kinds of adsorbed methoxide species were formed on MgO. One disappeared at ca. 473 K,hereafter referred to as "unstable methoxide", and the other remained on the magnesia surface up to 673 K (stable methoxide). It is interesting to note that unstable methoxide changes into stable methoxide around 473 K At 673 K, the IR spectral change of the stable methoxide species were followed with time, as shown in fig. 7-3.

The intensities of the bands at 2798 and 1092 cm^{-1} decreased gradually, however, no new species were observed.

Kagel and Greenler[1] have reported that at 433 K methoxide species change into formate ion on MgO. However, in the present study, the formate species appeared when

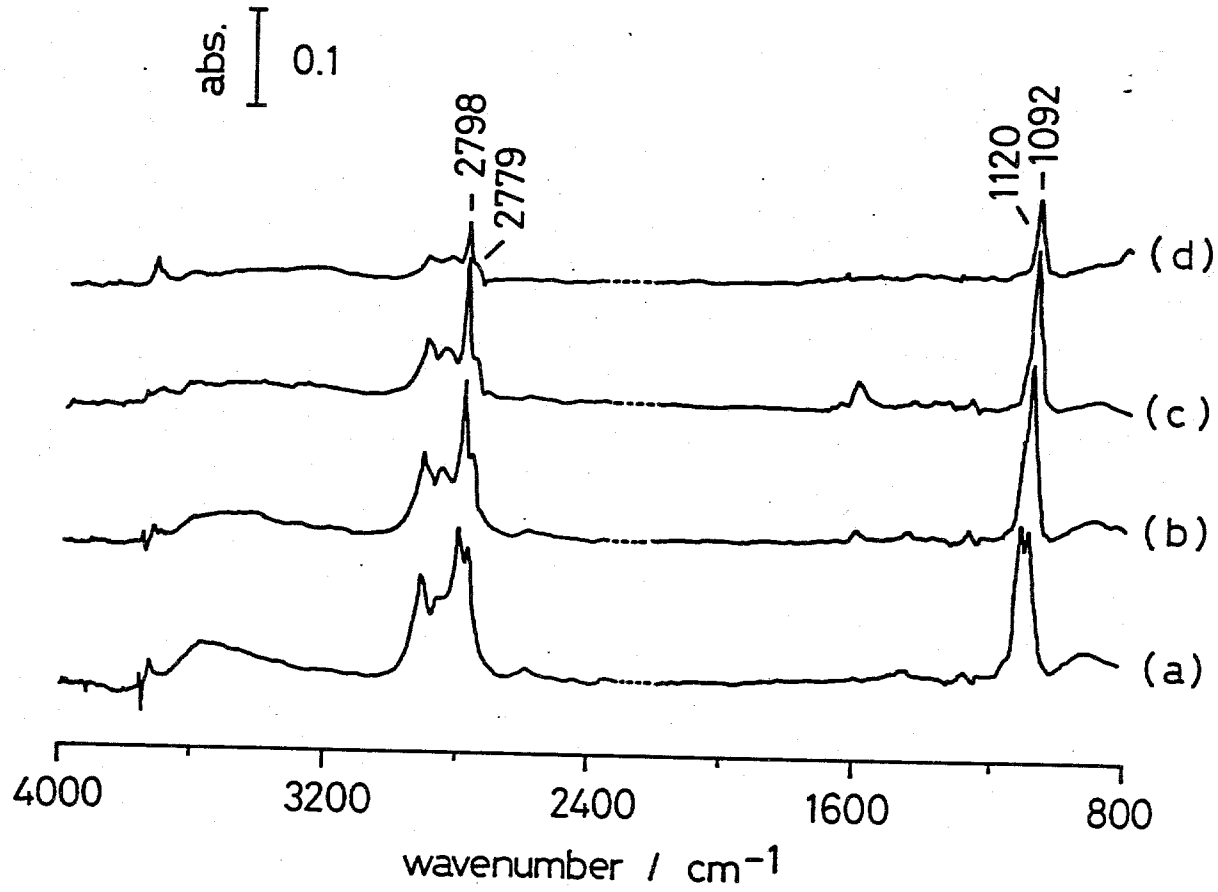

Fig. 7-1 Changes of IR spectra of methoxide species adsorbed on MgO at various temperatures:(a) 373 K, (b) 473 K, (c) 573 K and (d) 673 K.

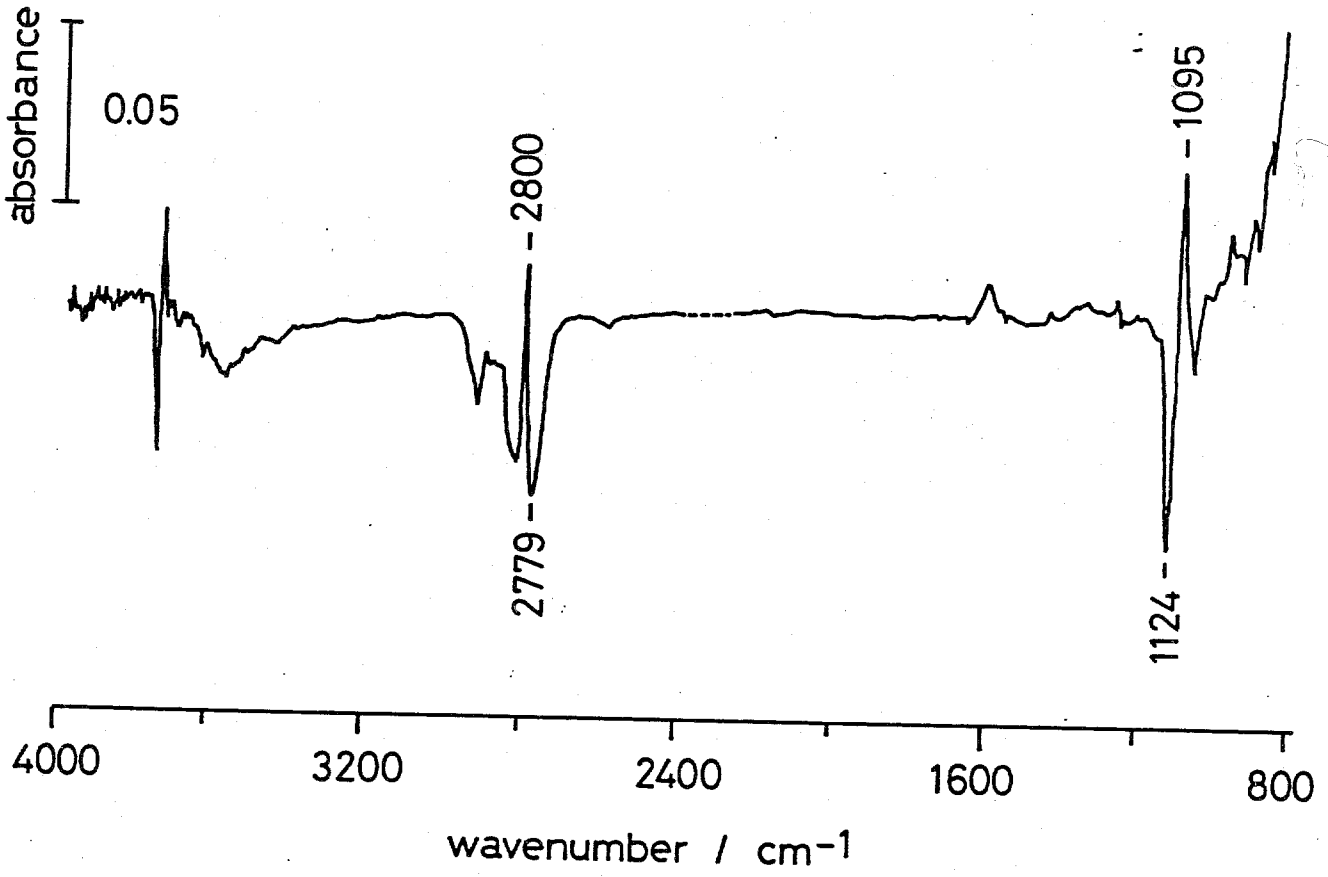

Fig. 7-2 Ratio spectrum of (b)/(a) in fig. 7-1.

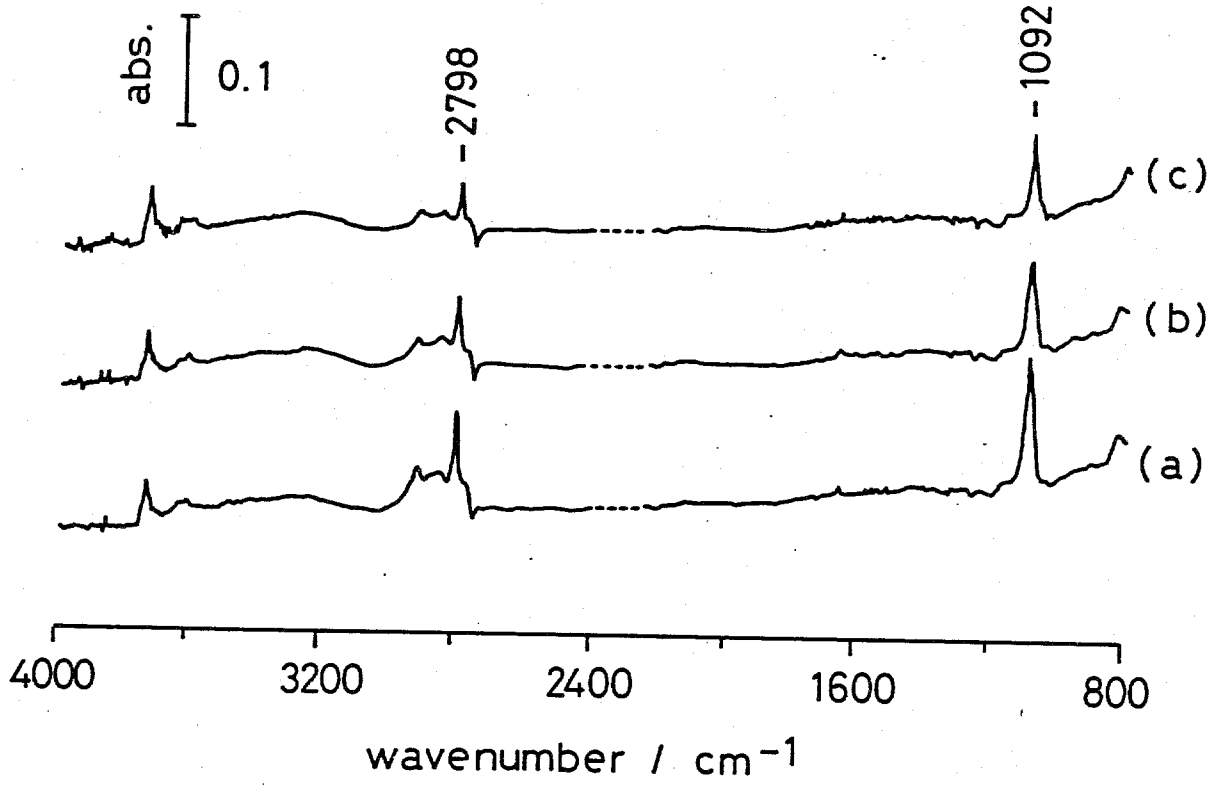

Fig. 7-3 IR spectra of adsorbed methanol on MgO at 673 K:
(a) 10 min, (b) 20 min and (d) 30 min.

the methoxide species were heated in the presence of O_2. At 438 K, the unstable methoxide species were easily oxidized to form formate species while the stable one remained unchanged. In fig. 7-4, at 503 K, the stable methoxide species, however, were also oxidized to form formate species.

When formic acid was introduced over MgO at 473 K, IR spectra of adsorbed species were observed as shown in fig. 7-4. The observed bands were reasonably assigned to the formate species[6]. The strong band at 1605 cm^{-1} due to an antisymmetric OCO^- stretching vibration has a shoulder at 1657 cm^{-1} and the bands around 1350 cm^{-1} can be assigned to an OCO^- symmetric stretching of the formates. This fact suggests that two kinds of formate species adsorbed on MgO are present similarly to the case of methoxide species.

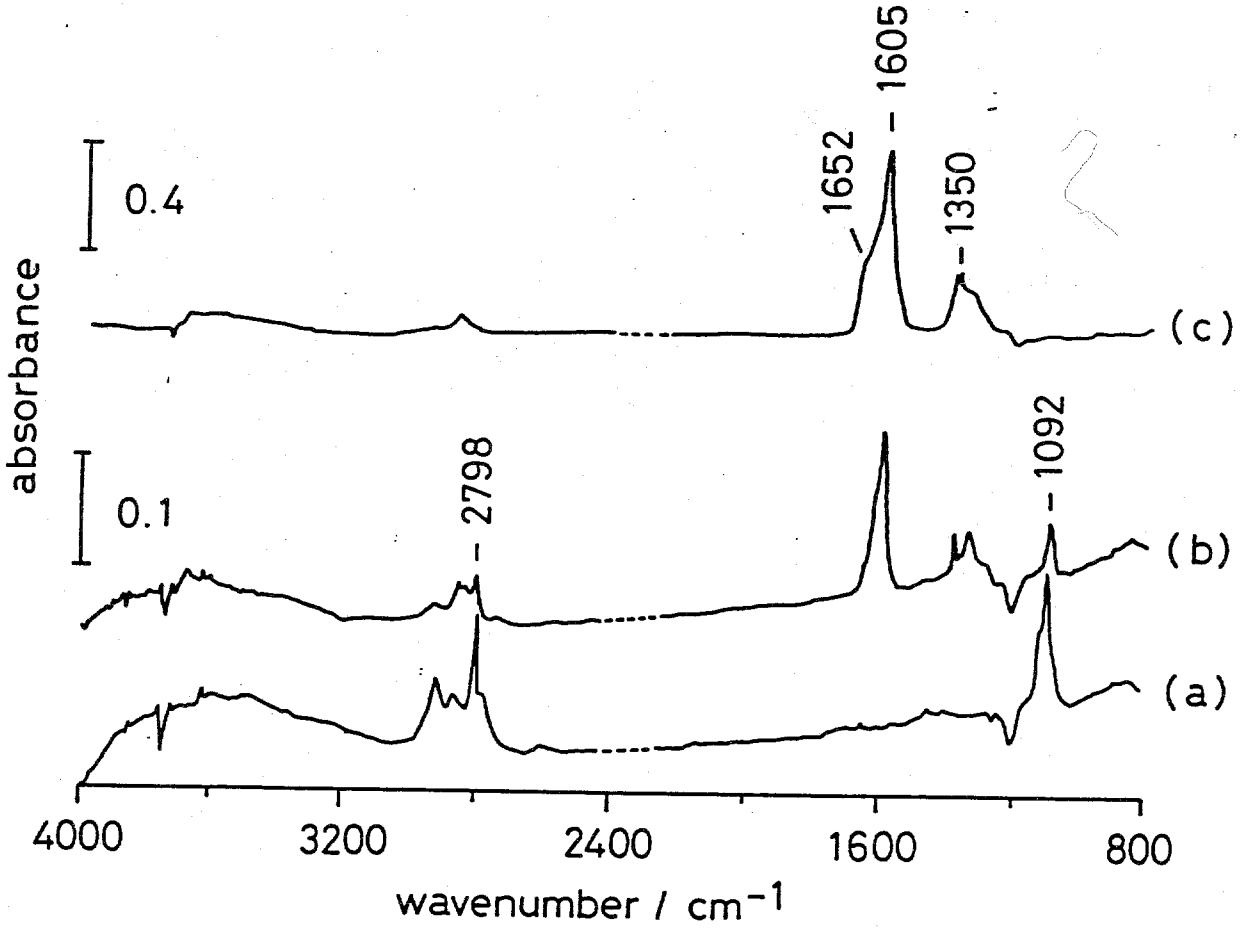

Fig. 7-4 IR spectra of adsorbed methoxide and formate species formed from methanol and O_2 over MgO at 503 K: (a) without O_2, (b) 15 min with O_2 and formic acid at 473 K.

7-5 Conclusion

From the results, it is concluded that there are two kinds of methoxide species formed from methanol adsorption on the magnesia surface and that one is stabler under heating and oxidation by O_2 compared to the other. These adsorbed species change into the formate species only when they are heated in the presence of O_2.

7-6 References

1 R.O Kagel and R.G. Greenler, J. Chem. Phys., 1968, 49, 1638.

2 J. Lamotte, O. Saur and J.C. Lavalley, J. Chem. Soc., Faraday Trans. 1, 1986, 82, 3019.

3. J.F. Edwards and G.L. Schrader, J. Phys. Chem., 1985, 89, 782.

4 H. Hattori and G. Wang, in: Proc. 8th Intern. Congr. on Catalysis II-219.

5 J.S. Chung, P.Miranda and C.O. Bennett, J. Chem. Soc., Faraday Trans. I, 1985, 81, 19.

6 H. Abe, K. Maruya, K. Domen and T. Onishi, Chem. Lett., 1984, 1875.

Chapter 8

Conclusion

One of the simplest catalytic reactions involving hydrocarbons is the hydrogenation of ethene to ethane. Because of its relative simplicity, this reaction has been the subject of numerous fundamental studies designed to determine the detailed surface chemical mechanism by which the reaction occurs. Several different mechanisms have been proposed for the reaction over metals[1]. Comparing a great deal of the researches on metal catalyst, much less investigation have been done over metal oxide catalysts. ZnO is the only oxide on which the mechanism of ethene hydrogenation has been studied in detail. The proposed mechanism is that π-adsorbed ethene is first hydrogenated to ethyl species, which then forms ethane. In this mechanism ZnH and OH species are regarded to be intermediates.

On ZrO_2 a reaction mechanism is proposed with detailed analysis of IR spectroscopy, as schematically described below (chapter 5):

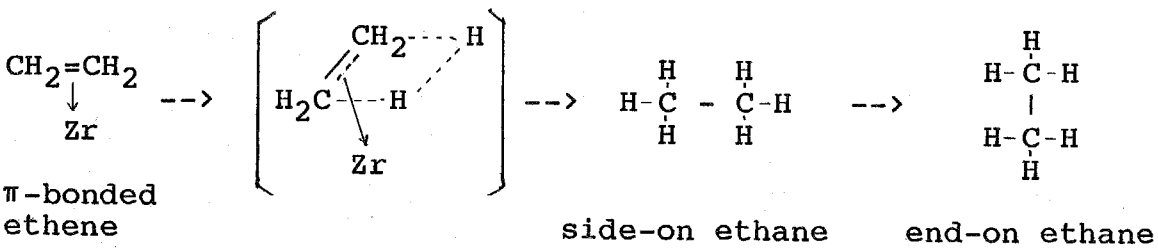

π-bonded ethene

side-on ethane

end-on ethane

Three adsorbed species: π-bonded ethene, side-on and end-on ethane; were directly observed by IR following the time course of the reaction (chapter 3 and 4). The activated complex is thought to involve an associated hydrogen molecule, not separated hydrogen atoms. This mechanism

differs from the one over ZnO on the point that the reaction proceeds without individual activation of hydrogen. Furthermore the probability of this mechanism to work as a catalytic process was confirmed by kinetic studies of both IR and conventional volumetric methods (chapter 5).

Among the first ideas, the mechanism of ethene hydrogenation through an immediate attack of hydrogen molecules on the adsorbed ethene has been suggested. However this present study is the first direct observation of the adsorbed species which might prove the mechanism.

An important notification is provided by this study: the activation process of hydrogen. Nowadays a common way of pursuing studies on a mechanism of a hydrogenation is to first examine the activation of each related molecule and then combine them. Yet, the actual activation process can not be often concluded only from each separated study. Then it becomes very important to carry out the observation studies in the reaction conditions (or "in situ") to disclose the real reaction mechanisms.

Activation of hydrogen over ZrO_2 was examined as a fundamental study to consider the hydrogenation mechanisms. The energetic interpretation of heterolytic dissociative adsorption to form ZrH and OH species was examined in detail. As a result an isotope effect was found between H_2 and D_2 for this adsorption. Besides this heterolytic dissociative adsorption, an adsorbed species, which is regarded as $Zr<^{H}_{H}$, resulting from homolytic

dissociative adsorption was identified for the first time on metal oxides (chapter 2).

Also a reaction mechanism for hydrogenation of CO to methanol is proposed (chapter 6). In case of this reaction, ZrH and OH species which are derived from the heterolytic dissociative adsorption are considered to be intermediates. Below room temperature, unstable formyl species (Zr-CHO) were identified by IR spectroscopy. The existence of formyl species suggests the reaction mechanism as described below:

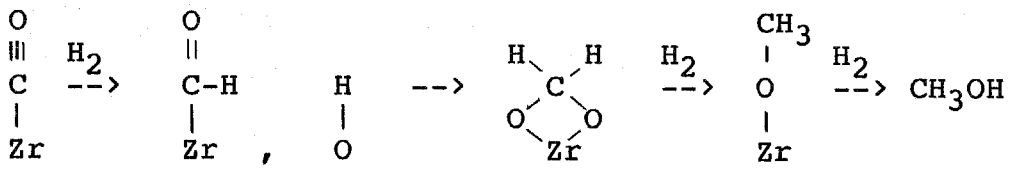

It is made clear that the formate species exists stably on ZrO_2 surface and that it might be a spectator for methanol synthesis reaction. This mechanism is in good agreement with one proposed mechanism over ZrO_2 in the literature[2,3], where the formyl species were not detected.

References

1 J. Horiuti and K. Miyahara, "Hydrogenation of Ethylene on Metallic Catalyst", NSRDS-NBS, 1968, No. 13.

2 K. Klier, "Methanol Synthesis", Academic Press, 1982.

3 N.B. Jackson and J.G. Ekerdt, J. Catal., 1986, 101, 90.

List of Publication

On the chapter 2;

1) J. Kondo, Y. Sakata, K. Domen, K. Maruya and T. Onishi, "Infrared Study of Hydrogen Adsorbed on ZrO_2", J. Chem. Soc., Faraday Trans., 1990, 86, 397.

On the chapter 3;

2) J. Kondo, K. Domen, K. Maruya and T. Onishi, "Infrared Studies of Ethene Hydrogenation over ZrO_2, 1. Ethene Adsorption", J. Chem. Soc., Faraday Trans., 1990, 86, 3021.

On the chapter 4;

3) J. Kondo, K. Domen, K. Maruya and T. Onishi, "Infrared Studies of Ethene Hydrogenation over ZrO_2, 2. Ethane Adsorption", J. Chem. Soc., Faraday Trans., 1990, 86, 3665.

On the chapter 5;

4) J. Kondo, K. Domen, K. Maruya and T. Onishi, "Infrared Studies of Ethene Hydrogenation over ZrO_2, 3. Reaction Mechanism", J. Chem. Soc., Faraday Trans., received.

5) J. Kondo, N. Akamatsu, K. Domen and T. Onishi, "Infrared Studies of Ethene Hydrogenation over ZrO_2", J. Electron Spectrosc. Related Phenomena, 1990, 54/55, 805.

On the Chapter 6;

6) J. Kondo, H. Abe, Y. Sakata, K. Maruya, K. Domen and T, Onishi, "Infrared Studies of Adsorbed Species of H_2, CO and CO_2 over ZrO_2", J. Chem. Soc., Faraday Trans. 1., 1988, 84, 511.

7) T. Onishi, K. Maruya, K. Domen, H. Abe and J. Kondo, "The Mechanism of CO Hydrogenation over Zirconium Oxide Studied by FT-IR", Proc. 9th Intern. Congr. Catal.(Canada), 1988, 2, 507.

On the Chapter 7;

8) J. Kondo, Y. Sakata, K. Maruya, K. Tamaru and T. Onishi, "Infrared Studies of Methanol Adsorbed on Magnesium Oxide", Appl. Surf. Sci., 1987, 28, 475.

Others;

9) Y. Sakata, H. Abe, J. Kondo, K. Maruya, K. Domen and T. Onishi, "Dinitrogen Species Adsorbed on ZrO_2 Studied by Infrared Spectroscopy", Chem. Lett., 1989, 711.

10) M. Anpo, T. Nomura, J. Kondo, K. Maruya, K. Domen and T. Onishi, "Photoluminescence and FT-IR Studies of the Dissociative Adsorption of H_2 on the Activated ZrO_2 Catalyst and its Role in the Hydrogenation of CO", Research on Chemical Intermediate, 1990, 13, 195.

Acknowledgemensts

First of all I wish to thank the persons who guided me the last six years on my way to become a researcher: professor T. Onishi and professor K. Domen. I really appreciate the fact that they made me become interested in research.

Also my sincere thanks to professor K. Aika and Dr. K. Maruya for their time and effort. Professor K. Tamaru, thanks for introducing me to the laboratory I worked the past six years. And I appreciate Dr. Y. Sakata for getting me started on working with IR spectroscopy.

Takahito, thank you for not letting me suffer alone during our master and doctor courses. And to all the students of Onishi and Aika's group, you all encouraged me a lot. I really shared good time with you. Other professors working in the same building share my gratitude for inviting me very often to their parties.

Finally I would like to appreciate my parents for their warm encouragement as well as their financial support.

1991

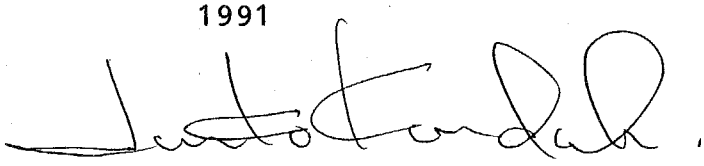

Junko Kondo